DEVELOPMENT AND FABRICATION OF COST EFFECTIVE GOLD- POLYPYRROLE ACTUATOR FOR UNDERWATER APPLICATION

A Thesis Submitted in Partial Fulfillment of the Requirements
for the Degree of

DOCTOR OF PHILOSOPHY

by

Samir Kumar Panda

(Roll No. 10610312)

Department of Mechanical Engineering
Indian Institute of Technology Guwahati
Guwahati-781039
INDIA

Department of Mechanical Engineering

Indian Institute of Technology

Guwahati - 781039

India

CERTIFICATE

It is certified that the work contained in the thesis entitled "**Development and Fabrication of Cost Effective Gold - Polypyrrole Actuator for Underwater Application"** submitted by **Mr. Samir Kumar Panda** to the Indian Institute of Technology Guwahati for the award of the degree of Doctor of Philosophy has been carried out under my supervision in the Department of Mechanical Engineering, Indian Institute of Technology Guwahati. This work has not been submitted elsewhere for the award of any other degree or diploma.

The thesis, in my opinion, has reached the standard fulfilling the requirements for the award of degree of Doctor of Philosophy in accordance with the regulations of the Institute.

Dr. Dibakar Bandopadhya

Associate Professor

Department of Mechanical Engineering

Indian Institute of Technology Guwahati

Guwahati - 781039

INDIA

Dedicated To.....

Mr. Antaryami Panda
Mrs. Manorama Panda
My parents for their blessing and guidance

Mrs Pratyasa Adhikari
My wife for her great understanding, support and encouragement

Master Sathvik Panda
My son for his love and affection

Mr. Prasanta Adhikari
Mrs. Prabhamanjula Panda
My parents-in-laws for their blessing

Mr. Sandip Kumar Panda
Mr. Sambit Kumar Panda
Mrs Sasmita Mishra
Mr. Manoranjan Mishra
Mrs Khetramani Panda
My brothers, sister and paternal aunty for their blessing, support and guidance

Mr Sambit Mallick
Mr Sasanka Sekhar Tripathy
My best friends for their affection, support and encouragement

Acknowledgement

I wish to express my deep gratitude to all those who have helped me in various ways during the tenure of my PhD work at IIT Guwahati. I have been supported and accompanied by many people and each one has played an indispensable role during my work. I am grateful to all of them.

I am greatly indebted to my supervisor Dr. Dibakar Bandopadhya who inspired me to pursue research in the field of design and advance materials. I am highly grateful to him for his guidance and encouragement during the research work. Without his support, advice and motivation, it would have just been an impossible task for me to carry over this research work. I am always gratitude to my supervisor for his endless freedom, encouragement, and motivation which he has provided to achieve this goal.

I would like to thank my doctoral committee chairman, Professor S. K. Kakoty for his valuable suggestions and encouragement during the period of my research work. Also, I would like to extend my appreciation to my doctoral committee members Dr. Karuna Kalita and Professor H. B. Nemade for their constructive criticisms and helpful suggestions which make thesis improvement. I am also grateful to the past and present heads of the mechanical engineering department, Professor D. Chakraborty, Professor A. K. Dass and Professor Santosha K. Dwivedy for extending various facilities during the tenure of my doctoral programme.

I wish to express my sincere thanks to Mr. Sanjib Sarma, Mr. Nip Borah, Mr. Suren Saloi, Mr. Narayan Kalita and Mr Manoranjan Dourah for their assistance whenever needed during experimentation and academic work. I am very much thankful to Professor P. K. Iyer and his research students for their efficiency and cheerful readiness to help me in fabricating the experimental setup precisely and accurately. I am very much thankful to Dr. Sambit Mallick for his support, encouragement and advice during my PhD work.

I am very much thankful to former director of Tezpur University, Dr. M. K. Choudhury and Professor S. K. Dolui and his research team for their help in fabricating the working prototype.

My sincere thanks go to my friends Dr. Aravinda Kumar M. S., Dr. Mithun Chakraborty, Dr. Bheem Reddy, Dr. Basudev Behera, Mr. Sudhir Yadav, Dr. Hema Gurung, Dr. Bigyan Jali, Dr. Avinash Kumar, Mr. Uttam K. Tarai, Dr. Mrutyinjay Maharana, Mr. Ankan Mishra, Mr. Bighna and my senior colleagues Dr. Himanshu S. Jena, Dr. Biswajit Nayak, Dr. Dilip Biswal, and Dr. Jagannath Sardar for their help, support and advice in different occasions of my PhD work. I shall always be grateful to my parents Mr. Antaryami Panda and Mrs. Manorama Panda for their great encouragement, love and warm wishes. The mental support I got from my brother (Sambit), Sister (Sasmita) and friend (Sasanka) is very effective and highly appreciable. Most deeply, I thank Ms Pratyasa for her constant encouragement, support, patience and motivation for the completion of this thesis work. I may have missed out a few names in the following list; my sincere apologies are due for any such inadvertent oversight.

Finally, I bow my head to the God Almighty in deepest gratitude and ask for his blessings.

13th September, 2019

Samir Kumar Panda

IIT Guwahati

Abstract

Polypyrrole, an ionic electroactive polymer (i-EAP) recently emerged as artificial muscle material and used for various cutting edge applications in defence, aerospace, biomedical and robotics. As an ionic EAP, the Polypyrrole (PPy) actuator exhibits strain through ion transfer upon applying electric potential and generates mechanical bending. In addition to this, promising properties like light weight, flexibility and biocompatibility attract researchers to develop smart and miniaturized systems particularly in biomimetic robots by effectively replacing the large, heavy and cumbersome conventional motor actuators.

The PPy is organic polymer which exhibits conductivity due to conjugated carbon bonds in chemical structure; hence categorized as Conducting Polymer (CP). The ionic transfer between electrolyte and PPy upon applying electric potential results in dimensional changes leads to generate mechanical work, and thus makes the PPy suitable to be used as actuator. PPy actuator has been used in various forms such as disc, rectangular, circular or cylindrical with both single layer and multilayer structure. While single layer structures essentially required an electrolyte fluid medium to operate, multilayer structures effectively operate in non electrolyte medium by using solid polymer electrolyte membrane on which PPy is electrochemically deposited. Beside, multilayer structure provides more strength and stiffness, hence suitable for bending applications. Further in multilayer structures, bilayer and trilayer structures are used for unidirectional and bidirectional bending applications respectively. The trilayer PPy actuator is exhibits large bending displacement and work density with low driving power and its bimorph like behaviour makes it suitable for underwater applications. However, high fabrication cost, low life cycle, slow response and low bending displacement in nonelectrolyte fluid medium are major limitations restricted its usage in real time applications.

The current state-of-the-art procedures to fabricate the Polypyrrole (PPy) actuator is expensive due to conductive coating made from platinum or gold, expensive dopants like ionic liquids (IL) and TBA based salts and organic solvents and complex synthesis process. It is anticipated that changes in processing parameters, materials and operating conditions may be able to reduce the cost and improve the performances as well. Recent literatures indicate that limited success has been achieved for successful fabrication of PPy actuator for efficient underwater performances with reasonable cost. The proposed work deals with fabrication, characterization, theoretical and experimental analysis of Gold-Polypyrrole (Au-PPy) actuator for underwater operation. The Au-PPy actuator is fabricated by using electrochemical polymerization and layer by layer deposition of PPy from aqueous solution of pyrrole (Py) and sodium dodecynbenzenesulfonic acid (NaDBS) at room temperature on both sides of gold (Au) coated polyvinylidene fluoride (PVDF). The in-depth fabrication procedures are outlined in this work. Scanning electron microscope is used to analyze the microscopic and morphological characteristics of PPy samples that show dense packed PPy-DBS on the surface of the Au-PVDF that acts as solid polymer electrolyte. The crystal structure of PPy membrane is investigated by X-ray diffraction analysis. Thermo-gravimetric analysis (TGA) and differential scanning calorimetry (DSC) test are carried out and thermal stability of the actuator is assessed. Dynamic-mechanical analysis (DMA) and thermo-mechanical analysis (TMA) are performed to evaluate the viscoelastic properties and performance of the actuator.

An experimental setup is developed to carry out the underwater bending and dynamic analysis of the developed PPy actuator. Bending test is performed in fixed-free configuration for measuring tip displacement, tip force and surface resistance under DC and AC operating voltage. The present Au-PPy actuator is cost effective and exhibits superior performances, hence can be used as artificial muscle actuator for real time applications. Several studies have been carried out to find out the effect of hydrodynamic loading on the actuation performance of the developed Au-PPy. It is well established fact that the fluid viscosity and forces act on the PPy actuator with applied electric potential significantly affects the actuation and hydrodynamic

performances like thrust and speed of PPy actuator. The effect of damping, time dependent viscoelastic modulus and hydrodynamic loading on PPy actuator is also studied to predict the life cycle of the actuator. The effect of excitation frequency on bending and hydrodynamic performances is analyzed to predict the accurate performances and efficiency of the actuator in underwater medium.

In order to analyze the underwater behaviour and hydrodynamic performances of PPy actuator a simple but robust empirical electro-chemo-visco hydrodynamic bending model is developed. The electrochemical strain is estimated in terms of output current by using RC transmission line mechanism with second order diffusion equation. Then by using electrochemical strain as input, the hydrodynamic mechanical model is developed. Here, viscoelastic effect is taken into consideration and Wiechert viscoelastic model is used for the same. The effect of underwater environment on PPy actuator performances is studied by using the complex hydrodynamic function in terms of fluid inertia and viscosity. Multi mode approximation has been taken into consideration and extended Hamilton's principle is applied for developing the governing equation of motion of the actuator. The solution of the numerical model is developed in transform form of equation to estimate the output bending displacement in terms of input voltage. The linear vibration responses are analyzed from numerical model and its results are compared with experimental results to predict the fundamental natural frequency and damping the actuator. Theoretical steady-state results are compared with the experimental results for validation.

Further modelling is extended, where a compressive study on effect of surrounding fluid on the actuator performance by considering the nonlinear fluid damping. The nonlinear governing equation of motion and a closed form expression for the response amplitude has been developed that can be used to obtain the nonlinear hydrodynamic force and amplitude response for any PPy actuator operates in fluid medium. The fluid flow around the actuator is studied by vortex shedding mechanism and the nature of force exerted on actuator is analyzed. The results obtained from numerical model solved by Fourier transform are compared with the experimental results and are found to be in good agreement.

In recent years, conducting polymers particularly PPy based artificial muscle actuator has been used in robotics and its large bending displacement and high work density makes it suitable for underwater microrobotic applications. In the present work, a tadpole like undulatory swimming robot has been developed using the fabricated PPy actuator making it suitable for underwater locomotion. The developed low cost Au-PPy actuator based robotic system is also potentially suitable in defence, security and environment monitoring applications.

The novelty of the present works is; a low cost, high performance delivering Au-PPy actuator has been fabricated from aqueous solution of Py and NaDBS at room temperature. The actuator exhibits superior performance index in reverse polarity beyond 8 h - 10 h and thus can be easily extended for micro-switching applications as well.

Content

List of Figures

List of Tables

Nomenclature

Abbreviations

AC	Alternating Current
ACN	Acetonitrile
AUV	Autonomous Underwater Vehicle
CP	Conducting Polymer
CV	Cyclic Voltametry
DE	Dielectric Elastomer
DC	Direct Current
DMA	Dynamic Mechanical Analysis
DSC	Differential Scanning Calorimetry
EAP	Electroactive Polymer Actuator
EIS	Electrochemical Impedance Spectroscopy
EDX	Energy Dispersive X-Ray
FESEM	Field Electron Scanning Electron Microscope
GMA	Giant Magnetostrictive Actuator
GPa	Giga Pascal
IPMC	Ionic Metal Polymer Composite
ICF	Intrinsic Conjugated Fiber
IL	Ionic Liquid
LBL	Layer by Layer
NM	Natural Muscle

PPy	Polypyrrole
Pani	Polyaniline
Pth	Polythiophene
PEDOT	Poly(3,4-ethylene)dioxythiphene
PVDF	Polyvinyledene Flouride
PC	Propylene Carbonate
pTS	p-Toluene Sulfonate
PZT	Piezoelectric
RC	Resistance Capacitance
SMA	Shape Memory Alloy
SPE	Solid Polymer Electrolyte
TFSI	Trifluromethanesulfonimide
TBA	Tetrabutylamonium
TMA	Thermo- mechanical Analysis

Notations

A	Area of Actuator
A(x)	Amplitude envelop of tadpole tail
A_m	Modal participation factor
A_n	Fourier coefficient
B	Amplitude of bending mode
B_n	Fourier Coefficient
c_m	Fluid added mass co-efficient
c_f	Modal hydrodynamic coefficient

c_d	Fluid drag co-efficient
C_{dl}	Double layer capacitance
E_e	Equilibrium modulus
E_{vm}	Elastic modulus in Maxwell element
E_0	Initial Modulus
E (t)	Relaxation modulus
E'	Storage modulus
E''	Loss modulus
e_m	Prony constant
F_b	Blocking force
F_{ec}	Electrochemical force
F_{fluid}	Fluid force
f_m	Fluid force due to mass
f_d	Fluid force due to drag
F_d	Drag force on tadpole
F_n	Reactive force on tadpole head in normal direction
F_t	Reactive force on tadpole head in tangential direction
h	Height of actuator
h_{PPy}	Height of PPy layer
h_{PPy_l}	Height of lower PPy layer
h_{PPy_u}	Height of upper PPy layer
h_{PVDF}	Height of PVDF layer
h(x)	Lateral undulation of tadpole tail

I	Moment of Inertia
I_c	Current output
κ	Wave number
L	Length of actuator
l(t)	Vortex shed at actuator surface
$l_u(t)$	Vortex shed at upper edge
$l_l(t)$	Vortex shed at lower edge
M_{ec}	Electrochemical bending moment
M_a	Actuator bending moment
m_a	Mass of actuator
m_f	Mass of fluid
m_c	Virtual mass co-efficient
m_v	Virtual mass density
P	Power consumption
p	Velocity potential at any arbitrary point on actuator
P_{avg}	Average power consumption
Q	Charge density
Q_t	Total Quality factor
Q_f	Quality factor in fluid
Q_a	Quality factor of actuator
q(t)	Generalized time co-ordinate
R_{PPy}	Resistance of PPy
R_{PVDF}	Resistance of PVDF

R_C	Charge transfer resistance
Re	Reynold's number
r	Displacement in Z axis
s	Laplace variable
St	Strouhal number
t_r	Random time
t	Time
T	Kinetic Energy
t_{dl}	Thickness of double layer capacitance
T_f	Thrust force
$\overline{T_f}$	Average thrust force
u	Displacement along X axis
U_s	Tadpole swimming speed
U	Strain energy
V	Tadpole body wave speed
V_{in}	Input voltage
V_x	Tadpole velocity along X direction
V_y	Tadpole velocity along Y direction
V_n	Normal component of tadpole velocity
V_t	Tangential component of tadpole velocity
v	Displacement along Y axis
W	Width of actuator
w	Transverse displacement of actuator

w_d	Work density
w_{nc}	Non-conservative work
w_f	Transverse displacement of actuator in fluid
X	Reference axis
x	Distance along length
x_p	Any point on actuator to calculate velocity potential
$\hat{x}$	Unit normalized mode function
y	Distance along thickness
Y	Reference axis
Y_a	Admittance
z	Impedance
Z	Reference axis
z_{eq}	Equivalent impedance
z_d	Diffusion impedance

Greek Symbols

ε_{ec}	Electrochemical strain
ε_a	Actuator strain
α	Strain to charge ratio
γ_{PPy}	Conductivity in PPy
γ_{PVDF}	Conductivity in PVDF
μ	Kinematic viscosity of water
μ_m	Viscosity of Maxwell element
ρ_f	Fluid density

ρ_{PVDF}	Density of PVDF layer
ρ_{PPy}	Density of PPy layer
σ	Applied stress
σ_a	Actuator stress
σ_m	Mechanical stress
σ_e	Stress in elastic component
σ_v	Stress in viscous component
σ_{PPy}	Stress in PPy layer
σ_{PVDF}	Stress in PVDF layer
τ_m	Viscoelastic time constant
ω	Actuation frequency
ω_n	Natural frequency
ω_{n_a}	Natural frequency in air
ω_{n_f}	Natural frequency in water
φ	Bending mode shape
η	Loss factor
ζ_a	Damping ratio of actuator
ζ_f	Damping ration due to fluid
ζ	Total damping
ψ	Tadpole tail bending angle
λ	Wavelength
η_{swim}	Swimming efficiency
τ	Propulsive force

∇	Laplace operator
χ	Complex conjugate variable
Ψ	Single mode approximate mode shape
Ψ_m	Unit normalized mode shape in air medium
ς	Complex conjugate velocity
ϕ_z	Normal velocity at fluid along z direction
ϕ_u	Complex vortex sheet strength at upper edge
ϕ_l	Complex vortex sheet strength at lower edge
ϕ	Complex vortex sheet strength at surface

1
Introduction

With the advancement in the field of science and engineering, conventional actuators are being replaced by smart materials particularly electro active polymer (EAP) actuators. Promising properties like low actuation potential, light weight, flexibility, high strain, biocompatibility and natural muscle like working and performances make it suitable for used as artificial muscle actuator for various macro to micro scale applications in robotics, health care, aerospace, defence and automobile sectors [1-4].

Being as artificial muscle, PPy has gained momentum for developing miniaturized underwater systems, soft and flexible bio-inspired robots and biomimetic propulsive systems. Biomimetic underwater swimming robots are of great interest for exploring underwater environments as the most part of the underwater environment is still unknown. The design of highly manoeuvrable underwater micro robots is often based on swimming mechanism, natural fish like undulatory body motion, highly controllable fins and optimal thrust. Recently various smart materials such as giant magnetostrictive (GMA), piezoelectric (PZT) and its derivatives actuators, ionic polymer metal composites (IPMC), shape memory alloy (SMA), integrated conjugated fibre (ICF) and dielectric elastomer (DE) based actuators have been developed for underwater robotics application [5-6]. However, there are many challenges like high cost, poor cycle life, low stiffness, bending displacement and mechanical stability limits their real time applications.

In this thesis the underwater working and performances of Polypyrrole, a conducting polymer are studied and are used to demonstrate the feasibility of using this material in developing bio-inspired propulsion based small swimming robot for

underwater applications. The results of these studies and experimental investigations will contribute to the understanding of underwater operation and performances of polypyrrole actuator and is extremely useful in developing effective artificial muscle based swimming devices for various underwater applications. The polypyrrole actuator driven swimming robot is also an important step towards the advanced bio-robotics for defence, security and medical applications.

In this chapter an overview of Conducting polymer and polypyrrole as artificial muscles actuator is presented at first. Then the fabrication methods and parameters affects the actuation and characteristic properties are studied with the improvements have done so far. Following this, the modelling techniques and methodologies have been used for studying the bending actuation of Polypyrrole actuators are discussed along with the method is adopted to study the underwater operation of Polypyrrole actuator. Then the recent applications of polypyrrole actuator in various fields particularly in underwater environment are discussed. This will be followed by the motivation and objectives of the present work and at last highlights of the contributions of the thesis is presented.

1.1 Conducting Polymer

Conducting Polymer (CP) as the name suggests, a polymer exhibits conductivity. In the mid of 19^{th} century, conducting polymer was first synthesized as aniline, though then the conductivity was not noticed. Later by 1963, the conductivity was reported up to 1 S/cm with the production of Polypyrrole (PPy) [7]. By 1977, CPs significantly showed large conductivity of nearly 10^3 S/cm has been reported with halogen doped [8]. Subsequently various conducting polymers such as Polypyrrole (PPy), Polyaniline (PANi), Polythiophene (Pth) and its derivatives were successfully synthesized later in that year. Because of this property, CPs are known as organic metals and hence gained attention for further research on synthesis, fabrication and uses of CP for real time applications.

The conductivity in CPs is primarily due to the polarons and bipolarons were generated from the chemical and electronic structure of the as shown in Fig.1.1.

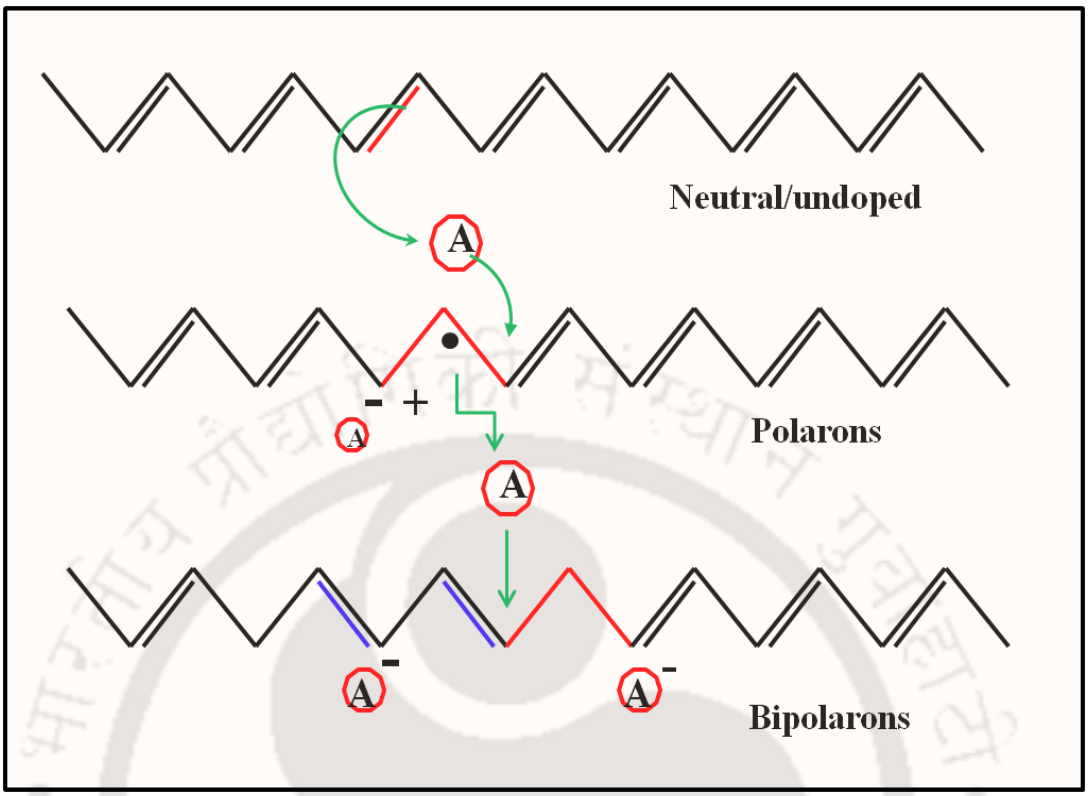

Figure.1.1 Schematic diagram of conjugated chemical structure of CPs with polaron and bipolaron

Fig.1.1 shows the CP posses intrinsic conjugated structure with alternate carbon-carbon double bond. The overlapping and delocalization of π molecular orbital electron generates the polarons and bipolarons. The lower energy based bipolarons are widely exists in the conducting polymer, hence the CP conducts the charge due to the movement of bipolarons upon applying electrical field [9]. The chemical structure alone is not sufficient for conductivity and dopant is required for the same [10]. The polymer is doped by changing its oxidation state (adding or removing electron from the backbone), which, when performed electrochemically, leads to the migration of ions into the bulk polymer, balancing charge. Doping results in creation of states in the band gap and leading to nearly metallic conduction.

The electrochemically controllable charging of conducting polymers makes them attractive materials to be used as energy storage devices, micro electro-mechanical systems, electronics and drug delivery devices [11-13]. An interesting property of conducting polymers is that their volume changes as a result of the change in oxidation state and the corresponding charging. This effect has provided an exciting

application for conducting polymers as artificial muscle actuators [14]. Among those tremendous applications, actuators attract a lot of scientists because of its similarity to natural muscles and potentially wide application. In this thesis conducting polymers as electrochemically driven actuators are studied for its underwater operations and an example of their application in bio-robotics is discussed.

1.1.1 Conducting Polymer as Artificial Muscle Actuator

Because of the similarities in terms of working and performances with natural muscles as shown in Fig.1.2, the use of conducting polymers as artificial muscles actuator is first proposed in early 1996 [14].

Figure.1.2 Natural muscle and conducting polymer working concept

Generally, the size and shape changes in CPs are the result of ions and solvent molecular influx and efflux in between polymer chain and electrolyte, as shown in the schematic diagram of actuation mechanism in Fig.1.3. Such volume changes

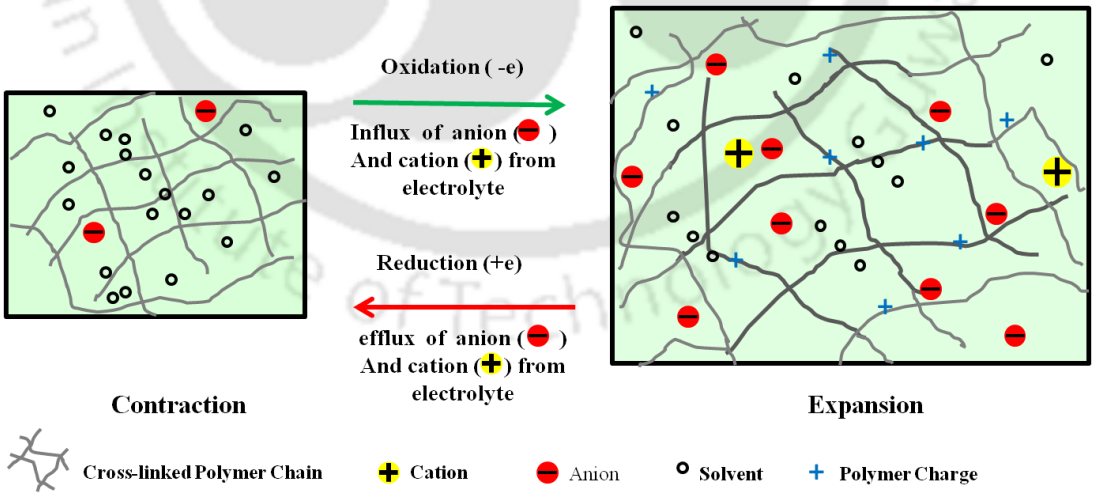

Figure1.3. Actuation mechanism via ions insertion accompanied by solvent.

are due to accommodate the anions, cations and sometimes the solvent molecules which accompanied by the redox reactions in CPs. Reversible redox reactions i.e. simultaneous reduction and oxidation reactions in CPs lead to electrochemical

charging and discharging. These processes generate charged sites on the polymer backbone where each site is charged by an oppositely charged "counter-ion". Counter-ions enter and leave into the polymer from and to an external electrolyte; leads to volumetric changes, hence generate strain and subsequently the stress.

The above actuation principle of CPs attracts researchers to develop actuator and implement this in practical applications like active catheter system, drug delivery system and micro robotic etc [15-17]. Although CP actuators and natural muscles have many features in common such as both of them are driven by electro stimulation and flux of ions, both are soft and flexible, operate in contact with electrolyte, transfer chemical energy to mechanical energy and are, the working life cycle of CP actuators is very less as compared to natural muscles [18].

In recent times, including CP there are various other smart and active materials have been used as artificial muscle materials such as ionic polymer metal composites (IPMC), piezoelectric materials (PZT), dielectric elastomer (DE), macro fibre composites (MFC) and Shape memory alloys (SMA) [19-20]. The characteristics properties and performance parameters of various smart materials including CPs and their comparison with natural muscle is shown in Table 1.1.

Table 1.1 Comparison of CP with natural and other artificial muscle materials

Material	**Strain (%)**	**Stress (MPa)**	**Work Density (kJ/m^3)**	**Strain Rate (%/s)**	**Efficiency**	**Advantage**	**Disadvantage**
NM	20	0.35	8	>50	~40	heat and waste removable, energy deliver, regeneration	Required specialized environment, cannot produced synthetically
DE	Upto 380	~1	Upto 3400	4500	Typically 30 upto 90	Very high strain and strain rates	High voltage (>1kV) & field (>150MV/m)

CP	**max 39%, avg. 5**	**Upto 30**	**100**	**12**	**20**	**Low voltage, high stress and strain**	**Slow response, Creep, Low life**
IPMC	0.5 - 3	3	Upto 5	3	1.5 - 3	Low voltage large displacement	Only bending (not linear) motion
SMA	5	Upto 200	>1000	300	<5	high power (> 100 kW/kg) low voltage	Difficult to control (run at peak, not in between)
NM = Natural Muscle, DE=Dielectric Elastomer CP=Conducting Polymer, SMA = Shape Memory Alloy IPMC=Ionic Polymer Metal Composite							

It is observed that the weight to actuation capability of CP is much higher and advantages include operation at low voltage (typically $1-1.5$ V or less); light weight (density is roughly $0.5\sim2$ g/cm^3); relative large dimensional changes (as large as 40% in some special cases); and high power density (up to 300 kJ/m^3). Besides similarity with natural muscle, unique characteristics such as low density, high toughness, low driving energy and inherent vibration damping makes it suitable for developing biomimetic systems. In this thesis conducting polymer (CP) has been studied and applied for actuator application.

1.1.2 Materials Used for Conducting Polymer Actuator

From the literature it has been seen, over the years polyaniline (PANi), polythiophene (Pth) and its derivative poly (3,4-ethylenedioxythiophene) (PEDOT) and polypyrrole (PPy) are widely used CPs. Layout of the chemical structures of these materials is shown in Fig.1.4.The brief detail of each material is given below followed by the primary characteristic properties and performances of these materials.

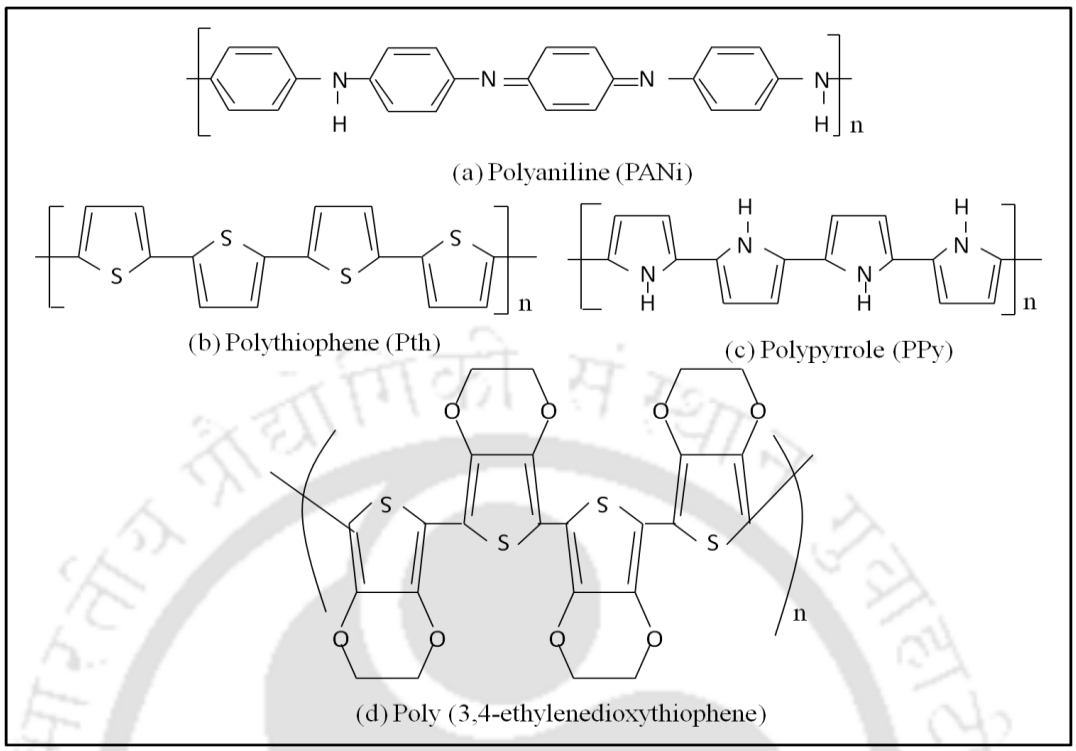

Figure.1.4 Schematic diagram of chemical structure of (a) Polyanilene (b) Polythiophene (c) Polypyrrole and (d) Poly (3,4-ethylenedioxythiophene)

1.1.2.1 Polyaniline (PANi)

Polyaniline as the first CP material was discovered and where Nitrogen (N) atom is present outside the aromatic cycle as shown in Fig.1.4 (a). PANi is synthesized by using chemical and electrochemical polymerization methods. Polyaniline is acidic in nature hence the actuators are operated in an acidic environment in both aqueous and organic solution. Strain generated by PANi actuator is usually below 2% at free load, which is small as compared PPy actuator. The interesting part of PANi is perhaps its high mechanical strength and actuation strain from $1\% - 3\%$ has been obtained at stresses of 5 MPa, which is attractive to engineers [21]. It has been seen PANi with carbon nanotubes reduced the actuation strain to 0.8% but greatly enhance the strength so that actuation could be achieved at 125 MPa [22]. These materials showed a large work output ($320\ kJ/m^3$) [23]. Another advantage of using PANi is its capability of processing suitable for mass-production, which makes the material attractive for commercialization. There are also some limitations in using PANi as an actuator material. The acidic aqueous

environment perhaps limits the further application of the PANi actuators due to fast material degradation. Further, small strain and non-biocompatibility limits the real time actuator application to great extent. However, it has been seen PANi is suitable for sensor application [24].

1.1.2.2 Polythiophene (Pth)

Polythiophene (Pth) and its derivative poly (3,4-ethylenedioxythiophene) (PEDOT) both are sulphur containing conducting polymer where Sulphur atom present in the aromatic cycle as shown in Fig.1.4 (b) and (d). Pth and PEDOT can be prepared by both chemical or electrochemical polymerization. The advantages of using Pth in electrochemical applications include its high conductivity, wide potential window and structure stability where PEDOT is used as both sensor and actuator. However Pth actuator shows low strain of 0.5% – 2% in organic and ionic liquid based electrolyte [25, 26]. It has been found that elastic modulus is usually lower in the expanded state and the actuation strain diminishes with an increasing applied load. Strain is as high as 11.5% were recorded, although the strain diminished rapidly with increasing voltage scan rate and higher isotonic loads [27].

Poly (3,4-ethylenedioxythiophene) (PEDOT) is a oxygen and sulphur contained conjugated polymer. Tough PEDOT exhibits conductivity, mechanical stability with low actuation potential, low band gap and poor solubility limits its application. PEDOT is synthesized by chemical polymerization method and its composite forms are suitable for sensor application [28]. PEDOT with polystyrene sulfonate (PEDOT.PSS) and PEDOT with Polypyrrole (PEDOT.PPy) were also used for actuator applications [29].

1.1.2.3 Polypyrrole (PPy)

Polypyrrole (PPy) is a nitrogen contained organic chemical compound formed from a number of connected pyrrole in ring structure as shown in Fig.1.4 (c). Pyrrole is the monomer of polypyrrole polymer having chemical formula C_4H_4NH. It is a volatile liquid that darkens readily upon exposure to air thus need to be distilled before use. PPy is the first derivative of polyacetelene which shows high conductivity [8]. The properties of Polypyrrole are primarily dependent on its synthesis process.

PPy is the most attractive conducting polymers due to its high conductivity, stability in both of the aqueous and organic solvent, high mechanical strength, biocompatibility and large actuation strain. The strain of polypyrrole actuators is typically $2\% - 10\%$ [30]. Polypyrrole synthesized with DBS that achieved 12% strain however stress is very low of 0.5 MPa [31]. The free-standing PPy/TFSI films, without load, can show extremely high strain as much as 40% by carefully selecting dopants and solvents [32].

The summary of important properties of various CPs is shown in Table 1.2. It has been observed that PPy is the potential candidate for actuator application in versatile [21-23, 25-26, 28, 30-34]

Table 1.2 Summery of important properties of various conducting polymers

Properties	**Polyaniline (PANi)**	**Polythiophene (Pth & PEDOT)**	**Polypyrrole (PPy)**
Strain (%)	1-2	0.5-2	**2-8**
Stress (MPa)	10	8	**40**
Operating Voltage (V)	3-5	3-5	**1.3-3**
Suitable Application	sensor	sensor	**Sensor and Actuator**
Work density(kJ/m3)	20	10	**100**
Stability	Low life	Low life	**Moderate to high**

environments. PPy can generate large strains (typically 6% and maximum39%), relatively low strain rates (typically 1%/s and maximum 12%/s), high stresses (typically 5 MPa, and maximum 100 MPa) and work density ($80 - 100\ kJ/m^3$ makes it suitable for underwater applications. Hence in this thesis the details of fabrication and characterization of PPy actuator has been studied for its underwater operations.

The Young's modulus of PPy is between 0.2 GPa to 1 GPa [33]. These properties along with biocompatibility, light weight, low actuation voltage and

natural muscle like working, make it suitable to be used as artificial muscle actuator and the present work is focused on fabrication and application of PPy based actuator. However slow response, low operational life and high fabrication cost are some major limitations were reported earlier, these can be overcome by careful selection of materials and synthesis process.

1.2 Polypyrrole (PPy) Actuator

Recently Polypyrrole has gained attention to develop artificial muscle actuator due to its low operating voltage, large strain, stress and work density, flexibility and biocompatibility, hence used for various applications in robotics, defence, aerospace and biomedical [33, 35-36]. From the literature, it has been seen the PPy actuators were used broadly categorized as axial and bending type actuator. For these two types, various configurations such as sheet (strip), helical, laminated, multilayer strip based actuator have been proposed. For axial bending particularly sheet and helical forms are suitable while for bending laminated and multilayer structures similar to beam configurations have been used [37-38]. Further based on the working environment such as electrolyte and non-electrolyte medium, laminate structures are suitable as the laminates can be used for internal storage of electrolyte in case of non-electrolyte medium of operation particularly in air and water medium. The helical type actuator has been used for underwater microrobotics operations however to immersed in fluid it need a guiding tube which limits their application. Unlike this, the laminated structure with internal electrolytic storage has proven more efficient for bending operations in non-electrolyte fluid medium [39-40]. Again laminated structure with internal electrolyte storage can be classified as bilayer and multilayer based on number of layers of PPy and electrolyte storage. Among multilayer structures, bilayer and trilayer laminated structures are of great interest because of simple fabrications and operation process. Though the bilayer structure is the simplest one, the disadvantages like low strength, delamination and unidirectional operations may hinder its continuous bending applications. Alternatively, the trilayer actuator is suitable for bidirectional bending and exhibits

significant strength makes it suitable for continuous bending operation in non-electrolyte medium especially in water.

1.2.1 Actuation Mechanism of PPy trilayer actuator

PPy undergo deformation due to change in oxidation state upon applying electric potential i.e. yields mechanical work or motion from a membrane or beam like structure by converting input electrical energy, hence suitable to be used as actuator. The actuation mechanism of laminated PPy strip actuator is shown in Fig.1.5.

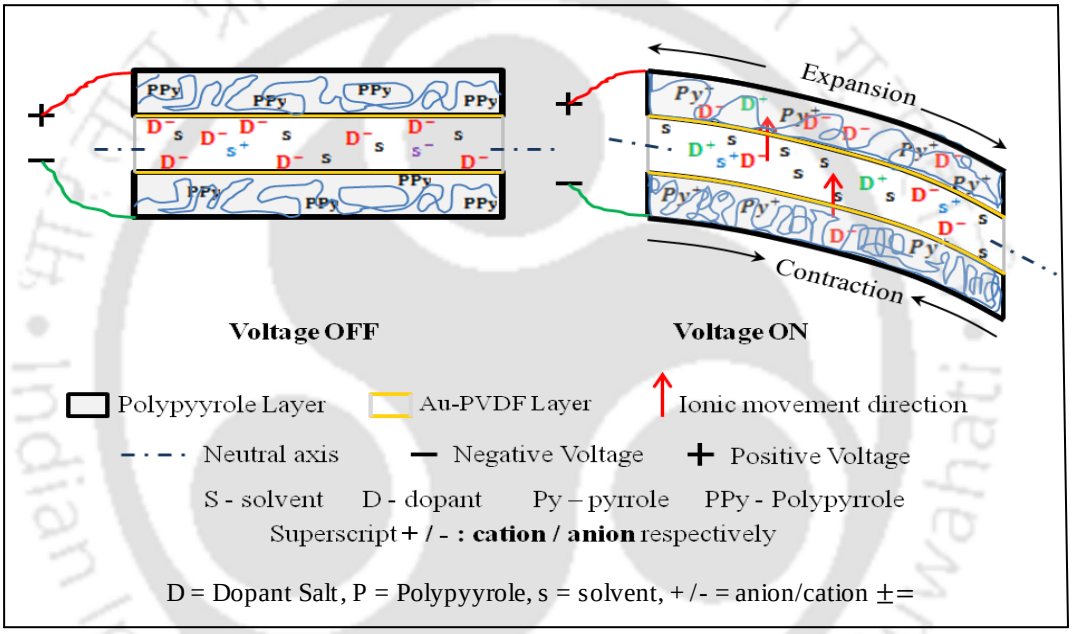

Figure.1.5. Schematic diagram of PPy trilayer actuator working

The middle layer is a porous membrane that acts as solid polymer electrolyte (SPE) while the top and bottom layers are Polypyrrole. During synthesis the cation and anion of the salt along with solvent absorbed and trapped in the SPE membrane and later take part in ionic exchange between electrolyte and PPy on applying voltage. This validate that PVDF is used frequently as compared to other SPEs such as cellulose and nylon [41]. The SPE is also contributing stiffness to the actuator as well. The working principle of PPy actuator is based on reversible redox reaction i.e. Simultaneous oxidation (removal of electrons from the polymer) and reduction (gain of electron into polymer matrix to maintain the neutrality) occurs between the polypyrrole and electrolyte upon applying electric potential. The ionic movement is

primarily dependent upon the size of ions i.e. the small ions are highly mobile and can easily penetrate and move in the polymer chain. Therefore, the actuation is named as cationic, anionic and mixed actuation based on type of mobile ions transfer between electrolyte and polymer chain. Due to this ionic movement, the actuator experiences volumetric changes which generates strain and subsequently stress in the actuator. If one side of the actuator is fixed like a cantilever, bending induces in the actuator due to the strain and stress.

This bending mechanism makes the PPy actuator suitable for robotics application particularly bio-inspired robotics has gained a lot of interest. Recently Polypyrrole bending actuators have been used in numerous micro to macro scale application while it has shown more efficient in developing miniaturized and soft robots [15, 33, 35]. Further, the similarity of bending behaviour with fish tail like movement, large bending displacement and high work density makes the Polypyrrole suitable for underwater operation.

1.3 Synthesis and Fabrication of PPy Actuator

Like other conducting polymers, the Polypyrrole (PPy) is synthesized by both chemical and electrochemical polymerization methods. It has been reported that the properties of the PPy are largely dependent on the synthesizing conditions such as temperature, time, substrate, concentration and doping materials [42-43]. The details of the synthesis of process are described in following section.

1.3.1 Chemical Synthesis

In chemical polymerization, a monomer, a dopant, and an oxidant are dissolved in a solution kept at a certain temperature. The monomer is first oxidized into a radical cation and then the coupling of two radical cations results in a dimer. The dimer can then be oxidized into a dimer radical cation and continuation of these reactions produces oligomers followed by polymers until termination of the chain. The polymerization time ranges from minutes up to a few days, depending on reaction conditions. The mixture is then filtered, washed, and dried to yield pure conducting polymers. The PPy synthesized by chemical method is obtained in powder form.

Though various oxidants have been used for chemical polymerization of Polypyrrole $FeCl_3$ is typically used frequently as it provides stability and enhances the conductivity as well. The conductivity of chemically synthesized PPy is very low roughly around 10^{-4}S/cm and including this low thermal stability, poor mechanical strength, complex fabrication and processibility of the powder form limits their actuator applications [44]. However, PPy fabricated by chemical deposition method has shown reliable active performances with chemical activities thus mainly used to develop various sensors such as gas sensor, electronic and mechanical sensor [45-46].

1.3.2 Electrochemical Synthesis

In electrochemical synthesis, the radical cation is generated at the initial step via electric potential is applied across an electrolyte solution containing a monomer and a dopant. A three-electrode (working, reference, counter electrodes) or a two-electrode (working, reference electrodes) mode may be used. Electrochemical polymerization is convenient and controllable process and develops the stable PPy in solid film form.

Electrochemical deposition is generally preferred by researchers to prepare PPy materials as it provides a good control on film thickness, morphology, improved mechanical properties and higher conductivity. Electrochemical synthesis is based on the transfer of electrons between a substrate and an electrode. A complete electrochemical reaction system requires both an anode and cathode as the working and counter electrodes, respectively, a reference electrode is to maintain the right voltages in the system, as well as an electrolyte for the migration of ions. Upon oxidation of the anode, electrons are removed to attract the anions and pyrrole monomers to be simultaneously polymerized and deposited onto the working electrode. The conductivity of electrochemically polymerized PPy may reaches up to 200 S/cm and shown active mechanical performances, hence suitable for used as actuator [47, 48].

Electrochemical techniques are superior under these conditions as the oxidation is localized to the interface at the working electrode. Over the course of a reaction,

the continued polymerization coats the surface with a layer of increasing thickness. It is the ability to grow films that enables a great deal of further testing and remains a critical step in the synthesis of conducting polymer actuators. The electrochemical process has become more popular for developing actuator as it is suitable to produce PPy films and can control process parameters during synthesis. For electrochemical synthesis aqueous electrolyte solution is preferred as water helps to capture the reaction-released protons and prevents pyrrole from being protonated. The comparison between chemical and electrochemical synthesis is shown in Table 1.3.

able 1.3. Comparison of chemical & electrochemical synthesis process.

Synthesis Process	Advantages	Disadvantages
Chemical	• Large Scale Production • Modify CP backbone after synthesis	• Complex synthesis process • Can't prepare thin film
Electrochemical	• Prepare thin film • Ease & better control of synthesis • Simultaneous polymerization & film formation	• Difficult to modify after synthesis. • Hard to separate film from substrate.

Further in electrochemical polymerization layer, by layer (LBL) polymerization and deposition method has been used. It has been reported that the conductivity and stability of the film synthesized by LBL method is increased as compared to the continuous polymerization and deposition method [49]. In the present work layer by layer electrochemical polymerization and deposition method is adopted to fabricate the PPy actuator.

1.3.3 Factors affecting the Electrochemical Synthesis

The actuation characteristics and performances of PPy actuator is mainly depend on the factors such as type of electrode materials, mobile ions and dopants, solvent type, temperature and deposition techniques. This section covers the effect of each

factor on the actuation and and improvements have been carried out to enhance the actuation characteristics and electro-chemo-mechanical properties of PPy actuator.

1.3.3.1 Electrodes

PPy films can be electro-polymerised on a wide range of metal electrodes. Glassy carbon, platinum (Pt) and gold (Au) are mostly used. However, Indium-tin oxide (ITO) coated glass, Titanium (Ti), Aluminium (Al), mild steel, and brass, mercury, tin-oxide and silver have also been tried [50]. In comparison with Pt electrode, the oxidation potential of pyrrole is increased and current density reduced when Ti, Fe, or Al are used. This is a consequence of metal-oxide film formation which impedes electron transfer during electro polymerisation. Metals such as silver or aluminium, which oxidise more readily than the pyrrole monomer, would obviously not be a good choice. PPy films electro-polymerized on platinum or Gold (Au) have much smoother surfaces when compared with PPy prepared on other electrodes. While the cost of Pt is high, Gold is the most suitable material for use as electrode. The Gold electrode is fabricated by using various coating methods like sputter coating, vapour and vacuum deposition techniques. However the sputter coating techniques have been used frequently; however, the expensive sputter targets increase the fabrication cost to a significant extent. Unlike the sputter coating, vapour and vacuum deposition techniques provide more uniform coating thickness at low cost, hence the use of later one is explored in the current work to further minimized the fabrication cost for developing high performance PPy actuator.

1.3.3.2 Method of Polymerization

Electrochemical deposition of polypyrrole can be achieved using controlled potential or current densities. Low polymerization current density allows better alignment of polymer chains, leads to high compactness of PPy, which might have slow down transfer of ions and strain rate. Different current intensity leads to different porosity which directly influences the conductivity and mechanical property [51]. It has been observed that the polymerization process, and in particular the polymerization potential, influences which ion dominates the actuation properties [52]. With potentiostatic polymerization mainly cation-driven actuation was found in both organic and aqueous electrolytes. To have movement of only one ion type

(anions or cations with solvent molecules) at anodic or cathodic potentials to dominate the actuation has been a major goal in the development of CP actuators. The polymerization techniques such as galvanostatic, potentiostatic and potentiodynamic were used for synthesis and fabrication of PPy actuator [53]. However galvanostaic method is widely used as the deposition thickness is uniform and PPy exhibits high stability due to applying the constant current density.

1.3.3.3 Temperature

Temperature of the electro-polymerization reaction has substantial influence on the mechanical properties and electrical conductivity of PPy films. In general, PPy polymerized at low temperature shows high stability and conductivity [54]. It is important to note that polymerization at low temperature avoids any other unpredictable side reactions that can occur at the same time during the polymerization reaction. Further, the ionic movement is in moderate speed at low temperature, hence promoting a more ordered molecular structure of PPy, thus improves the conductivity. To maintain the low temperature during synthesis, glove box setup or low temperature box setup has been used, however these setups increases the fabrication cost. It has been observed that PPy actuator synthesized in room temperature may also exhibits high conductivity by proper tuning of other synthesis parameters [55]. In the present work the synthesis and fabrication is carried out in room temperature setup to further reduce the fabrication cost.

1.3.3.4 Mobile ions and Dopant Salt

The dopant plays the major role for exhibiting conductivity while their ions sizes are solely contributed to the actuation strain in the PPy. Based on ionic movement, the actuation may be cation or anion dominated while very few mixed ion actuations based actuator has been reported so far [56]. Cation-dominated actuation in PPy is more frequent which polymerized with large anion based readily available dopant as reported in many papers [57]. Polypyrrole doped with dodecyl-benzenesulfonate (PPy/DBS) and *p*-toluene sulfonic acid salt (PPy/PTS) are two typical cation driven actuators as Na^+ can penetrate into the polymer while pTS and DBS were unable to move due to large size [58]. It has been reported that the actuation strain was observed to be linearly proportional to the size of the cation in

cation dominated PPy [59]. From literature it has been seen that, the strain is exceptionally high for few anion dominated actuation particularly in Ionic liquids and TFSI derivative based dopant salts [60], however these dopants are expensive and not readily available in market. The anion incorporated into the polymer (counter ion) during synthesis has the greatest influence on the general properties of the polymer and the thermal stability. The mixed ion actuation is generating moderate to high strain with easily available low cost dopants like sodium or lithium based DBS salts [61]. These actuators show good mechanical strength and can operate for long time.

The polymers are molecular composites maintaining charge neutrality by containing ions in the polymer backbone and with accompanying " dopant" counter ions. During electrochemical synthesis, as a result of simultaneous oxidation and polymerisation of the pyrrole monomer, the conducting form of the polymer with a delocalized positive charge on the electron system is formed. The counter-ions used as supporting electrolytes in electro-polymerisation should be very soluble in the monomer solution, chemically inert (toward the solvent or electrodes), electrochemically stable at the redox potential of monomer. Therefore, easily oxidisable anions with a lower oxidation potential than the monomer, such as iodide or bromide, decrease the electro polymerisation efficiency or reduce the selectivity for film formation [61]. In the present work DBS based dopant is used to develop the high performance PPy actuator with low cost.

1.3.3.5 Solvent

For efficient electrochemical actuation, a solvent plays a major role as it facilitates the ionic movement. It has been observed the PPy exhibits high strain in case of organic solvents like propylene carbonate (PC), acetonitrile (ACN) and methyl benzoate and ionic liquid based solvents [59]. However, high cost of these materials and faster material degradation of PPy in organic solvents restricts their real time applications. Further these solvents are suitable for certain electrolyte ions, hence only uses for specific applications. Unlike these, the use of an aqueous deposition medium would offer considerably larger selection of supporting electrolyte anions. Although the conductivity and strain are moderate, PPy actuator synthesized with

aqueous solvent shows life operating life and the actuation performances can be further improved by proper tuning of synthesis conditions [59, 60, 62]. In the present work deionized water is used as solvent for fabrication and actuation of PPy actuator.

1.4 Limitations of PPy Actuator

Polypyrrole (PPy) exhibits many promising properties which make it suitable for artificial muscle actuators, however delamination, slow response and creep are the major reported reasons limits its real time application. It has been observed multilayered PPy actuators have been widely used due to its higher mechanical strength and bending strain however delamination is the major challenge in multilayered actuator. Experimental evidences show that, delamination could occur as a result of excess interfacial stress arising from thermal expansion mismatch or strain mismatch during redox reactions [63]. PPy films electropolymerized on a metal-coated surface usually extended onto the uncoated edges of the thin substrate, forming a U-shaped enclosure, might play a pivotal role against delamination [64]. It has been observed, any type of coating on a synthesized PPy film is prone to delamination that initiates from the unenclosed edges, hence bilayered PPy strip actuator and encapsulation on PPy layers may be mechanically vulnerable against delamination. Therefore, simple trilayer configuration actuator is suitable for mechanical bending application.

Another most common limitation is the slow response or low rate of actuation. It is essential to understand the rate of actuation to design and develop a high performance actuator. The rate of actuation depends upon the time required for complete movement of ions from electrolyte to polymer chain during redox reaction upon applying electric potential. It is believed that the ion transfer mechanism in redox reaction is based on diffusion. The distance of ionic movement is directly proportional to the square root of diffusion co-efficient by Fick's law of diffusion. It has been reported that the rate of actuation is lower in case of thick PPy film and low actuation frequency. Further, the diffusion co-efficient is estimated experimentally and evidences show the diffusion co-efficient depends upon the type

of solvent, dopant ions and state of redox reactions [43]. Hence the response of the actuator depends on thickness of the PPy layer and voltage scan rate [65]

Creep in Polypyrrole actuator during the operation is the common cause of failure, which is believed due to material degradation and viscoelastic nature of polymer. It has been noticed that PPy experiences material loss due to higher applied operating voltage, high load and or highly acidic operating environment [66]. Although these issues can be easily overcome by proper tuning of actuation parameters, creep due to viscoelasticity is unavoidable as it is the material property of PPy. PPy exhibits loss of energy under applied load and the current behaviour is influenced by the past hence it is a history dependent phenomenon. For dynamic condition, it is essential to consider the viscoelasticity as under dynamic loading, the modulus of the PPy actuator is varying over time, frequency and amplitude of loading. The details of various models and their uses are discussed in the following section.

1.5. Modelling of Polypyrrole Actuator

A key challenge for the designers of Polypyrrole actuator driven devices is the prediction of the actuation response. Modelling of the PPy actuator not only is useful as a design tool, but also can serve to understand the effects of different physical properties, working environment and applied electric potential on the PPy actuator performance. For real time applications of PPy actuator, it is essential to develop an efficient model to study all possible dynamics of the PPy actuator prior to fabricate the prototype. The modelling of PPy actuator is contributed by electrical, chemical and mechanical parameters, hence various electro-chemo-mechanical model have been developed in recent times.

A diffusive elastic model has been previously developed, that predicts the electrical and mechanical behaviour of a thin film conducting polymer actuated in an electrochemical cell [16]. The success of this model for polypyrrole suggested that actuation is dominated by ion diffusion through an elastic and metallic polymer matrix. In addition, this model highlighted the relationship between strain, charge and time constants pertinent to polypyrrole actuation, which corresponds to the

diffusion time into the polymer and the capacitive charging time of the polymer. This model includes RC transmission line model analogous to trilayer actuator to predict the electrical and chemical parameters effectively.

Then, the admittance transfer function model of polypyrrole has been developed to predict the strain associated with electrolyte over the potential range in which polypyrrole is highly conductive. The admittance is well described by treating the polymer as a volumetric capacitance whose charging rate is limited by the electrolyte resistance and by diffusion within polypyrrole. The admittance of the circuit is analysed in frequency domain [67]. Later this model is extended to estimate the total charge transfer as function of time and position of the actuator; hence predict the strain more accurately.

Including this, various other models have been proposed to estimate the total impedance associated with ion diffusion, double layer capacitance and charge transfer resistance along with the accurate prediction of charge density and electrochemical strain in time and frequency domain for various types of input voltage [68-70]. From all these models, it has been observed that the resistances and capacitances are not constant during the oxidation and reduction of the polymer and they depend on the local charge. This means that the electrical and ionic conductivity and capacitance of the PPy are functions of local charge or voltage. Hence for electrochemical modelling, RC transmission line based diffusive elastic model is suitable for estimating the essential electrical parameters like surface resistance, charge density and conductivity and chemical parameters like ionic conductivity and diffusion co-efficient for wide range of voltage, frequency and electrolytes. In the present work the similar method has been adopted to model the dynamic bending of PPy actuator.

The strain obtained from electrochemical model acts as input to the mechanical model and subsequently associated with mechanical strain and material properties generate bending displacement. There are numerous bending models have been proposed to study the bending performances and dynamics of the actuator. At first, linear elastic bending models have been proposed for quasi-static mode operation in air medium [67, 71-74]. In these predict the bending performances and reported that

the increase of bending displacement with increase in voltage amplitude. However, fails to predict the real time dynamics hence gained attention for further improvement. Later the dynamic bending models have been developed for PPy actuator for various applications like manipulation, propulsion and catheter system [75-80]. The lumped-parameter model is developed and experimentally validated for bending-type polypyrrole (PPy) actuators for use in improving their displacement and force outputs. It has drawn an analogy between the thermal strain and the real strain in the PPy actuators due to the volume change to set up the mathematical model, which is a coupled structural/thermal type model. The finite element method (FEM) is used to solve the model. The effect of propagation of the ion migration into the PPy layers is mimicked with a temperature distribution model. Theoretical and experimental results demonstrate that the model is practical and effective enough in predicting the bending angle and bending moment outputs of the PPy actuators quite well for a range of input voltages, and the PPy layer thicknesses. In these models, constant elastic modulus has taken into consideration and Hamilton's method is used to develop the governing equation of motion. The bending dynamics are estimated from the multimode solution methods and the tip velocity is obtained from frequency response analysis. Though the bending dynamics and vibration can estimate more accurately as compared to quasi-static model, fails to predicts the creep behaviour and nonlinearities associated with the dynamic actuation of PPy. It has been reported creep is one of the major limitations of PPy actuator. Besides PPy is exhibited viscoelasticity, hence the modulus is not constant due to its intrinsic viscous nature which needs to consider in modelling to develop a robust model to predict the accurate position in dynamic condition.

There are various linear and nonlinear viscoelastic dynamic bending modelling has been proposed [75,76,81]. Among popular viscoelastic models such as Maxwell, Kelvin-Voight and Standard linear solid model, most of the models based on Kelvin-Voigt viscoelastic model due to its simple structure and easy calculation. Though the viscoelastic behaviour is history dependent, the Kelvin-Voigt model may not predict the variation in strain, modulus and creep behaviour accurately for over a long operational time. To further improvement, Maxwell – Weiechert

viscoelastic model has been used. The integral form of constitutive equation along with Boltzmann's time superposition principle can predict the viscoelastic behaviour by considering the past history effectively. In recent times the nonlinear viscoelastic dynamic bending modelling of PPy actuator has been developed for geometrically nonlinear structure along with shear deformation principle [81].

Although there are numerous models have been developed for PPy actuator in recent time, all of them are focused on air medium operation. There are very few underwater bending model has been proposed however a comprehensive underwater bending model is still a challenge. PPy actuators based biorobotic fins that are designed to create and control forces like the pectoral fin of the bluegill sunfish. For this application, trilayer bending actuators were used successfully to reproduce the cupping motion of the sunfish pectoral fin by controlling the curvature of the fin's surface. However, the speed of these large polymer films was slow, and must be increased if the fin's shape is to be modulated synchronously with the fin's flapping motion [82, 83]. At earliest, kinematic model PPy based camber foil is developed for use in the propeller blade of an autonomous underwater vehicle. The model is based on bilayer and linear actuator designs. This model predicts the camber angle effectively however effect of hydrodynamic forces is not clear [84]. Underwater swimming robots have been developed by using PPy actuator for estimating the thrust and swimming speed by using linear hydrodynamic loading function. However various hydrodynamic bending and propulsion models have been proposed, the nonlinear effect due to underwater environment is still not clear. [84-87]. In the present work, a comprehensive underwater visco-electro-mechanical model for PPy actuator is developed to predict the real time underwater performances.

1.6 Applications

Promising characteristic properties of the PPy actuator like; low operating voltage, large bending deformation, ease of miniaturization, and light weight, distinguishes them from the other class of active actuators. The low actuation potentials can be easily implemented by simple control circuits and well suited to battery-operated devices. As a

polymer, PPy can be easily designed into various shapes; their properties can be tailored to a specific application by following different manufacturing process. The most attractive feature of PPy is their ability to mimic the biological muscles with large strain, stress and geometrical deformation, and inherent vibration damping. The use of PPy actuators could eliminate the need for gears, bearings, and other components that complicate the construction of micro-robots and other similar devices, which reduce the cost and the weight.

In last two decades, PPy actuator based robots and robotics systems have been used various sectors like medical, industry, aerospace, marine and defence [15, 33, 35, 82, 84-86]. Because of the similarity with artificial muscles, PPy actuator based biomimetic miniaturized robots are attracting researchers particularly for defense and medical application. While the shape and size plays major role in miniaturized robots, PPy actuator is the potential candidate which can replaces the present conventional actuator technologies to develop efficient miniaturize robotic system. It has been observed PPy based robots and robotics systems have been used for various applications like locomotion, planning and manipulations. As the nature and biological systems are the most efficient systems, bio-inspired robotic system has gained attention and recently various biomimetic robot such as insect inspired flying robots, humanoids robot, soft robots have been developed for defence, security and industrial applications [88-89].

Polypyrrole behaves as artificial muscle and exhibited biocompatibility, hence suitable for biomedical applications. The biomedical applications could be further divided into two categories, those where PPy as an anticorrosion coating applied on metallic implants [90,50] and those where PPy films acting as a conducting substrate to deliver electrical stimuli to cells to promote their proliferation or differentiation rate. It has been found that PPy can be used for human primary osteoblasts which in good agreement with the observations reported on human neural stem cells [91]. The better biocompatibility was ascribed to the higher affinity between the cells and the smooth surface of PPy. Later the design has been improved with multilayer strip actuator on opposing sides of the catheter in order to achieve bidirectional bending or circular motion is demonstrated [92].

1.6.1 Application of PPy actuator in Underwater Medium

In recent times, there are considerable research has been carried out in design and developing underwater propellers and propulsion system for autonomous underwater vehicles (AUV). AUV technologies have been discussed, where mature methods of swimming locomotion based on principles of steady state hydrodynamics have already developed and are readily implemented analogous to the biological swimming organism. Biomimetic fish-like propulsion has been developed by using various smart material actuators [93]. However, high manoeuvrability, efficient and quiet propulsion systems for real time application is still a challenge.

The low operating voltage, large bending displacement and high work density makes the PPy suitable for underwater operation. Besides the PPy bimorph actuator can analogues to body or fin undulation of biological fish, makes it suitable for developing bio-inspired fish like efficient propulsion system. At first, Polypyrrole actuator based crab like swimming robot is developed for various types of motion however it could not operate other than propylene carbonate solution [83]. Then the PPy based camber foil has been developed to use in propeller blade to effectively change the camber angle [84]. Although few PPy actuator based underwater robots have been developed, high fabrication cost, slow response, low life and efficiency of PPy actuator restrict their use in real time applications. The present work is focused on developing a low cost and efficient PPy actuator based swimming robot for real time underwater applications.

1.7 Motivation of the Present Work

Natural muscles are highly evolved material systems that enable the production of large deformations by repetitive molecular motions. There is currently no widely used technology to replace natural muscle or developing synthetic muscles, which is a strong motivation for the proposed research work.

Till date, Polypyrrole proved to be research-worthy and with tremendous potential in biomimetic systems and robotics application. A key advantage is that it requires very low actuating voltage of around 1.5 V - 3 V, while the widely used

PZT actuator normally operates around 200 V – 500 V. This eliminates the extra mass and cost associated with the power electronics which makes the PPy actuator based system compact and light weight. Again, PZT actuators are manufactured with relatively small dimension due to high brittleness hence may lead to failure under fatigue loading. While IPMC exhibits low bending displacement and strain to the applied voltage, Magnetostrictive materials undergo huge hysteresis loss and difficult to fabricate in actuator form. However, the large bending displacement at relatively low voltages (1.2 V – 2 V), high work density makes PPy actuator suitable for underwater operation over other frequently used smart materials.

Even though, there are very less commercial applications of Polypyrrole as actuator till date. One reason could be that, the technology is still new and the working mechanism and its applications were not well explored; another reason is that the expensive fabrication cost due to the expensive experimental setup, organic solvents and ionic liquid based dopant salts and Platinum (Pt) or gold (Au) conductive coating by sputter coating technique. Considering the range of applications of these polymers, have great future potential to be used in defence, aerospace, robotics and other research applications, but are limited due to the high manufacturing cost. This motivates to use simple cost effective fabrication setup in room temperature, water as solvent, easily available DBS based low cost salts and vacuum coating technique for conductive coating with enhanced performances shown research potential for PPy actuator. Hence the low cost high performance PPy actuator to be used as an artificial muscle actuator particularly in real time biomimetic robots and other artificial muscle applications.

Several studies have been carried out to find out the major limitation of the PPy actuator are slow response and the creep effect which restrict the real time applications of PPy actuator. Further, it has been observed the actuation performances of the PPy actuators are greatly influenced by the working environment. Hence the detailed research on effect of viscoelasticity and hydrodynamic loading on PPy actuator helps to develop a real time underwater actuator which will be suitable for various underwater applications like exploration, pollution detection, scanning and surveillance etc.

This motivates to develop a simple but robust empirical electro-visco-mechanical hydrodynamic underwater actuation model for PPy actuator. As the viscoelasticity is time-history dependent phenomenon, Weichert viscoelastic model along with Boltzmann's superposition principle can be used to predict the accurate dynamic bending responses of PPy actuator with respect to amplitude and frequency of input voltage. Literature shows very few mathematical models on underwater operation of PPy actuator have been proposed, most of them are based on linear modelling. However, a linear dynamic model is not enough to predict the underwater dynamics of the PPy actuator because of its high flexibility due to low thickness and viscous damping of fluid. Further, it has been observed that a little research has been carried out to find out the nonlinear vibration responses viscoelastic PPy actuator in quiescent viscous fluid domain.

Though development of a comprehensive model is still going on, factors such as hydrodynamic responses, viscoelastic effect and nonlinearities have received less attention in the previous work. This motivates the development of both linear and nonlinear hydrodynamic model that is capable of better describing the behaviour of Polypyrrole during underwater operation. The precise prediction of stable and unstable zone of performance responses for an applied electric potential is important for any miniaturize system utilizing PPy actuator. The vibration in the PPy actuator causes due to both structural damping and fluid damping which plays the major role for steady state operation. Hence a comprehensive model is essential to predict all possible dynamics precisely, helps to develop the real time underwater actuator and study the bending and hydrodynamic performances like thrust, speed and efficiency for a wide range of input voltage, frequencies and working medium.

Smart materials are nowadays utilized successfully in robotics for their flexibility, light weight, biocompatibility and low driving power with efficient locomotion. Undulatory motion mechanism is one such mechanism which is followed by most of the swimming organism, hence over few years various smart materials such as shape memory alloy (SMA), electroactive polymers (EAPs) and piezoelectric materials are used for developing undulatory robots. However, such robotic systems are not yet used for real time application due to high cost and low life cycle. This motivates to

develop an efficient undulatory robot by using a low cost high performance PPy actuator which can be used for long operation hours for various underwater applications like exploration, scanning and surveillance.

1.8 Objectives of the Present Work

The focused objectives of the present research work are outlined below along with the specific contribution to the field of polypyrrole actuator. The main objectives are stated below.

- Fabrication and characterization of Polypyrrole (PPy) with low cost fabrication setup.
- Investigation and calculation of viscoelastic dynamic modulus and damping of PPy actuator under electric potential.
- Performance quantification of PPy actuator in underwater environment under DC and AC electric potential.
- Analyze the underwater hydrodynamic performances by developing a transform form of equation for output bending displacement with input electric potential.
- Study and analyze the linear and nonlinear vibration responses numerically and experimentally for underwater operation of viscoelastic PPy actuator.
- Develop an underwater undulatory robotic mechanism using the fabricated PPy and study the feasibility for underwater applications of PPy actuator based robots.

1.9 Organization of the Thesis

The thesis consists of seven chapters, and is organized as follows:

First chapter deals with a brief introduction, actuation mechanism, synthesis and applications of Polypyrrole (PPy) and PPy actuator followed by literature review. Motivations of the present work, objectives and thesis organization are outlined in this chapter. The details of fabrication procedure, thermal, electrical and mechanical characterization of a PPy actuator are discussed in chapter two. The underwater bending characterization and the hydrodynamic performances of PPy actuator are

studied and analyzed in chapter three. In chapter four, a simple robust mathematical model is developed using multimode approximation of a fixed-free Euler-Bernoulli beam and the governing equation of motion of the actuator has been derived by using the extended Hamilton's principle incorporating viscoelastic dynamic modulus to predict the underwater bending displacement and hydrodynamic performances such as thrust in terms of input voltage and time. Including these, the linear vibration responses, natural frequencies and damping ratio are also estimated and compared with the experimental results. In continuation, the effect of nonlinear hydrodynamic damping and fluid flow behaviour at the edges of the PPy actuator on the performances and hydrodynamic loading behaviour are studied in chapter five. The theoretical results have also been experimentally validated. Chapter six deals with an application of PPy actuator in underwater swimming robot mechanism by developing a tadpole like robot and analysed its motion during fish tail like movement of the PPy actuator.

Finally, chapter seven provides the summary of the contributions of the thesis and scope for future work.

2

Fabrication and Characterization of Gold - Polypyrrole Actuator

2.1 Introduction

Polypyrrole (PPy), a Conducting polymer has been recently used as actuator in various applications as sensor and actuator. PPy exhibits promising properties like lightweight, flexibility, metal like conductivity and generate high strain with low driving voltage. In order to develop an effective actuator for range of applications, particularly in underwater or fluid medium, a key factor is the synthesis and fabrication process of PPy which in turn determines its performances and life time.

Various methods, materials and technologies have been adopted to synthesize and fabricate Polypyrrole based actuators with superior performance are found to be costly because of expensive and complex tetrabutyl ammonium (TBA) and ionic liquids (IL) based doping salts, organic solvents, low temperature fabrication setup, precious metal like Platinum (Pt) for electrode and conductive coating by sputtering technique etc. Further, slow response, low life cycle and creep are the major disadvantages that limit its commercial applications. However, most of the recently developed Polypyrrole actuator focused in air medium operation, while limited success has been achieved for underwater applications as compared to other leading EAP based actuators [6,15]. Therefore, modifying the synthesis and fabrication procedures may enhance the performance of Polypyrrole actuator with reduced cost makes it suitable for real time applications can be extended its operation in underwater medium as well.

In this chapter the proposed research objective is to develop a cost-effective high performance PPy actuator suitable for efficient underwater operations. The particular

works have been discussed step by step with schematic diagram and flow chart format. The objectives of the present chapter as follows:

- Fabrication of Polypyrrole (PPy) actuator where gold (Au) acts as the conductive coating material.
- Topographical analysis of properties of the developed Au-PPy actuator
- Comparative study on various properties of the present Au-PPy with the recently developed actuators.

For the fabrication of PPy actuator, electro-chemical polymerization and deposition method is followed. Further, topographical characterizations have been carried out by microscopic and morphological analysis, X-ray diffraction (XRD) analysis, thermo-gravimetric analysis (TGA), differential scanning calorimetry (DSC) tests and field transition infrared (FTIR) analysis is done to study the structural properties of PPy actuator. The electro-chemical parameters were estimated by using cyclic Voltammetry (CV) and electrochemical impedance spectroscopy (EIS) analysis followed by stability analysis of the present actuator estimates the strain and cycle life of the actuator. The details of the fabrication, characterization process with experimental setup and materials used are discussed in the following section.

2.2 Fabrication of Polypyrrole Actuator

State-of-the-art studies show that several fabrication techniques like chemical deposition, electrochemical deposition, vapour deposition and solution casting method are available to synthesize and fabricate Au-PPy actuator. However, electro-chemical polymerization and deposition technique is mostly acceptable method for fabricating PPy actuator as it's the most controllable and tuneable method over the others.

In electrochemical polymerization, layer by layer deposition technique can be used so the process can monitored and tuned the process parameters at each layer of deposition to enhance the performance unlike the continuous deposition electrochemical method [49]. Hence, in this work layer by layer electrochemical deposition method is used for fabricating the PPy actuator. The flow chart of the

fabrication process is shown in Fig.2.1 and the details of various steps starting from the materials are described below.

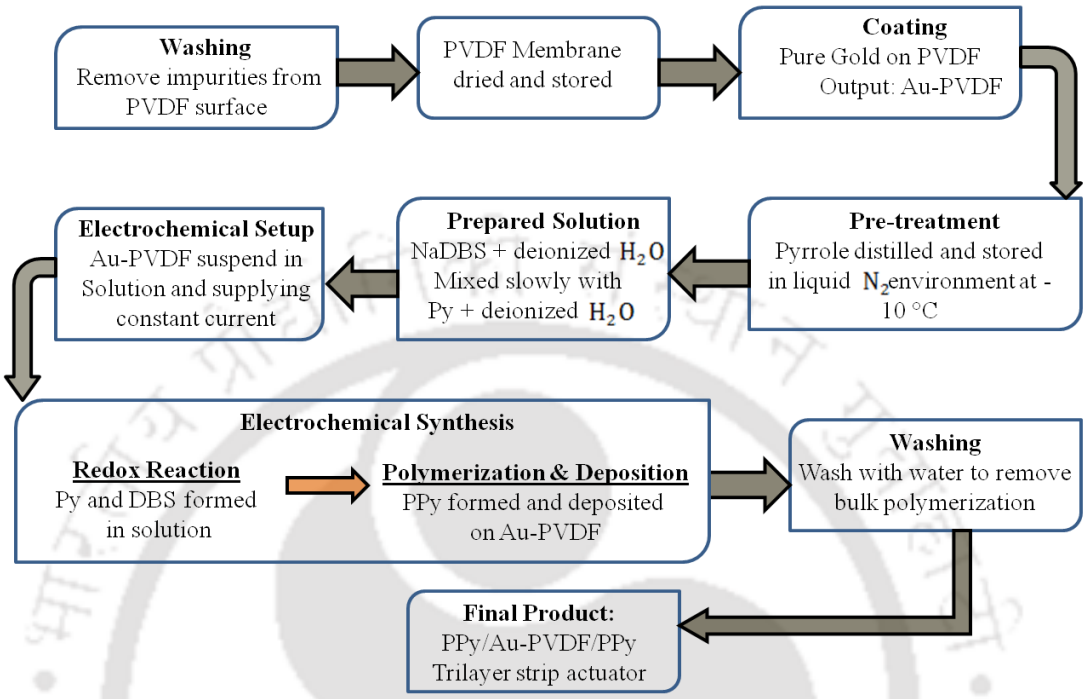

Figure.2.1 Schematic diagram of Flow chart of fabrication process

Material Required: Monomer: Pyrrole (Py) (98% pure), **Doping salt:** Sodium dodecylbenzenesulfonic acid (NaDBS) reagent grade, **Solvent:** MilliQ water, **SPE:** commercially available PVDF membrane (110 μm thickness). All the materials are purchased from **Sigma-Aldrich**. Py was vacuum distilled and stored in cool and dark place prior to use; other chemicals were used as received. Pure Gold (Au) (99.9% purity) purchased from **Tanishq, India** for making conductive coating on PVDF membrane. The flowchart for the fabrication process is given in Fig. 2.1 and the step-by-step procedure is described below.

Step 1: Pre-treatment of monomer and Surface preparation for coating

First cut $60mm \times 15mm$ of rectangular size PVDF membrane from the roll and placed in a cleaned glass plate. Both sides of the membrane are washed thoroughly in deionized water, dried at room temperature and stored in clean glass box for 48 h prior to the electrochemical synthesis.

Pyrrole (Py), the monomer (C_4H_5N) is a colourless volatile liquid that darkens readily upon exposure to air. Prior to the experiment, the pyrrole double distilled and stored in cool, dark and liquid Nitrogen (N_2) environment with nearly -10° C. The equipment were used in this step are shown in Fig.2.2.

Figure 2.2 Equipments used in fabrication process (a) Vacuum double distillation setup (b) Vacuum coating unit (c) Magnetic stirrer (d) Electrochemical setup

Step 2: Conductive Coating

The preliminary process of fabrication starts with making of the conductive coating on PVDF membrane, act as working electrode and on which Polypyrrole (PPy) will be deposited during electrochemical synthesis. This coating is an essential process as it diminishes the voltage drop across the length of PVDF and ensures uniform deposition of polymer during synthesis. The conductive coating material properties had great impact on the stability of the deposited thin film and rate of the actuation as well. While various conductive materials such as Platinum, Gold, Gold/Palladium

alloy, Silver and Copper has been used frequently as coating material, pure gold provides good conductivity and efficient actuation in good price. For coating, sputter coating technique has been used frequently, where expensive sputter target(Platinum and Gold/Palladium) and non-uniform coating in large surfaces are the major disadvantages. Therefore vacuum coating techniques is followed, that reduce the fabrication cost and developed pure gold based high conductivity coating on PVDF surface. In comparison with low cost conductive material such as Silver and Copper, Gold is most suitable for PPy actuator as both Ag and Cu particles interact with PPy films involving a strong complex formation affecting its electrochemical behaviour. Further, Gold coating is much less reactive, highly porous and exhibit higher contact resistance than copper and silver which makes it suitable to maintain the uniform conductivity, long term conductor with electrical contacts and allows faster ion transfer without forming tarnishes in low operating voltage.

The dried PVDF membrane fixed in the work plate and 0.6 g of small pieces of pure Au kept in tungsten filament inside the vacuum chamber of vacuum coating unit (**Vacuum Technologies Pvt. Ltd, Bangalore**) and closed tightly. Then starts the water flow and run the vacuum pump to achieve the required pressure inside the chamber. When the pressure reached up to 10^6 bar, set the deposition thickness at 5000 A° and slowly apply the voltage. It has been observed that the deposition starts on 50 mV with 30 mA current and maintain the same upto the deposition thickness reached at 5000 A°. The final output obtained from this step is gold coated PVDF membrane (Au-PVDF).

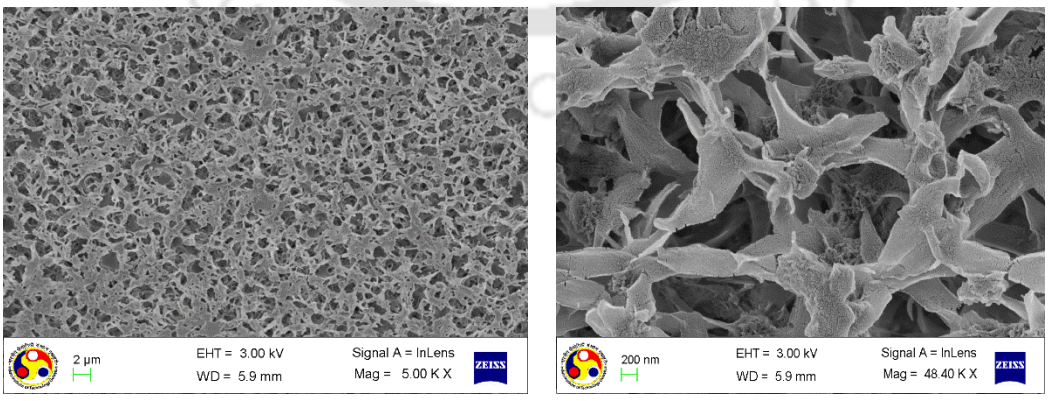

Figure 2.3 Microstructure of PVDF after Gold Coating

The deposition thickness is monitored by the scale given in the top panel. For avoiding the finger prints in the PVDF surface, the membrane should not be hold with bare hands. The depositing voltage and current should maintain properly for avoiding material loss due to melting as well as damaging of the PVDF membrane. From the microstructure analysis shown in Fig.2.3, it has been observed that the deposition is uniform with pore size of Au-PVDF membrane is 0.43 μm approximately which is nearly same as the PVDF (0.45 μm) before deposition.

Step 3: Electrochemical Setup

For electrochemical synthesis, the CHI 760D (**CH Instruments Inc**.) three electrode electrochemical setup (**CIF, IIT Guwahati**) is used as shown in Fig. 2.4. The Au-PVDF membrane suspended vertically on a three electrode electrochemical cell,

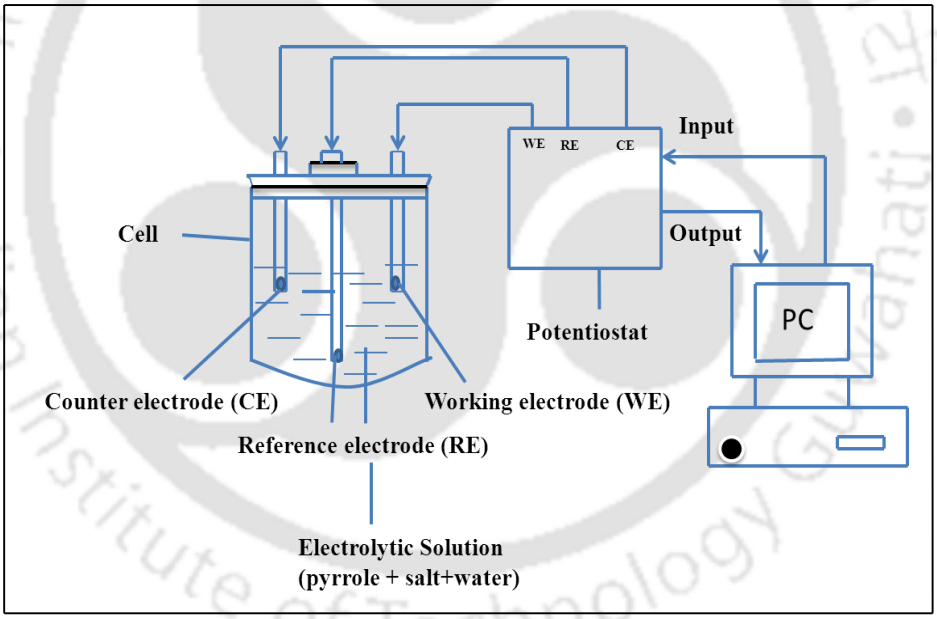

Figure 2.4 Schematic diagram for experimental setup of electrochemical synthesis

which acts as the working electrode on which Polypyrrole (PPy) get deposited while glassy carbon is used as counter electrode where Ag/AgCl is used as reference electrode. The other ends of the electrodes are connected to the corresponding ports in Potentiastat/Galvanostat **(Gamry 3000 series, Gamry Inc.)** that connects the PC and power source. The electrochemical solution: aqueous solution of 0.2M of NaDBS (4.2 g) and 0.2M of Pyrrole (0.78 ml) in 60 ml of MiliQ water prepared separately. The molar concentration of monomer and dopant maintained at 1: 1. The complete

synthesis process carried out at room temperature i.e $22℃ - 30℃$. Unlike the use of expensive salt and solvents, higher concentration of pyrrole (Py) monomer and NaDBS in deionised water is used here to develop the Au-PPy actuator.

Step 4: Eletro-chemical Polymerization and Deposition

A constant current density of $0.15\, mA/cm^2$ is applied for $3\, h$ and during the deposition the working and counter electrode potential was monitored carefully. After $3\, h$, the working electrode is taken out from the solution and washed with distilled water for several times and reused in freshly prepared solution maintaining the same parameters for further synthesis. Unlike continuous depositions for $15\, h$, the process is continued until five individual layer depositions are made.

Step 5: Post – Synthesis and Final Product

The PPy deposited Au-PVDF membrane is taken out from the solution, washed several times with distilled water removing the bulk polymerization of PPy. In the following, the final product output is the PPy-Au-PVDF-PPy sheet dried at room temperature for $48\, h$, prior to characterization of the actuator. The step by step fabrication process and output of each step is shown below in Table 2.1.

Table 2.1 Step by step process for fabrication of Au-PPy actuator

Steps	Processes	Details	Output
S -1	Sizing Solid Polymer Electrolyte (SPE)	PVDF membrane of $60mm \times 15mm$ cut from the roll, washed with de-ionized water to removing impurities and dried.	PVDF as SPE 
	Pre - Treatment	Pyrrole double distilled and stored in cool, dark and N_2 environment	

S - 2	Conductive Coating on PVDF	Pure gold coated on both sides of PVDF by vacuum coating tech.	Au – PVDF 
S - 3	Preparation: Electro -chemical Solution and setup	Separately prepared aqueous solution of Py slowly mixes into the aq.solution of NaDBS in a 3-electrode cell. Au-PVDF, vertically suspended into solution and other end connected to potentiostat with PC.	Electrochemical setup 
S – 4	Electrochemical reaction and Polymerization	Redox Reactions Py – e- ---→ Py+ NaDBS ---- Na+ + DBS-	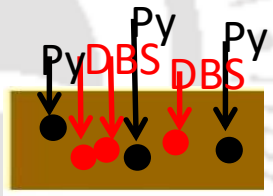
	Deposition	The pyrrole cation and DBS anion continuously deposited on Au-PVDF for nearly 3 h then repeat it 4 times in separately prepared fresh solution.	 1st Layer PPy deposition
S - 5	Post-Synthesis Treatment and Final product	Washed thoroughly with distilled water and obtained Gold – Polypyrrole (Au-PPy) trilayer actuator	 PPy-Au/PVDF-PPy

2.3. Characterization of the Gold - Polypyrrole Actuator

In this section, the topological, electrical and mechanical characterizations of PPy/Au-PVDF/PPy trilayer actuator are discussed. The topological characterization involves the measurement of conductivity, deposition thickness, EDX analysis, XRD analysis, FTIR analysis of surface morphology. The thermal characterization includes the DSC and TGA analysis while in mechanical characterization the DTMA analysis, stress – strain analysis and estimation of viscoelastic modulus of Au-PPy actuator in wet condition. The equipment used for characterization and detail of the characterization processes are described in the following section.

2.3.1 Topographical Characterization

In this section the surface morphology of Polypyrrole (PPy) along with the components present in the PPy layers are analysed. The surface morphology, chemical structure and chemical bonds are present in PPy chain is primarily affect the essential properties like conductivity and strain. Various types of topographical characterization techniques followed in the present work are described in the following section.

2.3.1.1 Microstructure Analysis

The morphology of the PPy-DBS synthesized can be analyzed by investigating the microstructure of the PPy surface, ion content in the PPy film, chemical structure of the electrochemically polymerized PPy film, the intensity of the ions and bonds between various elementary particle and diffraction angle. The details of various analysis are discussed below.

The surface morphology of the PPy surfaces and ion contents in the polymerized PPy film along with penetration depth are studied by using ΣIGMA Field Emission

Figure.2.5 Equipment used for microstructure analysis

Scanning Electron Microscope (FESEM) equipped with energy dispersive x-ray (EDX) **(Model: Carl Zeiss NTS GmbH)** analyser. The experimental setup is shown in the Fig.2.5.

The microstructure of Au- PPy film surface obtained from FESEM analysis is shown in Fig 2.6. It is observed that the PPy surface is compact, globular, uniform and smooth as shown in Fig.2.6 (a). The size of the globules is approximately 0.3 μm and uniformly present in the surface as shown in Fig. 2.6 (b)**.** There is no significant large bumps and discontinuity present in the surface unlike the PPy film synthesized with propylene carbonate.

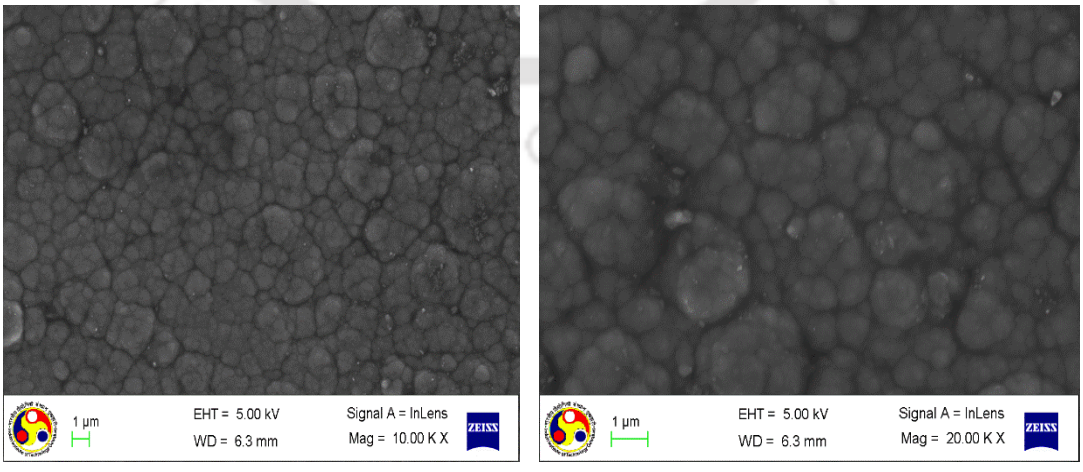

(a) Microstructure of PPy-DBS surface (b) High resolution Microstructure of PPy-DBS

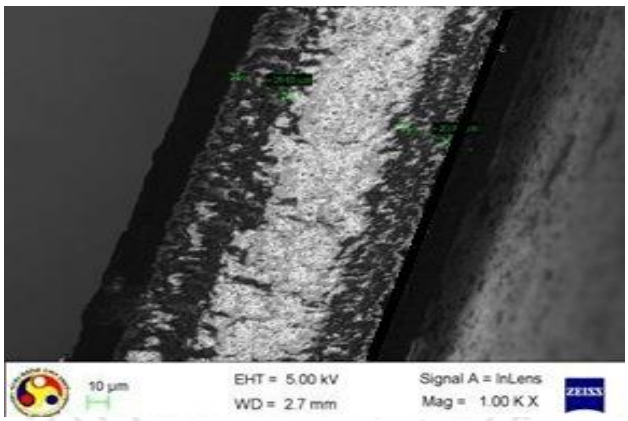

(c) Microstructure of PPyDBS cross section

Figure.2.6 FESEM analysis of Polypyrrole film surface and cross section

The surface is porous and the particles are uniforms distribute which enhances the accessibility for electrolytes and subsequently enhance the actuation performances, conductivity and strain. The cauliflower like surface pattern is similar to the PPy film synthesized with TBA based salt and methyl benzoate solvent at low temperature range($< 0℃$) [94]. It is believed that, higher monomer (Pyrrole) and salt (NaDBS) concentration in water and layer by layer electrochemical deposition produce PPy with improved performances in comparatively at low cost.

The uniform thickness of PPy layer can be clearly visible from cross sectional view of actuator as shown in Fig.2.6 (c). The total thickness of trilayer actuator is approximately 150 μm where each layer of PPy is approximately20 μm. However, the deposition thickness of PPy layer was 23 μm on both sides, PPy layers penetrates into the Au-PVDF membrane by approximately 2-3 μm due to high porosity of Au-PVDF. Due to this penetration, the DBS anions are more close to the PPy chain and hence may enhances the rate of transfer could lead to higher strain.

Subsequently EDX analysis shows the ions content in the PPy surface and cross section as shown in Fig.2.7. It is clearly observed that the surface of PPy film primarily contained carbon (C) and sulphur (S) which is believed to be present due to PPy and DBS respectively. Including this nitrogen (N) and oxygen (O) both are present significantly while sodium (Na) is present in traces as shown in Fig.2.7 (a). While presence of Nitrogen and oxygen is due to PPy and DBS, sodium (Na) ions are trapped during polymerization because it cannot move easily due to its bulky size. Although

the actuation here dominates by DBS^- due to its small size, small amount of Na^+ might also move during actuation.

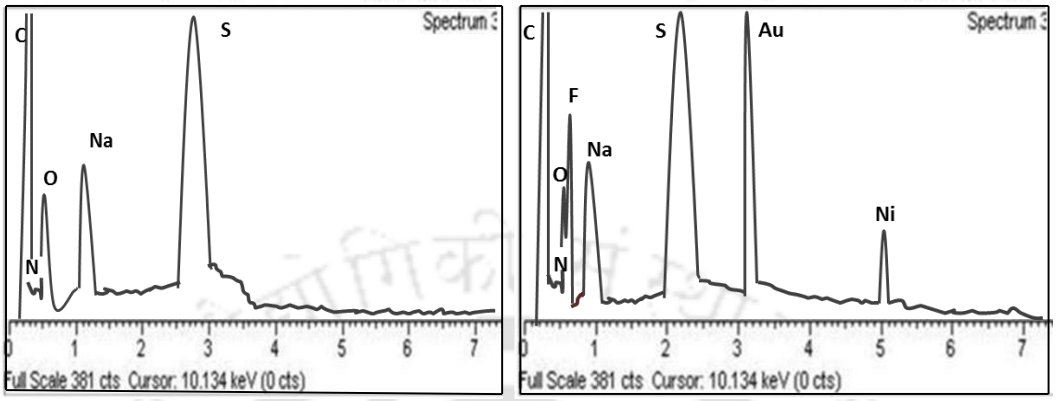

(a) EDX analysis of PPy-DBS surface (b) EDX analysis of PPy-DBS cross section

Figure.2.7 EDX analysis of PPy-DBS surface and cross section

This is one of the primary reasons that the higher concentration of NaDBS generates high strain due to movement of both dominating anions and small amount of cations.

The cross section of the actuator contains same elements present in surface and including this Fluorine (F), Gold (Au) and Nickel (Ni) are also present because of Au-PVDF film. It is also observed that the entire surface elements are present in the cross section confirms the penetration of PPy layer into the PVDF as discussed in microstructure analysis. The nature of EDX analysis curve is similar and has good agreement with the earlier published results [94].

2.3.1.2. *FTIR and X-Ray Diffraction Analysis*

The chemical structure of the polymerized PPy film can be studied by using X-Ray Diffraction (XRD) Analysis while the presence of various functional groups in the raw materials is studied by using Fourier transform infra-red spectroscopy (FTIR). These studies helps to study the nature of PPy film and bonds present in PPy which later helps predict the conductivity of PPy film.

The experimental setups are used for XRD **(Model: Seifert XRD 3003 PTS)** analysis and FTIR **(Model No.: IRAffinity-1; Make: M/s Shimadzu, Japan)** analysis shown below in Fig.2.8.

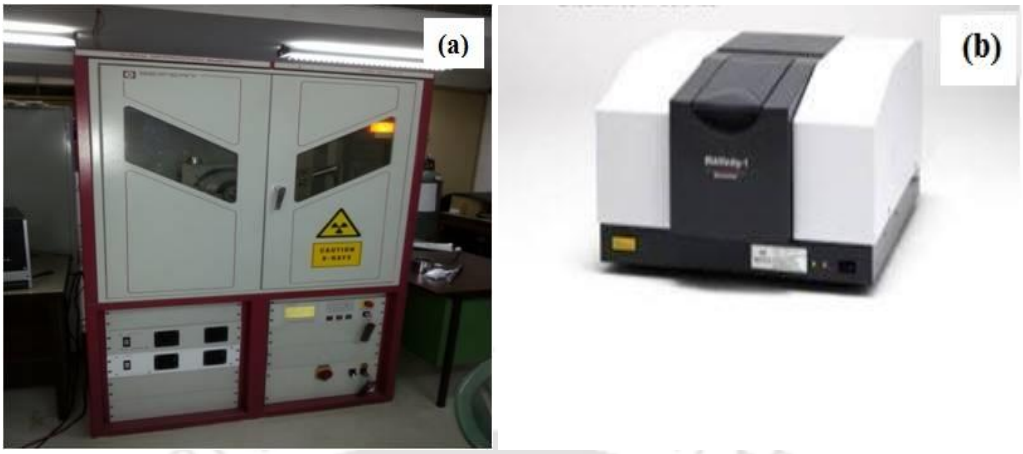

Figure.2.8 Equipments used for (a) XRD and (b) FTIR analysis

X-ray diffraction curve of PPy film is show in Fig.2.9. Three major characteristics diffraction peaks of Au-PPy are observed at $38.15°, 44.3°, and\ 64.45°$ which are corresponding to the crystal faces of $(111), (200), and\ (220)$. The broad peak is characterize its amorphous nature due to the scattering from PPy chains at the inter-planar spacing [95-97].

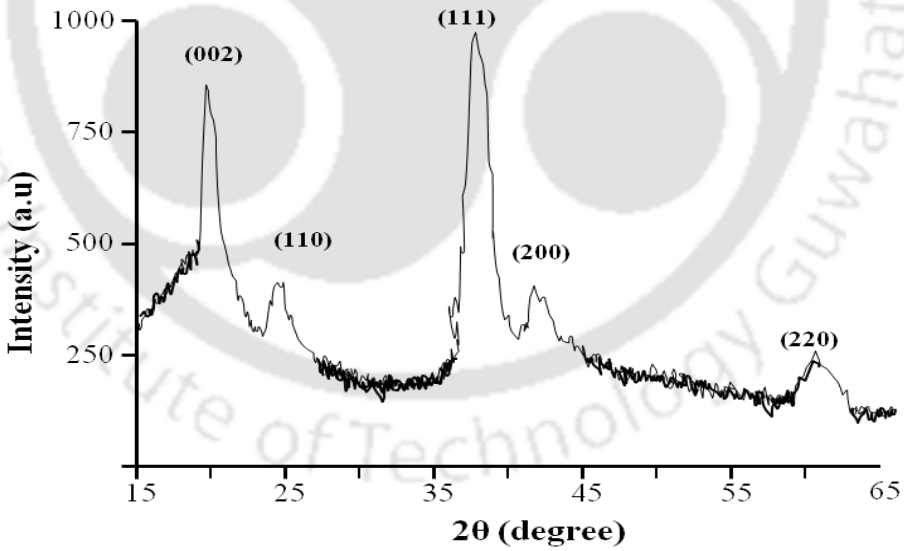

Figure.2.9 XRD analysis of Polypyrrole thin film

In fact, it shows the characteristics of face centred cubic (FCC) structure and validated that Au-PPy exhibited good conductivity property. The characteristics diffraction peak of PPy membrane at $2\theta \approx 24°$ is in good agreement with the previous results [95].

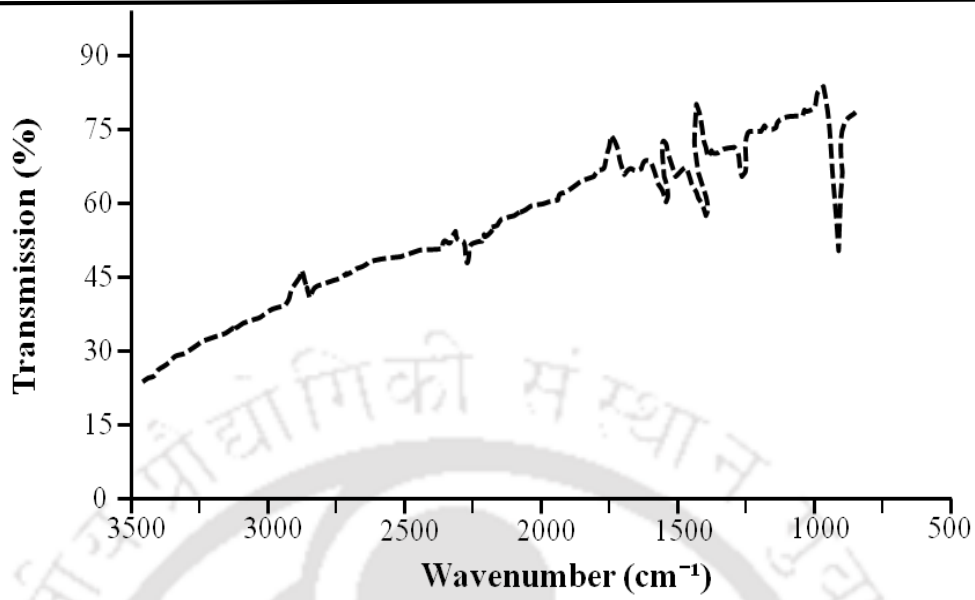

Figure.2.10 FTIR analysis of Polypyrrole thin film

The peaks at 820 cm^{-1} are attributed to C–H. The characteristic peaks at 1558.4 $cm^{-1}$and 1487 cm^{-1}correspond to the C=C stretching, whereas peaks at 1685.7 $cm^{-1}$and 1315.4 cm^{-1}represent C=N and C–N bonds respectively as shown in Fig.2.10. The occurrence of small peaks at 2800 $cm^{-1}$is assigned to be the presence of N–H stretching vibrations. The peaks observed in the present work match well with the results available in the literature [95-97] confirming the formation of Polypyrrole

2.3.2 Thermo-Mechanical Analysis (TMA)

Thermo-mechanical analysis of the actuator is necessary relating to the temperature fluctuation in underwater condition affecting performances and the thermal stability of the actuator.

Thermo-gravimetric analysis (TGA) and Differential Scanning Calorimetric (DSC) analysis are carried out to investigate the thermal behaviours and also the effect of temperature on the PPy performances. TG and DSC measurements are carried out by **NETZSCH STA 449 F3, Jupiter® instrument** as shown in Fig.2.11.

PPy actuator is cut into small pieces to provide a suitable sample size of about 5 – 10 mm. TG and DSC curves are recorded on wet PPy actuator at a heating rate of 10° C/min under Argon atmosphere (60 ml/min) from room temperature (15℃) to 300℃ (TG curves) and 250℃.

Figure.2.11 Photograph of DSC and TGA Equipment

The TGA curve of wet PPy film is shown in Fig. 2.12. The solid line represents the percentage of mass loss where the dashed line represents the first derivative (DTG) curve.

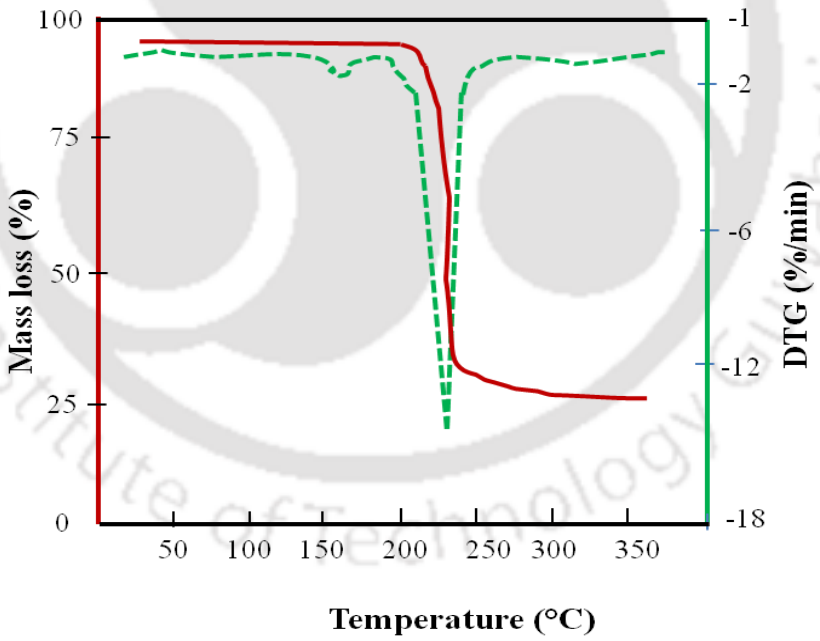

Figure 2.12 TGA Curve of wet Polypyrrole film

Thermal behaviour of PPy-DBS follows the decomposition proceeded in two stages which are correspond removal of DBS anion and rest of structure decomposition, respectively. The removal of DBS anion is an exothermic process. The average peak temperatures of exothermic reaction (removal of DBS anion) is nearly 220℃ . The

mass loss occurs at two stage in the range of 200℃ – 250℃. The thermogravimetric analysis confirms that the PPy-DBS exhibits higher thermal stability, hence this suggested the better performance of the PPy-DBS actuator in underwater medium

Fig. 2.13 shows the DSC thermographs of PPy membrane in wet condition. DSC thermograph for PPy shows a strong endothermic peak near 88ºC as glass transition temperature (T_g), and another peak near 143ºC as crystallization temperature.

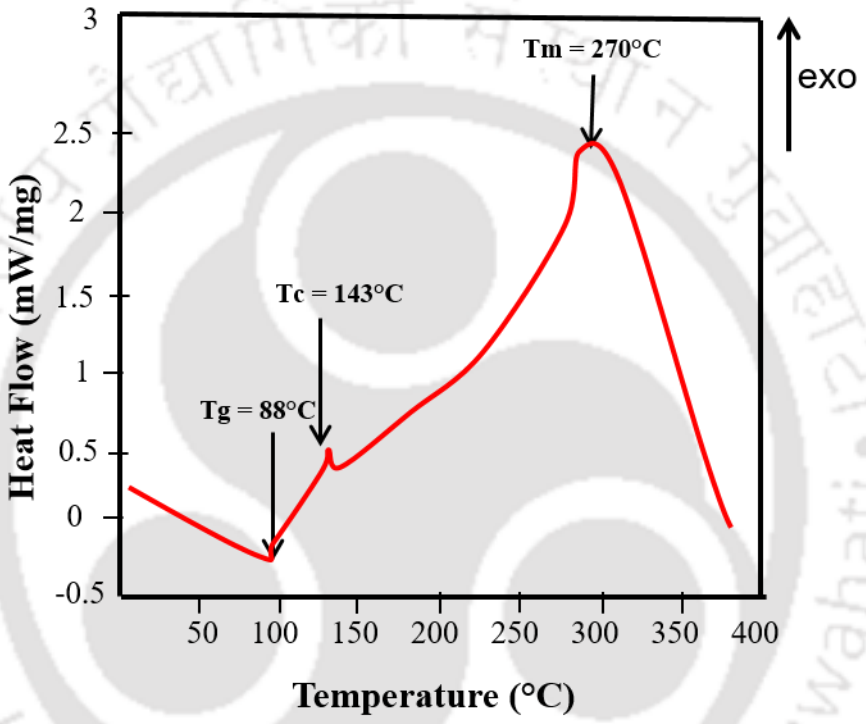

Figure. 2.13 DSC Curve for wet PPy film

Thermal transition above 200℃ may be associated with the thermal degradation of the PPy film. The exothermic peak near 270ºC indicates the melting point of PPy.

2.3.3 Electrical Characterisation

The electrical parameters such as surface resistance of PPy and PVDF, charge transfer resistance and conductivity were determined experimentally. The electrochemical actuation and strain primarily depend upon these electrical parameters.

The electrical conductivity of the material is a measure to their ability to pass electricity. The electrical conductivity is known as a basic requirement for many applications for polypyrrole including actuators. The actuation performance is improved when the polymer has higher conductivity [47, 43] that can be modified by

varying polymerization parameters such as current density, temperature and dopant. The conductivity of the PVDF (γ_{PVDF}) and PPy layer (γ_{PPy}) was measured by the digital multimeter (**45CF Meco Pvt. Ltd.**). The film conductivity is estimated by taking average of all individual conductivity recorded at numerous points on the film.

In present study the conductivity of the PPy film is estimated as $136\ S/cm$, close to the conductivity obtained from TBA based dopants [43]. The electrical conductivity of present actuator is compared with actuator developed with various dopant, solvent and temperature range as shown Fig.2.14.

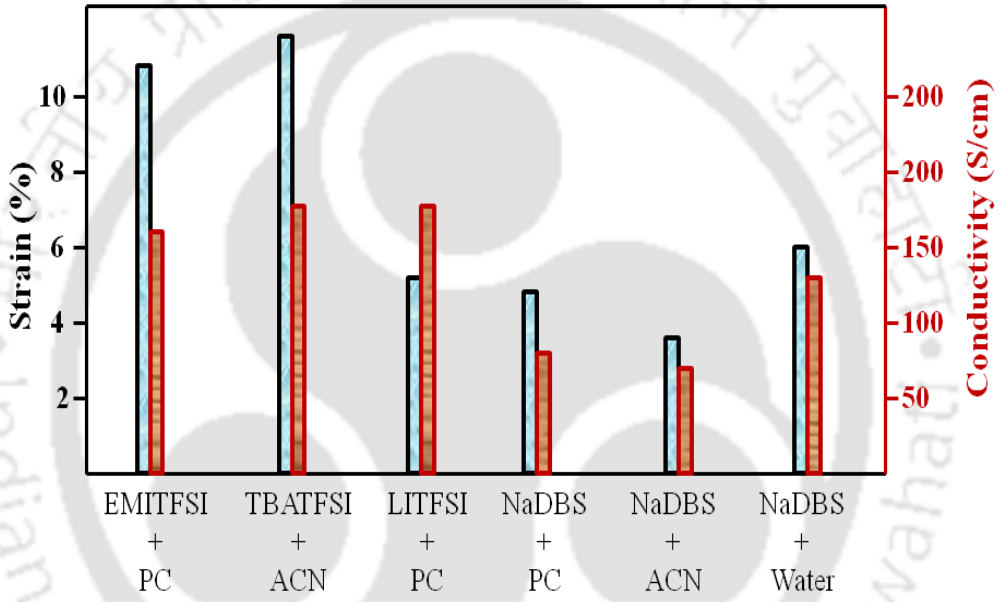

Figure.2.14 Conductivity and strain of PPy actuator with various dopant and solvent

This is observed that the conductivity of the PPy actuator with water as solvent is nearly same with the PPy actuator fabricated by using ionic liquid (IL) and propylene carbonate (PC) or acetonitrile (ACN) as doping agent and solvents [43,47,50]. Then the charge transfer resistance, is estimated using the current passed through the actuator when it is applied with a constant voltage and obtained as $8.4 \times 10^3 \Omega$ (for the actuator with a length of $(L = 35\ mm)$.

The resistance of the gold-coated PVDF layer is first measured in wet condition while immersed in electrolytic solution, where the resistance of PPy is measured by a multimeter. The resistance of individual element of PPy and PVDF layer obtained by using [68] the Eq.2.1

$$R_{PPy} = \frac{2h_{PPy}}{W*\gamma_{PPy}} \text{ and } R_{PVDF} = \frac{1}{W*h_{PVDF}*\gamma_{PVDF}} \quad (2.1)$$

Where γ_{PVDF} and γ_{PPy} is the conductivity of the Au-PVDF and PPy respectively and h_{PPy} is the height of the PPy layer.

2.3.4 Electrochemical Characterization

Electrochemical characterization is an essential for PPy actuator as it involves the study of electrochemistry behind the actuation mechanism and quantifies the electrochemical actuation performance parameters. Here, the electrochemical characterization is carried out through cyclic voltammetry and impedance spectroscopy method to estimate the range of actuation voltage and frequency respectively. Besides, the primary actuation parameters like rate of charge transfer, current density and performance such as electrochemical strain and cycle are also estimated to study and validate the present actuator.

2.3.4.1 Cyclic Voltammetry and Electrochemical Impedance Spectroscopy

For cyclic voltammetry (CV) and electrochemical impedance spectroscopy (EIS) the actuator was vertically dipped in an electrochemical cell containing aqueous NaCl solution. One end of the actuator is fixed and placed between two gold coated electrode plates acts actuator holder and connected to the Data Acquisition system **(NI Instruments Inc.)** and Potentiostat **(Gamry Inc.)** for providing input voltage and works in two electrode mode operation respectively. In two electrode mode operation, one layer of PPy is connected with working electrode while other layer is connected to counter and reference electrode to the potentiostat. For CV experiment the actuator sweeps between $-1V$ to $+1V$ with $50\ mV/s$ scan rate where the EIS experiment was conducted with the same voltage amplitude for a range of frequencies 0.1 to $5Hz$. This experiment is useful to predict and analyze various important electrochemical parameters like charge transfer rate, diffusion co-efficient and strain at various amplitude and frequencies of input voltage. Fig.2.15 shows the CV curve for PPy actuator for various actuation cycles. The cyclic voltagram, from which the oxidation (doping) and reduction (de-doping) potential peaks as well

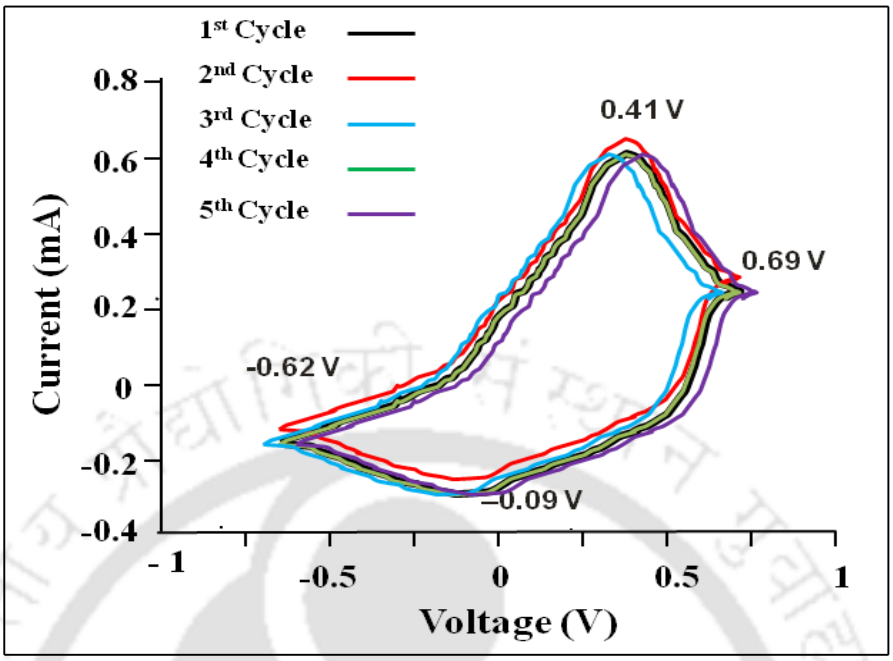

Figure 2.15 Cyclic Voltagram of Polypyrrole-DBS Actuator

as the voltage range for real time application can be identified. The operational voltage should not be less than 1.3 V for fully oxidation and reduction of actuator as oxidation and reduction peaks roughly estimated as $+0.4\,V$ and $-0.08\,V$.

The peak values are shifted according to the voltage range used but the oxidation peak stabilize at 0.60 V even increasing in voltage. The range of redox peak is nearly 0.48 V, hence the minimum voltage required for actuation of PPy-DBS actuator is 0.48 V. But the oxidation curve extends up to $+0.69V$while the reduction curve terminates at $-0.60\,V$. The electrochemical strain increases during oxidation and decreasing during reduction as it depends upon the charge density. The EIS of PPy trilayer actuator is shown in Fig.2.16**,** where the frequency response of the impedance is analysed. On applying a sinusoidal voltage of 1.3 V amplitude and frequency range 10^{-2} to 10^{-4} Hz, the frequency response of magnitude and phase of impedance is measured. The magnitude of impedance abruptly decreases after 10^{2} Hz while the phase and distortion keep increasing. Thus it is found that the PPy actuator can effectively work with a broad bandwidth of 0.01 Hz to 100 Hz.

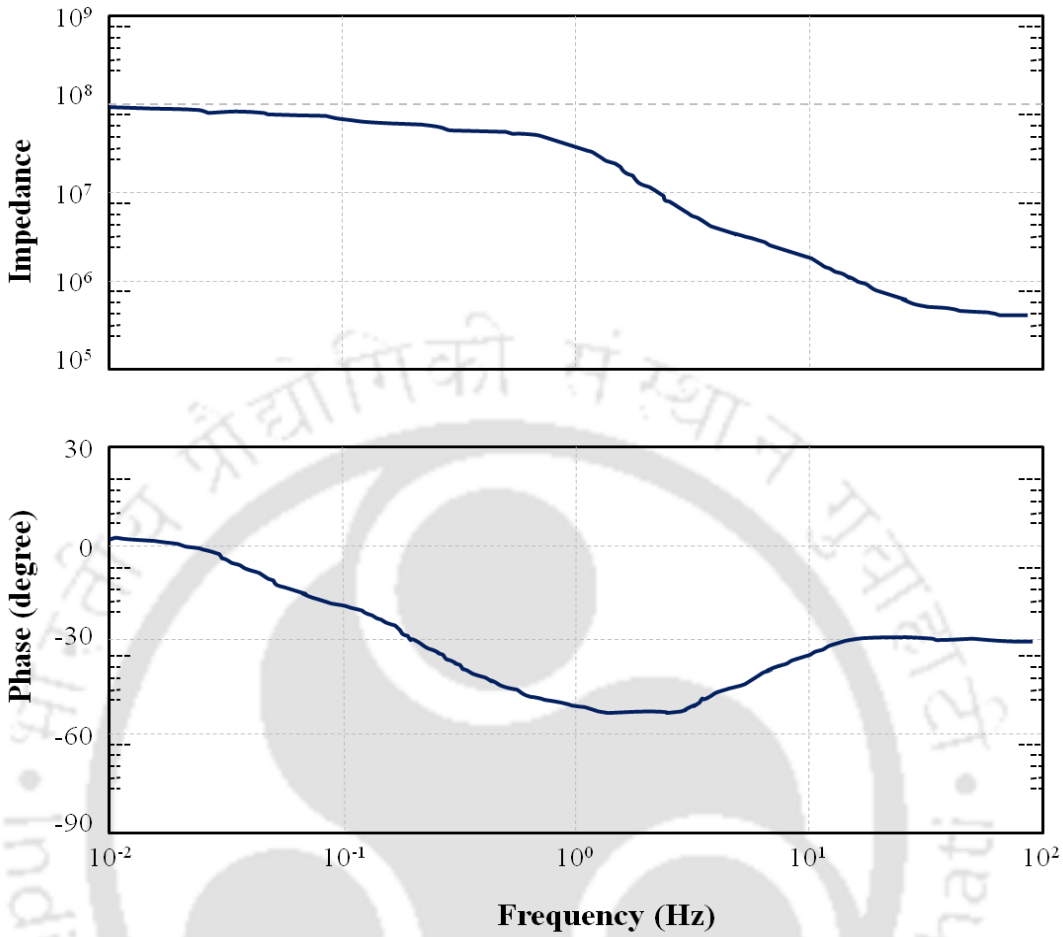

Figure 2.16 The electrochemical impedance spectroscopy of PPy actuator

2.3.4.2 Electrochemical strain and stability

The electrochemical actuation characteristics like strain and stability of the actuator are important properties which primarily enhances the performances of the actuator. The strain obtained from various sweeping cycles is shown in Fig.2.17. It has been observed that the maximum strain is obtained in the first cycle is nearly 6% which is close to the natural muscle however less than the strain obtained from TFSI based salts [31, 33]. At higher strain, stability of the PPy actuator deteriorates in a faster rate as compared to moderate strain as the actuator experience strain hardening and creep. From the results it can be concluded that the strain in PPy actuator is decreasing with increase in cycle numbers. In TFSI doped PPy, the strain decreases from 16% at first cycle to below 5% in just 25 cycles [43] and the rapid decrease in strain leads to degradation of electro activity and failure of the actuator. However, in the present

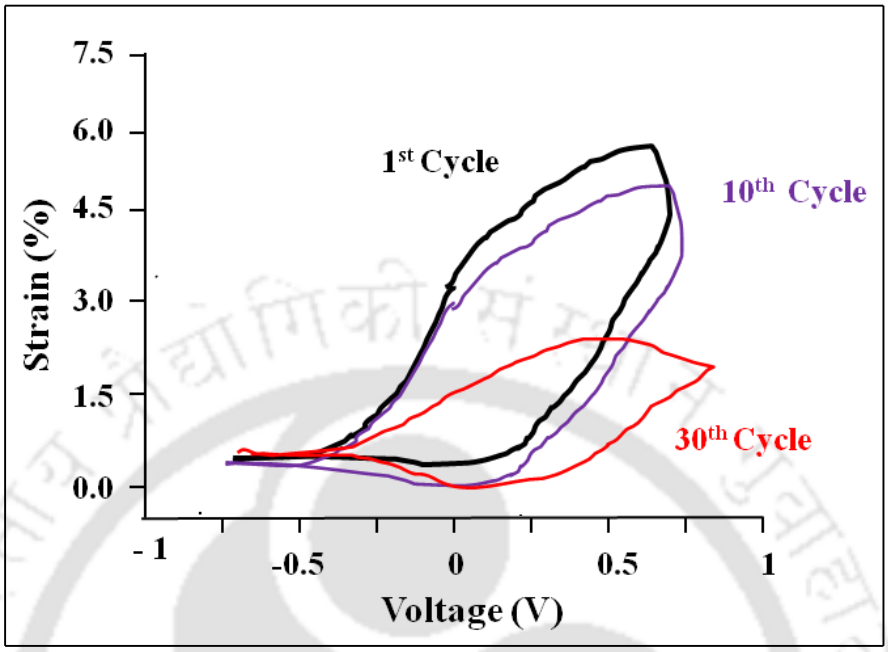

Figure.2.17 Actuation strain of PPy trilayer over actuation cycles

case the rate of decreasing in strain is less as compared to the former one, hence the stability may be increased that makes it suitable for real time application

2.3.5 Mechanical Characterization

Mechanical properties such as elastic modulus and tensile strength of the PPy trilayer actuator in wet condition are estimated. The mechanical properties are obtained from tensile test. Prior to the experiment the actuator was dipped in aqueous NaCl solution for 24 h. Dynamic-mechanical analysis (DMA) of the PPy actuator is carried out in wet condition.

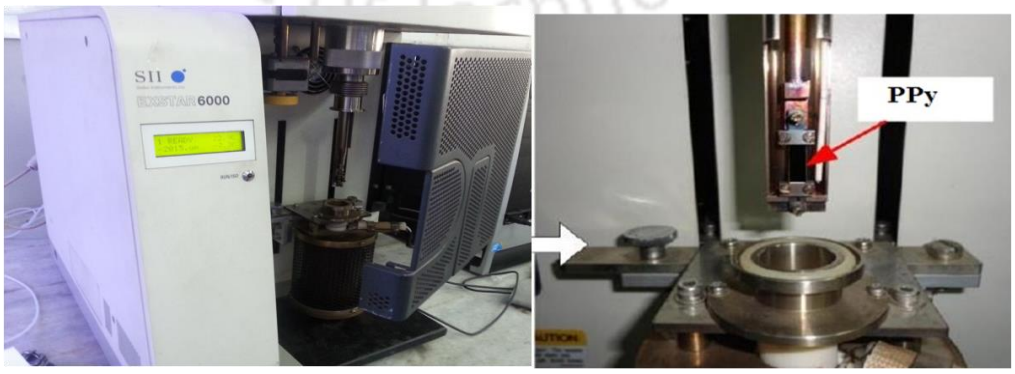

Figure.2.18. Experimental setup for Dynamic Mechanical analysis of PPy actuator

The DMA test is conducted in open environment in tensile mode in an **EXSTAR TMA/SS 6000 instrument (SII Seiko Instruments Inc)**. The experimental setup is shown in Fig.2.18. The frequency of applied load is taken as 0.1 Hz while the heating rate is kept constant at $2°C/min$ for DMA experiment.

The modulus of the PPy actuator is one of the important parameter for analysing the mechanical properties of the actuator. The storage (E') and loss modulus (E'') along with the loss factor ($tan\ \delta$) of the PPy actuator are obtained from the DMA analysis in the temperature domain with steady increase of time. From Fig.2.19 (a) it has been clearly showed that the storage and loss factor varies with temperature.

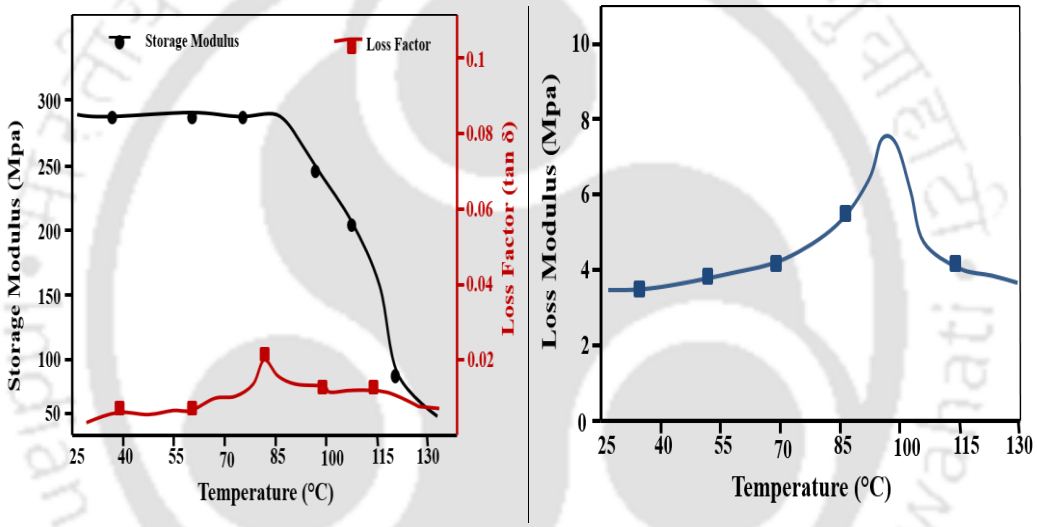

(a) Viscoelastic storage modulus and Loss factor

(b) Viscoelastic loss modulus of PPy actuator

Figure.2.19 Dynamic mechanical analysis of PPy Actuator

The maximum storage modulus is obtained nearly 284 MPa, loss factor is nearly 0.023 while the maximum loss modulus is obtained up to 7 MPa in the temperature range of $25°C - 130°C$ which makes it suitable for underwater operation.

The relatively flat regions in low temperature zone correspond to the glassy state of polymer. The glassy transition starts from the peak (85°C) where the curve initially bend downward. Beyond this point, the modulus decreases rapidly as shown the stiff drop of the curve which results from softening and rubbery form of the PPy. Again the modulus will increase after the crystallization of PPy. As the actuator operates in underwater medium the specific temperature range has been focused here. The glass

transition temperature is found in the range of 85℃ −90℃ which is very close to the value obtained in DSC analysis. The peak maximum of loss modulus corresponds to the beginning of segmental motion of polymer chain, which eventually causes damping in PPy. The loss factor peak represents the longer-range cooperative molecular motion in PPy which is consistent with rubbery flow and permanent deformation due to conjugated PPy structure.

The stress – strain curve is obtained from the tensile test is shown below in Fig.2.20. During relaxation, the actuator losses energy, hence the gap created between the loading and relaxation curve. The area under the curve in the stress strain diagram confirms its viscoelastic property.

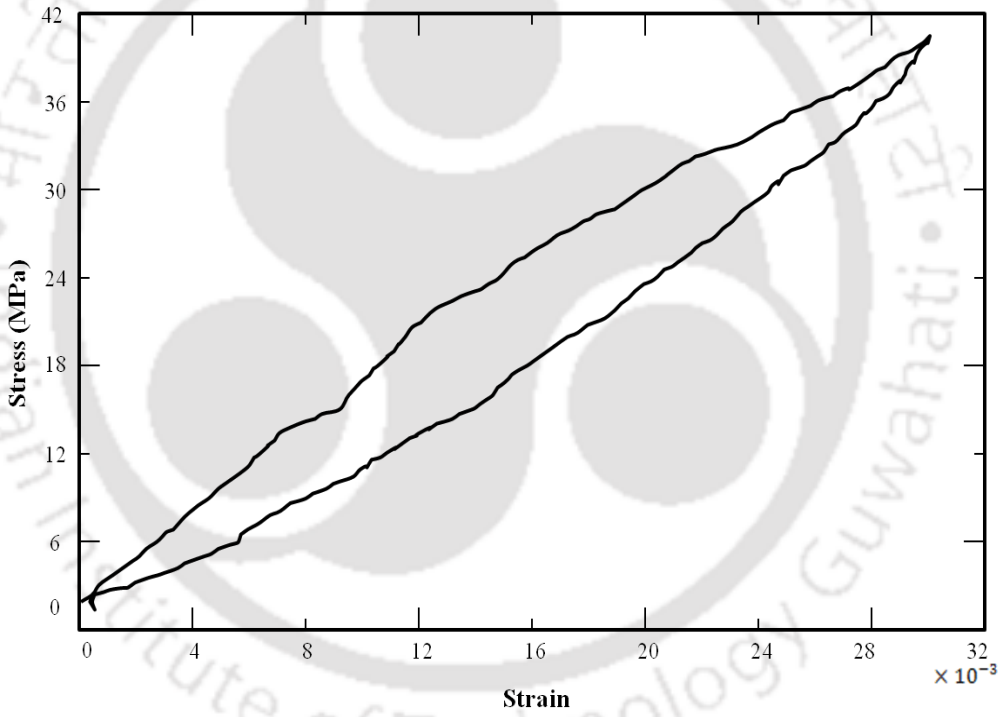

Fig.2.20 Stress-strain Curve for PPy actuator

The tensile strength of wet PPy is estimated nearly to be 32 MPa. The stiffness is reduced significantly upon immersion in the fluid as compared to dry PPy-DBS [98]. Soaking also leads to a 14 % strain and 25 % increase in mass over the first 8 h. The decrease in stiffness suggests that polypyrrole is being plasticized by the solvent, which likely forms hydrogen bonds with the polypyrrole backbone.

Work density is another important property of PPy actuator to quantify the performance. The work density of the PPy actuator for each cycle can be estimated by using the mathematical expression [43] as shown in Eq.2.2

$$W_d = \frac{work\ done\ in\ each\ cycle(J)}{volume\ (m^3)} = \sigma\varepsilon \qquad (2.2)$$

Where σ is the applied stress and ε is the strain generated from actuation. The work density of the present actuator is estimated over a range of stress and it is found that with increasing stress, the work density increases up to the breaking stress point and after that it decreases as shown in Fig.2.21. The breaking stress of the present actuator is near to 9 MPa and the maximum work density occurs at this point as 84 kJ/m^3, is improved as compared to the existing actuators [43].

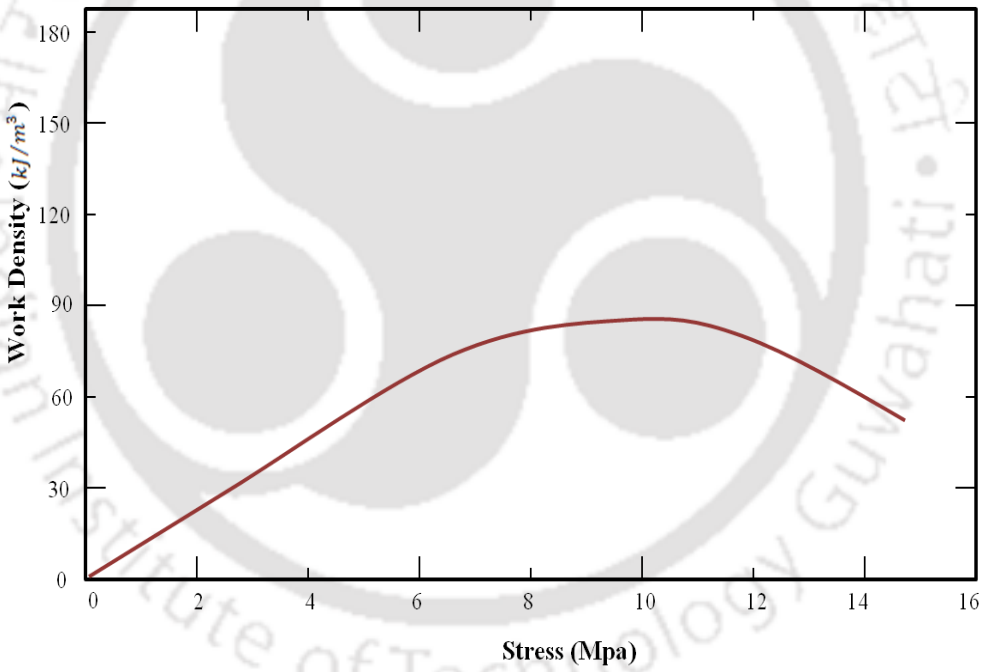

Figure 2.21 The work density of the PPy actuator

The characteristics properties of the present PPy actuator are obtained during experiment are summarized below in Table 2.2.

Table 2.2 Characteristics properties of the fabricated PPy actuator

Parameters	**Experimental Value**
Electrochemical Strain	6%
Actuation Voltage	1.3 V and 1 Hz
Conductivity	136 S/cm
Charge transfer resistance	$8.4 \times 10^3 \Omega$
Melting Point	$270°C$
Electrochemical Stability	$8 - 10\ h$
Viscoelastic Loss Modulus	7 MPa
Viscoelastic storage Modulus	284 MPa
Loss Factor	0.023
Tensile strength	32 MPa
Breaking Stress	9 MPa
Work density	83 kJ/m^3

2.4 Summary

The layer by layer electrochemical decomposition method is followed for synthesis and fabrication of Polypyrrole trilayer actuator for underwater operation. Experimental study is carried out to characterize the electro-chemical, thermal and visco-mechanical of PPy trilayer actuator.

Topographical features are examined by scanning electron microscope suggested that there is uniform deposition of PPy-DBS over the gold coated PVDF film and also confirm adequate bonding between the PPy (Polymer) and PVDF (Electrolyte) layer. Also, SEM images show that PPy layers were penetrated through PVDF membrane up to $2\mu m - 3\ \mu m$. Further, morphological studies of the fabricated PPy show no crack formation in the micro-structure (with 2kX magnification). XRD analysis confirms that deposited PPy-DBS layer is polycrystalline in nature without any unwanted phase formation. In fact, it shows the characteristics of face-centred cubic

(FCC) structure validates that PPy layers have perfect conductivity property. DSC and TGA tests of the developed PPy confirm improved thermal stability to suitable for underwater operation.

The electrical conductivity results of the PPy film shows the conductivity of the PPy film is significantly increased upto $136\ S/cm$. The optimal operating voltage amplitude is 1.3 V and frequency 1 Hz for the PPy actuator is estimated from the CV experiment and EIS analysis. The present actuator shows significantly high electrochemical strain of 6% and improved stability, may be due to the high concentration of monomer and salt.

The modulus of the PPy actuator is estimated from the DMA is 284 MPa while the tensile strength is 32 MPa. The stress strain curve shows the energy loss which confirms the viscoelastic property of the PPy. It has been noticed the modulus is changing over temperature and time. The tensile strength and work density of the PPy actuator is makes it suitable for underwater operations.

3

Hydrodynamic Characterization and Performance Evaluation of Gold-Polypyrrole Actuator

3.1 Introduction

Polypyrrole actuator has gained attention to use in underwater medium due to its promising properties of large bending displacement and high work density with low driving voltage. In addition to this, light weight, flexibility and biocompatibility make it suitable to develop miniaturized underwater systems particularly bio-inspired propulsion mechanism and biomimetic robots. Past researchers proved that various smart materials such as SMA, IPMC, DE and PZT including CPs were used to develop underwater actuator propulsor [99-111]. However, an efficient versatile underwater actuator propulsor for real time application is highly desirable. In order to develop a realistic actuator, the hydrodynamic performances of the actuator need to be improved.

This chapter focuses on the hydrodynamic characterization of the PPy actuator in underwater environment and estimates the hydrodynamic performances to study the feasibility of the present actuator. The hydrodynamic bending and performances of the actuator estimated for both DC and AC electric potential to study the quasi static and dynamic behavior of PPy actuator. The hydrodynamic loading and its effect on bending displacement, thrust generated, power consumption and efficiency of the present PPy actuator are the important aspect of this chapter. Beside, the tip velocity, bending frequency, vibration in PPy actuator while operate in underwater medium were determined experimentally to study the feasibility of the actuator. Finally estimate the life cycle of the actuator and compared the performances with published results to show its feasibility for underwater operations.

3.2. General Experimental Techniques

In this section the details of the actuator configuration, equipments and methods were used necessary for hydrodynamic characterization and estimating the hydro-dynamic performances of the PPy actuator has been discussed in details.

3.2.1 Actuator Configuration

In the present work, the rectangular trilayer strip actuator having dimension $35mm \times 8mm \times 0.15\,mm$ is used for underwater experiment. One end of the actuator is fixed and placed in between copper electrode plates while the other ends free to move. The copper electrodes are used to supply electric voltage to the actuator. The electrode and the electrical connection shielded properly and ensure leakage proof as the actuator operates inside the fluid medium. The details of the experiments and experimental setup are discussed in the following section.

3.2.2 Underwater Bending Experiment

The underwater bending experiment is carried out in both quasi static and dynamic mode by applying DC and AC voltage respectively. The schematic diagram of in-house experimental setup is used with DC voltage supply are shown in Fig.3.1.

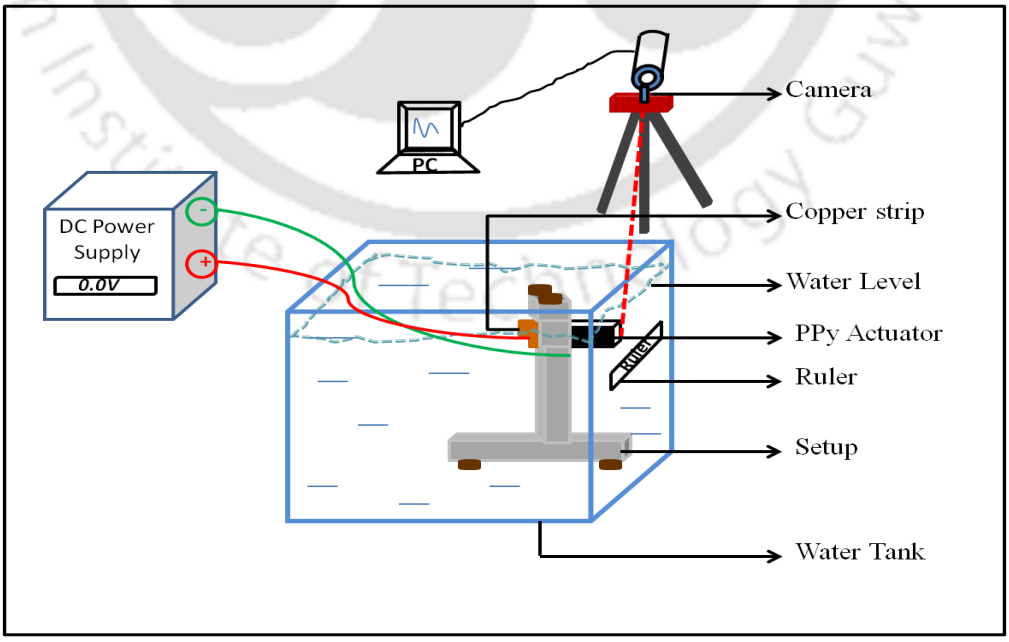

Figure 3.1 Schematic diagram for experimental setup of underwater experiment

For the underwater environment an artificial open face glass tank is fabricated having the dimension of $75 \times 60 \times 60\ cm^3$. Here, the experiments were conducted in quiescent water having zero flow velocity and the height of water level in tank is up to 45 cm. The actuator with the holder setup is placed inside the tank where the actuator is located 15 cm below the free water surface. The real time bending experiment photograph is shown below in Fig.3.2.

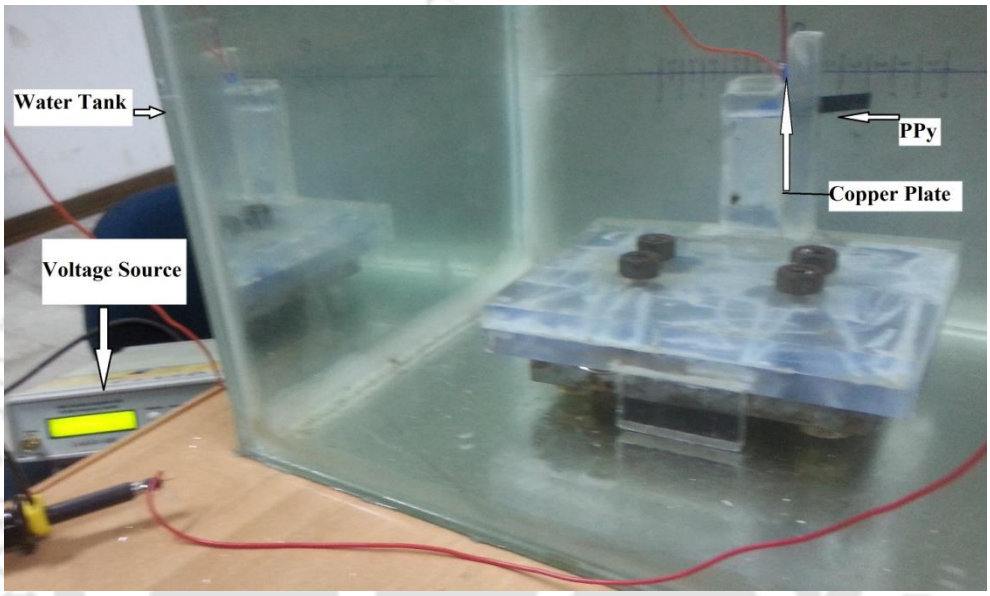

Figure 3.2 Photograph of real time bending experiment under DC voltage

At first the quasi static bending experiment is conducted on applying DC voltage by the DC power supply ($0 - 32$ V, $0 - 2$ A) and the bending displacement is recorded using digital camera (**Maker: Sony, RX 110**). The camera is connected to PC and use the ImageGrab software to estimate the hydrodynamic parameters. The bending displacement is recorded for a range of voltages starting from 0.6 V to 2 V with a step size of 0.2 V

For the dynamic condition, similar experimental setup is used along with the function generator to convert DC to AC voltage and laser sensor to detect the bending displacement as shown in Fig.3.3. The fixed end is connected with voltage source which is connected to the function generator (**Sony/Tektronix AFG 320**) and PC. A rotational laser vibrometer (**RLV-5500, Polytec, GmbH**) is used detect the bending displacement along with the high speed camera (**SONY RX 110**) with ImageGrab software. The bending experiment is recorded with high speed camera of

100 fps to study the bending motion of the PPy actuator. In dynamic bending, sinusoidal voltage is applied to the actuator exhibiting continuous bending in both sides.

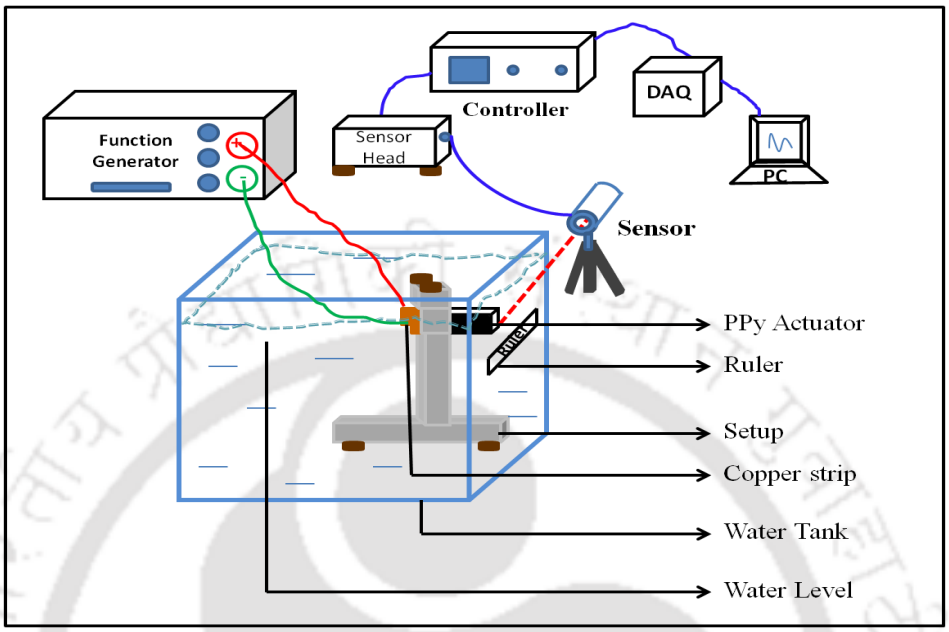

Figure 3.3 Schematic diagram of underwater bending experiment with AC voltage

The laboratory bending experiment of PPy actuator under AC voltage is shown in Fig.3.4.

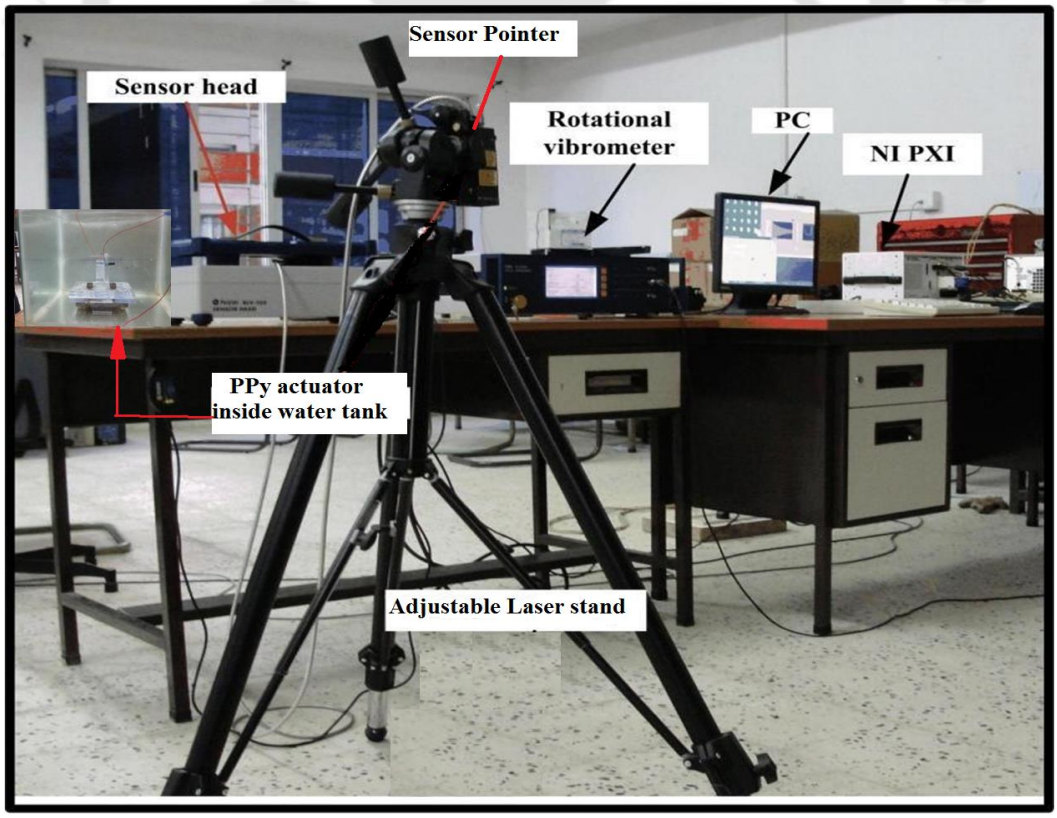

Figure 3.4 Photograph of bending experiment under AC voltage

The frequency response of bending displacement is analysed to estimate the tip velocity and bending frequency. The underwater bending displacement is recorded for 1.3 V of amplitude for a range of frequencies of 0.1 Hz ~ 10 Hz.

In the follow up of bending experiment, the actuator tip force is measured for both DC and AC voltage is acting the same experimental setup along with a pointed needle in connection with a physical balance (**maker: Sartotius, model: BSA2245-CW**). The force measurement experimental setup is shown in Fig.3.5. Before applying voltage at the fixed end of the actuator, the other end (free end) is just allowed to touch the digital measuring balance and the initial reading is set to zero at time $t = 0$. A PPy actuator of size $30 \times 8 \times 0.15\, mm^3$ is experimented to measure the tip force. Voltage is applied gradually (not the step input) and the tip force is measured for an input of $0.5\ V - 2\ V$. The simillar setup is used for estimating the force under AC voltage with the same parameters used for bending experiments. The behaviour of force is studied under various frequencies of input voltage.

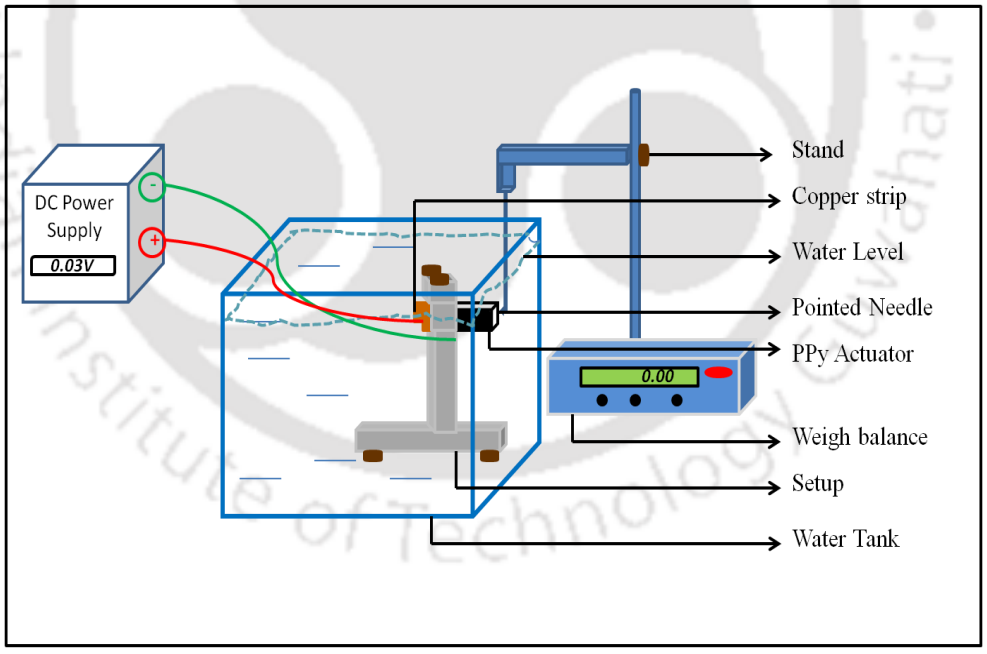

Figure.3.5 Schematic diagram for tip force measurement of PPy actuator

3.2.3 Experimental Method for Hydrodynamic Performances

The primary hydrodynamic performance is the thrust force for any underwater system. The other performances like speed, power consumption and efficiency primarily depend upon the thrust force and measured from thrust experiment also.

The thrust measurement is carried out in two main steps i.e. calibration and actuation. Further the calibration is done before and after the actuation to ensure the actuator starts working from zero deflection point and maintain the equilibrium position with appropriate boundary conditions. It is ensured that the pre and post calibration data necessary to be approximately constant and identical even with minor disturbances. This leads to determination of the equilibrium position from the average of pre and post calibration data after each actuation cycle. Following the pre-calibration, the AC voltage supplied to the actuator for actuation by using voltage source and the amplitude and frequency is regulated by using LabVIEW module software.

A 10 g load cell (**FC 2311, TE Connectivity**) was used to measure the thrust force of the PPy actuator operates in underwater medium. The load cell was connected to a data acquisition system (**National Instruments**), where the time and force of the propulsor were measured and recorded. The propulsor was placed horizontally in water tank and connected to the load cell, via an extensor, as shown in Fig.3.6. The load cell force value was set to zero, thus eliminating the force contributions of gravity.

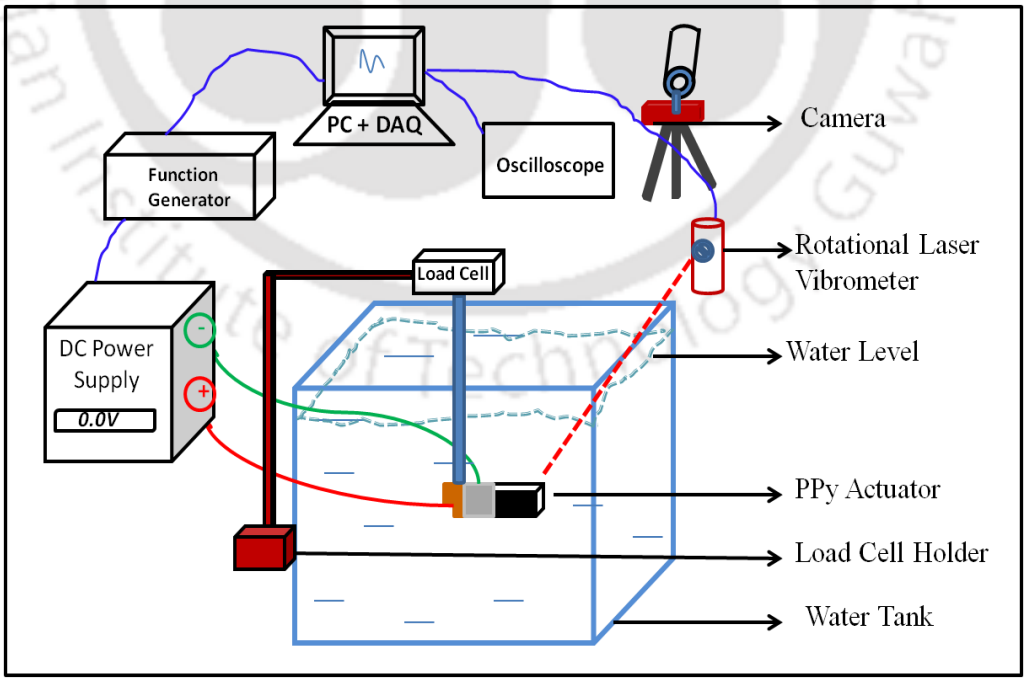

Figure.3.6 Schematic diagram of experimental setup for measuring thrust

Once the proper setup is complete, the voltage applied in varying amplitude and frequencies to record the data. For actuation of the PPy actuator, 1.3 V of potential is applied as the PPy actuator exhibits optimum and stable bending as explained in chapter 2. The frequency of excitation is varying from 0.1 Hz to 10 Hz to estimate the optimum frequency for generating high thrust force and correlated the thrust with bending displacement and tip force. The experimental data is collected when the actuator reaches its steady-state equilibrium position, eliminating transient data from the experimental data set. More number of actuation cycles was recorded by measuring each cycle for 10 s and recorded the data. In the underwater bending, the tip deflection of the actuator primarily depends upon the actuator dynamics and hydrodynamics, as the hydrostatic pressure effects cancel out. Therefore the tip displacement can be used to calculate the mean thrust of the actuator. Further the other hydrodynamic parameters like drag and mass co-efficient are also estimated from the experiment. The equipments were used in underwater bending experiment for the present study is shown below Fig.3.7.

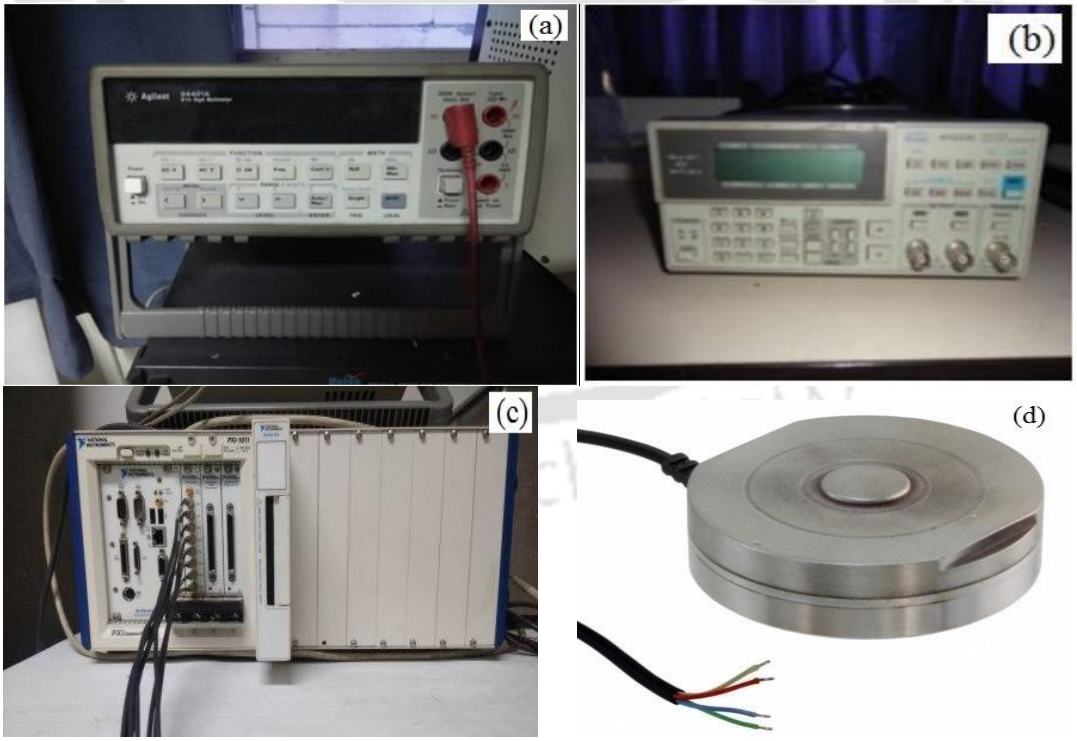

(a) Oscilloscope (b) Voltage Source (c) Data Acquisition System (d) Load Cell

Figure.3.7 Equipments used for hydrodynamic characterization of the PPy actuator

3.3 Results and Discussion

In this section the results obtained from the underwater bending experiment in quasi static and dynamic condition are analyzed and discussed in details. The hydrodynamic performances like speed, effectiveness, power consumption, operating life cycle etc are studied and compared with the literature showing the feasibility of the present actuator for underwater actuations. The frequency response analysis along with vibration and damping of the actuator were also studied.

3.3.1 Underwater Bending Displacement under DC voltage

Fig.3.8 shows the displacement vs time for various input voltage. It is observed that nearly after 4 s of voltage applied the PPy actuator attains its equilibrium. The actuator exhibits highest displacement over 7 mm however within few seconds of operation the displacement decreases. It may be believed that the actuator experience material degradation due fast actuation and increased temperature at actuator holder, hence the bending performances fluctuates and decreases suddenly

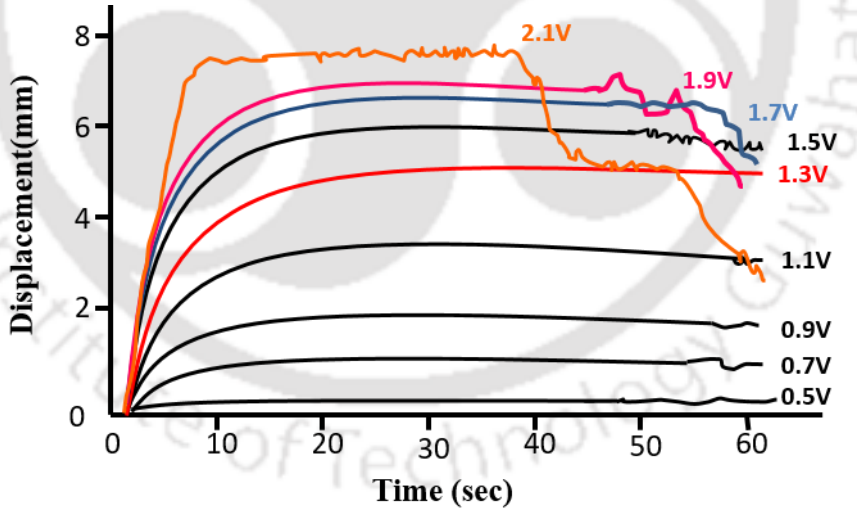

Figure.3.8 Displacement Vs Time for various amplitude of DC voltage

at high voltage. The actuator shows steady bending at 1.3 V with displacement amplitude of 5.4 mm which is slightly higher as compared to the existing underwater actuators [111]. In lower voltage, the rate of actuation is lower hence the bending displacement is low. Therefore the optimum actuation voltage for the PPy actuator for underwater medium is 1.3 V for steady and improved bending

performances. Fig.3.9 shows the comparison on bending displacement of the developed actuator with the existing actuators. This is observed that the present PPy actuator exhibits tip displacement up to 5.4 mm at 1.3 V with more stability as compared to earlier developed actuators [102,105,108,110,111]. Although in some cases the tip displacement is more than present actuator, the stability is poor due to high or low voltage.

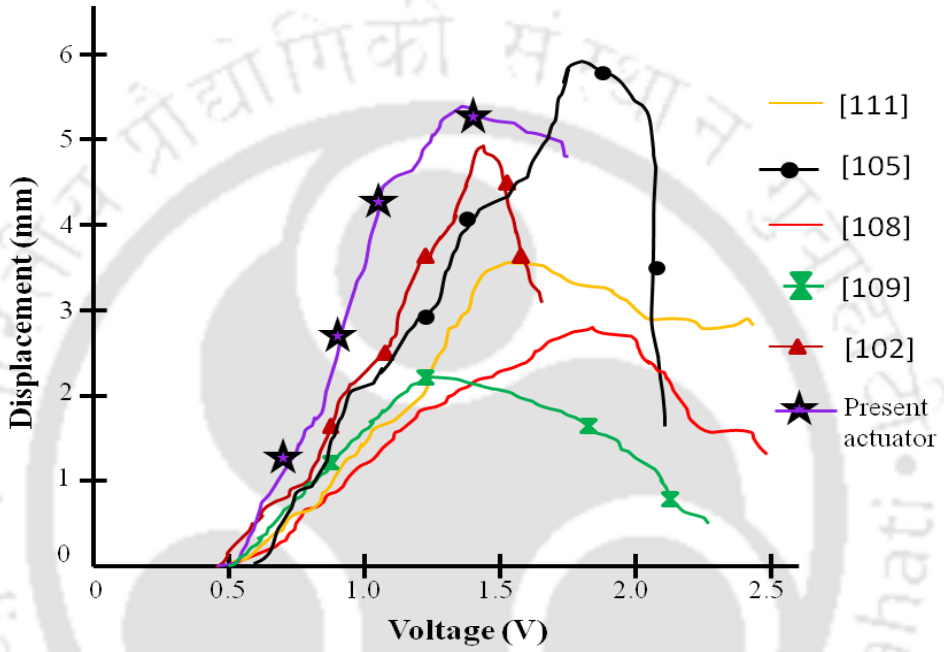

Figure.3.9 Comparative analysis of PPy actuator bending displacement

3.3.2 Tip force Measurement under DC Voltage

Fig.3.10 shows the tip force vs time for various amplitudes of DC input voltage. It has been observed that the actuator generates maximum of 4.2 mN force at 1.3 V. Further it has been observed that the tip force increases with the input voltage beyond 1.3 V however instability was notices from the experimental results. The tip force is following the similar trend as the displacement varies with voltage amplitudes. Tough the max tip force is generated with the zero deflection point; hence the force is decreases with the increase in bending displacement. The tip force is primarily control the manoeuvring of the under swimming system.

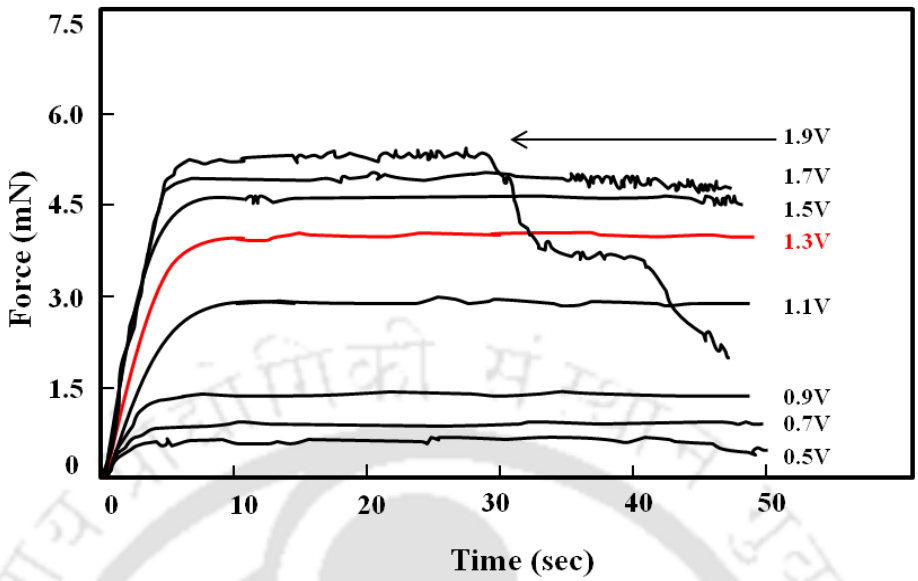

Figure 3.10 PPy actuator tip force for various amplitude of DC voltage

Fig.3.11 shows the behaviour of displacement and force with voltage amplitudes. It can be observed that both are varying similarly with voltage but oppositely varies with each other. For underwater propulsion both displacement and force affect the thrust force and hydrodynamic performances

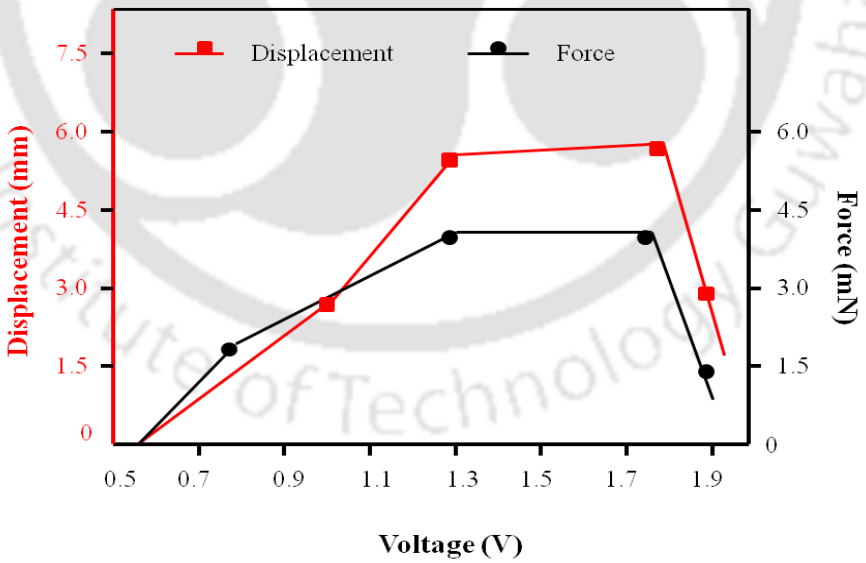

Figure. 3.11 Displacement and force with DC voltage input

The comparison of tip force is estimated here for the fabricated actuator with the existing actuators [105,106,109-111 is shown in Fig.3.12. It has been observed that the actuator tip force is not uniform in few cases and it may be due to the uneven

PPy film. The tip force plays a major role for underwater operation to generate thrust and maintain the stability of the system in underwater environment particularly in viscous fluid.

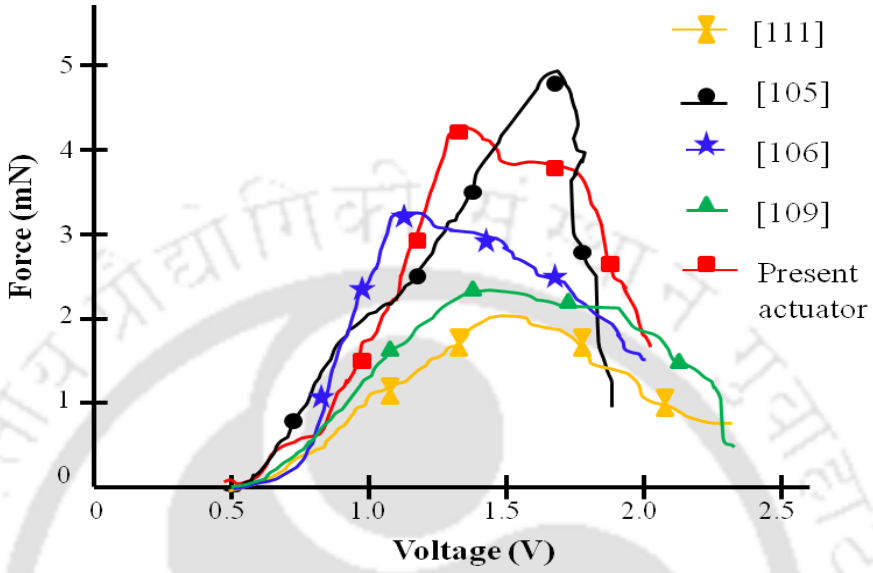

Figure.3.12 Comparative analysis of tip force of PPy actuator with existing actuator

3.3.3. Operational Life Under DC Potential

Operational life or the cycle life is an essential parameter for real time PPy system as reported low life due to creep and fatigue is the major disadvantage of PPy actuators. Fig.3.13 shows the life of the actuator over thousands of operation cycles.

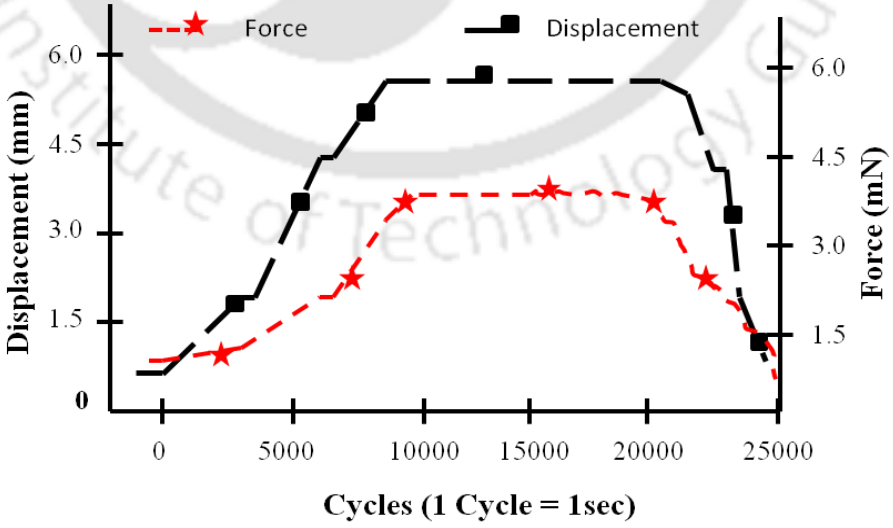

Figure.3.13 Displacement and Force over 25000 operational cycles

Dynamic fatigue is of extreme importance because a cyclic or fluctuating load causes a component to fail at much lower stresses than it does under monotonic loads [66]. From the experimental results, it has been seen that the bending output displacement and force curves are constant, hence it may concluded that the actuator operates in underwater medium for nearly 20,000 of cycles without any significant failure. This long term continue operation might make it suitable for underwater system for various applications like scanning and surveillance.

3.3.4 Underwater bending characterization under AC voltage

The bending displacement and force are measured for a time period of 10 s under sinusoidal voltage amplitude 1.3 V over a frequency range of 0.1 to 10 Hz. The time vs bending displacement for AC input voltage is shown in Fig.3.14.

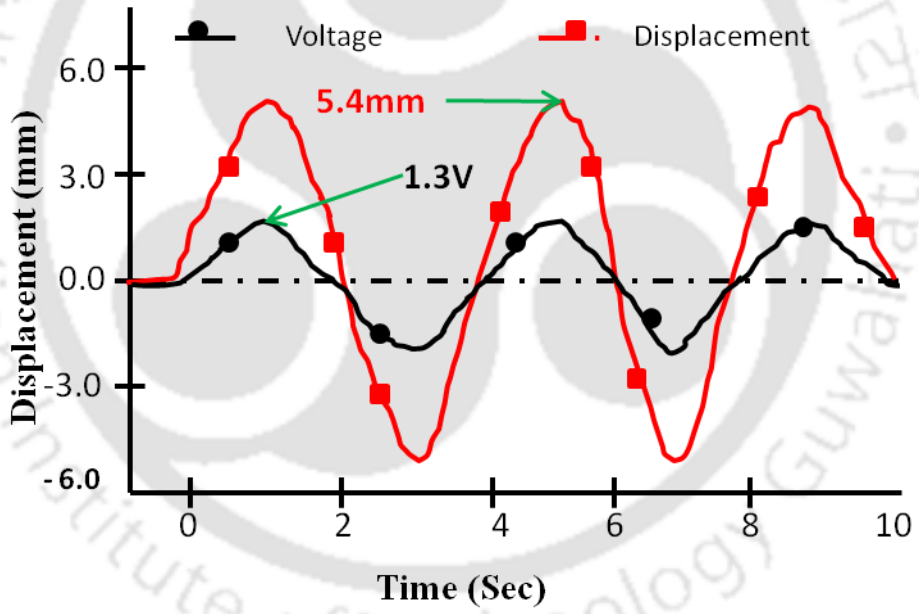

Figure 3.14 Bending displacement with time varying input voltage

The actuators exhibits maximum bending displacement of 5.4 mm and the bending behaviour is sinusoidal in nature as the input voltage is sinusoidal. Due to the AC voltage, the actuator bends in both direction continiously similat to the fish tail like movement. The variation in bending displacement with the actuation frequency is shown in Fig.3.15. The actuator shows the maximum displacemet at nearly 1 Hz and gradually decreses the displacement with increases or decreases with frequency.

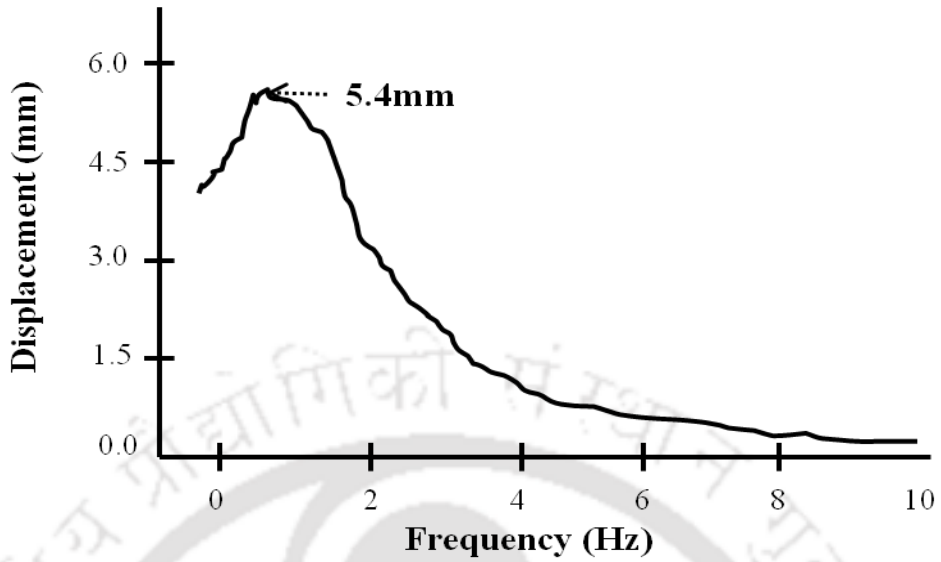

Figure 3.15 Bending displacement of PPy for various frequencies

At higher frequency the rate of transfer ions are faster and could not get enough time to reach the required point inside the polymer chain, hence the displacement is lower. While at the lower frequency, the rate of ionic transfer is slow and the ions need more time to reach the required position in the polymer chain, hence could not generate the required displacement. Therefore, the optimal frequency of the PPy actuator for underwater operation is nearly 1 Hz, the PPy actuator exhibits stable and improved performances. The photograph of bending experiment of PPy actuator under AC potential is shown in Fig.3.16.

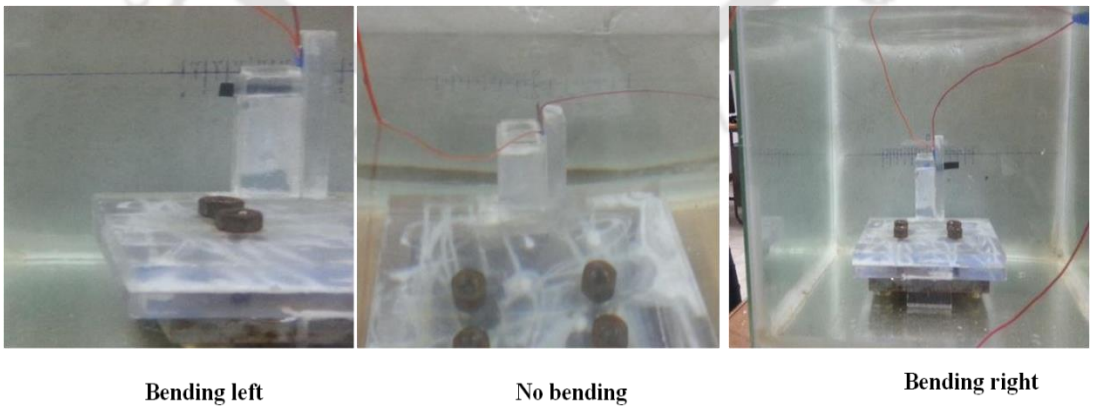

Figure.3.16 Photograph of bending experiment of PPy actuator under AC voltage

The tip velocity (U_{tip}) can be obtained from the tip displacement (w) and input frequency (ω) in rad/s by using the following [112] relation

$$U_{tip} = \omega w \quad (3.1)$$

Fig.3.16 shows the tip velocity of the actuator with the input frequency. It has been

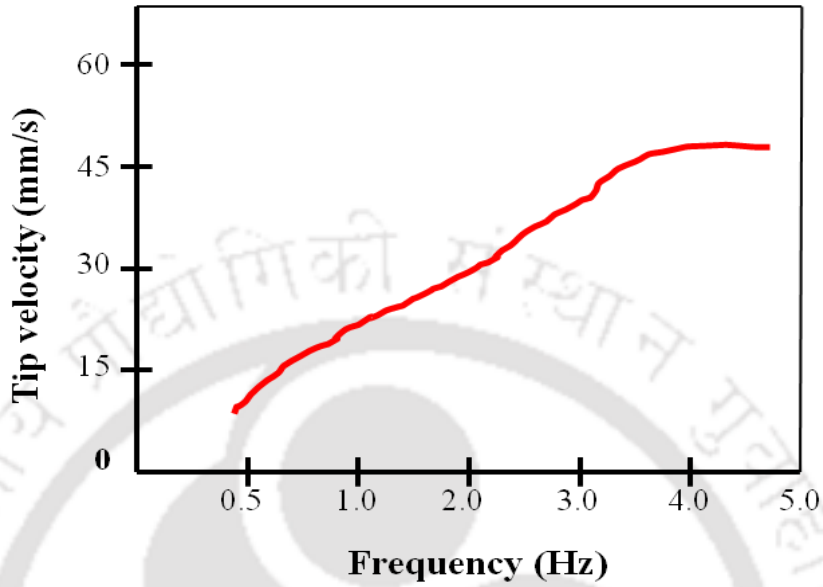

Figure 3.17 Tip velocity of the actuator with input frequency

observed that the tip velocity is increases with increase of frequency and the trend is opposite to the variation of displacement with frequency. At the highest displacement the velocity is less at low frequency and follows the similar trend with earlier developed actuators [112].

3.3.5 Tip Force measurement Under AC Potential

Fig.3.18 shows the time varying force generated by the actuator under AC voltage.

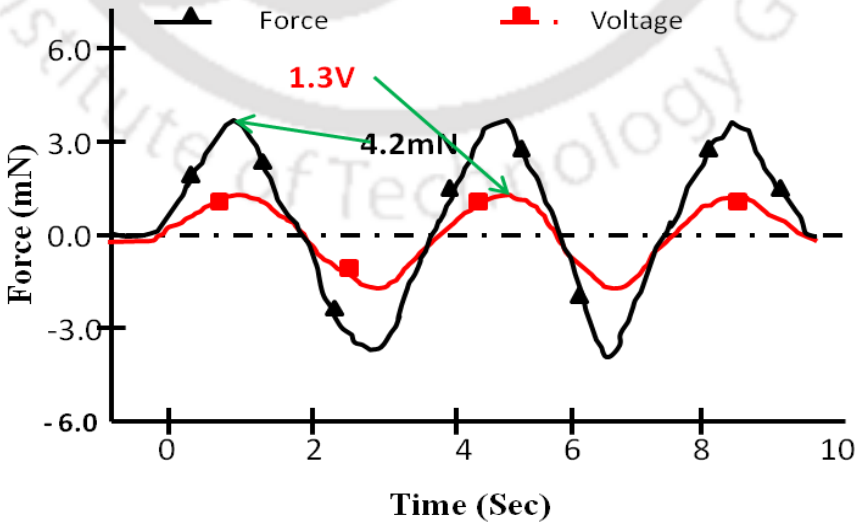

Figure 3.18 Tip Force in response to time varying voltage

The force generated due to bending is obtained from the physical balance as 4.2 mN and follows the same pattern as the input voltage is sinusoidal. As the force is generated by the blocking strength of the actuator, the tip force is maximum at zero bending and decreases with increase in displacement. Fig.3.19 shows the variation of force over the actuation frequency of PPy actuator operated in underwater environment. It has been observed at nearly 1 Hz the actuator exhibits maximum force of 4.2 mN and gradually decreases with increase in frequency.

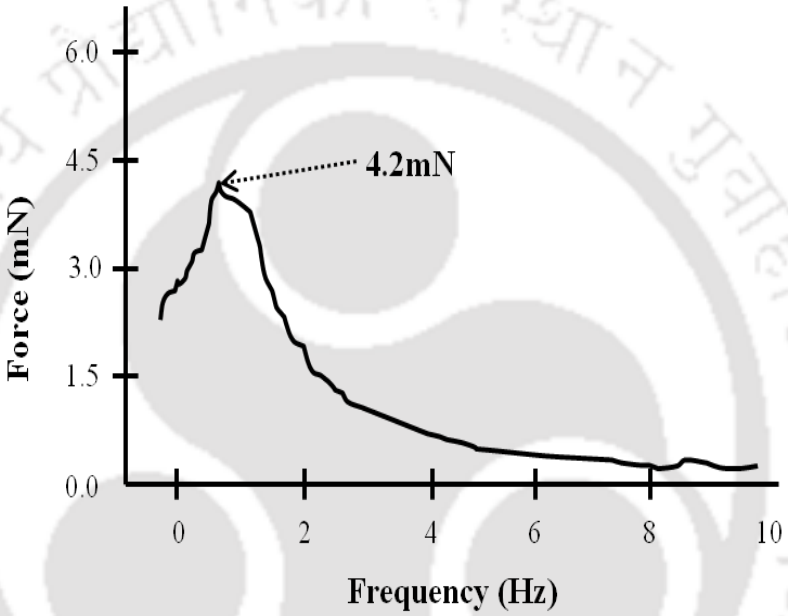

Figure 3.19 Frequency response of tip force of PPy actuator

3.3.6 Damping and Vibration Characteristics

The damping characterization of PPy actuator is to estimate the damping ratio and damping coefficient which helps to predict the accurate dynamic of the actuator in underwater medium. As the PPy actuator is very thin and flexible and operates in viscous fluid medium, it experiences higher order vibration. Further the PPy actuator exhibits viscoelasticity, hence the damping in present PPy actuator is contributed by both viscoelastic damping and fluid viscous damping. The study of damping properties helps to achieve the stable underwater operation by reducing the vibrations. The damping property of PPy actuator is studied for both free and forced vibration of submerged PPy actuator.

3.3.6.1 Free vibration of PPy in underwater medium

The free vibration characteristic of PPy actuator of size $30mm \times 8mm \times 0.15\,mm$ in fixed-free mode inside the water tank with zero flow velocity is studied using Rotational Laser Vibrometer (**RLV-5500, maker:Polytec, GmbH**). The experimental setup is used is similar to the underwater bending experiment. The actuator is allowed to vibrate under a small deflection at the tip for a time span before it comes to rest. The vibration response is then measured using **NI PXI-1031** controller with **NI PXI-4472** module and LABVIEW software, supplied by **NI Inc**.

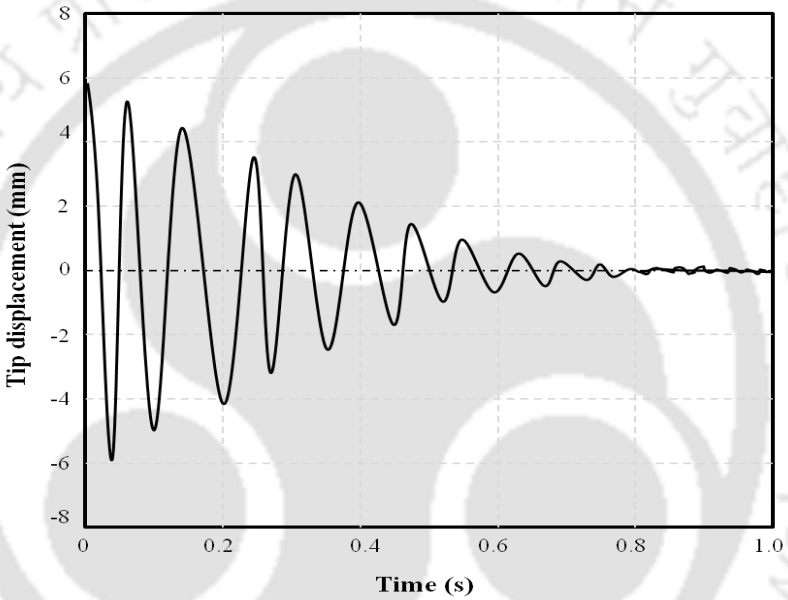

Figure 3.20 Free Vibration of Au-PPy in underwater medium

The damping ratio and loss factor of the PPy actuator are estimated from the free vibration of PPy in underwater environment. Fig.3.20 shows the free vibration and Fig. 3.21 shows the frequency response of the PPy actuator in underwater medium.

The logarithmic decrement method is used estimate the damping ratio. The logarithmic decrement method is expressed as

$$\delta = \frac{1}{n}\ln\left(\frac{z_i}{z_{i+n}}\right) \tag{3.2}$$

Where δ is the logarithmic decrement, n is the number of cycles, z_i is the displacement amplitude of i^{th}cycle and z_{i+n} is the displacement amplitude of $(i+n)^{th}$ cycle.

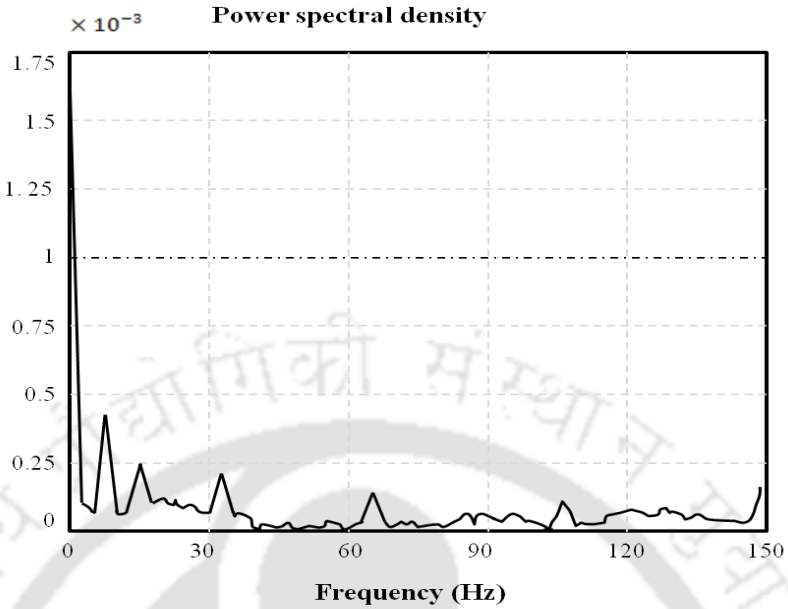

Figure 3.21 Frequency response of free vibration of Au-PPy in underwater

Following the logarithmic decrement, the damping ratio (ζ) can be determined by using the mathematical expression as

$$\zeta = \sqrt{\frac{\delta^2}{4\pi^2+\delta^2}} \tag{3.3}$$

As the PPy is exhibits viscoelasticity, the loss factor can be estimated from damping ratio by using the relation

$$\eta = 2\zeta \tag{3.4}$$

Taking 15 successive cycles ($n = 15$), the damping ratio of PPy actuator in underwater environment is determined as 0.012. The loss factor of PPy actuator is estimated 0.023. The loss factor is significantly more than the loss factor obtained from DMA analysis of dry PPy actuator is $0.012 - 0.014$ [43], hence it may be concluded that the damping increases due to fluid, almost half of structural viscoelastic damping. Therefore due to high fluid damping, the actuator may exhibits nonlinear responses which is discussed in chapter 5.

3.3.6.2 Forced Vibration of Au-PPy actuator in Underwater Medium

From the underwater dynamic bending experiment the vibration characteristics are studied. Fig.3.22 shows the vibration response of the actuator for DC voltage of 1.3 V and Fig.3.23 shows vibration response for sinusoidal voltage of 1.3 V for 1 Hz.

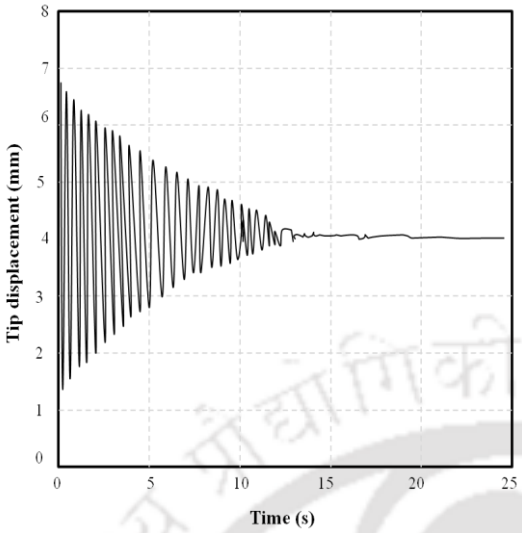

Figure,3.22 Vibration under DC voltage

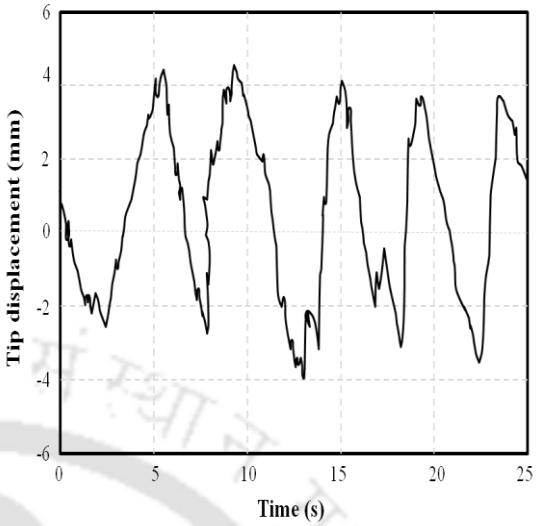

Figure.3.23 Vibration under AC voltage

It has been observed the vibration is approximately linear in case of DC potential where the nonlinearity noticed in responses under AC potential. The frequency response of bending displacement under AC potential is shown in Fig.3.24.

From the FRF analysis of bending displacement, the first natural frequency of PPy actuator is 6.5 Hz followed by the second, third and fourth mode natural frequencies are 13.4 Hz, 31 Hz and 58.2 Hz.

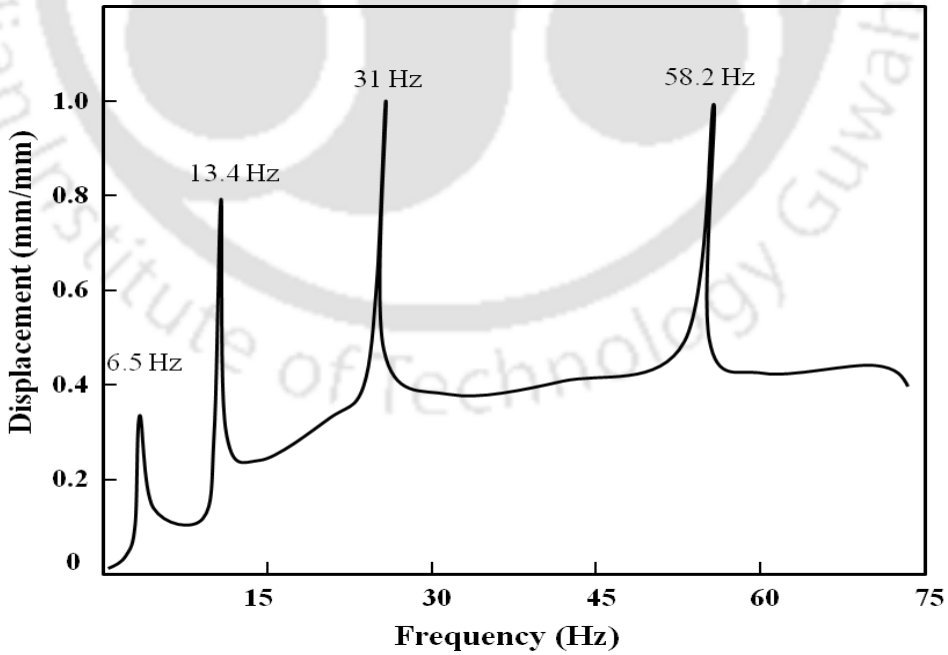

Figure. 3.24 Frequency response of bending displacement

From the bending experiment the FRF of the tip velocity of the PPy actuator in underwater medium is estimated and shown in Fig.3.25.

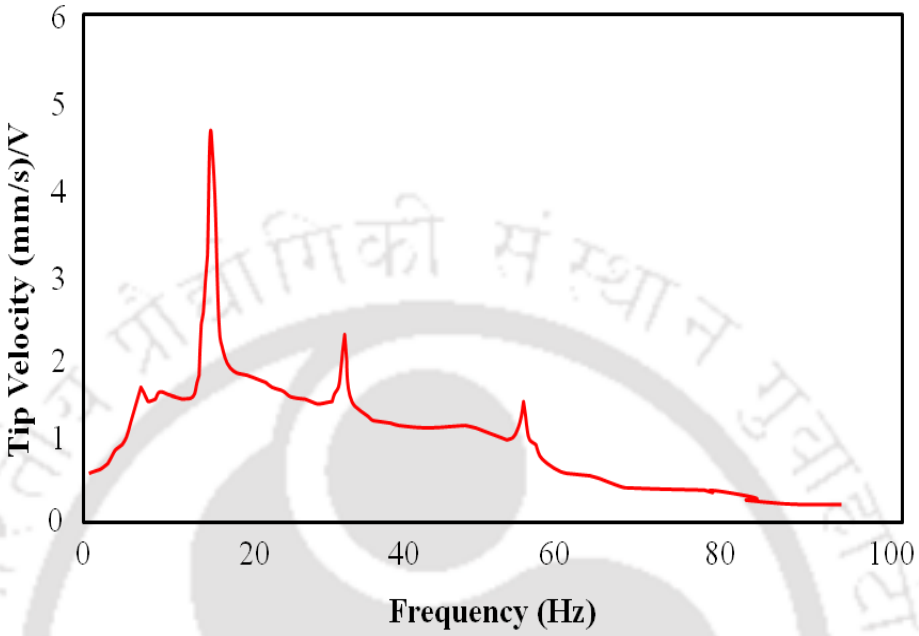

Figure.3.25 FRF of the underwater tip velocity of PPy actuator

The fundamental frequency is 6.5 Hz as it is obtained from FRF of displacement; however the tip velocity is not significantly high in this frequency. In the second mode at around 13 Hz the actuator exhibited high tip velocity.

3.3.7 Hydrodynamic Thrust

Although recently various smart material actuators based propulsion systems have been developed for underwater applications, bio-inspired actuators are still under research. PPy actuator based propulsor can be used as efficient bio-inspired propulsor as it exhibited promising hydrodynamic bending displacement. Besides, for real time underwater application, hydrodynamic thrust is the major characteristic properties of underwater system. The thrust force regulates the manoeuvrability and affects the hydrodynamic efficiency of any underwater system. The time varying thrust output for PPy actuator is shown in Fig.3.26

The maximum thrust is measured as nearly 1 mN while average thrust is obtained as 0.84 mN and the trends have shown good agreement with the existing actuator [110].

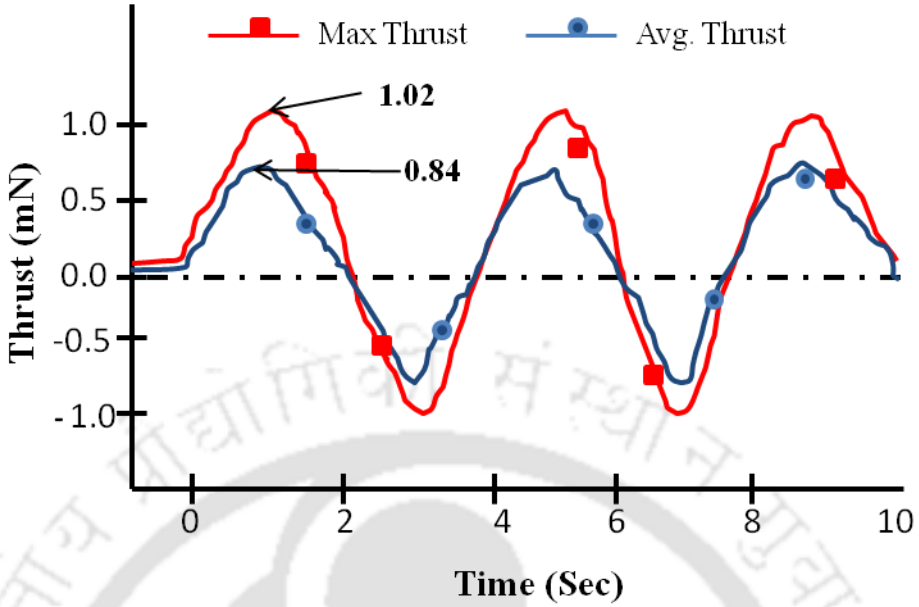

Figure 3.26 Thrust of PPy actuator with time varying voltage

The thrust varies over actuation frequency has revealed that the dominant actuation is at 1 Hz and at this frequency the maximum thrust can be observed as shown in Fig.3.27.

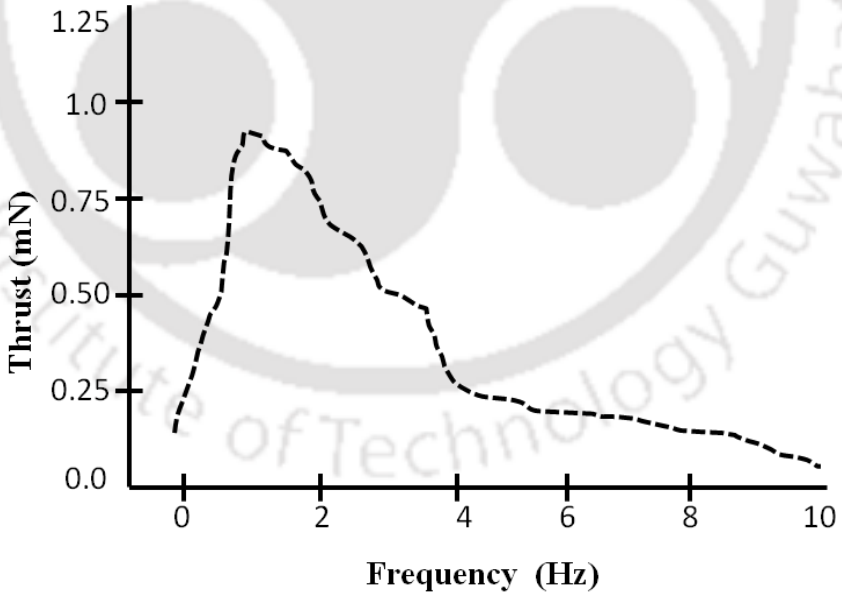

Figure 3.27. Frequency response of thrust force of PPy actuator

Further it can be observed that at zero displacement the thrust is also zero and the thrust frequency is twice of actuation frequency. The thrust follows the same

behaviour as the displacement i.e. one can observe the maximum thrust nearly at the displacement peak and the phase lag is same as of displacement with input voltage.

3.3.7.1 Thrust Co-efficient

The thrust co-efficient (c_t) can be estimated from the experimental tip displacement, thrust force and actuation frequency by using the mathematical relation as

$$c_t = \frac{2\overline{T_f}}{\rho_f \mu \omega^2 w^2 L} \tag{3.5}$$

Where $\overline{T_f}$ is average thrust force, ρ_f is the water density, μ is the kinematic viscosity of water, w is the tip displacement, L is the actuator length and ω is the actuation frequency in rad/s.

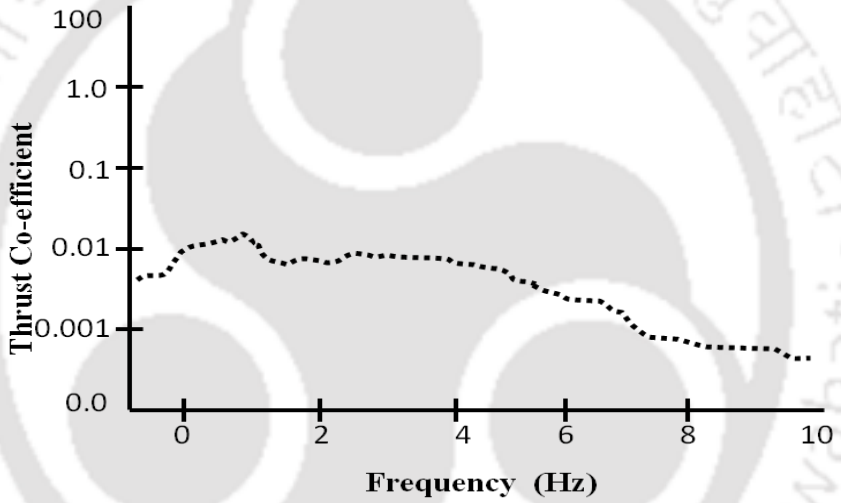

Figure 3.28 Variation of thrust co-efficient with actuation frequency

Here the thrust co-efficient is around 0.012 and its maximum at nearly 1 Hz and earlier it has been seen thrust is also maximum at this frequency. Fig.3.28 shows the variation of thrust coefficient with the actuation frequency and it shows the similar trend with published results [112]

3.3.8 Power Consumption and Effectiveness

Power Consumption by the actuator can be estimated from the underwater bending experiment. The laser sensor is measured the tip displacement and an oscilloscope is used to plot the graph for tip displacement. From the oscilloscope data recorder, the input voltage and output current of PPy actuator during underwater experiment is recoded. The applied voltage and current were monitored via LabVIEW software. The power consumption is determined by calculating instantaneous power

consumption over a minimum of ten actuation cycles and then taking the mean over the course of the cycle. By using this voltage and current the average power consumption of PPy actuator is calculated by using the formula [113], as follows in Eq.3.4

$$\bar{P} = \frac{1}{1/f}\int_{t_r}^{t_r+1/f}(V_i I_o)dt \qquad (3.6)$$

Where $\bar{P}$ is the average power consumed by PPy actuator for underwater bending, t_r is any random time during PPy actuator operates in underwater medium, V_i is the input voltage and I_o is the output current, f is the frequency of operating voltage. In order to find the propulsion efficiency quantitatively, the ratio of average thrust generated to average power requirement for one cycle of actuation is taken into consideration [103, 113].The power consumption of PPy actuators is primarily dependent on the input voltage, size of mobile ion due to which the actuation occurs. The actuation voltage of the PPy actuator is found to be 0.54 V but at this voltage the redox reaction is very slow which generates very low displacement. However the maximum and steady displacement is produced at a voltage of 1.3V and 1Hz, beyond this point the performances are not steady due to loss of material leads to increases the output current, hence the power consumption increases as shown in Fig.3.29

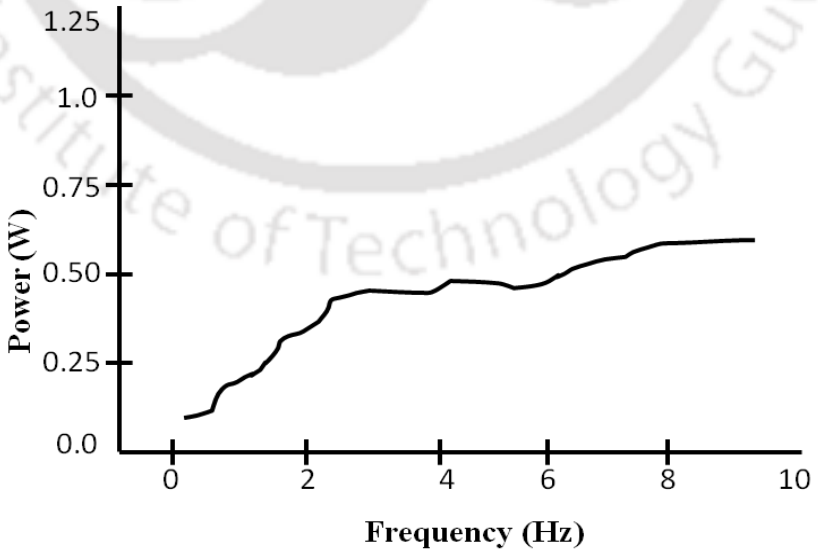

Figure.3.29. Frequency response of Power consumption

The power consumption is calculated as average power as the data recorded for eight to ten actuation cycle to enhance the accuracy. The resulting power consumption for the PPy actuator is 0.23 W and significantly lower than existing actuator [113]. With the increase in frequency, the power consumption increases, subsequently the performance of the PPy actuator based underwater system lowers.

The effectiveness is the parameter used to quantify the overall performance of the actuator. It is defined as the ratio of average thrust to average power consumption of the PPy actuator for certain number of actuation cycle [103]. As the thrust and power primarily depend upon actuation voltage; effectiveness varies with the frequency of operating voltage. Fig.3.30 shows the variation of effectiveness with actuation frequency.

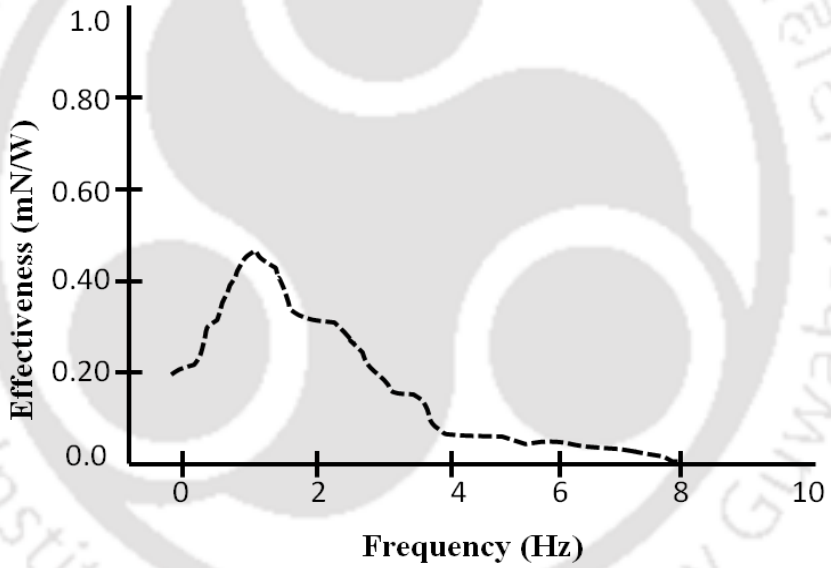

Figure.3.30 Effectiveness of the PPy actuator with actuation frequency

The effectiveness of the PPy actuator is 0.48 and shows the good agreement and significantly improved as compared to the earlier developed EAP actuators [112, 113].

From the present study it can be summarized that, the bending and propulsive performances of the actuator can be monitored and controlled by controlling the frequency alone and it will help to develop precise control system for any real time applications. The summery of the hydrodynamic bending and performance parameters are given in Table 3.1.

Table 3.1 Experimental results obtained from underwater bending experiment

Parameters	Experimental Value
Bending Displacement	5.4 mm
Tip Force	4.2 mN
Operative Voltage	1.3 V, 1 Hz
Thrust	Max: 1.02 mN Avg: 0.84 mN
Power	0.23 W
Hydrodynamic Damping	0.012
Total Damping	0.023
Operational Life	10-12 h
Effectiveness	0.48

3.4 Summary

In this chapter, hydrodynamic bending characterization and performances of the gold-polypyrrole (Au-PPy) actuator were studied. At first the underwater bending displacement, force and operational life cycle was measured for DC voltage. The experimental results show that the bending displacement and force increases with voltage amplitude. The maximum displacement is estimated as 5.4 mm while the maximum force is recorded as 4.2 mN at 1.3 V. Although the displacement increases at higher amplitude of voltage, it suddenly decreases may be due to material degradation. Under Dc potential the actuator can work upto 10-12 h without reposrting any significant failure. Following this, the bending characterizations are recorded for AC potential of 1.3 V amplitude with a range of frequencies. Experimental result shows the actuator exhibits stable performances at nearly 1 Hz. At higher or lower frequencies the ions don't get appropriate time to enter into the polymer chain hence the actuator performances were degraded. The tip velocity of the actuator estimated from the frequency response of displacement. The tip velocity is maximum around 4 Hz while the displacement lowers. At higher displacement the tip exhibits lower velocity. The damping and vibration of actuator is studied from

vibration experiment. The damping ratio of the PPy actuator is estimated as 0.012 and it is contributed by both viscoelasticity and fluid damping. The actuator operates under AC potential shows the nonlinear vibration which is believed to due to nonlinear viscous damping of fluid.

The hydrodynamic performances like thrust, power and effectiveness are estimated from the underwater bending experiment. The trust is measured from the load cell mounted on the water tank. The actuator exhibits maximum thrust of 1.02 mN while the average thrust is 0.84 mN calculated over 10 actuation cycles. Frequency response of thrust shows similar pattern like displacement. It has been observed thrust is higher at higher displacement nearly at 1 Hz. The present actuator consumes low [power as compared to other existing actuator hence the effectiveness of the PPy actuator is higher.

The present actuator shows superior performances and enhanced cycle which makes it suitable for underwater applications.

4

Underwater Dynamic Bending Modelling of Gold - Polypyrrole Actuator

4.1 Introduction

The underwater working medium influences the actuation properties and performances of Polypyrrole actuator. The inertia and viscosity of underwater medium reduces the bending displacement and effectiveness of PPy actuator during working conditions. Further, for efficient operation, the stiffness of actuator should be enough to avoid the fatigue enhancing the cycle life. The hydrodynamic performances like thrust and bending speed of the actuator quantify the underwater operation and make it suitable for underwater robotics applications.

Past literatures established the fact that the bending displacement of the PPy actuator is function of electrical, chemical and mechanical parameters. However, very limited research has been carried out to address the effect of working environment and viscoelasticity together as most of the earlier developed actuators were focused on air medium operations with constant modulus. In this chapter, an effective robust and comprehensive model is developed based on a trade off between the complexity and accuracy to study the behaviour and performances of the PPy actuator operating in underwater medium. To address this issue, we define the following key factors which significantly influence the development of the present dynamic model of PPy actuators: (i) use of a physics based grey box modelling (ii) consideration of underwater dynamics along with electrical, chemical and mechanical parameters (iii) consideration of the time varying viscoelastic modulus of the PPy actuator and (iv) use elongated body theory to predict the hydrodynamic performances. These factors play a significant role in order to develop a simple

model and can more realistically predict the bending performances like bending displacement, tip force and hydrodynamic performances like thrust and speed in response to excitation voltage and frequency. Hence the mathematical model is function of electrical, chemical and mechanical parameter along with material properties and operating conditions. The schematic diagram of the flow chart of the process and parameters used to develop the model is shown in Fig.4.1.

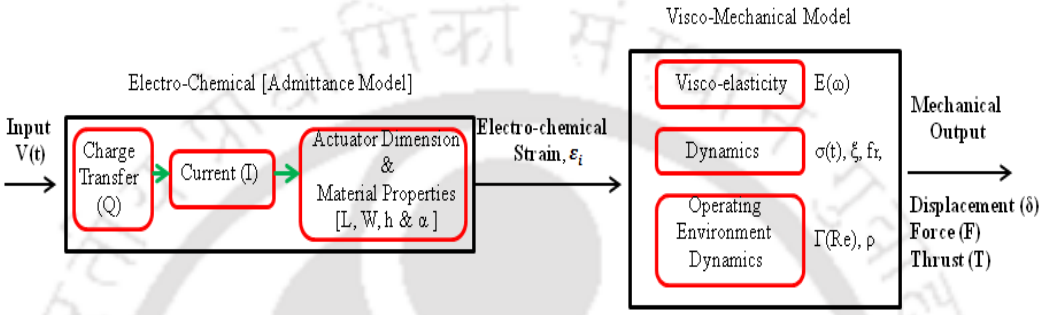

Figure.4.1 Flow chart of the modelling procedure

Finally, the results were compared with experimental results obtained in previous chapter followed by a comparative analysis with the recently published results to validate the model and study the feasibility of the present PPy actuator for underwater operations.

4.2. Modelling of the PPy actuator for Underwater Operation

In this section, the mathematical model for the underwater bending of PPy actuator is formulated in transform form of equation to predict the output tip displacement in terms of input voltage. The configuration of actuator and assumptions has been considered are discussed in details following by the formulation of governing equation and solutions.

4.2.1 Configuration of the PPy actuator

In present work, rectangular beam like trilayer structure has been considered. The schematic diagram of the trilayer PPy actuator is shown below in Fig.4.2. The free length and width of actuator L and W while the thickness of the actuator is $-h_2$ to h_2. The negative sign is used to represent the height in lower side of neutral axis.

The total thickness is divided into three layers: the thickness of the middle PVDF

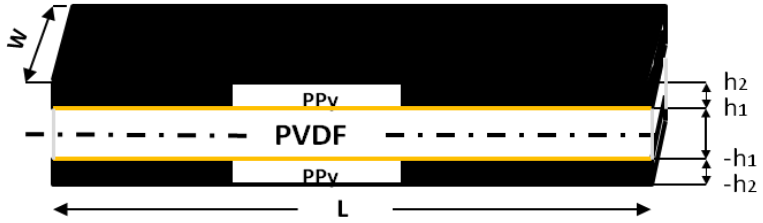

Figure.4.2. Schematic diagram of trilayer Polypyrrole actuator configuration

layer(solid polymer electrolyte) is $h_{PVDF} = -h_1$ to h_1, while the thickness of upper PPy layer is $h_{PPyu} = h_1$ to h_2 and lower PPy layers is $h_{PPyl} = -h_1$ to $-h_2$.

On applying voltage across the thickness of the trilayer actuator, the cations and/or anions set to move from PVDF (electrolyte) to PPy layer and vice versa. These redox reactions generate strain in the polymer layer by expansion and contraction of polymer chain. Due to the simultaneous expansion and contraction in both layers induces bending in the actuator. By fixing one side of the actuator, the PPy trilayer actuator behaves like a cantilever beam as shown in Fig.4.3, and is suitable for underwater propulsion systems.

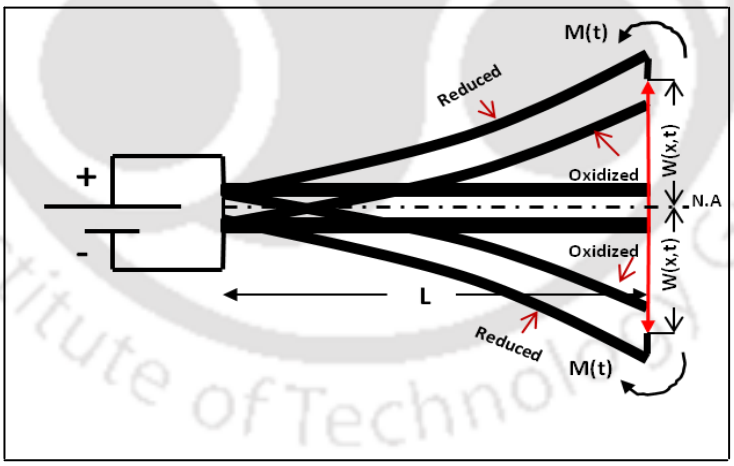

Figure.4.3. Schematic diagram of bending behaviour of PPy trilayer actuator

To develop the model, here some assumptions have been considered as follows:

(a) The actuator is symmetric in structure and the thicknesses of PPy layers are same for both sides of the middle PVDF layer.

(b) The actuator behaves like an inextensible Euler-Bernoulli cantilever beam i.e. shear and rotary inertia are negligible.

(c) The trilayer actuator behaves like a single layer i.e. no slip between inter-layers.

(d) The transverse (out of plane) bending is considered in XZ plane where it is uniform along the length.

(e) Strain distribution varies along the thickness with respect to the distance from neutral axis and the plane cross section remains unchanged during bending.

(f) The charge transferred is uniform along the thickness but opposite in direction. The stress induced in the actuator solely due to this charge transfer upon applying voltage.

(g) At time $t \leq 0$ the actuator is quiescent i.e. stress and strain is zero.

(h) The actuator exhibit visco-elasticity which leads to loss of energy during operation.

(i) The actuator operates in incompressible Newtonian fluid (water) medium which is in rest condition.

4.2.2 Electrochemical Modelling

On applying voltage V_{in}, the ion exchange starts between the middle PVDF and side PPy layers of the actuator. As the rate of charge transfer across the thickness and along the length is uniform, this can be analogous to the cantilever beam with uniform distributed load. The rate of charge transfer i.e. moving of DBS- into and out of PPy chain, can analogous to the current and subsequently the strain generated due to DBS- movement can be easily obtained. The DBS- stored in the interface of PVDF-PPy before entering into the polymer chain and diffuse into a certain distance as both PPy and PVDF elements exhibit resistance. Therefore, here the distributed RC transmission line mechanism along with diffusion impedance based admittance model has been adopted [68] to predict the output current as follows

$$Y_a(s) = \frac{1}{z(s)} = \frac{I(s)}{V_{in}(s)} = \frac{1}{\sqrt{2R_{PPy}Z_{eq}(s)}\ tanh\left(\frac{2R_{PPy}}{Z_{eq}(s)}L\right)} \tag{4.1}$$

here, R_{PPy} is the resistance of PPy, L is the length, s is the Laplace variable and z_{eq} is the equivalent impedance for unit element of the trilayer actuator.

The equivalent impedance, z_{eq} for an unit element of the trilayer actuator can be obtained from the electrolyte resistance (R_{PVDFi}), charge transfer resistance (R_c), diffusion impedance (z_d) and double layer (PPy-PVDF interface) capacitance (C_d), which can be written as,

$$z_{eq}(s) = R_{PVDFi} + \frac{(z_d + R_c)}{(z_d + R_c)sC_d + 1} \tag{4.2}$$

The equivalent transmission line circuit model for Polypyrrole actuator and its reduced form can be modelled as shown in Fig. 4.

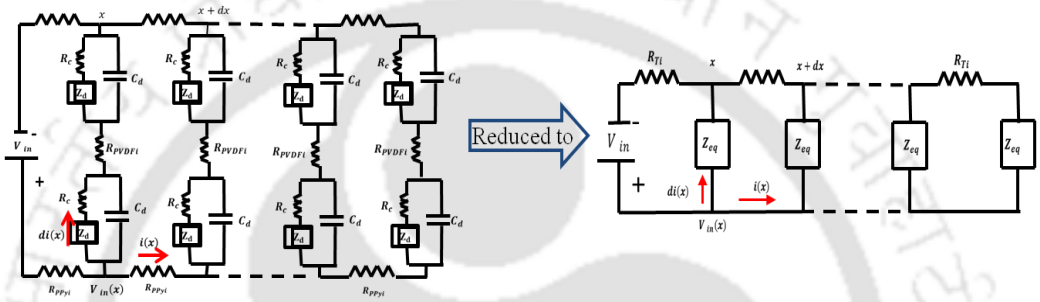

Figure.4.4. Schematic diagram of the equivalent circuit of PPy actuator

The diffusion impedance for a trilayer actuator depend on the double layer thickness (t_{dl}) and diffusion co-efficient (D) of the PPy and can be expressed as

$$z_d(s) = \frac{t_{dl}\coth\left(h_1\sqrt{s/D}\right)}{C_d\sqrt{sD}} \tag{4.3}$$

Due to the movement of $Na^+$and DBS^-, the actuator experiences the strain known as electrochemical strain, ε_{ec} as follows

$$\boldsymbol{\varepsilon_{ec}}(s) = Q(s)\alpha(s) \tag{4.4}$$

Where $Q(s)$ is the current or charge density and α is representing the strain to charge ratio. The charge density can be obtained as

$$Q(s) = \frac{I_c(s)}{sLWh_1h_2} \tag{4.5}$$

While the strain to charge ratio is a material property but varies with time as both the strain and charge density varies with time. The time dependent strain to charge ratio mathematically expressed as [43]

$$\alpha(t) = \frac{d\varepsilon_i}{dQ} \tag{4.6}$$

The strain obtained in Eq. (4.5) i.e. the electrochemical strain further combined with

mechanical properties of the actuator to generate primary mechanical output like bending displacement which is discussed in detail in the following section. As the total stress in the actuator is contributed by both electrochemical and mechanical stress, the electrochemical strain or stress will be the input to the mechanical model.

4.2.3 Mechanical Modelling

The displacement of any point of the actuator along X, Y, Z direction are represented as $u, v \; and \; s$ which mathematically expressed as

$$u = -z\frac{\partial w(x,t)}{\partial x} \; , v = 0 \text{ and } \; r = w(x,t) \tag{4.7}$$

By using the displacement, the strain can be expressed as

$$\varepsilon_x = \frac{\partial u}{\partial x} = -z\frac{\partial^2 w(x,t)}{\partial x^2}, \varepsilon_y = \frac{\partial v}{\partial y} = 0 \text{ and } \varepsilon_z = \frac{\partial r}{\partial x} = \frac{\partial w(x,t)}{\partial z} \tag{4.8}$$

The PPy actuator is considered as inextensible and there is no strain in neutral axis. In the present case the actuator exhibited viscoelastic property. For any viscoelastic material, the mechanical stress (σ) in the actuator is contributed by both elastic (σ_e) and viscous (σ_v) nature of material which can be expressed as

$$\sigma(t) = \sigma_e(t) + \sigma_v(t) \tag{4.9}$$

Here the Wiechert's viscoelastic model along with Boltzmann's superposition principle is adopted for accurate prediction of dynamics over the working time period. The mechanical stress of the actuator by using Wiechert's viscoelastic model can be expressed as

$$\sigma(t) = E_e\varepsilon + \sum_{m=1}^{n} \int_0^t E_{v_m} e^{\frac{(t-t_i)}{\tau_m}} \dot{\varepsilon}(t_i) dt_i \tag{4.10}$$

In Eq.(4.10), m is the number of Maxwell elements, n is the total number of Maxwell element required to predict the total stress accurately, t is the current time, t_i is the previous time, $t - t_i$ is the time history and $\dot{\varepsilon}(t)$ is the time dependent strain (dot sign used for first derivative with respect to time), τ_m is the time constant, E_e is the elastic modulus or equilibrium modulus, $E_e\varepsilon$ is the instantaneous stress and E_{v_m} is the spring constant in Maxwell element and μ_m is the viscosity in Maxwell element. In the above model, the nonlinear elastic and linear viscoelastic stress-strain relationship is taken into account.

The term $\sum_{m=1}^{n} E_{v_m} e^{\frac{(t-t_i)}{\tau m}}$ represents the Prony series, which is used to solve the exponential function easily. The Dirichlet-Prony series function provides smooth relaxation modulus function and simple shortcut solution to the above equation with large scale computational approximation and simple recurrence, as we have taken the total time history of the operation [114]. The relaxation modulus, $E(t)$ can be expressed mathematically from Eq. (4.10) as

$$E(t) = E_e + \sum_{m=1}^{n} \int_0^t E_{v_m} e^{\frac{(t-t_i)}{\tau m}} \tag{4.11}$$

By using Prony series the modulus in time domain can be further simplified to,

$$E(t) = E_s + E_0 \sum_m e_m \exp(-t/\tau_m) \tag{4.12}$$

here E_0 is the initial modulus at the starting point of experiment and the E_e is the long term or equilibrium modulus can be expressed mathematically as

$$E_0 = E_s + \sum_m E_m \implies E_s = E_0(1 - \sum_m e_m) \tag{4.13}$$

In the above equation, e_m is the Prony constant and can be derived as, $e_m(t) = \frac{E(t)}{E_0}$

For the dynamic condition, the strain can be expressed in sinusoidal form as the input voltage is sinusoidal as follows

$$\varepsilon(t) = \varepsilon_0 \sin \omega t = \varepsilon_0 \exp(i\omega t) = \varepsilon_0 e^{i\omega t} \tag{4.14}$$

The above strain is used as input to the mechanical model, then the output stress in terms of relaxation modulus can be expressed by using convolution theorem in Fourier transform as,

$$\sigma_w(\omega) = i\omega \int_{-\infty}^{\infty} E(t)\, e^{-i\omega t} dt\ \varepsilon(\omega) = i\omega\ E(\omega)\varepsilon(\omega) = E^c(\omega)\varepsilon(\omega) \tag{4.15}$$

In the above equation, $E^c(\omega)$ is the complex modulus and can be expressed as

$$E^c(\omega) = E'(\omega) + iE''(\omega) = E'(1 + i\eta) \tag{4.16}$$

Where $E'(\omega)$ is the storage modulus and $E''(\omega)$ is the loss modulus. The magnitude of the complex modulus can be obtained by

$$|E^c(\omega)| = \sqrt{[E'(\omega)]^2 + [E''(\omega)]^2} \tag{4.17}$$

Further the storage modulus can be expressed in terms of time constants and frequency by using Debye's relation [114] as follows

$$E'(\omega) = E_s + \sum_m \frac{E_m \omega^2 {\tau_m}^2}{1+\omega^2 {\tau_m}^2} \text{ and } E''(\omega) = \sum_m i \frac{E_m \omega \tau_m}{1+\omega^2 {\tau_m}^2} \quad (4.18)$$

The boundary conditions are

For $\omega \to 0$: $E'(\omega) = E_s \; and \; E''(\omega) = 0$

For $\omega \to \infty$: $E'(\omega) = E_s + \sum_m E_m \; and \; E''(\omega) = 0$

From storage and loss modulus we can predict the loss factor i.e. $\eta = \frac{E''}{E'}$. By using Prony series expansion and Eq. (4.18) the storage and loss modulus can be expressed as

$$E'(\omega) = E_s + E_0 \sum_m \frac{e_m \omega^2 {\tau_m}^2}{1+\omega^2 {\tau_m}^2} \text{ and } E''(\omega) = E_0 \sum_m i \frac{e_m \omega \tau_m}{1+\omega^2 {\tau_m}^2} \quad (4.19)$$

The stress in Polypyrrole is due to both electrochemical and mechanical parameters whereas stress in PVDF is only due to its mechanical property. So the viscoelastic mechanical stress in PPy and PVDF are as follows

$$\sigma_{PPy}(t) = E_{PPy_e}(\varepsilon \pm \varepsilon_i(t)) + \sum_{m=1}^{n} E_{(PPy)v_m} e^{\frac{(t-t_i)}{\tau_m}} \varepsilon(\dot{t}_i) \quad (4.20)$$

$$\sigma_{PVDF}(t) = E_{PVDF_e}\varepsilon + \sum_{m=1}^{n} E_{(PVDF)v_m} e^{\frac{(t-t_i)}{\tau_m}} \varepsilon(\dot{t}_i) \quad (4.21)$$

The "$\pm$" has been used for opposite direction of charge transfer due to opposite potential for a trilayer symmetric structure. The redox reaction leads to simultaneous expansion and contraction of the both layer of PPy causes bending in the cantilever like actuator.

The dynamic equation of motion of the actuator can be formulated by using extended Hamilton's principle which can be expressed mathematically as

$$\int_{t_1}^{t_2} (\delta L + \delta W_{nc}) dt = 0 \quad (4.22)$$

In Eq. (4.22), δL is the Lagrangian Function which can be expressed as, $\delta L = \delta T - \delta U$ while W_{nc} is the work done by non-conservative force, δT is the total variation in kinetic energy and δU is the total strain energy of applied force.

The total variation in kinetic energy of the actuator can be expressed as

$$\delta T = \frac{1}{2} \int_0^L m_a \left(\frac{\partial w(x,t)}{\partial t}\right)^2 dx \quad (4.23)$$

Where $m_a = 2\rho_{PPy}A_{PPy} + \rho_{PVDF}A_{PVDF}$, is the mass of the actuator consisted two layers of PPy and one layer of PVDF. The strain energy can be expressed as

$$\delta U = \int_0^V \sigma_a \delta\varepsilon dV \tag{4.24}$$

$\sigma_a = 2\sigma_{PPy} + \sigma_{PVDF}$ is the total stress in the actuator and $\delta\varepsilon$ is the variation of strain along the x direction. Hence the Eq. (4.24) can be upgraded as

$$\delta U = \int_0^V \sigma_a \left(-z\frac{\partial^2\delta(x,t)}{\partial x^2}\right)dV = \int_0^L M_a \left(\frac{\partial^2\delta(x,t)}{\partial x^2}\right)dx \tag{4.25}$$

M_a is the total bending moment of the actuator and can be expressed as

$$M_a = \int_A \sigma . h_3 dA = W\left[\int_{h_1}^{h_2} \sigma_{u_{PPy}} h_3 dy + \int_{-h_1}^{h_1} \sigma_{PVDF} h_3 dy + \int_{-h_1}^{-h_2} \sigma_{l_{PPy}} h_3 dy\right] \tag{4.26}$$

By substituting Eq. (4.20 & 4.21) in Eq. (4.26), the actuator bending moment can be obtained as

$$M_a = \left\{2E_{PPy_e} I_{PPy} + E_{PVDF} I_{PVDF}\right\}\left(\frac{\partial^4 w(x,t)}{\partial x^4}\right) + (2E_{(PPy)v_m} I_{PPy} + E_{(PVDF)v_m} I_{PVDF}) \sum_{m=1}^{N} \int_0^t e^{\frac{(t-t_i)}{\tau_m}} \frac{\partial^5 w(x,t)}{\partial x^4 \partial t} - 2WE_{PPy_e}\left(\int_{h_1}^{h_2} Q(x.t)\alpha h_3 dy + \int_{-h_1}^{-h_2} Q(x.t)\alpha h_3 dy\right) \tag{4.27}$$

Where I is the moment of inertia and can be expressed as, $I = \frac{Wh^3}{12}$. From the equation it can be observed that the total bending moment of the actuator is contributed by conservative force (1st term), non conservative force (2nd term) and voltage induced bending moment (3rd term). The voltage induced electrochemical bending moment can be written as

$$M_e = 2WE_{PPy_e}\left(\int_{h_1}^{h_2} Q(x.t)\alpha h_3 dy + + \int_{-h_1}^{-h_2} Q(x.t)\alpha h_3 dy\right) \tag{4.28}$$

4.2.4 Hydrodynamic Model

While the actuator operates in water medium hence the fluid force act on the actuator due to the added mass and drag can be expressed as

$$F_{fluid} = -f_m - f_d \tag{4.29}$$

The added mass is defined as the fluid force applied to a structure by the inertia of the fluid displaced by the structure as it moves [115]. The inertia of the added mass has the same sign, frequency and phase as the inertia of the vibrating structure.

Therefore, the added mass may be expressed as an added mass per unit length along the length of the beam. For the immersed cantilever beam, the force due to the added mass per unit length is

$$f_m = \frac{\pi}{4}\rho_f W^2 c_m \frac{\partial^2 w(x,t)}{\partial t^2} \tag{4.30}$$

Where c_m, is the mass or inertial co-efficient which can be determined experimentally. The drag force, unlike the force due to the added mass, is a nonlinear force that always opposes the motion of the actuator. While in some instances it is possible to linearize the drag force, the classical drag expression shall be used for this analysis. Therefore, the drag force is expressed as

$$f_d = -\frac{1}{2}A\rho_f c_d \left|\frac{\partial w(x,t)}{\partial t}\right| \frac{\partial w(x,t)}{\partial t} \tag{4.31}$$

Where c_d is the drag coefficient. Further due to hydrodynamic force the work done is categorized as non conservative and can be expressed by using Eq. (4.29) as

$$\delta W_{nc} = F_{fluid}dt = (-f_m - f_d)dt \tag{4.32}$$

The equation of motion from Hamilton's method can be upgraded with Eq. (4.30 & 4.31) as

$$\left(2E_{PPy}{}_e I_{PPy} + E_{PVDF} I_{PVDF}\right)\frac{\partial^4 w(x,t)}{\partial x^4} + \left(m_a + \frac{\pi}{4}\rho_f W^2 c_m\right)\frac{\partial^2 w(x,t)}{\partial t^2} +$$
$$\left(2E_{(PPy)v_m} I_{PPy} + E_{(PVDF)v_m} I_{PVDF}\right)\sum_{m=1}^{N}\int_0^t e^{\frac{(t-t_i)}{\tau_m}}\frac{\partial}{\partial t}\frac{\partial^4 w(x,t)}{\partial x^4} +$$
$$\frac{1}{2}A\rho_f c_d \left|\frac{\partial w(x,t)}{\partial t}\right|\frac{\partial w(x,t)}{\partial t} = \frac{\partial^2 M_e(x,t)}{\partial x^2} \tag{4.33}$$

The boundary conditions for cantilever like actuator are,

$$w(0,t) = 0 \qquad \frac{\partial w(0,t)}{\partial x} = 0$$

$$M_a(L,t) = 0 \qquad \frac{\partial M_a(L,t)}{\partial x} = 0$$

Further simplification the above equation by using Eq. (4.11 & 4.19) can be expressed as

$$\left(2E_{PPy}{}_e I_{PPy} + E_{PVDF}{}_e I_{PVDF}\right)\frac{\partial^4 w(x,t)}{\partial x^4} + \left(m_a + m_f\right)\frac{\partial^2 w(x,t)}{\partial t^2} + c_f\frac{\partial w(x,t)}{\partial t} +$$
$$\sum_{m=1}^{N}\left(2E_{(PPy)v_m} I_{PPy} + E_{(PVDF)v_m} I_{PVDF}\right)\frac{i\omega\tau_m}{1+i\omega\tau_m}\frac{\partial}{\partial t}\frac{\partial^4 w(x,t)}{\partial x^4} = \frac{\partial^2 M_e(x,t)}{\partial x^2} \tag{4.34}$$

Thus the governing equation of motion of the PPy actuator operates in underwater medium can be expressed as

$$(E_eI)_{eq}\frac{\partial^4 w(x,t)}{\partial x^4}+\left(\sum_{m=1}^{N}(E_mI)_{eq}\frac{i\omega\tau_m}{1+i\omega\tau_m}\right)\frac{\partial}{\partial t}\frac{\partial^4 w(x,t)}{\partial x^4}+\left(m_a+m_f\right)\frac{\partial^2 w(x,t)}{\partial t^2}+c_f\frac{\partial w(x,t)}{\partial t}=\frac{\partial^2 M_e(x,t)}{\partial x^2} \quad (4.35)$$

Where,

$$2E_{PPy}{}_eI_{PPy}+E_{PVDF}{}_eI_{PVDF}=(E_eI)_{eq},\quad m_f=\frac{\pi}{4}\rho_f W^2 c_m,\quad c_f=\frac{1}{2}A\rho_f c_d\left|\frac{\partial w(x,t)}{\partial t}\right|$$

$$2E_{(PPy)v_m}I_{PPy}+E_{(PVDF)v_m}I_{PVDF}=(E_mI)_{eq} \quad (4.36)$$

4.3 Solution

For dynamic condition under sinusoidal electric voltage, the actuator generates sinusoidal bending displacement in fluid medium (w_f) can be expressed as

$$w_f(x,t)=\varphi(x)e^{i\omega t} \quad (4.37)$$

For approximate solution of $\varphi(x)$, a smooth function as an infinite series of weighted orthonormal functions is selected in combination of Eigen functions $\varphi_i(x)$ and time co-efficient $q_i(t)$ as

$$\delta_f(x,t)=\sum_{i=1}^{\infty}B_i\varphi_i(x)\,q_i(t) \quad (4.38)$$

Where subscript 'i' represent unit mode of bending, B_i represents amplitude corresponds to particular mode shape $\varphi_i(x)$ and $q_i(t)$ represents the time constant. Since the system is viscoelastically damped, the eigen function denoted by $\varphi_i(x)$ is indeed the mass normalized eigen functions of the corresponding undamped free vibration of cantilever. The general solution for the eigen function is obtained as

$$\varphi_i(x)=\sqrt{\frac{1}{m_aL}}\left[\left\{\cos\left(\frac{\beta_i}{L}x\right)-\cosh\left(\frac{\beta_i}{L}{}_i\,x\right)\right\}+\frac{\{\sin(\beta_iL)-\sinh(\beta_iL)\}}{\{\cos(\beta_iL)+\cosh(\beta_iL)\}}\left\{\sin\left(\frac{\beta_i}{L}x\right)-\sinh\left(\frac{\beta_i}{L}x\right)\right\}\right] \quad (4.39)$$

The PPy actuator behaves like a cantilever hence the boundary conditions are

At fixed end, x=0: $\varphi_i(0)=0$ and $\frac{d\varphi_i(0)}{dx}=0$

At free end, x=L: $\frac{d^2\varphi_i(L)}{dx^2}=0$ and $\frac{d^3\varphi_i(L)}{dx^3}=0$

and should satisfy the orthogonal conditions as

$$\int_0^L \varphi_i(x)\varphi_j(x)dx = \begin{cases} 1 \; for \; i = j \\ 0 \; for \; i \neq j \end{cases} \text{ for and } \int_0^L EI\varphi_j(x)\frac{d^4\varphi_i(x)}{dx^4}dx = {\omega_n}^2 \qquad (4.40)$$

On solving the characteristic equation is obtained as

$$\cos\beta_i L \cosh\beta_i L + 1 = 0 \qquad (4.41)$$

The above equation is a nonlinear equation and has infinite roots. The first five roots are $1.8751, 4.6941, 7.8598. 10.9955, 14.1372$. These values are converged to

$$\beta_i L = \frac{\pi}{2}(2i-1) \; for \; i > 5 \qquad (4.42)$$

The mode shapes $\varphi_i(x)$ of each individual mode, i, can then be plotted as a function of normalized length as shown in Fig.4.5.

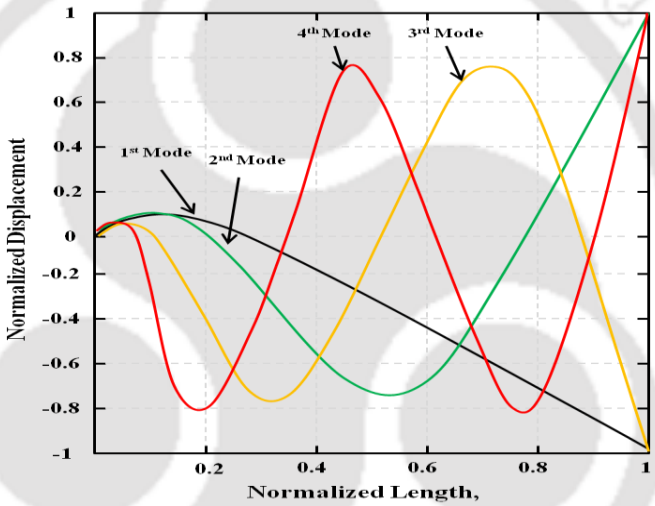

Figure 4.5 First four mode shapes of PPy actuator

In the Eq.(4.40), ω_n is the natural frequency for undamped cantilever configuration which can be obtained from the general equation as

$$\omega_n = (\beta_i)^2\sqrt{\frac{EI}{m_a L^4}} \qquad (4.43)$$

In present case, the natural frequency of PPy actuator in air, ω_{n_a} can be obtained as

$$\omega_{n_a} = (\beta_i)^2\sqrt{\frac{(E_e I)_{eq} + \left(\sum_{m=1}^{N}(E_m I)_{eq}\frac{i\omega\tau_m}{1+i\omega\tau_m}\right)}{m_a L^4}} \qquad (4.44)$$

As such, the natural frequencies and mode shapes for an immersed cantilever beam are influenced by the inclusion of added mass and the drag force. Accordingly, the natural frequencies for an immersed cantilever beam will be significantly lower

than those for a cantilever beam in air owing to the mass of the system and viscosity of the fluid environment has increased while the stiffness remains constant. When the system is operating in air, the effective mass per unit length is simply the mass per unit length of the beam, m_a neglecting the viscosity of the air medium. However, when the system is immersed in a fluid, the effective mass per unit length is the mass per unit length of the beam plus the added mass per unit length from the fluid. Therefore, by using the quality factor of Vancura model [116], the resonating frequency in fluid medium can be obtained as

$$\omega_r = |\omega_v| \left(\sqrt{1+\frac{m_f}{m_a}}\right)^{-1} \left(1-\frac{1}{2{Q_t}^2}\right)^{1/2} \tag{4.45}$$

Where Q_t is the total quality loss of the actuator in fluid medium which is contributed by both quality loss due to internal damping of actuator, Q_a and quality loss due to fluid damping, Q_f. As the internal damping of actuator is negligible as compared to fluid damping the total quality loss is equal to the quality loss due to fluid. The total quality loss can be expressed as

$$Q_t \cong Q_f = 2\pi|\omega_v| \frac{\sqrt{1+Lm_f/m_a}}{Lc_f/m_a} \tag{4.46}$$

By substitute the Eq.(4.38 & 4.40) in governing Eq.(4.35), the equation of motion yields

$$\sum_{i=1}^{\infty} B_i \left[(E_eI)_{eq}{\varphi_i}^4(x)q_i(t) + \sum_{m=1}^{2}(E_mI)_{eq}\frac{i\omega\tau_m}{1+i\omega\tau_m}{\varphi_i}^4(x)q_i\dot{(t)} + \frac{1}{2}A\rho_f c_d\left|\varphi_i(x)q_i\dot{(t)}\right|\varphi_i(x)q_i\dot{(t)} + \{M\}\varphi_i(x)q_i\ddot{(t)}\right] = \frac{\partial M_{ec}(x,t)}{\partial x^2} \tag{4.47}$$

By taking the total amplitude, $\sum_{i=1}^{\infty} B_i = B_L$, pre-multiplying $\varphi_i(x)$ and integrated over length of beam with the orthogonality conditions, Eq. (4.47) simplified as

$$B_L\left[{\omega_i}^2 q_i(t) + \frac{\sum_{m=1}^{2}(E_mI)_{eq}}{(E_eI)_{eq}}\frac{i\omega\tau_m}{1+i\omega\tau_m}{\omega_i}^2\, q_i\dot{(t)} + \frac{1}{2}A\rho_f c_d\left|q_i\dot{(t)}\right| q_i\dot{(t)}\int_0^L|\varphi_i(x)|\,{\varphi_i}^2(x)dx + q_i\ddot{(t)}\right] = \int_0^L \frac{\partial^2 M_{ec}}{\partial x^2}\varphi_j(x)dx \tag{4.48}$$

In the above equation, the right hand side term represents the actuation force i.e.

$$\frac{\partial^2 M_{ec}}{\partial x^2} = F_{ec}(x,t) = -WE_{PPy_e}\, Q(t) * \alpha\{{h_2}^2 - {h_1}^2\} \tag{4.49}$$

This is observed that the quadratic nonlinearity in the governing equation is due to the damping of fluid. However the approximate solution to the above equation due to the nonlinearity is difficult, hence the reduced to linear equation as follows

$$B_L\left[q_i\ddot{(t)} + \left(\frac{\sum_{m=1}^{2}(E_m I)_{eq}}{(E_e I)_{eq}}\frac{i\omega\tau_m}{1+i\omega\tau_m}{\omega_{n_f}}^2 + \frac{1}{2}A\rho_f c_d D\left|q_i\dot{(t)}\right|\right) q_i\dot{(t)} + {\omega_{n_f}}^2 q_i(t)\right] = F_{ec}(L,t)\varphi_i(L) \quad (4.50)$$

By further reduction

$$B_L\left[{\omega_r}^2 q_i(t) + 2\zeta\omega_r q_i\dot{(t)} + q_i\ddot{(t)}\right] = Q(t)\left[W\left(E'(\omega)\right)_{PPy} * \alpha\left\{{h_2}^2 - {h_1}^2\right\}\right] \quad (4.51)$$

The total mass, m or total damping ratio, ζ of the actuator when it operates in fluid medium is the sum of actuator mass (m_a) or viscoelastic damping with fluid added mass (m_f) and fluid damping (ζ_f) respectively as, $m = m_a + m_f$ and $\zeta = \zeta_a + \zeta_f$ respectively. The total damping co-efficient of the actuator can be expressed as,

$$c = 2m\zeta\omega_r \quad (4.52)$$

The mode shape at actuator tip i.e. $\varphi_i(L)$ can be obtained from equation as follows

$$\varphi_i(L) = \frac{2(1-sin\beta_i L\, sinh\beta_i L)}{cos\beta_i L + cosh\,\beta_i L} \quad (4.53)$$

As the input is sinusoidal the moment and hence the force varies sinusoidally as

$$F_e(x,t) = F_{e0}(x)e^{i\omega t} = -WE_{PPy_e}\, Q(t) * \alpha\left\{{h_2}^2 - {h_1}^2\right\}e^{i\omega t} \quad (4.54)$$

By using Eq.(4.51 & 4.54) the generalized time coordinate can be obtained as

$$q_i(t) = \frac{-WE_{PPy_e}\, Q(t) * \alpha\left\{{h_2}^2 - {h_1}^2\right\}}{{\omega_r}^2 + i2\zeta\omega_r\omega - \omega^2}e^{i\omega t} \quad (4.55)$$

The bending amplitude, B_L can be obtained as

$$B_L = \left(\frac{1}{m}\right)\frac{F_e(L,t)\varphi_i(L)}{q_i\ddot{(t)} + 2m\zeta\omega_r q_i\dot{(t)} + {\omega_{r_i}}^2 q_i(t)} \quad (4.56)$$

By substituting the Eq.(4.54, 4.55 & 4.57) in Eq. (4.37) the underwater bending displacement of PPy trilayer actuator tip can be obtained as

$$w_f(x,t) = \frac{Q(t)WE_{PPy_e} * \alpha\,(t)\left\{{h_2}^2 - {h_1}^2\right\}\varphi_i(x)}{{\omega_{n_f}}^2 + i2\zeta\omega_{n_f}\omega - \omega^2} \quad (4.57)$$

Similarly, the change density of the actuator can be expressed as, $Q(t) = Q_0 e^{jwt}$ and the transfer form of equation for the system thus obtained as

$$\frac{w_f(x,s)}{V_{in}} = \frac{Y(s)E_{PPy_e}\alpha\{{h_2}^2-{h_1}^2\}\varphi_j(L)}{{\omega_{n_f}}^2+i2\zeta\omega_{n_f}\omega-\omega^2} \quad (4.58)$$

The blocked force, F_b generates at the tip of the actuator due to bending of the tip can be formulated by using Castigliano's theorem as follows

$$F_b = \frac{3M_e}{2L} \quad (4.59)$$

The above equation clearly shows the blocking force depends upon the applied voltage. At the same time the blocking force can be predicted by using the bending deflection at tip in fluid medium as follows

$$F_b = \frac{3(EI)_{eq}w_f(L)}{L^3} \quad (4.60)$$

The thrust force produced due to the actuator bending can be derived from Lighthill's slender body theory [117]. By using this theory, the mean thrust of PPy actuator in fluid with flow velocity zero i.e. U=0, can be expressed in terms of bending displacement and virtual mass density, m_v as follows

$$T_f = \frac{1}{2}m_v\overline{\left(\frac{w_f(x=L,t)}{\partial t}\right)^2} = \frac{1}{2}\frac{\pi\rho_f W^2 m_c}{4}\overline{\left(\frac{w_f(x=L,t)}{\partial t}\right)^2} \quad (4.61)$$

In Eq. (4.61), m_c is the virtual mass co-efficient and $\pi\rho_f W^2 m_c/4$ is the mathematical expression of virtual mass density, m_v.

4.4 Results & Discussion

In this section, study the results are obtained from numerical solution of mathematical equations developed in previous section by using MATLAB solver with built-in curve fit functions. Then the numerical results were compared with the experimental results obtained in chapter 2 & 3, and study the validation of the developed model.

4.4.1 Electro-mechanical Characterization

For predicting the electrochemical results, the experimental values of R_{PPy}, R_{PVDF} and R_C were used in Eqs. (1) and Eqs.(2). From the impedance equation the transient current is obtained in response to the step potential of ± 0.1 V. Fig.4.6 shows the

measured actuation current along with the prediction of numerical model.

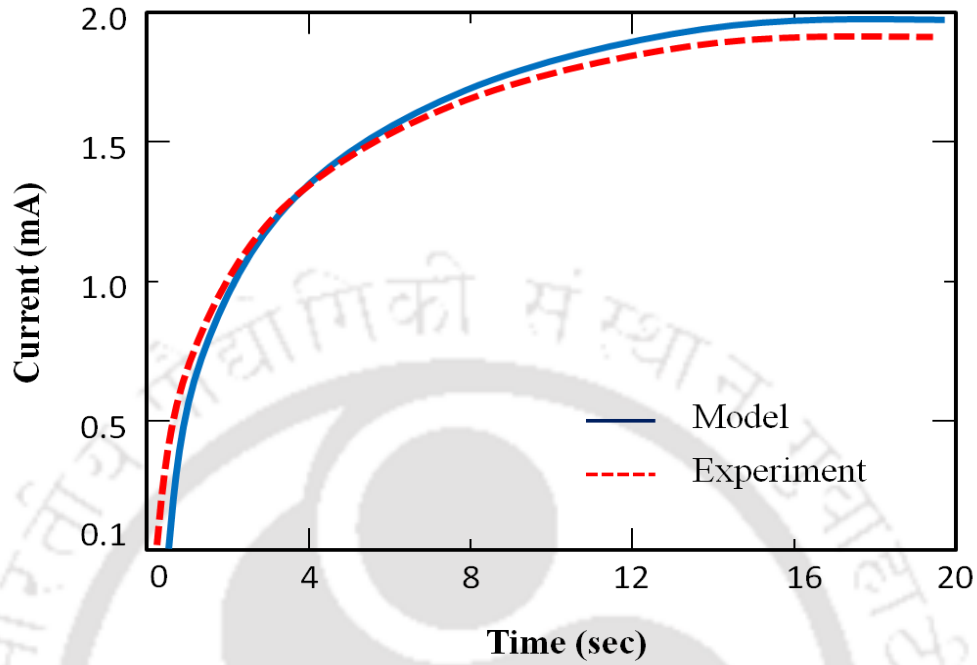

Figure.4.6 The current output in response to step voltage

It has been seen that the magnitude of initial current is low due to the surface resistance of PPy along the length. However the magnitude of the initial current is low and gradually increasing with time, the time constant is moderate hence the flow of current is stable and shows a good agreement with the experimental results.

The charge density in Eq.(4.3) is found to be time-position dependent which allows the prediction of charge and its corresponding strain along the polymer length as a function of time as shown in Fig.4.7. The degree of strain was predicted by coupling the charge transferred during the actuation with the strain to charge ratio which obtained experimentally. The present model can predict accurately the actuation response in short time also. For dynamic condition the behaviour of electrochemical strain and current in response to sine wave input voltage as shown in Fig.4.7 and Fig.4.8.

The experimental and result obtained from numerical model was compared and shown in Fig.4.7. It has been seen that the trends obtained is similar to the actuator developed earlier [16-17,31,33].

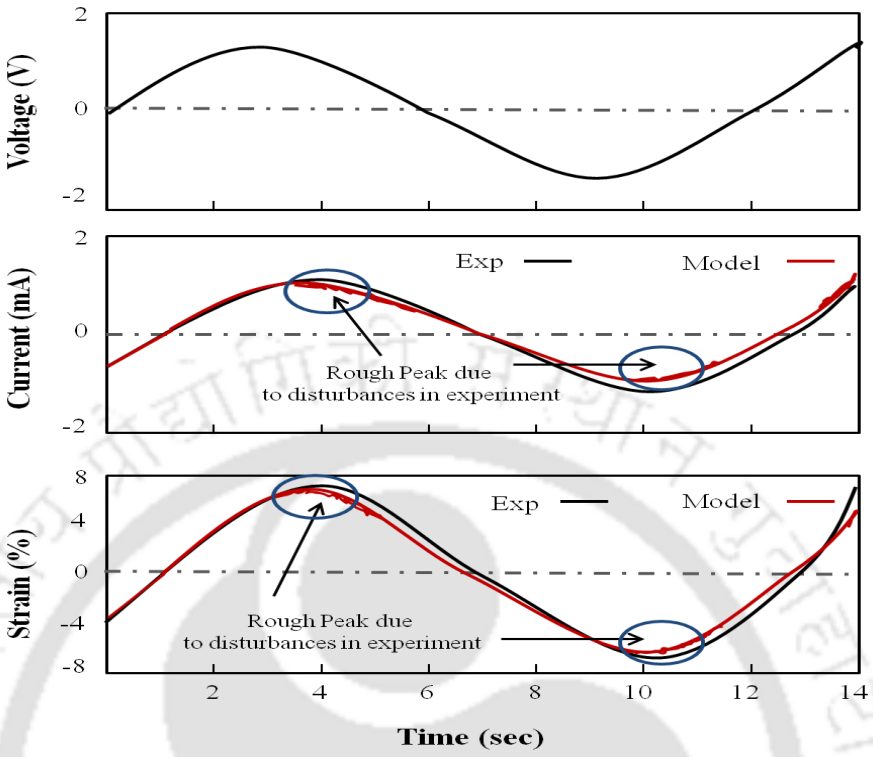

Figure 4.7 Time varying output current and strain on applying electric voltage

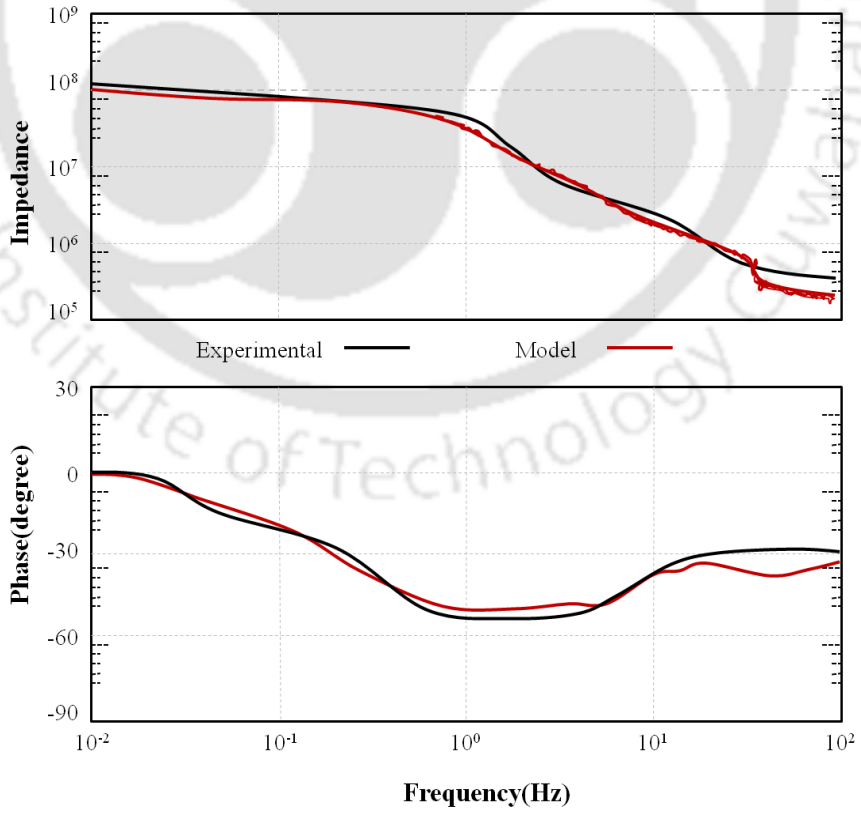

Figure.4.8 Frequency response of impedance of equivalent electrochemical circuit

The modulus of the PPy actuator is one of the important parameter for analyze the mechanical properties of the actuator. The storage (E') and loss modulus (E'') along with the loss factor ($tan\ \delta$) of the PPy actuator are obtained from the DMA analysis and numerical is shown in Fig.4.9.

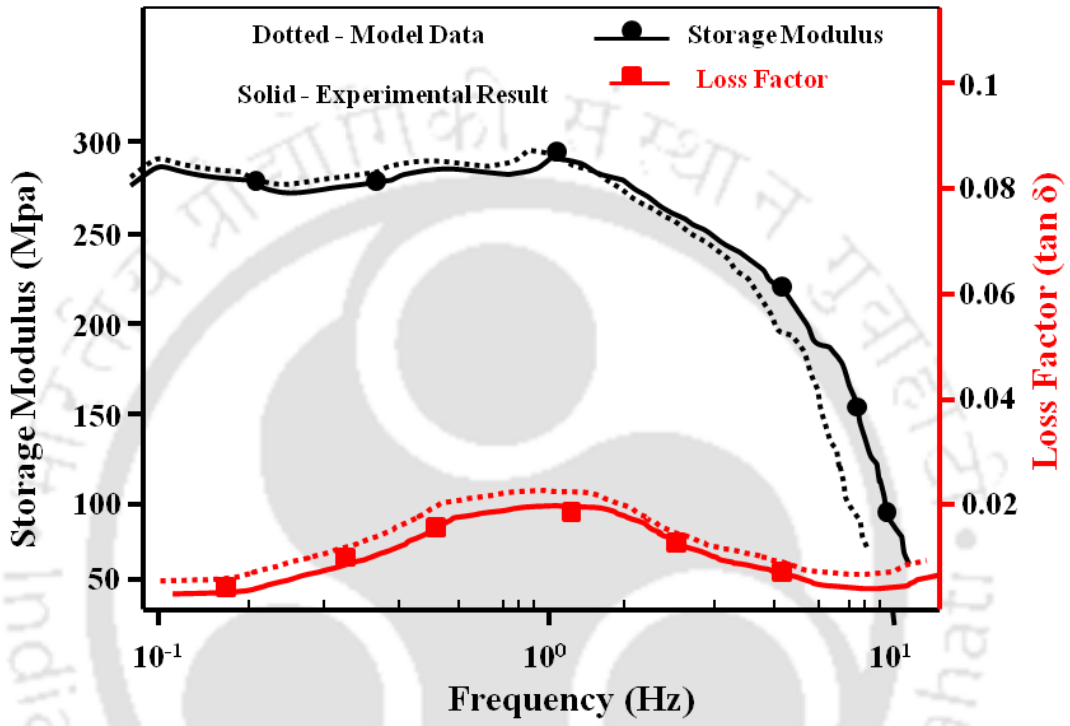

Figure 4.9 Experimental and numerical storage modulus and loss factor

The storage and loss modulus varies with frequency and hence with time. The storage elastic modulus is obtained nearly 284 MPa while the loss factor is nearly 0.024 experimentally while from numerically storage modulus is around 290 MPa and loss factor is 0.26, slightly more than the experimental value. However follow the same trend with the earlier published results [72]. The storage modulus and loss factor of the PPy actuator are function of time and determined by using fitting function. It has been observed the storage modulus and loss factor is high and stable at the actuation frequency of 1 Hz. At higher frequency, the modulus decreases rapidly due to material loss.

The relaxation modulus estimated from Eq. (4.11) is varies with time as shown in Fig.4.10. The elastic modulus of the PPy can be derived from the equilibrium modulus E_∞ in Young's relaxation modulus E(t). The modulus obtained from

DMA experiment and time dependent modulus by using Prony constants is shown good agreement with each other however the model value it little higher than experimental results even the starting value is same. The results shows that the modulus is decreasing over the time due to dissipation energy and material loss. Hence moderate enhancement of the modulus of PPy actuator helps it to operate for long time and improve the cycle life.

.

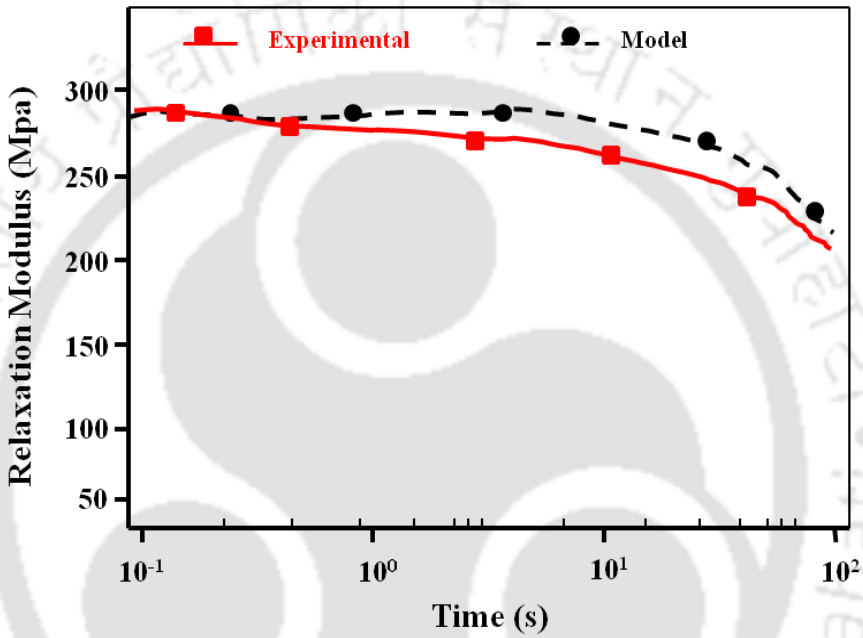

Figure.4.10 Theoretical and experimental relaxation Young's modulus vs time

The fitting function inputs are the applied stress and the measured strain as a function of time, from which the time derivative of strain is estimated. The fitting function inputs are the applied stress and the measured strain as a function of time, from which the time derivative of strain is estimated

Using the two parameters (i.e. E(t) and η), the fits function data (from the input stress and strain and the calculated strain rate) to Equation 8. Fig. 4.11 shows an example of fitting an experimental data (5 MPa at a frequency of 1 Hz) to the Weichert viscoelastic model. As shown in the figure the stress-strain response of the model using the fit parameters was in close agreement with the experimental data [33]. The waviness of the fit curve is due to the noise in the strain measurement data. The area under the curve represents the energy loss during loading and relaxation of the PPy actuator due to the viscous nature of the polymer.

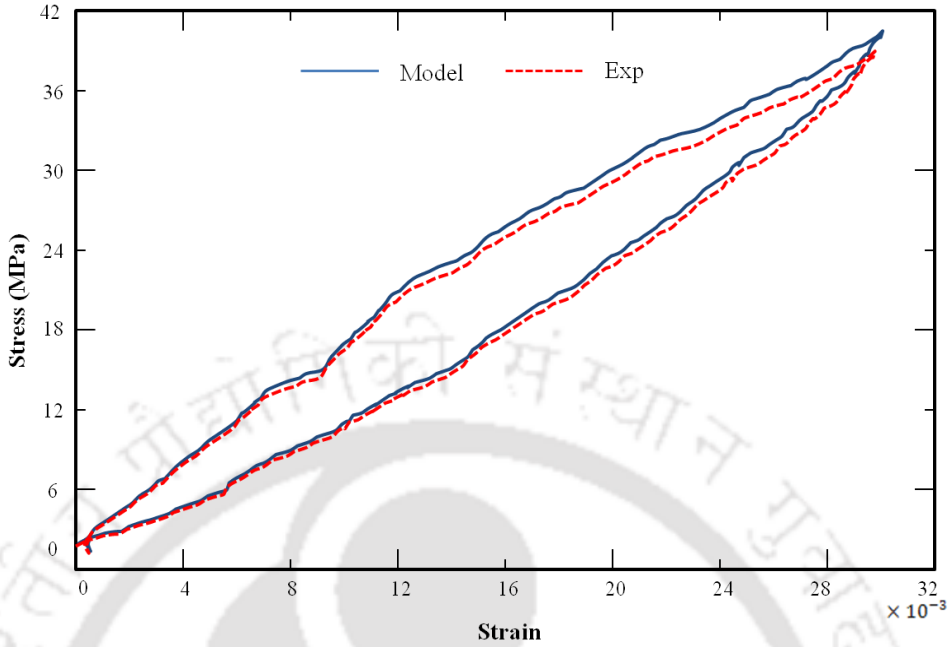

Figure.4.11 Stress-strain relationship of PPy actuator

4.4.2 Underwater Bending Characterization and Performance Analysis

Here, the dimensions of the PPy trilayer actuator used were 30 mm × 8 mmx0.15mm where 30 mm is the free length is. The actual length of actuator is 35 mm while 0.5 mm has been used to fix the actuator in electrode holder. Theoretical bending displacement is obtained from Eq.(4.57) is shown in Fig.4.12.

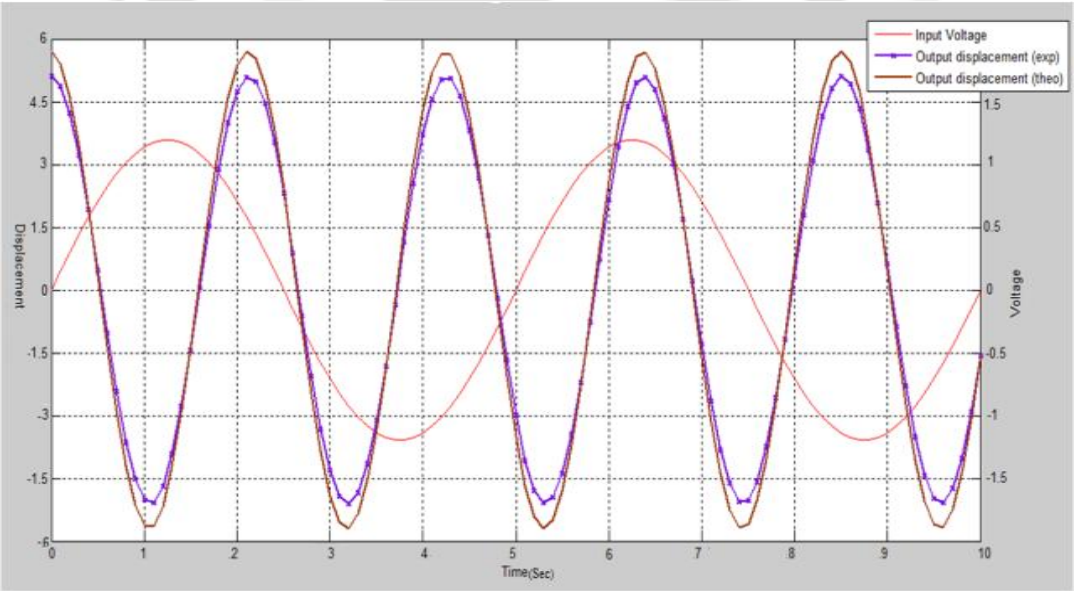

Figure.4.12 Time varying voltage and displacement of PPy actuator

The maximum bending displacement is estimated as 5.6 mm at 1.3 V while the displacement is obtained from experiment is 5.4 mm and in both cases the displacement is sinusoidal in nature as the input voltage is sinusoidal. Here, the bending displacement is significantly higher as compared to the other smart actuator including PPy actuator developed earlier [57,58]. Fig.4.13 shows the FRF of the underwater bending displacement of the PPy actuator

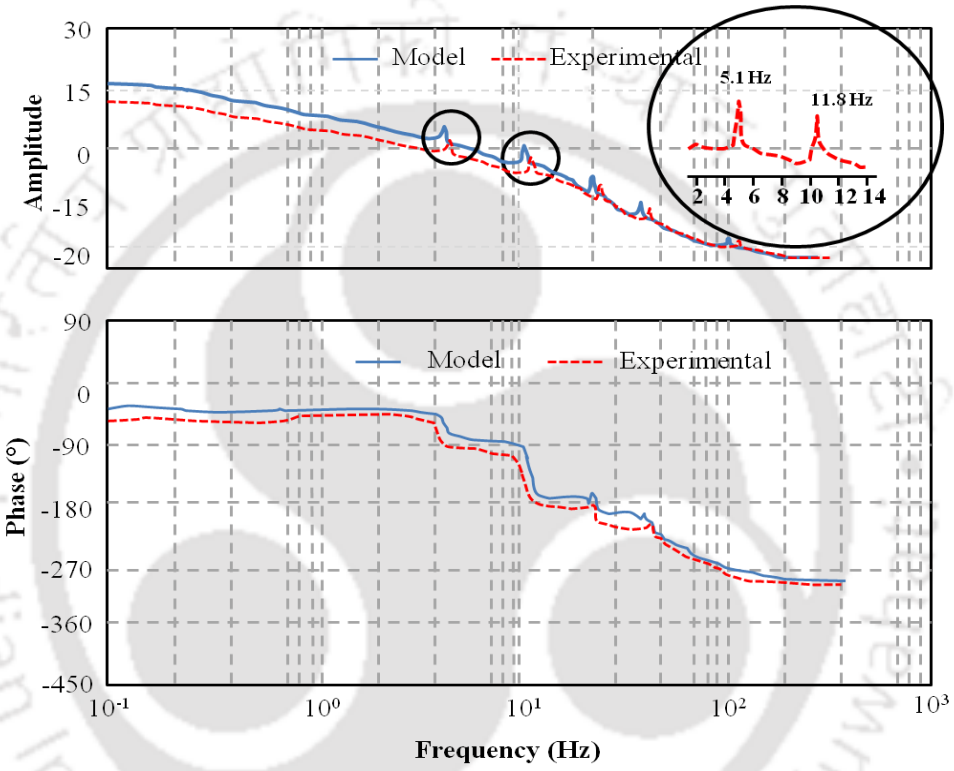

Fig.4.13 Frequency response of bending displacement of PPy actuator

From the frequency response of the displacement, the first resonating frequency observed at nearly 5.1 Hz and the second, third and fourth observed at nearly 11.8 Hz, 28 Hz. It has been seen there are nearly 2-3 % variation in frequencies obtained through analytical model and experimental results as shown in Fig.4.13. The damping ratio can be estimated from the vibration of PPy actuator

The FRF of the velocity curve is shown in Fig.4.14 which is obtained by using the modal damping ratio, drag and inertia coefficient which calculated experimentally. From this figure it has been confirmed the first natural frequency is around 5.5 Hz, which is significantly more than the recently developed IPMC and PZT based actuator [103, 105, 112].

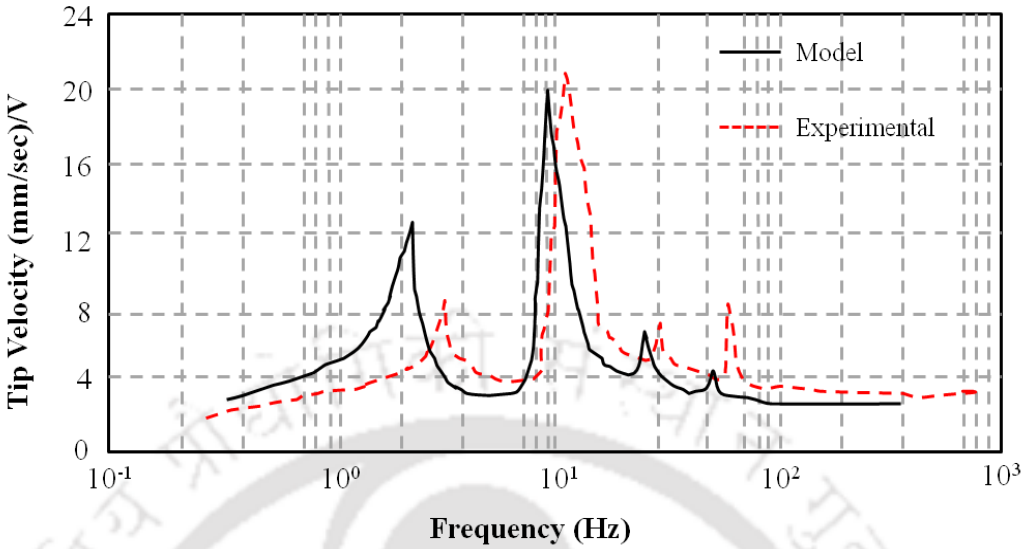

Figure.4.14 Tip velocity of PPy actuator with actuation frequency

From Eq. (4.46) and Eq. (4.52), the total damping of the actuator is estimated as o.042 while the actuator exhibits viscoelastic damping of 0.012 (estimated in previous chapter), hence the damping due to fluid is around 0.031. The damping due to fluid significantly more than the structural damping which affects the bending performances of the underwater actuator to a great extent. Tough the structural damping is very small; the responses are approximately linear while the actuator experiences non linear behaviours due to the fluid damping, discussed in Chapter 5. As the displacement varies with the input frequency, the tip velocity is also varying with the input frequency as shown in Fig.4.15. The experimental and numerical tip

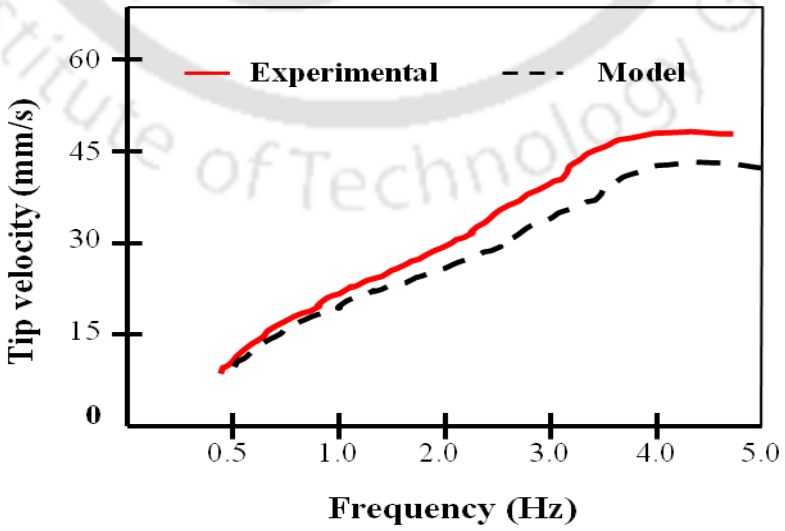

Figure 4.15 Experimental and theoretical tip velocity vs actuation frequency

velocity of the PPy actuator with the input frequency is compared and analyzed. Although slight difference has noticed in the results, both follow the same pattern and the high velocity at higher frequency and lower displacement.

Fig.4.16 shows the experimental tip force in comparison with force predicted from Eq. (4.59). The force generated due to bending is obtained from the physical balance as 4.2 mN while from numerical model it is estimated as 4.5 mN and follows the same pattern as the input voltage. As the force is generated by the blocking strength

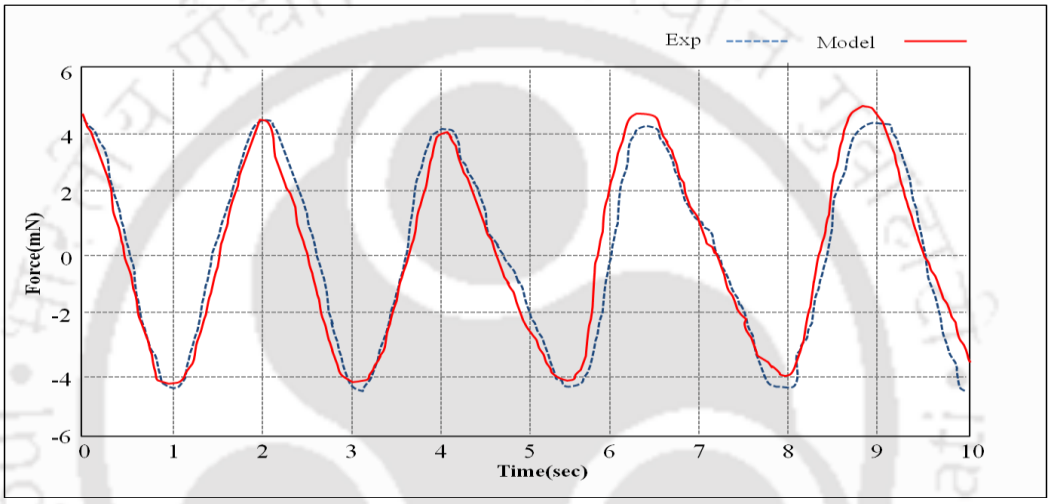

Figure.4.16 Time varying tip force of PPy actuator on applying sinusoidal voltage

of the actuator, hence the tip force is decreases with increase in displacement. Fig.4.17 shows the experimental and model tip force vs actuation frequency.

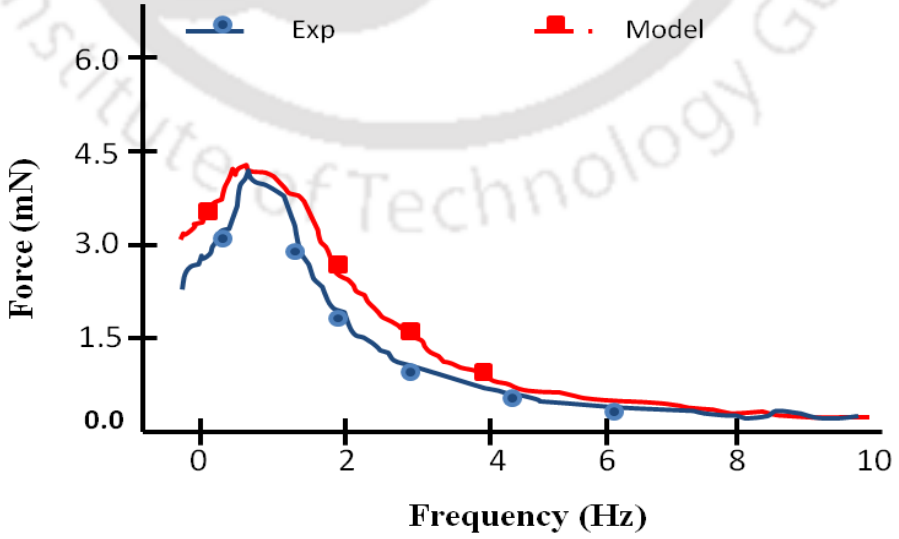

Figure.4.17 Frequency dependent tip force in underwater environment

From both theoretical and experimental results it has been observed that the actuator exhibits higher tip force at nearly 1 Hz as the displacement is also higher at this frequency. At higher frequencies, the ions could not get enough time to travel in the PPy chain; hence the strain is low which leads to displacement and subsequently the force decreases. Although there is little difference in results both follow the similar trend and it is believed that due to underwater noise and disturbances.

In the present work, the combination of displacement and force with optimum actuation voltage and frequency confirms the improvement in the bending performance of PPy actuator in underwater environment which makes it suitable for underwater propulsion applications.

4.4.3 Hydrodynamic Performances of Au-PPy actuator

The primary hydrodynamic performance for any underwater locomotives is the thrust and thrust co-efficient. Time varying thrust force generated under AC potential is shown in Fig.4.18.

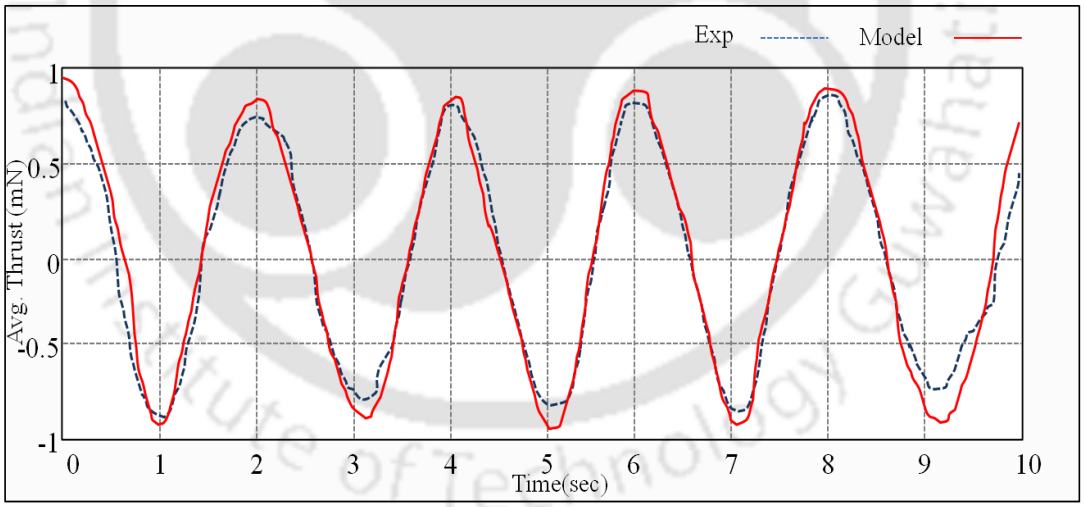

Figure.4.18 Time varying thrust for of PPy actuator for sinusoidal voltage

The maximum thrust is estimated as nearly 1mN and average thrust over 6 actuation cycle is obtained as 0.84mN. The trend has shown good agreement with the published results [82, 85, 87, 112].

The frequency response of thrust has revealed that the dominant resonance is at 1Hz and this frequency the maximum thrust can be observed as shown in Fig.4.19.

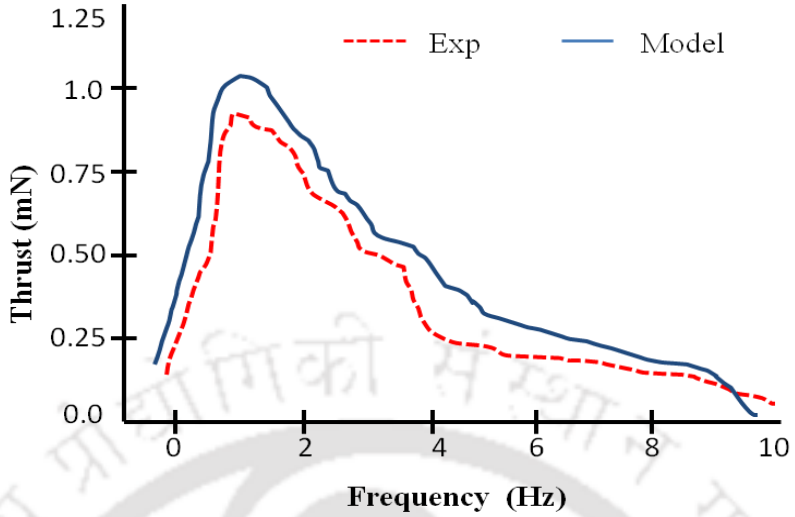

Figure.4.19 Thrust force in underwater environment vs frequency

Further it can be observed that at zero displacement the thrust is also zero and the thrust frequency is twice of actuation frequency. The thrust is follow the same behaviour as the displacement i.e. one can observe the maximum thrust nearly at the displacement peak and the phase lag is same as of displacement with input voltage. Tough the thrust is related to displacement, it may be believed that it also slightly depend on voltage amplitude. With the increases of amplitude the thrust peak is shifted along the increase in amplitude. From the results it can be observed that the hydrodynamic effects are relating to the actuator geometry; particularly at the tail end and its effect on thrust production. Similarly the thrust co-efficient is also varies with frequency as shown in Fig.4.20.

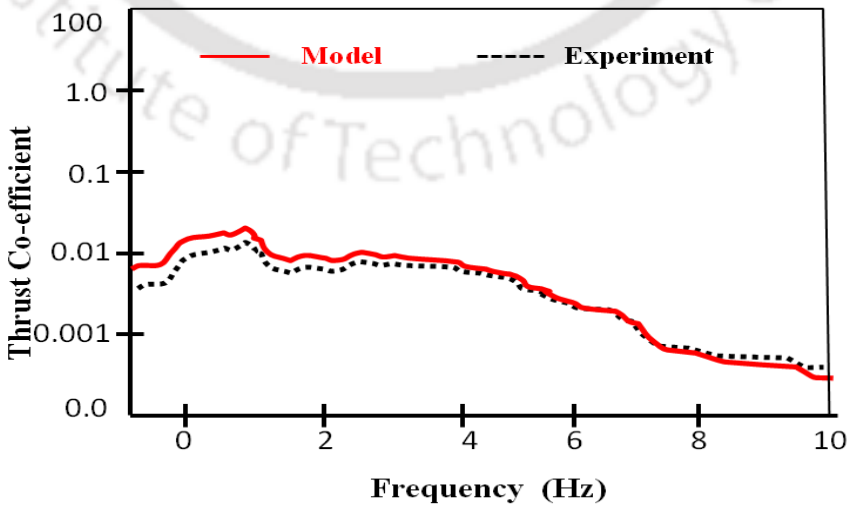

Figure.4.20 Theoretical and experimental thrust coefficient of PPy actuator

Fig.4.21 shows the variation in power consumption with input frequency. As the frequency is increases the power consumption is increases. The power consumed by the PPy actuators is further dependent on the input voltage, actuator geometry and size of mobile ion due to which the actuation occurs. As the size of the PPy actuator increases, the rate of charge transfer increases and subsequently consumes more power. The actuation voltage of the PPy actuator is found as 0.54 V but at this voltage the redox reaction is very slow which generates very low displacement.

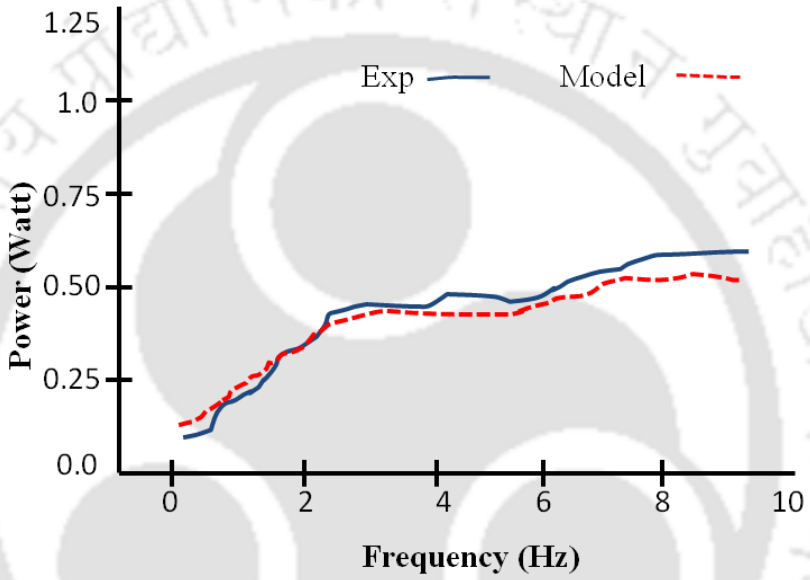

Figure.4.21 Power consumption vs actuation frequency of PPy actuator

However the maximum and steady displacement is produced at a voltage of 1.3V and 1Hz, beyond this point the performances are not steady due to loss of material leads to increases the output current, hence the power consumption increases. Further at higher voltage, electrolysis of water takes place which only consumes more power without any aid to the thrust generation. The result predicts the nonlinear relation between the power consumption and frequency at higher actuation frequency. The power consumption is calculated as average power as the data recorded for eight to ten actuation cycle to enhances the accuracy.

The effectiveness of the PPy actuator is estimated from the ratio of average thrust to power consumption. The effectiveness of the actuator in response to actuation frequency is shown in Fig.4.22. It has been seen that the trends shows the similar patterns as reported earlier with significant improvements [103]

Tough the effectiveness is primarily depending upon thrust and power consumption; it varies with the frequency of operating voltage.

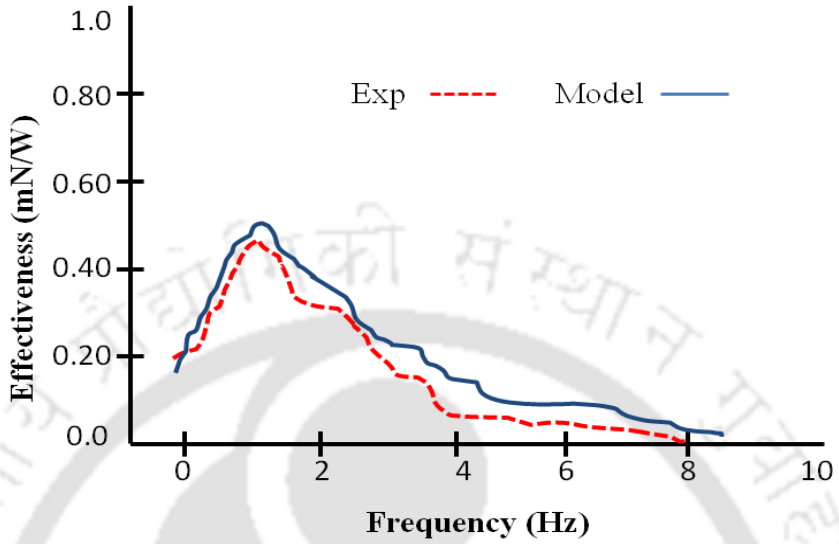

Figure 4.22 Effectiveness vs Frequency for the PPy underwater actuator

By increasing the frequency the power consumption increases which ultimately decreases the effectiveness or particularly the efficiency of the underwater actuator. The effectiveness of the present actuator is around 0.48 and has good agreement with the earlier published trends [113].

Here, the bending displacement, force and hence thrust is large as compared to the earlier reported actuators [112, 118, 111, 105, 108] however the delay is slightly more.

4.5 Summary

In this chapter, underwater actuation and bending of the PPy actuator is modelled to study the hydrodynamic bending performances. The model developed by considering electrochemical actuation of the cantilever like actuator for estimating the mechanical output like bending displacement, thrust and efficiency. Further the viscoelastic time dependent modulus has taken into consideration to predict the accurate performances in dynamic condition. The numerical results were estimated by using MATLAB programming with curve fitting function.

In section 4.3, modelling of bending characteristics following Euler-Bernoulli and pseudo-rigid body modelling approach for cantilever like trilayer actuator is

formulated in transfer function form, assuming it as a single layer multi-degree of freedom cantilever. An energy-based dynamic model has been derived using the Lagrange principle. Simulations are performed to demonstrate the bending response for various input voltages. The results demonstrate the gradual reduction of bending response of an actuator owing to high voltage and frequency in underwater medium. The frequency response analysis has been carried out for hydrodynamic bending displacement to estimate the tip velocity of the actuator. The results obtained here were shown a good agreement with the published results which makes it suitable for exploring its underwater application as propulsor.

5

Effect on Nonlinear Hydrodynamic Damping on Gold-Polypyrrole Actuator

5.1 Introduction

The operating or working medium of polypyrrole (PPy) actuator affects the performances of the actuator and plays a major role in estimating the accurate dynamics of the system. Generally, when the wing and fin like structures undergoes bending, the surrounding fluid gives rise to fluid forces that depend nonlinearly on the structural motion. In the recently developed underwater actuator, the effect of the fluid forces is considered as linear and studied only the effect of added mass acting on the actuator operating in underwater medium [119-121]. However, in order to develop a real time underwater propulsive system, the effect of nonlinear fluid damping is essential to predict the accurate dynamics and precise motion of the system. Past literatures showed that little research has been carried out to study the nonlinear response of the PPy actuator operating in liquid medium. This work is primarily focused to predict the nonlinear response of PPy actuator bending in underwater medium by developing a theoretical model followed by experimental validation.

The nature of the fluid loading on sinusoidal bending structure and the fluid flow theory used for modelling depend on the bending amplitude. Flexible structures like flapping wings, undulating fins and propulsive structures operate at moderate to large amplitudes to actuate large volumes of the surrounding fluid. When structures oscillate with amplitudes comparable to their characteristic length, the effects of the fluid viscosity in inducing vortex shedding is essential to consider. In such situations, the vortices shed from the structure's sharp edges produce a damping effect on the structural bending [122] Furthermore, this damping force depends

nonlinearly on the structural amplitude and frequency [123]. In this work, the vortex-shedding induced damping in rectangular PPy strip actuator is explored where the bending amplitudes are comparable to their widths. The focus is on developing experimentally validated theoretical models, which help to study the nonlinear bending responses of the PPy actuator along with the vortex-shedding-mechanism that generates the damping force.

Vortex is a region in a fluid in which the flow revolves around an axis line, which may be straight or curved. Kármán vortex street is a repeating pattern of swirling vortices, caused by a process known as vortex shedding, which is responsible for the unsteady separation of a fluid around blunt bodies. The shedding of these vortices imparts a periodic force on the object. The force is quite small and not enough to accelerate the object to any significant amount, especially if the object is relatively massive. If the object is flexible and light weight such that the object can vibrate about a fixed position, then the possibility of simple harmonic motion; and if the frequency of the periodic driving force matches the natural frequency of the oscillation, then resonance obtains and the amplitude of the oscillations can be significant [124,125].

For the nonlinear response analysis, three non-dimensional parameters, namely the Keulegan–Carpenter (KC) number, Reynolds number and the frequency parameter β, have been identified that governs the phenomenon of vortex-shedding-induced damping for flexible PPy actuator bending in quiescent fluid. The KC number signifies the distance that a fluid particle travels compared to the characteristic length of the structure before the fluid reverses the direction of flow, and is crucial for determining the size and the strength of the shed vortices as well as the nature of the fluid force acting on the structure [126]. The KC number mathematically defined as,

$$KC = \frac{2\pi A_b}{L} \tag{5.1}$$

Where A_b is the amplitude of bending envelop, L is the length of the actuator. The frequency parameter β signifies the importance of the unsteadiness of the fluid flow relative to the rate at which the fluid viscosity diffuses momentum in the fluid and can be expressed as

$$\beta = \frac{L^2 \omega}{2\pi\nu} \tag{5.2}$$

where ω is the angular frequency of bending and ν is the kinematic viscosity of the fluid. The Reynolds number (Re) indicates whether fluid flow past a body is steady or turbulent, can be expressed for flows around such periodic bending structures is the product of KC and β, as

$$Re = KC \times \beta = \frac{A_b L \omega}{\nu} \tag{5.3}$$

Specifically, we present experimental results for the hydrodynamic damping of PPy actuator with low KC numbers (ranging from 0 to 3) and moderately high values of β (ranging from 100 to 1200).

In this chapter, the nonlinear response of an underwater operated PPy actuator is analysed in a fixed-free configuration with Euler Bernoulli beam assumption with the effect of nonlinear hydrodynamic damping. Following the modelling, the PPy actuator is fabricated and experiments are conducted to validate the theoretical model and studied the nonlinear behaviour of PPy actuator operating in underwater medium under AC electric potential.

5.2 Mathematical Modelling

A nonlinear model is developed for PPy actuator operating in underwater medium taking into account of the hydrodynamic bending characteristics of the PPy actuator. This model will be suitable for any PPy actuator to evaluate and show the nonlinear response. The analysis will help to study the stability of the system under alternating electric potential.

5.2.1 Governing Equation of Motion

In the present work, rectangular beam like trilayer Polypyrrole actuator is considered having length L and area of cross section A, operated in an open face water tank having quiescent water. The actuator experiences nonlinear behaviour due to the surrounding quiescent water medium, hence this chapter only focuses on the nonlinear hydrodynamic loading effect on PPy actuator and all other material properties and working conditions will remain same as used in Chapter 4.

A schematic diagram of the flexible PPy cantilever actuator along with the XYZ coordinate system is shown in Fig.5.1. L is the length of the PPy actuator and W is the width of the actuator. The PPy actuator exhibits viscoelastic material property and its out-of-plane bending displacement in XZ plane is denoted by $w(x,t)$.

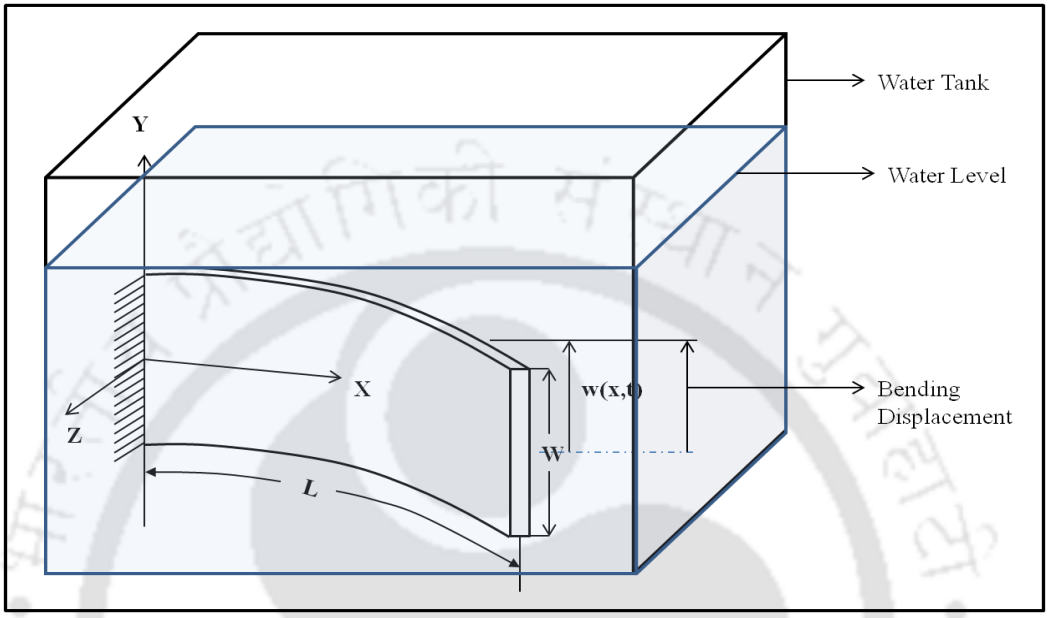

Figure 5.1. Schematic diagram of PPy actuator operates in underwater medium

Assuming that the wavelength of the bending motion is large and the slope of the deflection is small, the motion of the actuator as modelled using the Euler–Bernoulli beam theory. The equation of motion of the viscoelastic PPy actuator working under sine wave input voltage can be expressed by using Eq.(4.27) and Eq.(4.36) as follows,

$$(E_eI)_{eq}\left(\frac{\partial^4 w(x,t)}{\partial x^4}\right)+\left\{\left(\sum_{m=1}^{N}(E_mI)_{eq}\frac{i\omega\tau_m}{1+i\omega\tau_m}\right)\frac{\partial^4 w(x,t)}{\partial x^4}\right\}\frac{\partial w(x,t)}{\partial t}+m_a\frac{\partial^2 w(x,t)}{\partial t^2}=F_{ec}(x,t) \quad (5.4)$$

where $(E_eI)_{eq}$ is the equivalent modulus of the trilayer actuator due to the elastic component, $(E_mI)_{eq}$ is the equivalent modulus of the trilayer actuator due to viscous component (m is the unit Maxwell element). The actuator is modelled by using Wiecherts viscoelastic model with total N number Maxwell element as discussed in chapter 4. F_{ec} is the electrochemical actuation force generated on applying external voltage to the actuator, m_a is the mass of the actuator, ω is the angular frequency of actuation, τ_m is the time constant of viscoelastic model. As the PPy actuator

working in underwater medium, force due to surrounding is acting on the actuator. The Eq. (5.4) can be upgraded with the fluid force as,

$$(E_eI)_{eq}\left(\frac{\partial^4 w(x,t)}{\partial x^4}\right)+\left\{\left(\sum_{m=1}^{N}(E_mI)_{eq}\frac{i\omega\tau_m}{1+i\omega\tau_m}\right)\frac{\partial^4 w(x,t)}{\partial x^4}\right\}\frac{\partial w(x,t)}{\partial t}+m_a\frac{\partial^2 w(x,t)}{\partial t^2}=F_{ec}(x,t)+F_f(x,t) \quad (5.5)$$

Where F_f is the fluid force acting on the actuator. The boundary conditions are

At fixed end, $x=0; w(0,t)=0$ and $\frac{dw(0,t)}{dx}=0$

At free end, $x=L; \frac{d^2w(L,t)}{dx^2}=0$ and $\frac{d^3w(L,t)}{dx^3}=0$ (5.6)

For making the calculation simpler, non-dimensionalize the axial direction terms with the length L and the remaining two spatial directions with half-width $\left(\frac{W}{2}\right)$ of the actuator as the actuator is symmetric along the width and thickness. Taking the Fourier transform of Eq. (5.5) and after some rearrangement we obtain:

$$(E_eI)_{eq}\,w_{xxxx}(x,w)+\left\{\left(\sum_{m=1}^{N}(E_mI)_{eq}\frac{i\omega\tau_m}{1+i\omega\tau_m}\right)\,w_{xxxx}(x,w)\right\}w_t(x,w)-\left\{w(x,\omega)+\left(\frac{\rho_fW^2}{m_a}\right)\frac{F_f(x,\omega)}{\rho_fW^2\omega^2}\right\}m_a\omega^2=F_{ec}(x,\omega) \quad (5.7)$$

where, $()_x=\frac{\partial()}{\partial x}$, $()_t=\frac{\partial()}{\partial t}$, ρ_f is the fluid density, $\frac{m_a\omega^2L^4}{(E_eI)_{eq}+\left(\sum_{m=1}^{N}(E_mI)_{eq}\frac{i\omega\tau_m}{1+i\omega\tau_m}\right)}$ represents the flexibility of the beam relative to the beam inertia and the fluid force, and $\frac{\rho_fW^2}{m_a}$ represents the fluid to actuator mass ratio and characterizes the extent of fluid loading. It is assumed that the underwater medium surrounds the actuator is incompressible, inviscid with zero flow velocity. For large lengths $(L\gg W)$, the fluid flow along the X direction is small as compared to other two direction, hence the 2D plane parallel to YZ plane is considered for surrounding fluid. The governing equation for motion of the surrounding fluid is

$$\nabla^2p=0 \quad (5.8)$$

where ∇^2 is the Laplace operator and p is the velocity potential at a particular point on the actuator located at $x=x_p$ and denoted $p(y,z,t)$. The nonlinear boundary condition for the fluid flow is obtained by matching the velocity of the beam with the normal velocity of the fluid along the z direction, and is represented as

$$\phi_z=w(x_p,t) \quad (5.9)$$

By adopting the proposed method [127], a boundary integral method is used to express the complex-conjugate velocity field $\varsigma(\chi, t)$, where $\chi = y + iz$ acts as a combination of the flow fields caused by a actuator-bound vortex sheet and two free vortex sheets emanating from the edges of the beam. Then the complex-conjugate velocity field can be written as [130]

$$\varsigma(\chi, t) = \frac{1}{2\pi i}\left[\int_{l(t)} \frac{\phi(\lambda,t)}{\lambda-\chi} d\lambda + \int_{l_u(t)} \frac{\phi_u(\lambda,t)}{\lambda-\chi} d\lambda + \int_{l_l(t)} \frac{\phi_l(\lambda,t)}{\lambda-\chi} d\lambda\right] \quad (5.10)$$

where, $l(t)$ represents the vortex sheet for actuator surface, $l_u(t)$ is the free vortex sheet from upper edge and $l_l(t)$ is the free vostex sheet from lower edge of the free end of the actuator. Corresponding complex vortex sheet strengths are denoted by $\phi(\lambda, t)$, $\phi_u(\lambda, t)$ and $\phi_l(\lambda, t)$ respectively. As the input to the actuator is sinusoidal, the bending displacement is also sinusoidal and can be expressed as,

$$w(x_p, t) = B\cos(\omega t) \quad (5.11)$$

Where B is the amplitude of the actuator bending subsequently the fluid force $F_f\ (x_p, t)$ is found to be periodic in nature [128]. The time domain fluid force data converted into the added mass and hydrodynamic damping coefficients by representing them as a Fourier series. By expanding the periodic fluid force with Fourier series [126], the fluid force can be expressed as,

$$F_f\ (x_p, t) = \rho_f A^2 \omega^2 W[A_1 \cos(\omega t) + B_1\ sin(\omega t) + A_3\ cost(\omega t) + B_3 sin(\omega t) + \cdots.] \quad (5.12)$$

Where A and B are the Fourier coefficients and function of KC. Here only the odd coefficients are taken into account while the even coefficients, are zero because of the condition

$$F_f\ (x_p, t) = -F_f\ (x_p, t + {}^{\pi}/_{\omega}) \quad (5.13)$$

The Fourier coefficients are dependent on the *KC* number [128]. For low values of *KC*, such as *KC* <10, as is typically the case for the applications like electroactive polymer, the Fourier coefficients are expected to be small and the fluid force $F_f\ (x_p, t)$ may be well approximated by just the first harmonic of the Fourier series as

$$F_f\ (x_p, t) = \rho_f A^2 \omega^2 W[A_1 \cos(\omega t) + B_1\ sin(\omega t)] \quad (5.14)$$

Eq. (5.14) is an approximate representation of the fluid force acting on a particular actuator cross-section located at $x = x_p$, that is performing periodic bending with

amplitude B. Thus, for harmonic motion of the beam cross-section and small values of *KC*, the fluid force $F_f\ (x_p,t)$ is harmonic and can be thought of as being the instantaneous response of the fluid to the beam motion. This description of the fluid force is valid for a two-dimensional beam cross-section, and needs to be coupled with the mode shape of the beam deflection so that the fluid force acting on the entire beam can be obtained. The sinusoidal fluid force for total actuator can be written by using water medium mode shape of as [128],

$$F_f\ (x,t) = -\rho_f {A_m}^2 |\Psi_m| \Psi_m \omega^2 W (A_1 - iB_1) e^{i\omega t} \tag{5.15}$$

Where A_m is the modal participation factor, Ψ_m is any unit normalized air mode mode shape, m=1,2,3....number of modes, $|\Psi_m|$ represent the fluid force is dependent on local displacement. By using Eq. (5.14), the Fourier transform of fluid force can be expressed as,

$$F_f\ (x,\omega) = -\left\{-\rho_f \frac{|KC(x)|}{2\pi} \omega^2 W^2 (A_1 - iB_1) w(x,\omega)\right\} \tag{5.16}$$

Where $\rho_f \frac{|KC\,(x)|}{2\pi} W^2\ A_1(|KC(x)|)$ is the amplitude-dependent added-mass coefficient, while the term $\rho_f \frac{|KC(x)|}{2\pi} W^2 \omega^2\ B_1(|KC(x)|)$ represents the amplitude-dependent hydrodynamic damping coefficient and i stands for complex variable in the sinusoidal form. The fact that the Fourier coefficients A_1 and B_1 are functions of the spatially varying *KC* number is clearly indicated in the expressions for the added-mass and hydrodynamic damping coefficients. We also note that the aerodynamic damping coefficient depends linearly on the frequency ω. Thus, very flexible beams with low resonant frequencies experience smaller hydrodynamic damping compared to stiffer beams with high resonant frequencies. Substituting the above equation in the Eq. (5.7), the governing equation of motion of the PPy actuator is obtained as,

$$(E_e I)_{eq}\ w_{xxxx}(x,w) + \left\{\left(\sum_{m=1}^{N} (E_m I)_{eq} \frac{i\omega\tau_m}{1+i\omega\tau_m}\right)\ w_{xxxx}(x,w)\right\} w_t(x,w) -$$

$$m_a \omega^2 \left\{1 + \left(\frac{\rho_f W^2}{m_a}\right) \frac{|KC(x)|}{2\pi} (A_1 - iB_1)\right\} w(x,\omega)\ = F_{ec}(x,\omega) \tag{5.17}$$

5.2.2 Solution

To predict the aerodynamic damping for a particular Eigen mode of the actuator, single mode approximation of Galerkin's method is used as follows

$$w(x,\omega) = \Psi(x)q(\omega) \tag{5.18}$$

The above equation can be approximated to single mode as the fluid force nonlinearity does not couple the natural modes of the beam when the beam is excited with an external force. Specifically for an N - term Galerkin expansion, if ω is the excitation frequency and $\omega_1, \omega_2, \omega_3$ .... are the linear natural frequencies of the beam, then mode coupling can occur if (a)$p\omega = q\omega_k$ (case of secondary resonances where p, q, k are integers such that both p and q cannot be 1), or (b) $p\omega = a_1\omega_1 + a_2\omega_2 + \cdots + a_N\omega_N$ where p and a_n are integers such that [129]:

$$p + \sum_{n=1}^{N} |a_n| = M \tag{5.19}$$

By using Eq. (4.44) (previous chapter), the natural frequency of the actuator in underwater medium is obtained as,

$$\omega_f = \left| \sqrt{\frac{(E_e I)_{eq} + \left(\sum_{m=1}^{N} (E_m I)_{eq} \frac{i\omega\tau_m}{1+i\omega\tau_m}\right)}{m_a L^4}} \right| \left(\sqrt{1 + \frac{m_f}{m_a}}\right)^{-1} \left(1 - \frac{1}{2{Q_t}^2}\right)^{1/2} \tag{5.20}$$

where Q_t is the total quality loss of the actuator in fluid medium which is contributed by both quality loss due to internal damping of actuator, Q_a and quality loss due to fluid damping, Q_f. As the internal damping of actuator is negligible as compared to fluid damping the total quality loss is equal to the quality loss due to fluid. The total quality loss can be expressed as

$$Q_t \cong Q_f = 2\pi|\omega_v| \frac{\sqrt{1 + Lm_f/m_a}}{Lc_f/m_a} \tag{5.21}$$

By pre-multiplying the mode shape function $\Psi(x)$, non dimesionalize the Eq. (5.17) and integrated over non-dimensionalize unit length ($L = 1$) for both sides of the Eq.(5.17) and upgraded as,

$$\int_0^1 \Psi(x)\ \Psi_{xxxx}(x)dx - \frac{L^4}{(E_e I)_{eq}} \int_0^1 \rho_f A \Psi^2(x)\, dx\, \omega^2 q(\omega) +$$

$$\frac{\rho_f W^2 L^4}{(E_e I)_{eq}} \int_0^1 \frac{|KC(x)|}{2\pi}\ A_1(|KC(x)|)\Psi^2(x)dx\omega^2 q(\omega) +$$

$$\left(\frac{\sum_{m=1}^{2} (E_m I)_{eq}}{(E_e I)_{eq}} \frac{i\omega\tau_m}{1+i\omega\tau_m}\right) \int_0^1 \Psi(x)\ \Psi_{xxxx}(x)dxq(\omega) +$$

$$\frac{\rho_f \omega W^2 L^4}{(E_e I)_{eq}} \int_0^1 \frac{|KC(x)|}{2\pi} iB_1(|KC(x)|)\Psi^2(x)dxq(\omega) = \frac{L^4}{(E_e I)_{eq}} \int_0^1 \Psi(x) F_{ec}(x,\omega)dx \tag{5.22}$$

The modal hydrodynamic coefficient, c_f in the above equation depends on the fluid density, ρ_f the beam geometry (i.e. width W and length L), the beam oscillation

mode shape $\Psi(x)$ and the beam oscillation amplitude. In order to calculate c_f for a wide range of Underwater actuator with different widths, lengths and oscillation amplitudes, we can normalize the expression for c_f in the following manner:

$$\frac{c_f(E_eI)_{eq}}{\rho_f \omega L^6} = \frac{W}{L}\int_0^1 \frac{A}{L} B_1(|KC(\hat{x})|)|\Psi(\hat{x})|\Psi^2(\hat{x})d\hat{x} \qquad (5.23)$$

Where $\hat{x}$ is the unit-normalized mode function of a cantilever like actuator. The left side term of the Eq. (5.23) can be used to predict the vortex-shedding-induced damping. By simplifying

$$K_a q(\omega) - \omega^2(m_a + m_f)q(\omega) + i\omega(c_a + c_f)\, q(\omega) = -WE_{PPy_e}\, Q(\omega) * \alpha\{{h_2}^2 - {h_1}^2\} \qquad (5.24)$$

where $K_a = \int_0^1 \Psi(x)\, \Psi_{xxxx}(x)dx$ represents the flexural term associated with elastic component of viscoelastic PPy actuator, $m_a = \frac{L^4}{(E_eI)_{eq}}\int_0^1 \rho_f A\Psi^2(x)\,dx$ is the actuator mass, $m_f = \frac{\rho_f W^2 L^4}{(E_eI)_{eq}}\int_0^1 \frac{|KC(x)|}{2\pi} A_1(|KC(x)|)\Psi^2(x)dx$ added mass of surrounding fluid, $c_a = \left(\frac{\sum_{m=1}^{2}(E_mI)_{eq}}{(E_eI)_{eq}}\frac{i\omega\tau_m}{1+i\omega\tau_m}\right)\int_0^1 \Psi(x)\, \Psi_{xxxx}(x)dx$ is the viscoelastic damping in actuator and $c_f = \frac{\rho_f \omega W^2 L^4}{(E_eI)_{eq}}\int_0^1 \frac{|KC(x)|}{2\pi} iB_1(|KC(x)|)\Psi^2(x)dx$ is the non linear fluid damping, $F_{ec}(x,\omega) = -WE_{PPy_e}\, Q(\omega) * \alpha\{{h_2}^2 - {h_1}^2\}$ is the force to electrochemical actuation upon applying voltage, $Q(\omega)$ is the output current density which obtained from the electrochemical model Eq.(4.4) (chapter 4).

As the input voltage is sinusoidal in nature the displacement is also sinusoidal due to the output current density. For the sinusoidal $w(\omega)$, the expression for the generalized coordinate becomes $q(\omega) = W_u e^{-i\theta}$, where $W_u(\omega)$ and $\theta(\omega)$ are the amplitude and the phase of the approximate sinusoidal response, respectively. From the above equation, the approximate sinusoidal response W_u of the PPy actuator operating in underwater medium can be expressed as

$$W_u(\omega) = \frac{WE_{PPy_e}\, Q(\omega) * \alpha\{{h_2}^2 - {h_1}^2\}}{K_a - [\omega^2(m_a + m_f(W_u)]^2 + [\omega(c_a + c_f(W_u))]^2} \qquad (5.25)$$

where $m_f(W_u)$ and $c_f(W_u)$ represent the modal added mass and the modal hydrodynamic damping effects due to the surrounding air. Also, since $m_f(W_u)$ and

$c_f(W_u)$ depend on the magnitude of response $W_u(\omega)$, the above equation is solved by iterative method to estimate the response.

5.3 Experimental Method

The main objective of the experiments conducted in this work is to estimate the hydrodynamic damping during dynamic bending of flexible PPy sharp-edged actuator and study the nonlinear responses of the PPy actuator. This is achieved by measuring the amplitude and phase of the response of a dynamic bending of sharp edged PPy actuator under actuation voltage of 1.3 V and for a frequency range of 1 – 10 Hz. From the amplitude and phase response, the quality factor (Q-factor) is extracted by using the circle-fit method [130]. Physically, the Q-factor represents the sharpness of the frequency response of the periodic bending of actuator is a measure of the amount of damping ($Q - factor = \frac{1}{2\varsigma}$) is present for a particular Eigen mode, ς denotes damping ratio.

The PPy actuator dimension of $35\ mm \times 8\ mm \times 0.15\ mm$ is fabricated by electrochemical polymerization method from aqueous solution of $0.2M$ NaDBS solution at room temperature by applying $0.15\ mA/cm^2$ constant current density. In chapter 2 details of the fabrication process was presented. The experiments were carried out in an artificial open face glass made water tank of dimension of $75 \times 60 \times 60\ cm^3$ and filled with water up to aheight of $45\ cm$ having zero flow velocity. The actuator with the holder setup is placed inside the tank horizontally. AC voltage is applied to the fixed end of the actuator by using a voltage source connected with function generator (**Sony/Tektronix AFG 320**) and PC. A laser sensor (**RLV-5500, Polytec, GmbH**) is used to measure the response amplitude at the tip of the actuator as the deflection is maximum at tip. The voltage signal from the laser displacement sensor was collected by using a data acquisition unit (**NI Inc.**) and then analyzed by using MATLAB. The experiments and the theoretical predictions presented here focus on the case of single mode resonant harmonic motions of PPy actuator. The experimental setup is shown in Fig.5.2.

The experiments and the theoretical predictions presented in the present work focus on the case of single mode resonant harmonic motions of PPy actuator as the

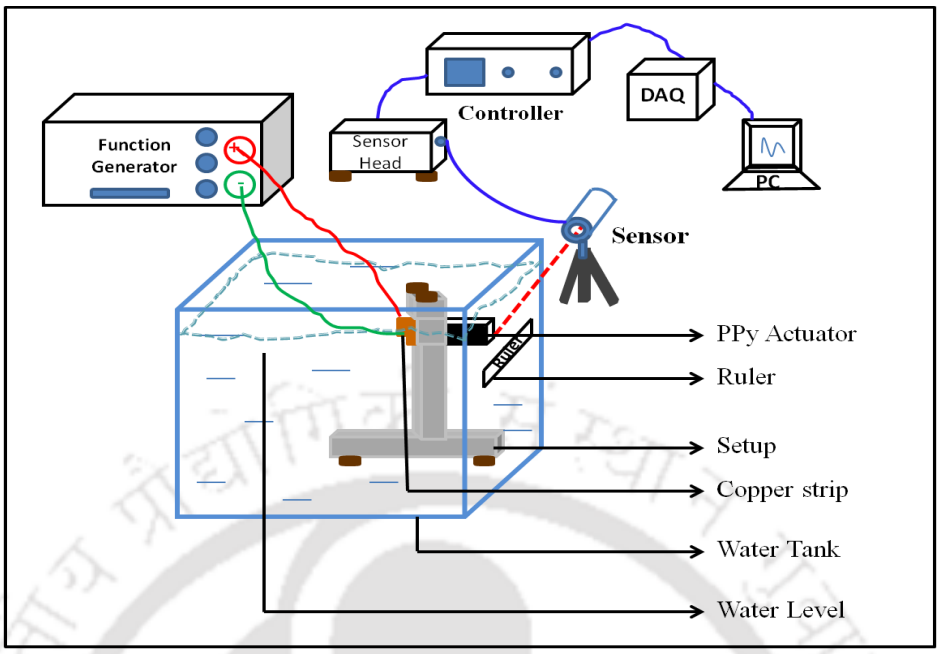

Figure 5.2 Schematic diagram of underwater damping experiment

underwater actuators [131] are operated under these conditions. Specifically, present study restricts the hydrodynamic damping of PPy actuator amid periodic bending in their first flexural mode.

5.4 Results and Discussion

In this section discusses the results obtained from theoretical modelling and the experimental results and their comparison. The fluid flow and vortex shedding results are limited only to theoretical model from the Eq. (5.10) and the results are adequately discussed. Along with this, studied the amplitude and vibration responses of the actuator obtained from both model and experiments for validation.

A PPy trilayer actuator is numerically studied and responses due to non linear hydrodynamic damping are investigated. A Gold-Polypyrrole actuator of length, $L = 35\ mm$, width, $W = 8\ mm$ and thickness, $h = 0.15\ mm$ has been considered for the numerical and experimental analysis. The actuator operates in water medium with density $(\rho_f) = 1\ g/cm^3$ on applying AC voltage of $1.3\ V$ amplitude and $1 - 10\ Hz$ frequencies. The PPy actuator exhibits viscoelasticity with storage modulus 284 MPa, loss modulus $7\ MPa$ and loss factor of 0.021 same as reported before. By solving the fluid flow equation, the Eq. (5.8) – Eq. (5.10), the time evolution of fluid flow

around the actuator transverse displacement generating from the applied sinusoidal voltage is shown in Fig.5.3.

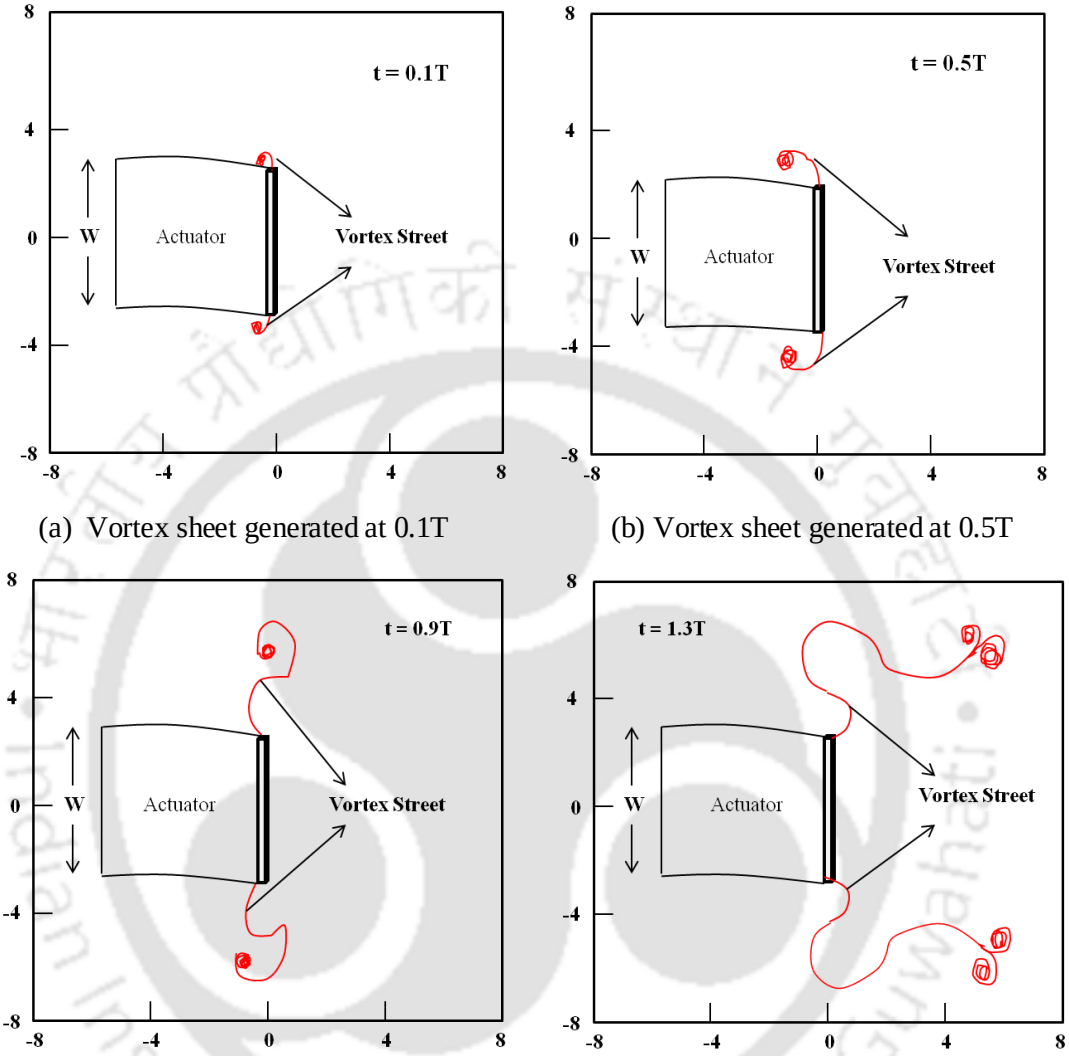

(a) Vortex sheet generated at 0.1T (b) Vortex sheet generated at 0.5T

(b) Vortex sheet generated at 0.9T (d) Vortex sheet generated at 1.3T

Figure 5.3 Fluid flow and vortex sheet generated at the edges of the actuator along the width (X and Y axis) for T = 1 s

It has been observed that the evolution of the free vortex sheet as the beam oscillates through 2 cycles. Note that for beam oscillations along the *z*-axis, the free vortex evolution exhibits symmetry about the y =0 axis even though no such constraint is imposed in the mathematical formulation. Fig.5.4 shows the normalized force (length normalization) acting on the actuator cross section along with a plot of the actuator acceleration. It is seen that the normalized force lags the beam acceleration by a small phase angle. This phase lag between the beam acceleration and the fluid

force gives rise to energy dissipation and is the main cause of the hydrodynamic damping.

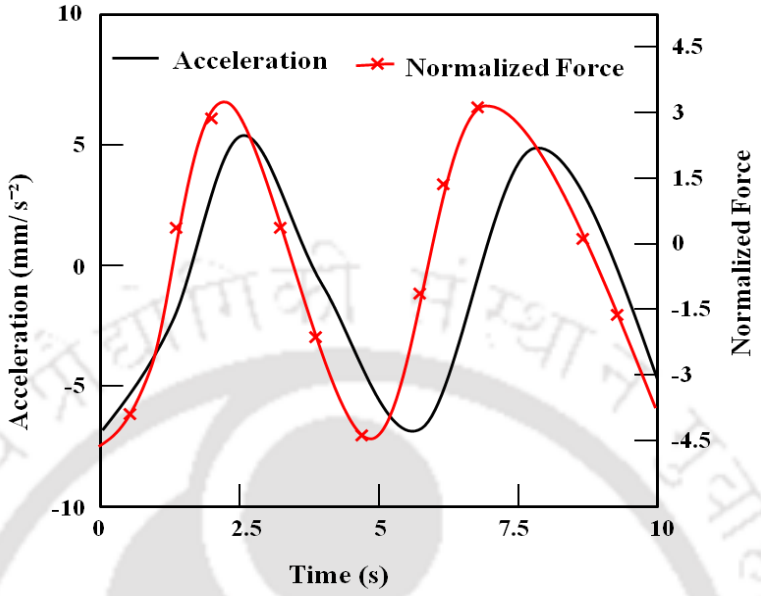

Figure 5.4 Time varying normalized force and acceleration of PPy actuator

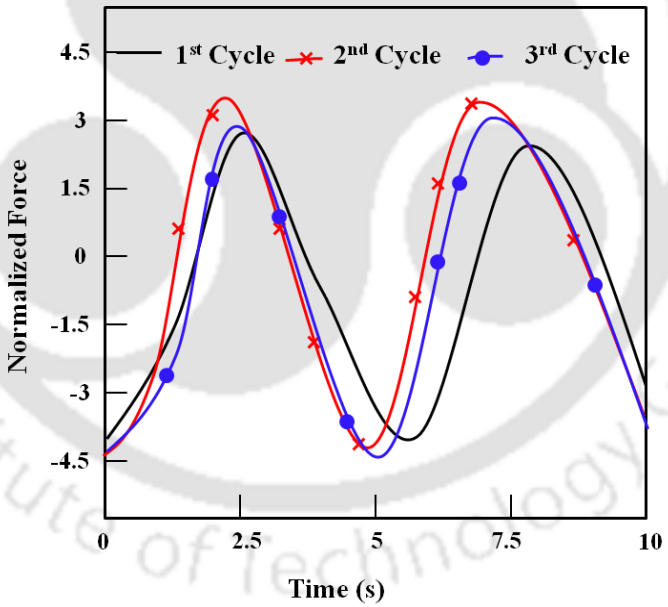

Figure 5.5 Time varying fluid force acting on the PPy actuator

Due to the sinusoidal input voltage, the actuator exhibits periodic motion, hence the fluid force is found to be periodic in time as shown in Fig.5.5. For the normalized fluid force during the second and the third cycle superimposed on top of the fluid force during the first cycle of bending.

In the absence of vortices around the cylinder, the force on the cylinder is proportional only to the fluid acceleration. However, when vortices are present, the

phase of the force component caused by the vortex pair is determined by the phase of the *y*-direction relative transport velocity. In general, the relative transport velocity of the vortex pair will not be in phase with the fluid acceleration, thus causing a portion of the fluid force to have a phase difference from the fluid acceleration. Thus, the transport of the vortices around a cylinder along *y*-direction relative transport velocities not in phase with the fluid acceleration can shift the phase of the fluid force acting on the cylinder. For the case of a bluff body oscillating in surrounding quiescent fluid, this phase shift between the fluid force and the structural acceleration gives rise to the vortex-shedding-induced fluid damping. Furthermore, increasing the oscillatory flow velocity causes both the strength of the shed vortices and the *y*-direction transport velocities to increase in magnitude, which subsequently cause the fluid force to increase in a nonlinear way.

Refer to the numerical model (Eq. (5.14)), it has been observed that the fluid force depends on the amplitude and the frequency. Additionally, the force depends on the Fourier coefficients A_n and B_n, which in this work are known to be functions of KC alone and independent of the value of frequency ω. As a consequence, the force depends on frequency ω only through the ω^2 term. For low KC numbers, as is the case for PPy actuator the computed fluid force reaches its steady-state periodic behaviour only after one to two cycles of beam oscillation.

To calculate the theoretical hydrodynamic damping for PPy actuator, Eq. (5.25) has been used. At first, the force is estimated due to actuation of PPy under AC potential of 1.3 V with a frequency range of 1-10 Hz. Along with the force, the natural frequency of first bending mode of PPy can be estimated by using the Eq. (4.28) and (4.45) (derived in chapter 4). Further the force is also estimated from the dynamic bending experiment as discussed earlier in section 5.3. From the frequency response of force, the hydrodynamic damping is estimated by using the logarithmic decrement method as discussed in Chapter 3.

Fig.5.6 shows the comparative study on theoretically predicted and the experimental amplitude response curve of PPy actuator operated in underwater medium. It has been observed that the error in predicting the resonant frequency is 7.28% (predicted value of 5.9 Hz and experimental value of 6.4 Hz), the error in

predicting the peak amplitude is 9.94% (predicted value from Eq. (5.21) is 1.5422 mm and

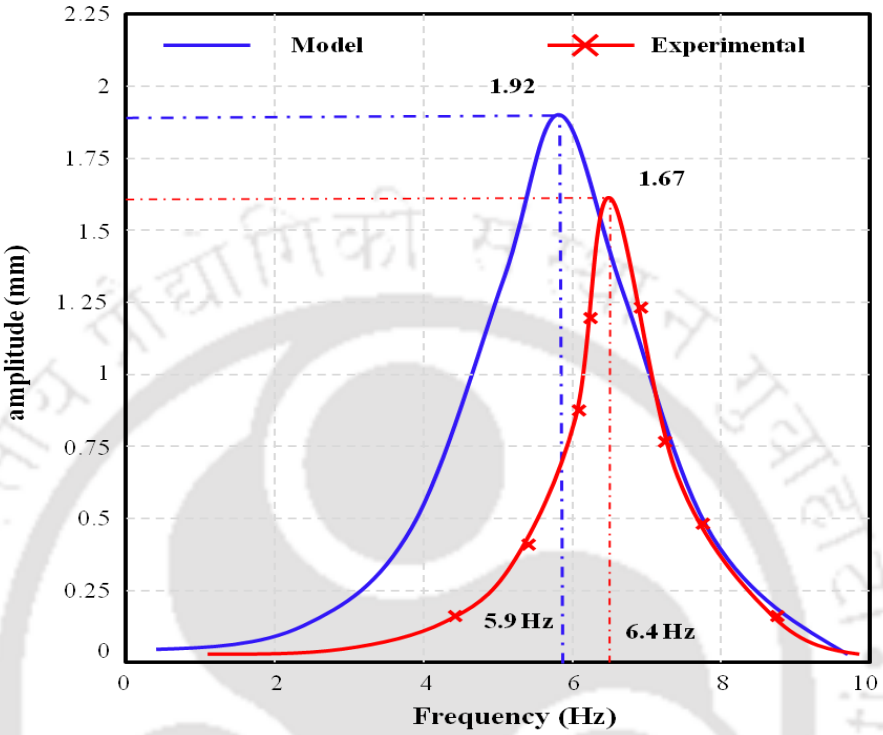

Figure 5.6 Comparison of theoretical and experimental amplitude response

experimental value is 1.39 mm). The model developed here is suitable in predicting the resonant amplitudes with an error of less than 10 % validating the similar trends of published nonlinear results [132, 133, 134]

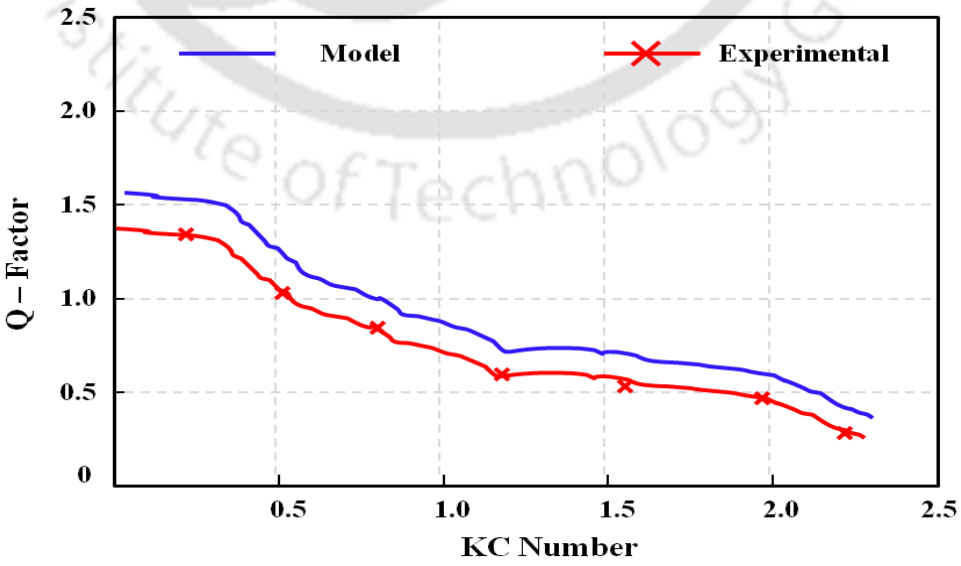

Figure 5.7 Comparison of theoretical and experimental quality factor

The Q – factor obtained theoretically and experimentally is shown in Fig.5.7. It is observed that the error in predicting the *Q*-factor is 16.6 % (predicted value of 2.17 mm and experimental value of 1.75 mm) and shows good agreement with published results [135]. Theoretical error is found to be more implies that the analysis was restricted in 2D flow where vortex shed is considered only in two edges thus failed to capture the 3D effects of the fluid force.

5.5 Summary

In this work, a theoretical model for the response amplitude of PPy actuator operating in underwater medium has been developed which can be used to obtain the nonlinear damping responses for any underwater operated actuator. This simplified expression can be used for finding the response of the system instead of solving the temporal equation of motion or perturbation method which is time consuming and requires more memory space. The numerical results are compared and verified by performing experiment. The precise predication of stable and unstable zone for an applied excitation voltage and frequency is of importance in many micromechanical systems utilizing PPy is the actuator. Both theoretical and experimental investigations confirm that the amplitude of vibration response decreases with the nonlinear hydrodynamic damping. This behaviour is excellently captured by the model that allows for flow separation and vortex shedding from the edges of the actuator. The hydrodynamic loading can be expressed in terms of two non-dimensional parameters KC and β making the results scalable and useful to predict the hydrodynamic loading of a wide variety of actuator operates in underwater environment. Further, in micro-scale applications, the amplitude of vibration can be easily increased and it may bring the system into non-linear regime, and therefore, it is useful to utilize the non-linear analysis to predict the behaviour of the system more accurately.

6

Polypyrrole Actuator for Underwater Undulatory Robot

6.1 Introduction

Smart materials are nowadays effectively used as actuator particularly in developing underwater miniaturized biomimetic robots due to their low weight, flexibility, biocompatibility, low power consumption and smooth operation. Biomimetic robotic systems are similar to biological organisms where smart materials such as electroactive polymers (EAP), piezoelectric materials (PZT), shape memory alloys (SMA) and dielectric elastomers (DE) successfully used over the years. Recently, there has been tremendous progress and demand for underwater miniaturized robots for defence, security and environmental monitoring as till now large part of underwater world is unstructured and unexplored. Most of the presents underwater vehicle or robots are operated by using conventional motor actuators and metallic joints. Drawback like high power driven heavy weight conventional motor and the complex electrical connection results in increasing the size and weight and poor manoeuvrability of these systems. Hence the movement of the system restricted to limited area and deficiency in getting the desired accuracy and repeatability at the desired destinations.

Shape memory alloy (SMA) actuators have been used for propulsion in underwater robot by utilizing their shape recovery effect with a heating above phase transformation temperature [136-138]. Literatures showed that to fabricating propulsion mechanism for robotic system, complex assembly processes, such as long wires and joints are required generating significant thrust [137]. Even though actuators made up of SMA are able to provide a large bending, their slow response and high operating temperature limits their applications. Dielectric elastomer (DE)

based actuator have been used as underwater actuator however low bending displacement and large operating voltage restrict its real time application [139-140]. Including these, Ionic polymer metal composite (IPMC) [141-144], Piezoelectric materials (PZT) and its composites (MFC) [145-147] actuators were among frequently used smart material actuator for underwater robotics. Low bending displacements of IPMC in fluid medium and low strain of PZT were the disadvantages that limit the underwater operation. Some of the effective actuator design with passive structures and controllable functions have been proposed and developed by using these materials. However, large bending displacement and high work density of PPy makes it suitable for underwater operation. Further, the moderate tip velocity, high thrust and low driving power of PPy are effective to develop miniaturized undulatory robots without using any passive fins.

In this chapter, a tadpole inspired undulatory prototype is developed by using bimorph PPy actuators as Tadpole has simple morphological structure and exhibit vertebrates like controlled undulatory movement by the lateral undulation of body without any extra fin. The image of natural adult tadpole is shown below in Fig.6.1. Undulatory swimming is a highly effective means of continuous locomotion by aquatic vertebrates [148]

Figure.6.1 Image of natural Xenopus Leavis Tadpole in adult stage

Tadpole swim by anguilliform motion i.e. lateral undulation of body by sending down alternatives waves from tip of head to tail end that create a jet in the wake may generate the forward force is known as thrust.

The tadpole is divided in two parts i.e. head and tail. The head consists of neural system and power system which control the movements while the tail consists of only the axial muscle which generates the locomotion. Hence the head exhibits major weight of the tadpole, therefore the centre of mass lies inside the head. The schematic diagram of tadpole body structure is shown in Fig.6.2. One side of the tail

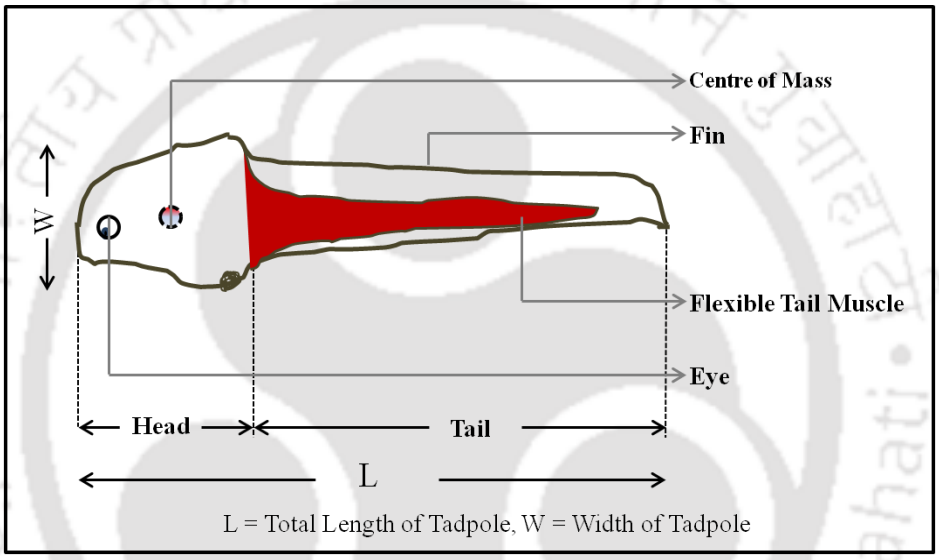

Figure 6.2 Schematic diagram of Tadpole

is fixed into the head where the other side is free to move similar to cantilever beam.

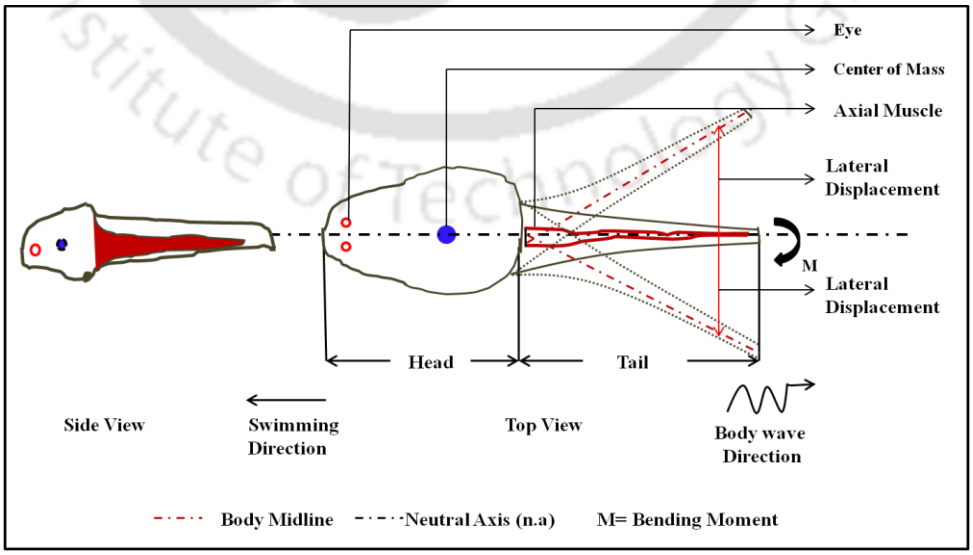

Figure.6.3 Schematic diagram of lateral undulation of Tadpole

The motion of tadpole is solely contributed by the lateral undulation of the tail [149]. The schematic diagram of lateral undulation of tail is shown in Fig.6.3. The lateral undulation of tail is analogous to bidirectional bending of bimorph actuator under AC electric potential. By using this mechanism there are various swimming robotics mechanism have developed for various underwater applications. Here PPy trilayer actuator is used as tail to develop a tadpole like undulatory robot.

6.2 Tadpole Robot

Tadpoles are unusual among vertebrates in having a globose body with a laterally compressed tail abruptly appended to it. Compared with most teleost fishes, tadpoles swim awkwardly with waves of relatively high amplitude at both the head and tail tip. Tadpoles don't have any extra fins like fishes and the undulatory motion generated only by the body [148,149]. However the tadpoles exhibit efficient motion with most simple body structure. Tadpoles can operate in low to medium Reynold's number based fluid, hence suitable for various applications like scanning, surveillance and exploration in uneven underwater environment.

Undulatory propulsion for most aquatic vertebrates is accomplished by sending alternating waves down the body towards the tip of the tail. These waves create a jet in the wake and hence a forward force, namely thrust. The high width-to-length ratio for tadpole bodies means a large frontal area and implies high pressure drag [150]. Undulatory swimming is a highly effective means of continuous locomotion by aquatic vertebrates. Tadpoles, however, are characterized by an awkward shape and equally awkward kinematics.

Xenopus laevis, is the tadpole with some exceptional features like continuous swimming, no lateral deflection of snout at low speed and high manoeuvrability and swim in low to medium Re number and have high efficiency as compared to other teleost fishes [150]. Therefore various tadpole models have been developed in recent time. An oscillating body of arbitrary 3D geometry based tadpole robot has been developed and studied the propulsion mechanism by using a three-dimensional computational fluid dynamic (CFD) model [149]. The undulatory locomotion of the tadpole is simulated in viscous and unsteady flow. Later a wireless tadpole robot has

been developed by using IPMC actuator [151]. Behaviour of TadRob is tested under various frequencies (1~8 Hz) to find the correlation between actuation frequency and velocity of the robot. The velocity of TadRob can be controlled by changing frequency of input voltage and the steering angle can be increased with increasing the duty ratio. The moving speed reached up to 23.6 mm/s for 4 Hz of driving frequency of the IPMC actuator. The numerical analysis of undulatory locomotion was carried out which provides a general understanding of the relationship between dynamic of vortex flow and the jet stream propulsion associated with undulatory locomotion of vertebrates [121]. Although various undulatory swimming devices have been developed, tadpole like small and efficient robots are still need improvement for real time application. In this thesis, a PPy actuator based tadpole like robot is developed followed by the comprehensive mathematical model of undulatory motion coupling with electrochemical actuation.

6.3 Tadpole Motion Modelling

The mechanical model of the robot is developed to predict the motion in underwater medium. The objective is to achieve tail deflections that resemble tail kinematics of a real fish. In order to accomplish this goal, models describing the dynamics of such flexible beams are needed. A required model is a function that would take as input to the actuator, material, and geometrical properties of compliant mechanisms and return as output motion. The simplest procedure is then to use such a model to fit kinematic data of a real fish. This process allows the designer to identify model parameters that allow the smallest fit errors. As a result, information regarding the appropriate material, geometry, and actuator properties required to achieve a good fit can be found.

The tadpole like can swim forward by the continuous bending of PPy actuator based tail on applying AC potential. The lateral bending of tail generates thrust which solely responsible for the forward movement of tadpole robot as the fluid flow velocity is zero. Due to the bidirectional bending, the rigid head exhibits force in normal and tangential direction. The resultant force on the head helps to move

forward and balance the drag force. The schematic diagram of lateral bending of tadpole tail in 2-D plane with reference frame is shown in Fig.6.4.

The kinematics for undulatory locomotion of tadpole is generally in the form of a backward travelling wave with the largest wave amplitude at the fish tail [148], which can be described by the following equations for the lateral undulations of the fish body (all lengths are non-dimensionalized with the fish length L):

$$h(x,t) = A(x,f).\sin 2\pi\{kz - \omega t\} \quad (6.1)$$

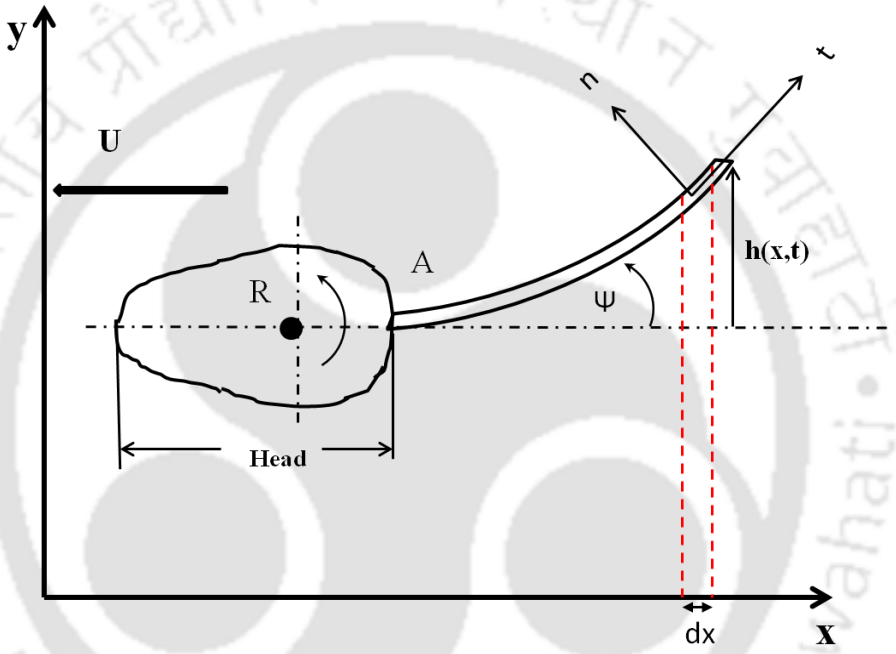

Figure.6.4. Schematic diagram of tadpole tail deflection

where x is the axial (swimming) direction measured along the fish axis from the tip of the fish's head; $h(x,t)$ is the lateral excursion of the body at time t; $A(x)$ is the amplitude envelope of lateral motion as a function of x; κ is the wave number of the body undulations that corresponds to a wavelength λ; and ω is the angular frequency. The amplitude envelop is the function of frequency of actuation voltage and axial body length.

The tail of the tadpole is made up of PPy actuator, hence dynamic modelling of the tail resembling the real fish tail motion is developed. The goal is to find relationships between the electrochemical actuation of PPy, material, and geometric features and the output lateral deflection $w(x,t)$ of the tail at a given point x and

time t in fluid medium. Fig.6.5 shows the PPy based tail end working mechanism equivalent to the natural tadpole motion mechanism. The deflection of the cantilever like voltage driven viscoelastic PPy actuator in a liquid environment is governed by the following equation

$$(E'(\omega)I)_{eq}\frac{\partial^4 w(x,t)}{\partial x^4} + m_a\frac{\partial^2 w(x,t)}{\partial t^2} + \left(c_a\frac{\partial^4 w(x,t)}{\partial x^4}\right)\frac{\partial x}{\partial t} = F_{ec}(L,t) - F_{fluid} \quad (6.2)$$

$$F_{fluid} = -c_f\frac{\partial w(x,t)}{\partial t} - m_f\frac{\partial^2 w(x,t)}{\partial t^2} \quad (6.3)$$

In Eq.6.2, $(E'(\omega))_{eq}$ is the equivalent viscoelastic modulus of PPy layers and PVDF, I is the moment of inertia, m_a and c_a is the mass and damping of the actuator, $w(x,t)$

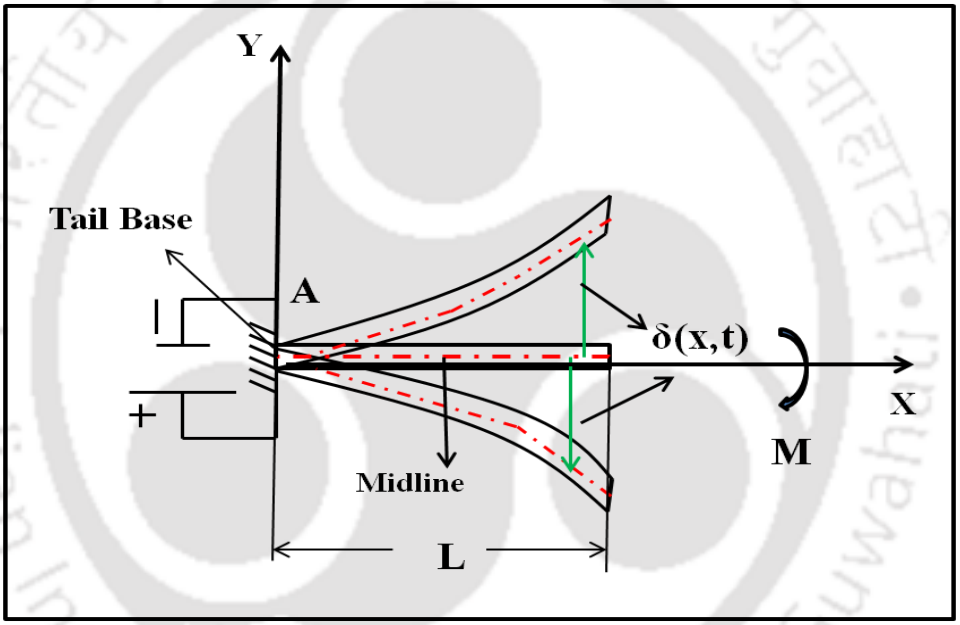

Figure.6.5 Schematic diagram of PPy actuator Tail working mechanism

is the deflection of the actuator, $F_{ec}(L,t)$ actuation force and F_{fluid} is the hydrodynamic force acting on the actuator. The details of the equation and solution are given in Chapter 4. The hydrodynamic force is contributed by both mass and damping due to fluid. By substituting the Eq. (6.3) into Eq. (6.2), the final governing equation of the viscoelastic PPy actuator is developed. The fluid damping term $c_f\frac{\partial w(x,t)}{\partial t}$ is otherwise known as resistive force in few literatures and is directly proportional to the normal components of the relative velocity between the tail and the liquid environment. For an undulating body with body wave speed V and the mean swimming speed U_s relative to the stream, a is given by

$$a = \frac{\partial \delta}{\partial t}\left(1 - \frac{U}{V}\right) \tag{6.4}$$

Hence, in steady motions a is directly proportional to the lateral speed of the tail. In the interest of simplicity we assume that the fluid damping displays a linear dependence on a. This would allow us to solve Eq. (6.2) but will make our results overestimate the actual behaviour since this assumption underestimates the environment resistive forces. Though, here flow of water is zero and constant, the resistive forces can be modelled by a term analogous to viscous damping, with a damping coefficient, c_f. As the actuator behaves like a cantilever beam, the boundary conditions are as follows

$$(w)_{x=0} = \left[\frac{\partial w}{\partial x}\right]_{x=0} = 0$$

$$\left[(E'(\omega)I)_{eq}\frac{\partial^2 w}{\partial x^2}\right]_{x=L} = \frac{\partial}{\partial x}\left[(E'(\omega)I)_{eq}\frac{\partial^2 w(x,t)}{\partial x^2}\right]_{x=L} = 0$$

The governing equation of motion in Eq. (6.2), is obtained by using multimodal method as,

$$w(x,t) = \sum_{i=1}^{\infty} B_i \varphi_i(x)\, q_i(t) \tag{6.5}$$

The 'i' subscript is used to represent unit mode of bending with shape function, $\varphi(x)$ and time frame, $q(t)$ for transverse bending of PPy trilayer actuator. The mode shape of a cantilever beam can be obtained as,

$$\varphi_i(x) = C_4\left[\{\cos(\beta_i x) - \cosh(\beta_i x)\} + \frac{\{\sin(\beta_i L) - \sinh(\beta_i L)\}}{\{\cos(\beta_i L) + \cosh(\beta_i L)\}}\{\sin(\beta_i x) - \sinh(\beta_i x)\}\right] \tag{6.6}$$

By using the boundary conditions and modal properties like orthogonality and mass normalized Eigen function, the shape function and time co-ordinate obtained as

$$\varphi_i(L) = \frac{2(1 - sin\beta_i L\, sinh\beta_i L)}{cos\beta_i L + cosh\,\beta_i L} \tag{6.7}$$

$$q_i(t) = \frac{F_{e0}}{{f_r}^2 + i2\zeta f_r \omega - \omega^2} e^{i\omega t} \tag{6.8}$$

As the input voltage is sinusoidal, the actuation force is sinusoidal in nature and expressed in exponential form in above equation simplifying the calculation. The steady state deflection of the PPy actuator can be expressed in terms of material geometry, properties and input voltage as

$$w_f(x,t) = \left\{\frac{1}{m}\sum_{i=1}^{\infty}\frac{-W\left(E'(\omega)\right)_{PPy}Q(t)*\alpha\{{h_2}^2-{h_1}^2\}\varphi_j(L)\varphi_i(x)}{{\omega_{n_f}}^2+i2\zeta f_r\omega-\omega^2}\right\}V_{in} \quad (6.9)$$

Furthermore, in addition to matching the kinematic behaviour of real fish, biomimetic mechanisms must maintain similar geometric features. This contributes to replicate the overall dynamic behaviour needed to achieve the required locomotion performance. As the robot moves in XY plane, the velocities along X and Y direction as follows

$$V_x = U \text{ and } V_y = \frac{\partial\delta}{\partial x} \quad (6.10)$$

This velocities in x and y direction determines the velocity of each point on actuator in normal and tangential direction during lateral bending of the actuator as follows

$$V_n = -Usin(\Psi) + \frac{\partial\delta}{\partial x}\,cos(\Psi) \quad (6.11)$$

$$V_t = Ucos(\Psi) + \frac{\partial\delta}{\partial x}\,sin(\Psi) \quad (6.12)$$

In above equations, Ψ is the angle of curvature of the actuator can be expressed as, $\Psi = \frac{\partial\delta}{\partial x}$. The principle of the model is based on the reactive force, generated by the fluid against the moving thin plate like PPy actuator. For any solid, the reactive force acting in normal and tangential direction according to the respective velocity components are as follows

$$F_n = -\frac{1}{2}\rho_f A c_n V_n \|V_n\| \quad (6.13)$$

$$F_t = \frac{1}{2}\rho_f A c_t V_t \|V_t\| \quad (6.14)$$

The propulsive force is generated from the tangential and normal components of the reactive force for the tadpole robots as follows

$$\tau = \int_0^L \frac{1}{2}\rho_f W(c_t V_t\|V_t\| - c_n V_n\|V_n\|\tan(\Psi))dx \quad (6.15)$$

The propulsive force is a periodic function; hence only focus on the analysis on propulsive force in a cycle. When area of one half cycles above the time axis is bigger than that of the other half cycle of below time axis, propulsive force acts as push force. In adverse, it acts as drag force, this feature can be expressed by mean propulsive force for robot as

$$\bar{\tau} = \frac{\int_0^T \frac{1}{2}\rho_f \int_0^L W(x)Ac_t(V_t\|V_t\| - Ac_n V_n\|V_n\|\tan(\Psi))dx}{T} \quad (6.16)$$

The above equation is for the tadpole; hence the width of the actuator varies along length. Further the thrust is dependent on the voltage induced bending displacement where the mean thrust function of actuation frequency as well as time. The drag force exerted on the tadpole robot in small scale can be expressed as

$$F_D = -\frac{1}{2}\rho_f A c_D U^2 \tag{6.17}$$

Where c_D is the drag co-efficient and U is the swimming speed of the robot. The drag coefficient depends on the Reynolds's number and the shape of the fish body. The Reynolds's number characterizes the relative speed U, the length of the body L and the kinematics viscosity ϑ of the fluid, and is defined as,

$$Re = \frac{UL}{\vartheta} \tag{6.18}$$

In steady state motion the mean thrust and drag force are equal relating to the mean swimming speed, U_s which can be derived as,

$$U_s = \sqrt{\frac{\int_0^T \frac{1}{2}\rho_f W \int_0^L (c_t V_t \|V_t\| - c_n V_n \|V_n\| \tan(\Psi)) dx}{T \rho_f A c_D}} \tag{6.18}$$

Finally the propulsive efficiency of the swimming tadpole is determined by using the formula as,

$$\eta_{swim} = \frac{U\bar{\tau}}{P_{avg}} \tag{6.19}$$

Where U is the speed, $\bar{\tau}$ is the mean thrust and P_{avg} is the average power consumption by the PPy actuator. The average power consumption can be estimated from the input voltage and output current [158], and is expressed as

$$P_{avg} = \frac{1}{1/\omega}\int_{t_r}^{t_r+\frac{1}{\omega}} (V_{in} I_o) dt \tag{6.20}$$

Where P_{avg} is the average power consumed by PPy actuator for underwater bending, t_r is any random time during PPy actuator operates in underwater medium, V_{in} is the input voltage and I_o is the output current, ω is the frequency of operating voltage.

To quantify the effectiveness of the PPy based propulsion system, non-dimensional Strouhal number (St) is widely used, which is defined as.

$$St = \frac{f_r w}{U} \tag{6.21}$$

Where f_r is the tail bending frequency w is the tail bending amplitude and U is the swimming speed. In flows characterized by a periodic motion, the Strouhal number is associated with the oscillations of the flow due to the inertial forces relative to the changes in velocity due to the convective acceleration of the flow field [153]. The Strouhal number is also indicative of the frequency at which reverse Karman vortices are generated in fluid. The K´arm´an vortices are the primary mechanism responsible for thrust production of an oscillating fin

6.4 Prototype Development

In this section, the design and development of the tadpole robot prototype is described in details. At first the geometrical dimension and computer aided design of the prototype is presented followed by the fabrication and assembly of the prototype. As the prototype is analogous to *Xenopus Leavis* tadpole species, the morphological features of this tadpole is taken into consideration for design and development of the prototype.

6.4.1 Design of Tadpole like Robot Prototype

Once the material, geometrical, and actuator properties are identified they can be used for designing prototype implementing the required locomotion kinematics for tadpole-like swimming. The swimming mechanism and morphology of the robot is to mimic natural *Xenopus Leavis* tadpole species.

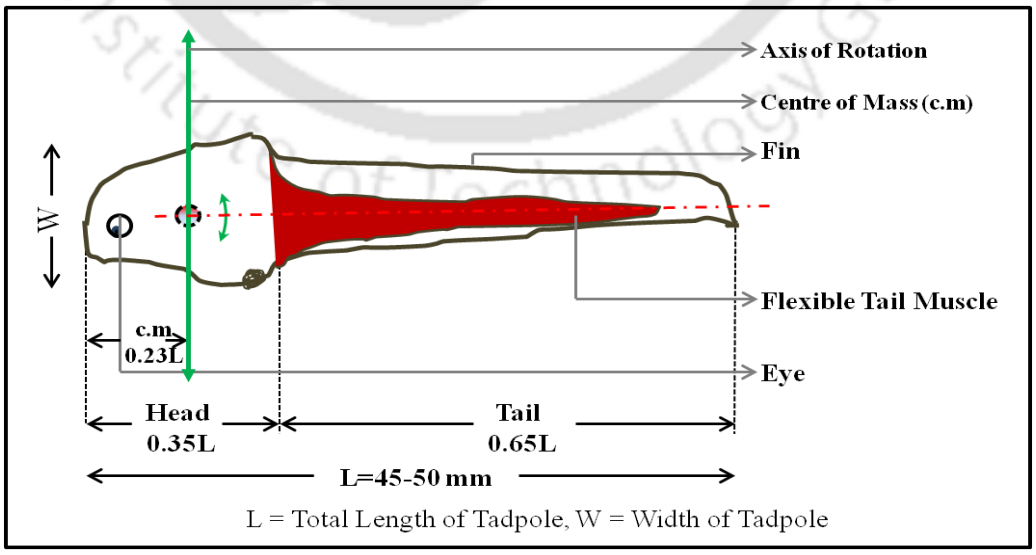

Figure.6.6 Schematic diagram of natural Xenopus Tadpole with morphology

The features of the proposed tadpole are shown in Fig.6.6 and the CAD model of the prototype is shown in Fig.6.7. The high width-to-length ratio for tadpole bodies means a large frontal area and implies high pressure drag.

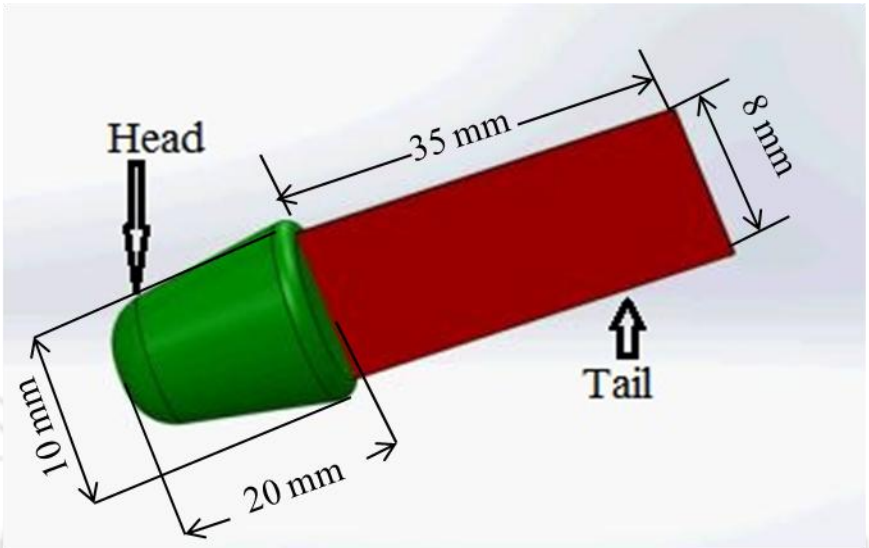

Figure.6.7 The image of CAD model of the tadpole like prototype

Rigid and flexible sections are jointed together forming a single tadpole prototype. Rigid section is working as head of the tadpole which carry the electrical connections and electrode holder while the flexible actuator behaves like tail of the tadpole that undergoes lateral undulation. The harmonically varying voltage input is applied to the actuator by electric wire connecting a voltage source.

The main advantages of this type of design are that the compliance is implemented by the structure itself, and the mechanism is self-contained. The design is monolithic and thus no sealing is required. The present robot swim and manoeuvre based on actuation of PPy and no extra passive fin is attached, hence the design is simple and cost effective.

In *Xenopus Leavis*, the length of head and body or tail is distributed as $0.35L$ and $0.65L$ respectively where L is the total length of the tadpole. The centre of mass lies in the range of $0.21L$ from the nose end. Though the average length of natural tadpole species is $4\ cm - 5\ cm$, here the prototype developed is slightly scaled up with respect to the natural one.

6.4.2 Fabrication and Assembly

In this section the details of materials and methods used for developing tadpole

robot prototype is discussed. For developing the prototype, the head and tail fabricated separately, followed by the assembly of this two.

6.4.2.1 Head

A streamlined body to house power electronics, provide structure, and clamp to hold the actuators was needed. For the effective undulating movement and to enhance the stability of the robot, the head should be rigid and leakage proof. To achieve this, the head is manufactured by two part 3D print moulding technique. The head is fabricated by using rigid fibreglass plastic due to its low cost and high durability.

The actuator holder is prepared by using a pair of copper plates with gold coating fixed into a breadboard for better delivery of power. The bread board is places inside the head and fixed in such a way that the centre of mass should lies around 14 cm from the nose end which is close to $0.2L$ as in case of natural tadpole. The power source, electronic components and electrical connections are made precisely in the breadboard and then the two halves were mated and sealed with fresh casting rubber leaving small slits for insertion of actuators later. The length of the head is around 20 mm, maximum width near the actuator holder is 10 mm and weight of the head with all components is nearly 15 g

6.4.2.2 Tail

The tail is made up of PPy trilayer actuator which is fabricated by using layer by layer electrochemical polymerisation and deposition technique. The fabrication of PPy based tail is carried out in a three electrode electrochemical cell by applying a constant current of $0.15\ \mathrm{mA/cm^2}$through potentiostat/galvanostat. PPy is polymerized from aqueous solution of 0.2 M Pyrrole and 0.2 M NaDBS at room temperature and deposited on both sides of gold coated PVDF membrane. The trilayer actuator is fabricated by using layer by layer deposition where each layer deposited for 3 h with freshly prepared solutions. The details of the synthesis and fabrication of PPy actuator is described in chapter 2. Following the fabrication, the PPy strip washed repeatedly with water and stored in a dried place. The dimension of the actuator is $40mm \times 8mm \times 0.15mm$ and the weight is nearly1 g.

The actuator is placed in between the two electrode in actuator holder inside the

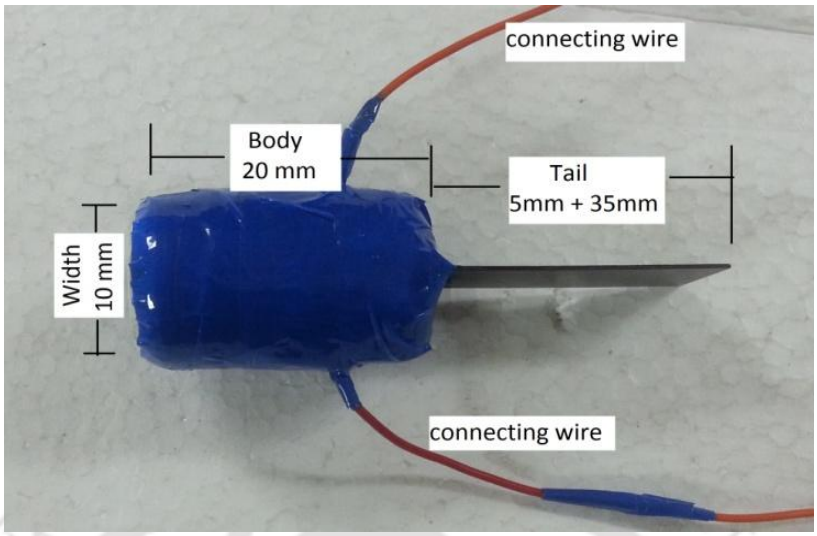

Figure.6.8 The image of the tadpole like underwater robot

head. The length of the actuator placed inside the head is around 5 mm and the free length of the tail is 35 mm as shown in Fig.6.8. The electrical wires are coming out through head through small holes. The wire output and the PPy actuator output zones are sealed with casting rubber properly to avoid any leakage.

6.5 **Experimental Setup**

The actuator is operated by external voltage source (**model: Caddo 4060**) connected to a function generator for providing sinusoidal voltage through thin electric wire. The swimming of the robot is recorded upon applying sinusoidal voltage amplitude of 1.3 V with range of frequency of $1 - 10$ Hz.

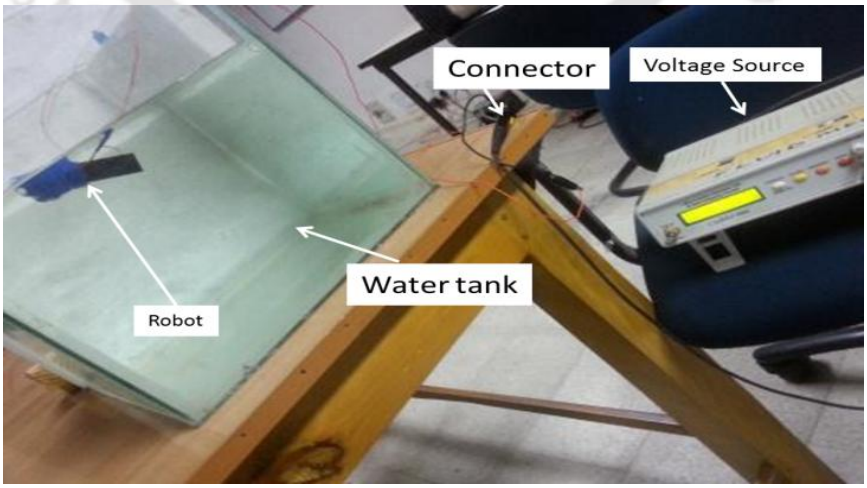

Fig.6.9.The laboratory setup for tadpole prototype experiment

6.6 Results and Discussion

The lateral displacement of tadpole tail is recorded and compared with the theoretical results as well as theoretical undulatory motion equation presented in Eq.6.1 as shown in Fig.6.10. It has been observed that the tadpole tail is followed

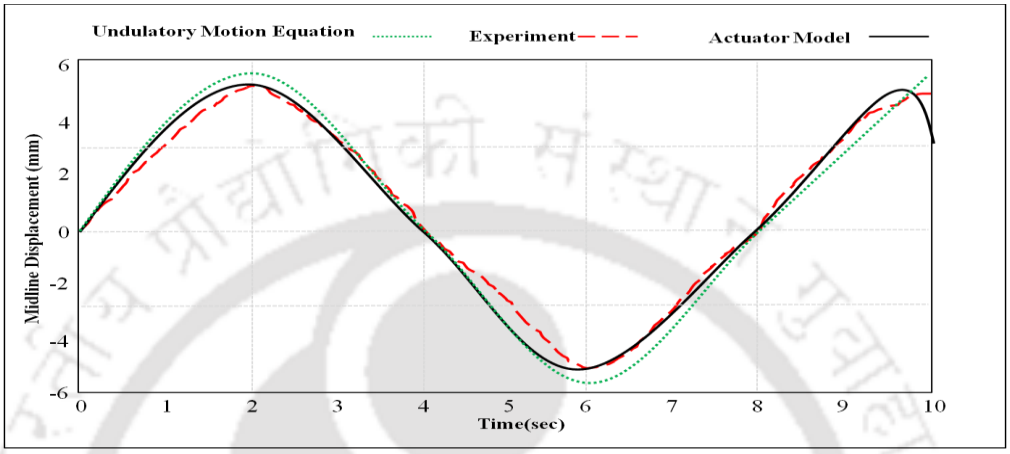

Figure 6.10 Bending displacement of PPy actuator based Tadpole robot

the same pattern with the theoretical results and shows good fit with the published results [120,142,144,147]. The tail exhibited 5 mm of lateral displacement, which is slightly lower than the actuator maximum displacement 5.4 mm. It has been observed the experimental curve not smooth as like the curve obtained from model, which may be due to noise and disturbances in underwater medium. The frequency response of the displacement curve is shown in Fig.6.11.

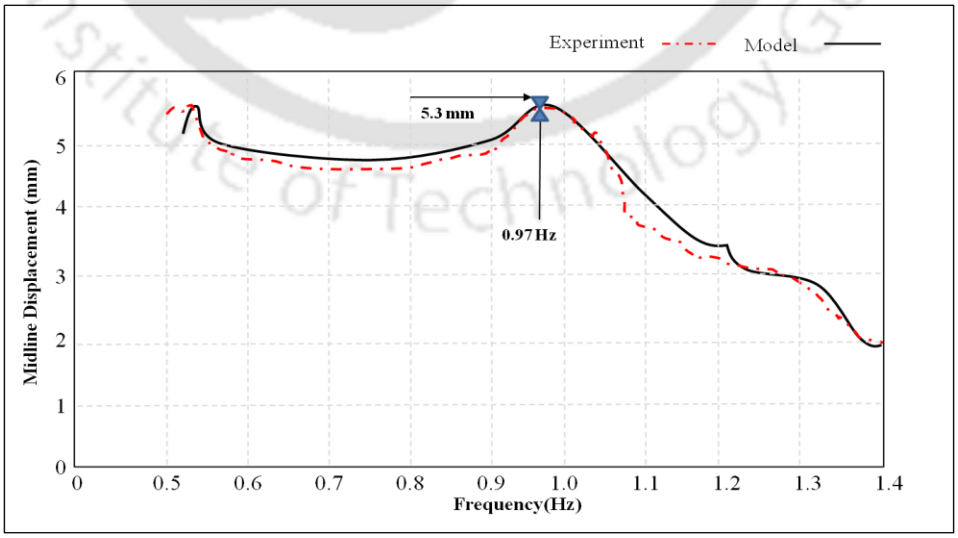

Figure 6.11 Displacement of tadpole tail at actuation frequency with 1.3 V

The maximum displacement occurs at 1.1 Hz which is slightly higher than the actuation frequency. It is believed that due to the weight of the head and fluid viscous the displacement is lower and the action frequency is slightly higher. This trend is shown good fit with the published results, however the tail achieved significantly higher displacement with low voltage [120,140,142,144,154].

The video was then analyzed to obtain an average velocity resulting in six measurements for each frequency. The average velocity of the robot as a function of the actuation frequency can be seen in Fig.6.12. The highest average velocity of 27 mm/s was found at an actuation frequency of 2.5 Hz.

Intuitively it would infer that the when the displacement lowers the robot achieve maximum speed. Upto 1 Hz of the actuation frequency, the speed is lowered as the displacement is high and it has been observed that the robot head is not stable and in due time of motion when the robot is achieving stability displacement is lower and the frequency increased.

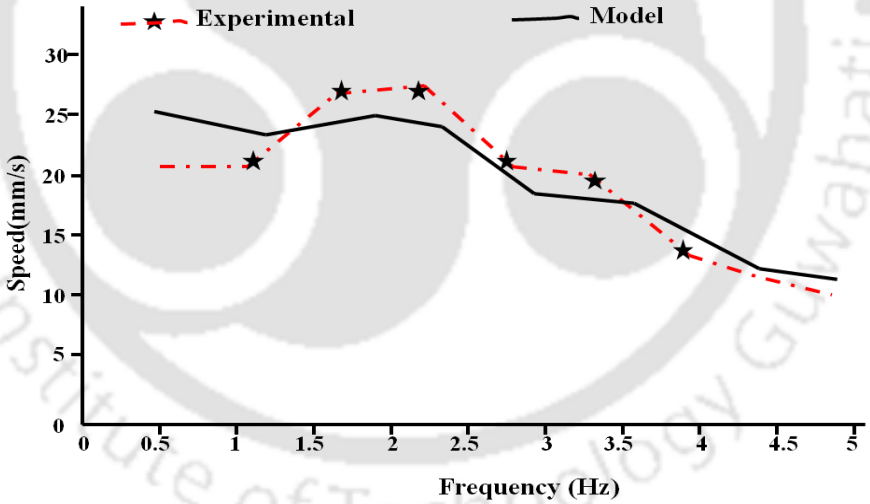

Fig.6.12 Speed of tadpole robot at various actuation frequency

Fig.6.13 shows the thrust obtained from the swimming experiment and the theoretical model over the range of frequencies. It has been observed the average thrust generated by the tadpole tail is 0.84 mN and follows the same trend as the displacement. It can be concluded that the displacement and thrust force are closely related. In other way, the thrust force is dependent on input voltage amplitude and it increases on increasing the voltage amplitude.

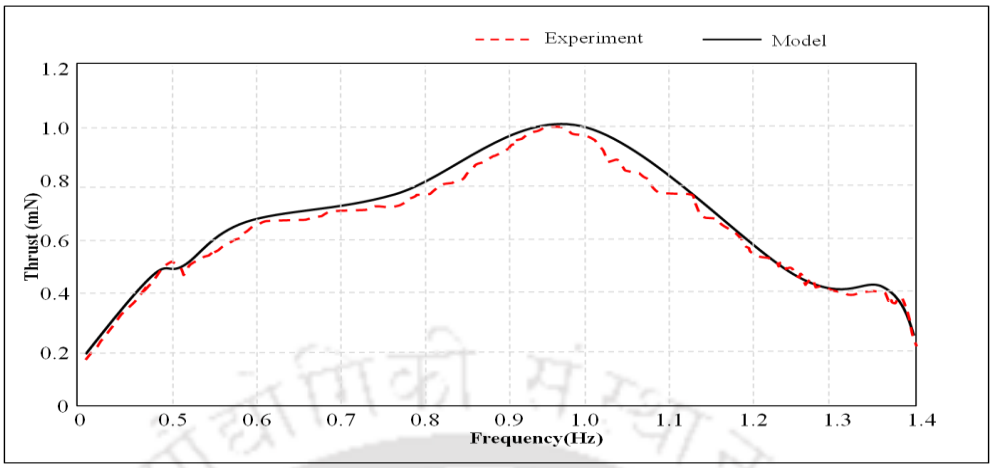

Figure 6.13 Thrust vs Frequency of PPy based tadpole robot

For swimming devices, Reynold number is being used frequently to estimate the application area of the system. The Reynolds number (Re), illustrates the ratio of inertial forces to viscous forces. When Re<1 viscous forces are dominate and govern the object's behavior. In contrast, when Re>>1 viscous forces play little role and inertial forces dominate the object's movement. This means that for small robotic systems or larger ones at low speeds (e.g., accelerating from rest) viscous forces are an important consideration. The Reynolds number of the prototype operating at maximum velocity is approximately 17303 which is close to the natural tadpole swimming pattern.

This Strouhal number (St) is a passive indicator of the effectiveness of thrust production and swimming. For angulliform swimmers the optimal strouhal number is between 0.4 and 0.5. [148], and the thrust and swimming behavior of the object is considered ideal. Indirectly it was shown that tadpole propulsion occurs where $0.4 < St < 0.5$ [148]. The Strouhal number of the robotic tadpole at maximum velocity was found to be 0.44.This value is close to optimal value and further improvements in body size and design could also generate accurate values.

The swimming efficiency or propulsive efficiency of the robot can be estimated from Eq. (6.19) and its variation with swimming frequency or tail beat frequency is shown in Fig.6.14. It has been observed the robot has maximum efficiency around 35% at nearly second mode shape frequency of 11 Hz. At higher frequency the actuator consumes more energy hence the efficiency lowers.

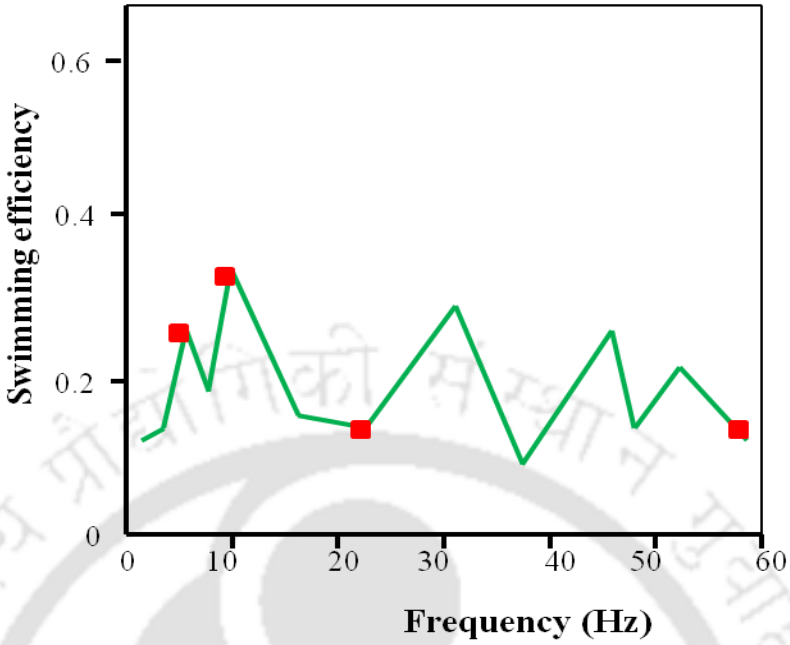

Fig.6.14 Frequency vs swimming frequency of tadpole robot

The comparative summary of the geometrical parameters and performances of the present tadpole with natural tadpole and earlier developed smart material based tadpole robots is presented in table 6.1.

Table 6.1 Performance comparison of present tadpole with natural tadpole and earlier developed tadpole robots

Properties	Natural Tadpole	Developed Model (PPy)	TadBot (IPMC) [134]
Dimension	45-55mm	55mm	96 mm
speed	24-30 mm/s	27 mm/s	23 mm/s
Operating condition	Normal water, sea water	Aqueous Nacl, water	water
weight	10 g	16 g	15.5 g
Operating Life		10-12 h continuously	5-6 h
Thrust		1.02 mN max 0.84 mN avg	0.72 mN
Tail beat frequency	10 Hz	9 Hz	8 Hz
Cost		90 USD	110 USD

6.5 Summary

Present work demonstrates the use of Polypyrrole, a special class of smart material to generate bio-inspired undulatory motion similar to tadpole and other swimming vertebrates. An analytical approach has been adopted to model the dynamic undulatory motion by using electro-visco-mechanical actuation of PPy bimorph actuator along with Lighthill's elongated body theory. Following this, a tadpole inspired prototype has been developed to estimate the undulatory motion performances and validate the model. The real time swimming experiments were carried out in quiescent water by applying voltage of 1.3V and a range of frequencies. The summery of the present work as follows:

- The PPy actuator works analogous to artificial muscle actuator and operates in very low voltage replacing the conventional motor actuator
- The bending displacement of PPy actuator based tail is achieved to be 5.4mm with a voltage of 1.3V and frequency of 1 Hz.
- The PPy tail can generate thrust upto 1mN and tail beat frequency utpo 11.2 Hz which makes it suitable for underwater application in still water.
- The developed model can swim at a speed of 27 mm/s which is very close to the natural tadpole.
- The motion parameters primarily depends upon the input voltage and frequency, hence it will be simple to develop the control system for precise motion

The present prototype has shown good agreement and improved performances with the developed systems, and enable used for various underwater applications like surveillance, environmental monitoring and pollution detection.

7

Conclusion and Future Work

7.1 Conclusion

In the present work, a low cost Polypyrrole (PPy) trilayer actuator has been fabricated. Several steps of trial-and-error attempts results in successful fabrication of the actuator, where vacuum coating deposition technique of Gold (Au) on middle polyvinylidene fluoride (PVDF) and layer-by-layer electrochemical polymerization process. Following that, several experiments have been carried out to characterize the developed PPy actuator. The effectiveness and performance of the actuator is studied for its underwater operation. The experimental investigation and comparative study demonstrates superior actuation capability of the actuator. Multiple experiments are conducted to ascertain the effect of viscoelasticity, hydrodynamic loading and environmental condition on actuation capability of the PPy actuator. An empirical model has been developed subsequently estimates the underwater performances of PPy actuator during working condition.

Further, extensive bending and vibration tests were performed under real time application criteria with AC input voltage. The experimentally obtained tip position data are used to develop theoretical models for prediction of linear and nonlinear vibration response of PPy actuator under AC voltage actuations. These responses are also obtained by incorporating time varying modulus and hydrodynamic parameters. The developed general purpose theoretical models can be used for any PPy actuator to predict the hydrodynamic performances and to study the effect of surrounding fluid on the vibration response of underwater operated PPy actuator. Finally, a tadpole like swimming robot has been developed demonstrating the applicability of the developed PPy actuator in bio-inspired underwater robotics application.

The specific conclusions of the present work can be summarized as follows:

- Polypyrrole trilayer actuator is successfully fabricated by using layer by layer electrochemical polymerization and deposition from aqueous solution of Pyrrole (Py) and sodium-dodecyl-benzene-sulphonic acid (NaDBS) followed by coating of Gold on PVDF membrane by using vacuum coating technologies.
- Morphological characteristics of PPy examined by scanning electron microscope illustrates that there is good bonding between the Au-PVDF and polymer layer and a uniform densely packed distribution of PPy is found over the Au-PVDF layer. The conductivity of the PPy actuator is found as 136 S/cm with a strain rate around 6%, are nearly equal to the PPy synthesized with expensive organic solvents, IL based salt and in low temperature fabrication setup.
- The actuation voltage and frequency obtained by using Cyclic Voltametry (CV) and Electrochemical Impedance Spectroscopy (EIS) as 1.3 V and 1 Hz. The coefficient of thermal expansion (CTE) of PPy shows negative value with low temperature, and changes from negative to positive value with rise in temperature.
- DSC and TGA tests of the PPy confirm improved thermal stability, and micro-tensile test confirms the increase in Young's modulus. The actuator shows steady state bending displacement of 5.4 mm and 4.2 mN tip force with voltage of 1.3 V and frequency of 1Hz for underwater operation. The improved work density, tensile strength and breaking stress of the PPy actuator makes it suitable for underwater operations.
- The cost of fabricating a $50mm \times 10mm \times 0.15mm$ Au-PPy synthesized from aqueous NaDBS solution is found to be around Rs.6500.00 (90 USD) which is much less compared to the Platinum-PPy synthesized from organic solvent/TBA based salt solution at low temperature based setup.
- The developed PPy shows significantly improvement in conductivity with increase in concentration of monomer and salt at room temperature setup. The actuator generates average thrust of 0.84 mN and continuously work upto 10-12 h makes it suitable for underwater operations.

- The superior performances of the actuator like large bending deflection, less surface resistance, larger tip force are compared with the actuator developed by using low temperature setup, costly salts like ionic liquids (IL) and organic solvents. The experimental investigation, characterization and performance of the developed IPMC demonstrate its effectiveness to be used for underwater operations.
- Tough creep is one of the major limitations of PPy actuator; here the viscoelasticity of PPy actuator was taken into account. The dynamic mechanical and thermal analysis of the actuator carried out to estimate the storage modulus, loss modulus and loss factor of the actuator. The actuator exhibits storage modulus of nearly 284 MPa which makes it suitable for underwater operation. For developing the robust model in real time applications, the time dependent modulus has also taken into account.
- The hydrodynamic bending characterization and performances have been studied by developing a comprehensive robot mathematical model. The transform function form of equation is formulated to predict the underwater bending displacement which is a function of electrochemical, mechanical, viscoelastic and hydrodynamic forces. The linear vibration response of the actuator has been studied from the frequency response analysis and estimated the damping and resonating frequencies. The actuator exhibits first fundamental frequency at around 5.5 Hz and the damping ratio is evaluated as 0.023. The improved performance of the actuator makes it suitable for small scale underwater robotics application.
- A closed form expression for the response amplitude has been developed to study the effect of surrounding fluid in terms of nonlinear hydrodynamic damping. The Keulegan Carpenter number and frequency parameters have been used to develop the theoretical model and validate with experimental results. The fluid flow around the actuator is numerically analyzed by using Fourier transformation and Von Karmen vortex mechanism. The non linear effect is quantified by evaluating the amplitude response and quality factor of the actuator operates in underwater environment. The simplified expression can be used for finding the response of the system instead of solving the temporal equation of motion which is time consuming and requires more memory space. The numerical results are compared and verified with experiment and the results

are found to be in good agreement. It is concluded that in macro-scale actuator, amplitude of vibration could change due to nature of surrounding fluid and a small change in excitation amplitude or input voltage occurs. Further, in micro-scale applications, the amplitude of vibration can be easily increased and it may bring the system into non-linear regime, and therefore, it is useful to utilize the non-linear analysis to predict the behaviour of the system more accurately.

The present PPy actuator based underwater robot can be precisely controlled by the input voltage and frequency. This robot can work in low Reynold's Number area and can move upto 27 mm/s for a longer time. Apart from this, the low cost Au- PPy based underwater robot has the potential applications in scanning, surveillance, defence, security and environment monitor etc.

7.2 Scope for Future Work

The research work reported in this thesis represents significant advancements in the field of fabrication, characterization and modelling of PPy actuator. Although, PPy applications in various fields and several other actuator related issues demand further investigation. Some scopes of further work are listed below.

- The fabrication procedure can be further optimized by understanding the physical actuation mechanism by exploring different low cost salts, varying concentration of polymer and varying the solvent materials. Further, fabrication procedures such as chemical polymerization, CVD or spin coating techniques may be employed to fabricate thicker and multilayered PPy. Similar analysis carried out in this work may be used for analyses of multilayered PPy and to study their effects on the actuation performance of PPy actuator.
- A similar study can be carried out to investigate the sensing properties for PPy actuator. This thesis focused mainly on the actuation of the PPy actuator; while sensing is also an important application area of PPy actuator. Further the simultaneous sensor actuator behaviour of PPy can be explored.
- In this work nonlinear vibration analysis has been carried out considering single frequency excitation. One may consider multi-frequency excitation to analyze the system.

- Controlling of robotic locomotion system can further be explored by using artificial intelligence technologies along with analysis and compensation for delay to the system response.

References

[1] Kim, K. J., Tadokoro, S., (2010), Electroactive polymers for robotic applications, Book, *Springer*

[2] Bar-Cohen, Y., (2001), Electroactive polymer (EAP) actuators as artificial muscles. *SPIE Press*

[3] Bar-Cohen, Y., (2004), Electroactive polymers as actuators for potential future planetary mechanisms." *Proceedings of the NASA DOD conference on Evolution Hardware, Seattle, USA*

[4] Carpi, F., Smela, E., (2009), Biomedical applications of Electroactive polymer actuators, *Book, John Wiley & Sons, Ltd.*

[5] Boyraz, P., Runge, G., and Raatz, A., (2018), Review: An overview of novel actuators for soft robotics, *Actuators*, **7(48)**

[6] Chu, W., Lee, K., Song, SH., Han, M., Lee, J., Kim, H., Kim, SK., Park., Y. J., Cho, K., Ahn, SH., (2012), Review of biomimetic underwater robots using smart actuators, *International Journal of Precision Engineering and Manufacturing*, **13(7),** pp 1281–1292

[7] McNeill, R., Siudak, R., Wardlaw, J. H., and Weiss, D., E., (1963) Electronic conduction in polymers, *Australian. Journal of Chemistry*, **16**, 1056-1075

[8] Chinag, C. K., Park, Y. W., Heeger, A. J., Shirakawa, H., Louis, E. J., and MacDiarmid, A. J., (1978), Conducting Polymers: Halogen doped Polyacetylene, *J. Chem. Phys.*, **69**, 5098-5104.

[9] Bredas, J.L., Street, G.B., (1985), Polarons, bipolarons, and solitons in conducting polymers. *Acc. Chem. Res.*, **18**, 309–315.

[10] MacDiarmid, A.G., Mammone, R.J., Kaner, R.B., Porter, S.J., Pethig, R., Heeger, A.J., and Rosseinsky, D.R., (1985), The concept of 'doping' of conducting polymers: The role of reduction potentials. *Phil. Trans. R. Soc. A*, **314**, 3–15.

[11] Gribkova, O.L., Omelchenko, O.D., Tameev, A.R., Lypenko, D.A., Nekrasov, A.A., Posudievskii, O.Y., Koshechko, V.G., Vannikov, A.V., (2016) The specific effect of graphene additives in polyaniline-based nanocomposite layers on performance

characteristics of electroluminescent and photovoltaic devices, *High Energy Chem.*, **50**, 134–138

[12] Tang, H., Kumar, P., Zhang, S., Yi, Z., Crescenzo, G.D., Santato, C., Soavi, F., Cicoira, F., (2015) Conducting polymer transistors making use of activated carbon gate electrodes. *ACS Appl. Mater. Interfaces*, **7(1)**, 969-973

[13] Yoon, H., (2013), Current trends in sensors based on conducting polymer nanomaterials. *Nanomaterials*, **3**, 524

[14] R.H.Baughman, R. H., (1996), Conducting polymer artificial muscles, *Synthetic Metals*, **78 (3)**, 339-353

[15] Kaneto, K., (2016), Research Trends of Soft Actuators based on Electroactive Polymers and Conducting Polymers, *J. Phys.: Conf. Ser.704 012004*,

[16] Madden, J., (2000) Conducting Polymer Actuator, *PhD Thesis, MIT*, 2000

[17] Jager, E., (2013), Conducting polymer actuators for medical devices and cell mechanotransduction, *IEEE/ASME International Conference on Advanced Intelligent Mechatronics, Wollongong*, 1661-1666

[18] Balint, R., Cassidy, N. J., and Cartmell, S. H., (2014), Conductive polymers: Towards a smart biomaterial for tissue engineering, *Acta Biomaterialia*, **10(6)**, 2341-2353

[19] Hunter, I.W., Lafontaine, S., (1992), A Comparison of Muscle with Artificial Actuators, *Technical Digest of the IEEE Solid-State Sensor and Actuator Workshop, Hilton Head, South Carolina*, 178–185

[20] Mirfakhrai, T., Madden, JD., Baughman, RH., (2007), Review: Polymer artificial muscles, *Materials Today*, **10(4)**, 30-38

[21] Kaneko, M., Fukui, M., Takashima, W., Kaneto. K., (1997), Electrolyte and Strain Dependences of Chemomechanical Deformation of Polyaniline Film, *Synthetic Metals*, **84(1-3)**, 795-796,

[22] Mazzoldi. A., DeglInnocenti, C., Michelucci, M., Rossi., D., (1998), Actuative Properties of Polyaniline Fibers under Electrochemical Stimulation, *Mater. Sci, Eng:C*, **6(1),** 65-72.

[23] Sprink, GM., Mottaghitalab., V., Bahrami-Saniani, M., Whitten., P. G., and Wallace, G. G., (2006), Carbon-Nanotube-Reinforced Polyaniline Fibers for High Strength Artificial Muscles. *Advanced Materials*, **18(5)**

[24] Alfano, B., Massera, E., Maria, A. De., Girolamo, A. DE., Francia, G. Di., Napolitano, T., Vineri, P. D., Borrielo, A., (2015), Polyaniline proton doping for sensor application, *XVIII AISEM Annual Conference*, Trento.

[25] Gonçalves, R., Pereira, E. C., and Marchesi, L. F., (2017), The Overoxidation of poly(3-hexylthiophene) (P3HT) Thin Film: CV and EIS measurements, *Int. J. Electrochem. Sci*., **12**, 1983–1991.

[26] XI, B., Truong V. T., Whitten, P., Ding, J., Spinks, G.M., Wallace, G. G., (2006), Poly(3-Methylthiophene.) Electrochemical Actuators Showing Increased Strain and Work Per Cycle at Higher Operating Stresses, *Polymer,* **47(22),** 7720-7725

[27] Lee, SH., Park, H., Son, W., Choi, H.H., and Kim, J. H., (2014), Novel solution-processable, dedoped semiconductors for application in thermoelectric devices, *J. Material Chemistry A*, **2(33)**

[28] Zein, A., Huppe, C., Cochrane, C., (2017), Development of a Flexible Strain Sensor Based on PEDOT:PSS for Thin Film Structures, *Sensors*, **17(6),** 1337.

[29] Li, Y., Tanigawa, R., and Okuzaki, H., (2014), Soft and flexible PEDOT/PSS films for applications to soft actuators. *Smart Materials and Structures*, **23(7),** 074010.

[30] Hara., S., Zama T., Takashima, W., and Kaneto, K., (2004), TFSI-Doped Polypyrrole Actuator with26% Strain, *Journal of Materials Chemistry*,**14(10)**: 15145-1517.

[31] Bay, L., West, K., Sommer-Larsen, R., Skaarup, S., and Benslirrane, M., (2003). A Conducting Polymer Artificial muscle with 12% Linear strain. *Advanced Materials*, **15(4)**, 310-313.

[32] Hara, S., Zama, T., Takashima, W., and Kaneto, K., (2005), Free-Standing Gel-Like Polypyrrole Actuators Doped with Bis((perfluoroalkylsulfonyl) Imide Exhibiting extremely large strain, Smart materials and Structures, 14(6), 1501-1510.

[33] Madden J.D., (2007) Polypyrrole Actuators: Properties and Initial Applications. *Electroactive Polymers for Robotic Applications. Springer*, London

[34] KIM, J., Deshpande, SD., Yun, S., Li, Q., (2006), A Comparative Study of Conductive Polypyrrole and Polyaniline Coatings on Electro-Active Papers, *Polymer Journal*, 38(7), 659–668

[35] Jager, E., Smaela, E., Inganas, O., Lundstrom, I., (1999), Application of Polypyrrole microactuator, *Synthetic Metals* **102**.

[36] Jager, E., Immerstrand, C., Magnusson, K., Inganas, O., and Lundstrom, I., (2000) Biomedical applications of polypyrrole microactuators: from single-cell clinic to microrobots, *IEEE-EMBS Special Topic Conference on Microtechnologies in Medicine and Biology. Proceedings*, Lyon, France, 58-61.

[37] Alici G., Mutlu R., Melling D., Jager E.W.H., Kaneto K., (2016) Conducting Polymers as EAPs: Device Configurations. Electromechanically Active Polymers. Polymers and Polymeric Composites: *A Reference Series. Springer*.

[38] Santa, A., D., Rossi, D. D., and Mazzoldi, A., (1997), Characterization and modelling of a conducting polymer muscle-like linear actuator, *Smart Materials and Structures*, **6(23),**

[39] Ding, J., Liu, L., Spinks, G. M., Zhou, D., Wallace, G. G., and Gillespie, J., (2003), High performance conducting polymer actuators utilising a tubular geometry and helical wire interconnects, *Synthetic Metals*, **138**, 391-398.

[40] Della Santa, A., Rossi, D. DE., and Mazzoldi, A., (1997), Performance and work capacity of a polypyrrole conducting polymer linear actuator, *Synthetic Metals*, **90**, 93-100

[41] Price, A. D., (2012), Fabrication, Modelling and Application of Conductive Polymer Composites, *PhD Thesis, University of Toronto*

[42] Ansari, R., (2006), Polypyrrole Conducting Electroactive Polymers: Synthesis and Stability Studies, *Journal of Chemistry*, **3(4)**, 186-201

[43] Zahang, W., (2011), Analysis of High performance Polypyrrole actuator, *PhD Thesis, University of Wollongong, Australia*

[44] Wu, A., Kolla, H., Manohar, S. K., (2005), Chemical Synthesis of Highly Conducting Polypyrrole Nanofiber Film, *Macromolecules*, 7873-7875.

[45] Bahraeian, S., Abron, K., Pourjafarian, F., Majid, R., (2013), Study on Synthesis of Polypyrrole via Chemical Polymerization Method", *Advanced Materials Research*, **795**, pp. 707-710

[46] Waghuley , S.A., Yenorkar, S. M., Yawale, S. S., and Yawale, S. P., (2008), Application of chemically synthesized conducting polymer-polypyrrole as a carbon dioxide gas sensor, *Sensors and Actuator B:Chemical*, **128(2)**, pp 366-373.

[47] Le, TH., Kim, Y., and Yoon, H., (2017), Electrical and Electrochemical Properties of Conducting Polymers, *Polymers*, **9(150)**

[48] Yamaura, M., Sato, K., Hagiwara, T., (1990) "Effect of counter-anion exchange on electrical conductivity of polypyrrole films" *Synthetic Metals*, **39**, 43-60.

[49] Danial, S., (2012), Optimization of the layer-by-layer synthesis method for polypyrrole actuators, *Research Thesis, University of Wollongong*.

[50] Yan, B., Wu, Y., and Guo, L., (2013), Review: Recent Advances on Polypyrrole Electroactuators**,** *Anal. Chem.*7230-7240.

[51] Zhou, M., Pagels, M., Geschke, B., Heinze, J., (2002), Electropolymerization of Pyrrole and Electrochemical Study of Polypyrrole:. Controlled Electrochemical Synthesis and Solid-State Transition of Well-Defined Polypyrrole Variants, *J. Phys. Chem. B*, 10065-10073.

[52] Kiefer, R., Bowmaker, G.A., Kilmartin, P. A., Travas-Sejdic, J., (2010), Effect of polymerization potential on the actuation of free standing poly-3,4-ethylenedioxythiophene films in a propylene carbonate electrolyte, *Electrochim. Acta*, **55**, 681–688.

[53] Hagiwara, T., M. Hirasaka, M., Sato, K., Yamaura, M., (1990), Enhancement of the electrical conductivity of polypyrrole film by stretching: Influence of the polymerization conditions, *Synthetic Metals*, **36**, 241–252.

[54] Warren, M., (2005), Electronic and Structural Effects on the Electrochemistry of Polypyrrole, *MS Thesis, University of British Columbia*

[55] Kassim, A., Basar, Z. B., Mahmud, HNME.,(2002), Effects of preparation temperature on the conductivity of polypyrrole conducting polymer**,** *Proc. Indian Acad. Sci. (Chem. Sci.)*, **114(2)**, pp 155–162

[56] Aydemir, M., Kilmartin, P. A., Travas-Sejdic, J., Kesküla, A., Liisa, A., Parcell, P. J., Harjo, M., Aabloo, A., Kiefer, R., (2015), Electrolyte and solvent effects in PPy/DBS linear actuators, *Sensor and Actuator B: Chemical*, **216,** 24-32

[57] Madden, J.D., Cush, R.A., Kanigan, T.S., Hunter, I.W., (2000), Fast contracting polypyrrole actuators, *Synthetic Metals*, **113**: 185–192.

[58] Madden, J.D., Madden, P.G., and Hunter, I.W., (2001), Characterization of Polypyrrole Actuators*: Modeling and Performance*. *Proceedings of SPIE 8th Annual Symposium on Smart Structures and Materials, Bellingham*, 72-83.

[59] Madden, J.D., Anquetil, P.A., Rinderknecht, D., Vandesteeg, N.A., Hunter, I.W., (2004), Large Strain Actuation in Polypyrrole Actuators. Smart Structures and Materials, *SPIE - International Society Optical Engineering: Bellingham*, 380-387.

[60] Madden, J.D., Vandesteeg, N.A., Anquetil, P.A., Madden, P., Takshi, A., Pytel, R.Z., Lafontaine, S.R., Wieringa, P.A., Hunter, I.W. Artificial muscle technology: physical principles and naval prospects. IEEE Journal of Oceanic Engineering, July 2004, **29(3):** 706-728.

[61] Maw, S., Smela, E., Yoshida, K., Stein, R. B., (2005), Effects of monomer and electrolyte concentrations on actuation of PPy(DBS) bilayers, *Synthetic Metals*, **155**, 18–26

[62] Masurkar, N., Jamil, K., and Reddy, L. M., (2017), Environmental Effects on the Polypyrrole Tri-layer Actuator, *Actuators*, **6(17)**

[63] Christophersen, M., Shapiro, B., Smela, E., (2006), Characterization and modeling of PPy bilayer microactuators: Part 1. Curvature. *Sens. Actuators B*, **115**, 596–609.

[64] Wang, J., Botelho, S.J., Naguib, H.E., Bazylak, A., (2013), Development of a novel active polypyrrole trilayer membrane. *ACS Sustain. Chem. Eng.*, **1**, 226–231.

[65] Zheng, W., Whitten, P. G., and Spinks, G. M., (2018). Polypyrrole actuators: the effects of polymer thickness and voltage scan rate on fractional charging and isotonic actuation strain, *Multifunctional Material*, **1**

[66] Madden, J.D., Rinderknecht, D., Anquetil, P.A., Hunter, I.W. (2007), Creep and Cycle Life in Polypyrrole Actuators, *Sensors and Actuators*, **133**: 210-217

[67] Madden, J. D., Madden, P. G., & Hunter, I. W., (2001), Polypyrrole actuators: modeling and performance. *Smart Structures and Materials*:

[68] Chuc Huu Nguyena,b, Gursel Alici a,b,∗, Gordon G. Wallaceb, Modelling trilayer conjugated polymer actuators for their sensorless position control, Sensors and Actuators A **185** (2012) 82– 91

[69] Secord, T. W., (2007), Modeling, Identification, and Application of Multilayer Polypyrrole Conducting Polymer Actuators, *MS Thesis, MIT*

[70] Bowers, T. A., (2004), Modeling, simulation, and control of a polypyrrole-based conducting polymer actuator, *MS Thesis, MIT*

[71] Mutlu, M., Alici, G., Xiang, X., Li, W., (2014), Electro-mechanical modelling and identification of electroactive polymer actuators as smart robotic manipulators, *Mechatronics*, **24(3)**, pp 241-251

[72] Fanga, Y., Tana, X., Shena, Y., Xia, N., Alici, G., (2008), A scalable model for trilayer conjugated polymer actuators and its experimental validation, *Materials Science and Engineering C* **28**, 421–428

[73] Du, P., Lin, X., Zhang, X., (2010), A multilayer bending model for conducting polymer actuators, *Sensors and Actuators A*, **163**, 240–246

[74] Alici, G., Mui, B., & Cook, C. (2006). Bending modeling and its experimental verification for conducting polymer actuators dedicated to manipulation applications. *Sensors and Actuators A: Physical*, **126(2),** 396–404

[75] Moghadam, AAA., Moavenian, M., Torabi, K., Tahani, M., (2011), Analytical dynamic modeling of fast trilayer polypyrrole bending actuators, *Smart Material and Structure*, **20,** 115020

[76] Alizadeh, V., Tahani, M., Ghassabi, A., (2014), Nonlinear dynamic modeling of fast trilayer polypyrrole (ppy) bending actuators with tip mass, *The 21st International Congress on Sound and Vibration13-17 July, 2014, Beijing/China*

[77] Moghadam, AAA., Torabi, K., Moavenian, M., Davoodi, R., (2013), Dynamic modeling and robust control of an L-shaped microrobot based on fast trilayer polypyrrole-bending actuators, *Journal of Intelligent Material Systems and Structures*, **24(4)**, 484–498

[78] John, S. W., Alici, G., and Cook, C. D., (2010), Inversion-Based Feed forward Control of Polypyrrole Trilayer Bender Actuators, *IEEE/ASME Transactions on Mechatronics*, **15(1)**, pp. 149-156

[79] Nguyen, N. T., Plesse, C., Nguyen, G. T., Dobashi, Y., Soyer, C., Vidal; F., Cattan; E., Grondel, S., Madden, JWD., (2018), Non-linear dynamic modeling of ultrathin conducting polymer actuators including inertial effects, *Smart Materials and Structures*, **27 (11)**, pp.115032.

[80] Wu, Y., Alici, G., Spinks, G. M., and Wallace, G. G. (2006), Fast trilayer polypyrrole bending actuators for high speed applications, *Synthetic Metals*, **156(16-17)**, 1017–1022.

[81] Alizadeh, V., and Tahani, M., (2014), Nonlinear viscoelastic dynamic modelling of high-speed polypyrrole-based trilayer bending plate-like actuators based on first-order shear deformation plate theory, *Journal of Intelligent Material Systems and Structures*, 1–17

[82] Alici, G., Spinks, G., Huynh, N., N., Sarmadi, L., and Minato, R., (2007), Establishment of a biomimetic device based on tri-layer polymer actuators – Propulsion fins, *Bioinspiration and Biomimetics*, **2**, pp. S18 - S30.

[83] Tangorra, J., Anquetil, P., Fofonoff, T., Chen, A., Zio, M. D., and Hunter, I., (2007), The application of conducting polymers to a biorobotic fin propulsor, *Bioinspiration & Biomimetics*, **2**

[84] Madden, JWD., Schmid , B., Hechinger, M., Lafontaine , S. R., Madden, PGA., Hover, F. S., Kimball, R., Hunter, I.W., (2004), Application of polypyrrole actuators: feasibility of variable camber foils, *IEEE Journal of Oceanic Engineering*, **29(3)**, pp. 738-749

[85] Mcgovern, S. T., Abbot, M., Emery, R., Alici, G., Truong, V., Spinks, G. M., and Wallace, G.G., (2010), Evaluation of Thrust force generated for a robotic fish propelled with Polypyrrole actuator, *Polymer International*, **59**, pp 357-364

[86] Alici, G., and Huynh, N., (2007), Performance quantification of conducting polymer actuators for real applications: a microgripping system, *IEEE – ASME Transl. Mechatronics*, **12 (1)** pp:73-84

[87] McGovern, S. T., Spinks, G., Xi, B., and Wallace, G., (2008), Fast bender actuators for fish-like aquatic robots, Proceedings Electroactive Polymer Actuators and Devices (EAPAD), **6927**

[88] Bar-Cohen, Y., (2003), Biologically inspired intelligent robots using artificial muscles, *Proceedings International Conference on MEMS, NANO and Smart Systems*, Banff, Alberta, Canada, pp. 2-8.

[89] Choi H.R., Jung K.M., Koo J.C., Nam J.D. (2007) Robotic Applications of Artificial Muscle Actuators. *Electroactive Polymers for Robotic Applications. Springer*

[90] Khan, W., Kapoor, M., Kumar, N., (2007), Covalent attachment of proteins to functionalized polypyrrole-coated metallic surfaces for improved biocompatibility. *Acta Biomater*, **3**, 541–549.

[91] Hardy, J. G., Sukhavasi, R. C., Aguilar Jr. D., Villancio-Wolter, M. K., Mouser, D. J., Geissler, S. A., Nguy, L., Chow, J. K., Kaplan, D. L., and Schmid, C. E., (2015), Electrical stimulation of human mesenchymal stem cells on biomineralized conducting polymers enhances their differentiation towards osteogenic outcomes, *J. Mater. Chem. B*, **3**, 8059-8064

[92] Shoa, T., Munce, N. R., Yang, V., and Madden, J. D., (2009), Conducting polymer actuator driven catheter: overview and applications", *Proc. SPIE 7287, Electroactive Polymer Actuators and Devices (EAPAD)*

[93] Chu, W. S., Lee, K. T., Song, S. H., Han, M. W., Lee, J. Y., Kim, H. S., Kim, M. S., Park, Y. J., Cho, K. J., Ahn, S. H., (2012), Review of Biomimetic Underwater Robots Using Smart Actuators**,** *International journal of precision engineering and manufacturing*, **13(7)**, pp. 1281-1292

[94] Viau, L., Hihn, J. Y., Lakard, S., Moutarlier, V., Flaud, V., & Lakard, B. (2014). Full characterization of polypyrrole thin films electrosynthesized in room temperature ionic liquids, water or acetonitrile. Electrochimica Acta, **137**, 298–310.

[95] Qia, G., Wub, Z., and Wang, H., (2013), Highly conductive and semitransparent free-standing polypyrrole films prepared by chemical interfacial polymerization, *J. Mater. Chem. C*, **1**, 7102

[96] Shah, SAA., Firlak, M., Berrow, S. R., Halcovitch, N. R., Baldock, S. J., Yousafzai, B. M., Hathout, R. N., Hardy**,** J. G., (2018) Electrochemically Enhanced Drug Delivery Using Polypyrrole Films, *Materials*, **11(7)**, 1123

[97] Su, N., Li, Yuan, S. J., Yi, S. P., Yin, E. Q., (2012), Synthesis and characterization of polypyrrole doped with anionic spherical polyelectrolyte brushes, *eXPRESS Polymer Letters*, **6(9)**, 697–705

[98] Melling D., Jager E.W.H. (2016) Conducting Polymers as EAPs: Characterization Methods and Metrics, *Electromechanically Active Polymers. Polymers and Polymeric Composites: A Reference Series. Springer, Cham*

[99] Zhang, Y., Li, S., Ma, J., and Yang, J., (2005), Development of an underwater oscillatory propulsion system using shape memory alloy, *IEEE International Conference Mechatronics and Automation, Niagara Falls*, **4**, pp. 1878-1883.

[100] Shinjo, N., and Swain, G. W., (2004), Use of a shape memory alloy for the design of an oscillatory propulsion system, *IEEE Journal of Oceanic Engineering*, **29(3),** pp. 750-755

[101] Wang, Z., Hang, G., Wang, Y., Li, J., and Du, W., (2008), Embedded SMA wire actuated biomimetic fin: a module for biomimetic underwater propulsion, *Smart Materials and Structures*, **17(2)**

[102] Hubbard, J. J., Fleming, M., Palmre, V., Pugal, D., Kim, K. J., and Leang, K. K., (2011), Characterization of Sectored-Electrode IPMC-Based Propulsors for Underwater Locomotion, *ASME Conference on Smart Materials, Adaptive Structures and Intelligent Systems, September 18–21, 2011 , Scottsdale, Arizona*, USA

[103] Hubbard, J. J., Fleming, M., Palmre, V., Pugal, D., Kim, K. J., and Leang, K. K.,(2014), Monolithic IPMC Fins for Propulsion and Maneuvering in Bioinspired Underwater Robotics, *IEEE Journal of Oceanic Engineering*, **39(3)**, pp. 540-551

[104] Chen, Z. (2017), A review on robotic fish enabled by ionic polymer-metal composite artificial muscles, *Robotics and Biomimetics*, **4(1)**, 24.

[105] Kim, K. J., Yim, W., Paquette, W. J., and Kim, D., (2007), Ionic Polymer-metal Composites for Underwater Operation, *J. Intelligent Material Systems and Structures* **18**,

[106] Chen, Z., Um, T., and Smith, H., B., (2012), Ionic Polymer-Metal Composite Artificial Muscles in Bio-Inspired Engineering Research: Underwater propulsion, *Smart Actuation and Sensing System - Recent Advances and Future Challenges, InTech Open*

[107] Shintake, J., Shea, H., and Floreano, D. (2016). Biomimetic underwater robots based on dielectric elastomer actuators. *IEEE/RSJ International Conference on Intelligent Robots and Systems (IROS).*

[108] Shintake, J., Ming, A., and Shimojo, M., (2011), A novel propulsion method of flexible underwater robots, *IEEE/RSJ International Conference on Intelligent Robots and Systems*, San Francisco, CA, pp. 4735-4740.

[109] Beker, F., Zimmermann, K., Volkova, T., Minchenya, V., T., (2013), An amphibious vibration-driven microrobot with a piezoelectric actuator, Regular and Chaotic Dynamics, **18(63)**

[110] Mcgovern, S. T., Abbot, M., Emery, R., Alici, G., Truong, V., Spinks, G. M., and Wallace, G. G., (2010), Evaluation of Thrust force generated for a robotic fish propelled with Polypyrrole actuator", Polymer International, **59**, pp 357-364

[111] Alici, G., Spinks, G., Huynh, N. N., Sarmadi, L., and Minato, R., (2007) Establishment of a biomimetic device based on tri-layer polymer actuators – Propulsion fins". *Bioinspiration and Biomimetics*. **2**, pp. S18 - S30

[112] Chae, W., Cha, Y., Peterson, S. D., Porfiri, M., (2015), Flow measurement and thrust estimation of a vibrating ionic polymer metal composite, *Smart Mater. Struct*.**24**

[113] TianMiao, W., Qi, S., Li, W., JianHong, L., (2012), On the thrust performance of an ionic polymer-metal composite actuated robotic fish: Modeling and experimental investigation, Science China: *Technological Science*, **55(12)**

[114] Roylance, D., (2001), Engineering Viscoelasticity, *Department of Materials Science and Engineering Massachusetts Institute of Technology*

[115] Blevins, R.D., (1979), Formulas for Natural Frequency and Mode Shape, *Van Nostrand Reinhold Company, Inc, New York*

[116] Vancuraa, C., Dufourb, I., Heinrichd, S. M., Jossec, F., Hierlemann, A., (2008), Analysis of resonating microcantilevers operating in a viscous liquid environment, *Sensors and Actuators A* **141**, 43–51

[117] Lighthill, M.J., (1976). Flagellar hydrodynamics: the John von Neumann lecture,. *SIAM Rev*, 161–230.

[118] Kim, K. J., Yim, W., Paquette, W. J., and Kim, D., (2007), Ionic Polymer-metal Composites for Underwater Operation, *J. Intelligent Material Systems and Structures* **18**

[119] Shahab, S., and Erturk, A., (2016), Electrohydroelastic Euler–Bernoulli–Morison model for underwaterresonant actuation of macro-fiber composite piezoelectric cantilevers, *Smart Mater. Struct*.**25**

[120] Cen, L and Erturk, A., Bio-inspired aquatic robotics by untethered piezohydroelastic actuation, *Bioinspiration and Biomimetic*.**8,** 13pp

[121] Wang, J., McKinley, P. K., Tan, X., (2017), Dynamic Modeling of Robotic Fish With a Base-Actuated Flexible Tail, *Journal of Dynamic Systems, Measurement, and Control*, **137**

[122] Graham, J. M. R., (1980), The forces on sharp-edged cylinders in oscillatory flow at low Keulegan– Carpenter numbers. *J. Fluid Mech*. **97 (2),** 331–346.

[123] Sarpkaya, T., (1995) Hydrodynamic damping, flow-induced oscillations, and biharmonic response, *J. Offshore Mech. Arct*. **117**, 232–238.

[124] Jessica K. Shang, J. K., Stone, H. A., Smits, A. J., (2014), Vortex and structural dynamics of a flexible cylinder in cross-flow, *Physics of Fluids* **26**,

[125] Schnipper, T., Andersen, A., Bohr, T., (2009) Vortex wakes of a flapping foil, *Journal of Fluid Mechanics* **633**:411 – 423

[126] Keulegan, G. H. and Carpenter, L. H. (1958), Forces on cylinders and plates in an oscillating fluid, *J. Res. Natl Bur. Stand*. **60 (5)**, 423–440.

[127] Jones, M. A., (2003), The separated flow of an inviscid fluid around a moving flat plate. *J. Fluid Mech*. **496**, 405–441.

[128] Bidkar, R., Kimber, M., Bajaj, A., Garimella, S., (2009), Nonlinear aerodynamic damping of sharp-edged flexible beams oscillating at low Keulegan-Carpenter numbers, *J. Fluid Mech*. **634**, pp. 269–289

[129] Nayfeh, A.and Mook, D., (1979), Nonlinear Oscillations, *1st ed. John Wiley & Sons*.

[130] Ewins, D. J. 2000 Modal Testing: Theory, Practice, and Application, 2nd ed. Baldock.

[131] Kimber, M., Garimella, S. V. and Raman, A. (2007), Local heat transfer coefficients induced by piezo electrically actuated vibrating cantilevers. *J. Heat Trans.-ASME* **129**, 1168–1176.

[132] Mahmoodia, S. N., Khadema, S. E., Kokabi, M., (2007), Non-linear free vibrations of Kelvin–Voigt visco-elastic beams, *International Journal of Mechanical Sciences*, **49** 722–732

[133] Facci, A. L., Porfiri, M., (2012), Nonlinear hydrodynamic damping of sharp-edged cantilevers in viscous fluids undergoing multi-harmonic base excitation, *Journal of Applied Physics*, **112**, 124908 (2012)

[134] Facci, A. L., Porfiri, M., (2012), Nonlinear hydrodynamic damping of sharp-edged cantilevers in viscous fluids undergoing multi-harmonic base excitation, *Journal of Applied Physics*, **112**, 124908 (2012)

[135] Ahasan S., Aureli, M., (2017), Three-Dimensional Analysis of Hydrodynamic Forces and Power Dissipation in Shape-Morphing Cantilevers Oscillating in Viscous Fluids, International Journal of Mechanical Sciences, **149**

[136] Roznowski, G., (2006), Underwater Robot Actuated by Shape Memory Alloy Wires," *Proceedings of the 2nd International Conference on Perspective Technologies and Methods in MEMS Design*, *Lviv*, pp. 149-150

[137] Raparelli, T., (2017), Design and realization of a Flexible Finger Actuated by Shape Memory Alloy (SMA) Wires, *International Journal of Applied Engineering Research* **12(24)**, pp. 15635-15643

[138] Huang, P. H., Wang, J., (2012), A New Design of Underwater Robot Fish System Using Shape Memory Alloy", *Applied Mechanics and Materials*, **187**, pp. 260-266

[139] Godaba, H., Li, J., Wang, Y., and Zhu, J. (2016), A Soft Jellyfish Robot Driven by a Dielectric Elastomer Actuator, *IEEE Robotics and Automation Letters*, **1**, 624-631.

[140] Xu, L., Chen, H. Q., Zou, J., Dong, W. T., Gu, G. Y., Zhu, L. M., Zhu, X. Y., (2017), Bio-inspired annelid robot: a dielectric elastomer actuated soft robot, *Bioinspiration & Biomimetics*, **12**,

[141] Shelton, R. M., Thornycroft, P. J., Lauder, G. V., (2014), Undulatory locomotion of flexible foils as biomimetic models for understanding fish propulsion, *Journal of Experimental Biology*, **217**, 2110-2120

[142] Gutta, S., (2011), Modeling and Control of a Flexible Ionic Polymer Metal Composite(IPMC) Actuator for Underwater Propulsion, *PhD Thesis, University of Nevada, Las Vegas*

[143] Guo, S., Shi, L., (2014), IPMC Actuator-Based Multifunctional Underwater Microrobots, *Soft Actuator*, pp 401- 421

[144] Neubauer, J., Stalbaum, T., and Kim, K. J., (2018), IPMC Embedded in a Pneumatic Soft Robotic Actuator: Preliminary Experiments in Actuation and Sensing Behaviors, *15th International Conference on Ubiquitous Robots (UR)*, *Honolulu, HI*, pp. 80-82.

[145] Cen, L., Erturk, A., (2013), Bio-inspired aquatic robotics by untethered piezohydroelastic actuation, *Bioinspiration and Biomimetic*.**8**

[146] Nagata, Y., Park, S., Ming, A., and Shimojo, M., (2008), Development of underwater robot using Macro Fiber Composite, *IEEE/ASME International Conference on Advanced Intelligent Mechatronics*, *Xian*, pp. 955-960

[147] Wang, H., Tjahyono, S. S., MacDonald, B., Kilmartin, P. A., Travas-Sejdic, J., and Kiefer, R., (2007), Robotic Fish Based on a Polymer Actuator, *Australian Conference on Robotics and Automation*,

[148] Hoff, K., Wassersug, R. J., (2000), Tadpole Locomotion: Axial Movement and Tail Functions in a Largely Vertebrae less Vertebrate, Integrative and Comparative Biology, **40(1),** Pages 62–076.

[149] Liu, H., Wassersug, R., and Kawachi, K., (1997), The three dimensional hydrodynamics of tadpole locomotion, *The Journal of Experimental Biology*, **200**, 2807–2819.

[150] Hoff, K. V. S., Wassersug, R. J., (1986), The Kinematics of Swimming in Larvae of the Clawed Frog, Xenopus Laevis, *Journal of Experimental Biology*, **122**, 1-12,

[151] Kim, B., Kim, D. H., Jung, J., Park, J., (2005), A biomimetic undulatory tadpole robot using ionic polymer–metal composite actuators, *Smart Materials and Structures*, **14(6)**

[152] Wang, J., McKinley, P. K., Tan, X., (2017), Dynamic Modeling of Robotic Fish With a Base-Actuated Flexible Tail, *Journal of Dynamic Systems, Measurement, and Control*, **137**

[153] Wen, L., Liang, J., Shen, S., Bao, L., and Zhang, Q., (2013), Hydrodynamic Performance of an Undulatory Robot: Functional Roles of the Body and Caudal Fin Locomotion, *International Journal of Advanced Robotic Systems*,**10(5).**

[154] Shintake, J., Ming, A., Shimojo, M., (2010), Development of Flexible Underwater Robots with Caudal Fin Propulsion, *IEEE/RSJ International Conference on Intelligent Robots and Systems October 18-22, 2010, Taipei, Taiwan*.

Publications

Conferences

1. Samir K Panda, Dibakar Bandopadhya, (2017), Fabrication and Characterization of Au-PPy Bimorph Actuator for Underwater Operation, *International Conference on Advance Materials Development and Process (AMDP), University of Pune, Pune, India,* 11-14 July
2. S K Panda, D Bandopadhya, (2017), Synthesis and Development of Au-PPy Actuator for Underwater Applications, *International Conference on Advances in Materials and Manufacturing Applications (IconAMMA), Amrita University, Bangalore, India,* 17-19 August.[(Published in IOP: Material science Conference series, 310 (1)]
3. Samir K Panda, Dibakar Bandopadhya, (2018), Gold Polypyrrole (Au-PPy) Bimorph Actuator for Underwater Robotic Motion, *International Conference on Systems, Computations and Networking (ICSCN), MVIT, Pondicherry, India,* 6-7 July. [Published in IEEE digital explore, pp: 1-8, 18273973]
4. Samir K Panda, Dibakar Bandopadhya, (2018), Hydrodynamic Characterization and Performances Evaluation of Gold Polypyrrole Actuator Propulsor, *International Conference on Advances in Materials and Manufacturing Applications (IconAMMA), Amrita University, Bangalore, India,* 16-18 August.
5. Samir K Panda, Dibakar Bandopadhya, (2019), Bioinspired Underwater Undulatory Motion by Using Polypyrrole Bimorph Actuator, *International Conference on Systems, Computations and Networking (ICSCN), MVIT, Pondicherry, India,* 29 - 30 March.

Journals

6. Samir K Panda, Dibakar Bandopadhya, (2019), Hydrodynamic Characterization and Performances Evaluation of Gold Polypyrrole Actuator Propulsor, *IOP: Material Science* (accepted)

7. Samir K Panda, Dibakar Bandopadhya, (2019), Bioinspired Underwater Undulatory Motion by Using Polypyrrole Bimorph Actuator, *IEEE Digital Xplore* (accepted)
8. Samir K Panda, Dibakar Bandopadhya, (2020), Modelling and Experimental Validation of Polypyrrole Actuator for Underwater Propulsion Application, *Smart Structure and Systems*, *Techno-press*. (Communicated).
9. S K Panda, D Bandopadhya, (2020), Modelling and Development of Gold-Polypyrrole Based Underwater Undulatory Robot, *Journal of Intelligent Material and System.* (communicated)